Développement de nouveaux supports basés sur des nanofibres de matériaux hybrides électrofilées pour le développement de biocapteurs électrochimiques

Eleni Sapountzi

UNIVERSITE CLAUDE BERNARD LYON 1

ECOLE DOCTORALE DE CHIMIE, PROCEDES, ENVIRONNEMENT

Thèse présentée pour l'obtention du grade de

Docteur en Chimie et Nanotechnologie de l'Université Claude Bernard Lyon 1

Soutenue le 23 Septembre 2015

par

Eleni SAPOUNTZI

DEVELOPPEMENT DE NOUVEAUX SUPPORTS BASES SUR DES NANOFIBRES DE MATERIAUX HYBRIDES ELECTROFILEES POUR LE DEVELOPPEMENT DE BIOCAPTEURS ELECTROCHIMIQUES

Membres du jury:

Mme Florence LAGARDE	Chargée de recherche, CNRS, Lyon	Directrice de thèse
M. Didier LEONARD	Professeur, Université Claude Bernard, Lyon	Examinateur
Mme Sophie TINGRY	Chargée de recherche, CNRS, Montpellier	Rapporteur
M. Francis Vocanson	Professeur, Université Jean Monnet, St Etienne	Rapporteur

Membres invités:

Mme Nicole JAFFREZIC-RENAULT, Directrice de recherche émérite, CNRS, Lyon

M. Jean-François CHATEAUX, Maître de conférences, Université Claude Bernard, Lyon

UNIVERSITE CLAUDE BERNARD LYON 1

ECOLE DOCTORALE DE CHIMIE, PROCEDES, ENVIRONNEMENT

Thèse présentée pour l'obtention du grade de

Docteur en Chimie et Nanotechnologie de l'Université Claude Bernard Lyon 1

Soutenue le 23/Septembre/2015

par

Eleni SAPOUNTZI

DEVELOPMENT OF NOVEL PLATFORMS BASED ON ELECTROSPUN NANOFIBROUS HYBRID MATERIALS FOR ELECTROCHEMICAL BIOSENSOR APPLICATIONS

Jury Members:

Mme Florence LAGARDE	Chargée de recherche, CNRS, Lyon	Ph.D. Director
M. Didier LEONARD	Professeur, Université Claude Bernard, Lyon	Examiner
Mme Sophie TINGRY	Chargée de recherche, CNRS, Montpellier	Reporter
M. Francis Vocanson	Professeur, Université Jean Monnet, St Etienne	Reporter

Invited Members:

Mme Nicole JAFFREZIC-RENAULT, Directrice de recherche émérite, CNRS, Lyon

M. Jean-François CHATEAUX, Maître de conférences, Université Claude Bernard, Lyon

UNIVERSITE CLAUDE BERNARD - LYON 1

Président de l'Université	**M. François-Noël GILLY**
Vice-président du Conseil d'Administration	M. le Professeur Hamda BEN HADID
Vice-président du Conseil des Etudes et de la Vie Universitaire	M. le Professeur Philippe LALLE
Vice-président du Conseil Scientifique	M. le Professeur Germain GILLET
Directeur Général des Services M. François-Noël GILLY	M. Alain HELLEU

COMPOSANTES SANTE

Faculté de Médecine Lyon Est – Claude Bernard	Directeur : M. le Professeur J. ETIENNE
Faculté de Médecine et de Maïeutique Lyon Sud – Charles Mérieux	Directeur : Mme la Professeure C.BURILLON
Faculté d'Odontologie	Directeur : M. le Professeur D.BOURGEOIS
Institut des Sciences Pharmaceutiques et Biologiques	Directeur : Mme la Professeure C.VINCIGUERRA
Institut des Sciences et Techniques de la Réadaptation	Directeur : M. le Professeur Y. MATILLON
Département de formation et Centre de Recherche en Biologie Humaine	Directeur : M. le Professeur P. FARGE

COMPOSANTES ET DEPARTEMENTS DE SCIENCES ET TECHNOLOGIE

Faculté des Sciences et Technologies	Directeur : M. le Professeur F. DE MARCHI
Département Biologie	Directeur : M. le Professeur F. FLEURY
Département Chimie Biochimie	Directeur : Mme le Professeur H. PARROT
Département GEP	Directeur : M. N. SIAUVE
Département Informatique	Directeur : M. le Professeur S. AKKOUCHE
Département Mathématiques	Directeur : M. le Professeur A. GOLDMAN
Département Mécanique	Directeur : M. le Professeur H. BEN HADID
Département Physique	Directeur : Mme S. FLECK
Département Sciences de la Terre	Directeur : Mme la Professeure I. DANIEL
UFR Sciences et Techniques des Activités Physiques et Sportives	Directeur : M. C. COLLIGNON
Observatoire des Sciences de l'Univers de Lyon	Directeur : M. B. GUIDERDONI
Polytech Lyon	Directeur : M. P. FOURNIER

Ecole Supérieure de Chimie Physique Electronique	Directeur : M. G. PIGNAULT
Institut Universitaire de Technologie de Lyon 1	Directeur : M. C. VITON
Institut Universitaire de Formation des Maîtres	Directeur : M. A. MOUGNIOTTE
Institut de Science Financière et d'Assurances	Directeur : M. N. LEBOISNE

"To see a World in a Grain of Sand
And a Heaven in a Wild Flower,
Hold Infinity in the palm of your hand
And Eternity in an hour."
— William Blake, Auguries of Innocence

Dedicated to the memory of my beloved grandmother, Maria,

Who has shown to me how it feels like to be truly, deeply and unconditionally loved,

forever.

I will always miss you.

Love,

your granddaughter,

Elena

Résumé

Les travaux présentés dans ce manuscrit décrivent le développement de trois supports innovants basés sur des nanofibres de matériaux hybrides obtenus par électrofilage pour la réalisation de biocapteur électrochimiques. La performance des biocapteurs est fortement améliorée du fait de l'utilisation de matériaux nanostructurés qui leurs confèrent des propriétés uniques. Les fibres obtenues par électrofilage trouvent des applications dans de nombreux domaines, mais leur utilisation pour l'élaboration de biocapteurs, bien que très prometteuse, est encore très peu abordée. Dans ce travail, différentes nanofibres polymériques contenant des nanotubes de carbone ou recouvertes de nanoparticules d'or ou d'un film de copolymère polypyrolle/poly(pyrolle-3-carboxylique acide) ont été utilisées comme support pour le développement de biocapteurs. La glucose oxydase a été utilisée comme enzyme modèle pour valider les performances des biocapteurs réalisés. Cette enzyme a été incorporée directement dans les nanofibres ou fixée de façon covalente à leur surface. Les biocapteurs ainsi obtenus, caractérisés par différentes techniques microscopiques et électrochimiques, ont permis la détection du glucose avec succès, en utilisant la voltammétrie cyclique et la spectroscopie d'impédance électrochimique, tout en montrant des performances (sensibilité, reproductibilité, stabilité) supérieures à celles des biocapteurs conventionnels.

Mots-clés:

Biocapteurs enzymatiques, voltammétrie cyclique, spectroscopie d'impédance électrochimique, nanofibres, électrofilage, nanoparticules d'or, nanotubes de carbone, polypyrrole.

Abstract

The work detailed within this manuscript describes the development of three novel efficient electroactive platforms based on electrospun nanofibrous hybrid materials for further application to electrochemical biosensors elaboration. The performance of biosensors is enhanced by their coupling with nanoscale materials, due to the unique properties that the latter exhibit. Although electroctrospun fibers find applications in various fields, their exploitation for biosensing is still in an early but promising stage. Herein, different polymeric nanofibers incorporating carbon nanotubes, decorated with gold nanoparticles or coated with conducting polypyrrole/poly(pyrrole-3-carboxylic acid) films were used as platforms for the development of biosensors. Glucose oxidase was used as a model enzyme to validate the performance of the developed biosensors. The enzyme was either incorporated into the nanofibers or covalently immobilized onto their surface. These innovative biosensors, characterized by different microscopic and electrochemical techniques, enabled successful detection of glucose by employing cyclic voltammetry and electrochemical impedance spectroscopy, whilst demonstrating enhanced performances over conventional biosensors in terms of sensitivity, reproducibility and stability.

Keywards:
enzyme biosensors, nanofibers, electrospinning, cyclic voltammetry, electrochemical impedance spectroscopy, gold nanoparticles, carbon nanotubes, polypyrrole

ACKNOWLEDGEMENTS

This work has been performed in the team of "Interfaces and Biosensors", a part of the group "Surfaces (bio) Intrefaces and Micro/nano Systems", at the Institut des Sciences Analytiques UMR 5280 CNRS-UCBL-ENS in collaboration with the Institut des Nanotechnologies de Lyon. The financement of this thesis was provided by the French government.

Firstly, I would like to thank my Ph.D. director, Dr. Florence Lagarde for giving me the opportunity to perfom my thesis in the institute of analytical sciences. I am grateful for your time and for all the help you have offered to me over the past three years.

Secondly, I would like to express my sincere gratitude towards Dr. Jean-François Chateaux, for all the guidance, support, help and encouragement you have given me over the past three years. I feel privileged to have had the opportunity to work with you and I can honestly say that the work performed during my Ph.D. time here would not have been the same without our collaboration. I feel the need to thank you for standing by me as a co-director of this Ph.D., maybe not as an official one but as a real one, even though your time has always been limited.

I would aldo like to thank the jury members Dr. Sophie Tingry, Prof. Leonard Didier and Prof. Francis Vocanson for kindly accepting to evaluate the present dissertation. Moreover, I would particularly like to thank Prof. Leonard Didier for being always cheerful, for always offering a good piece of advice and for creating a nice working environment.

Accordingly, I would like to express my deep appreciation and my gratitude towards Dr. Nicole Jaffrezic-Renault, for all the advice, guidance and kind help you have offered to me during my Ph.D. time. Thank you very much for everything.

A special thank you to Dr. Carole Chaix, for helping me start my experimental activity in the institute of analytical sciences, for the useful advice and for keeping the door of your laboratory and your office always open for me.

Mrs. Carole Farre, deserves an equal big thank you, not only for the help you have given to me in the lab but also for all the advice during the good and the bad moments of my Ph.D. life. Iwould also like to thank Dr. Joëlle Saulnier for happily offering her scientific advice whenever I would ask for it. Moreover, I would like to thank Ms. Barbara Savournin, the groups' secretary, for making my day with your sweet and cheerful "helloooo" as I was entering the building every day.

I would also like to thank all of my colleagues, past and present, for sharing with me all the laboratory equipment and for all the scientific conversations we have had. I would like to thank firstly the ladies of the team: Ms. Sylvia Ayu Bethari, for always being enthusiastic to talk about chemistry, for being a great person to have around and for all the fun times we had in and outside the lab, Ms. Fatma Dridi, for the great environment in the office that we have all benefitted from over the past three years, for sharing lots of laughs but also the same agonies and for all the scientific and non-scientific conversations, and Dr. Magalie Faivre for helping me settling in at the Institut des Nanotechnologies de Lyon and for the help she has

offered to me in the lab. To this point, I would like to particularly thank from the bottom of my heart Dr. Anca Florea, for being a great colleguage but most importantly for being a great and true friend to me. Thank you for all the great times, sober and drunk, inside and outside the lab (respectively), for sharing lots of laughs and endless conversations of all kinds but most importantly for being there for me throughout the most difficult time of my life so far.

Continuing with the gentlemen of the team, firstly I would like to say a big thank you to Dr. Mohamed Braiek, for the excellent collaboration we had and for all the help he offered to me whenever it was needed, Dr. Abdellatif Baraket, for the help and the conversations in the lab, Mr. Mickaël Desbrosses (Debs), for all the music you have been playing in the office over the past three years, for the help and the funny conversations but most importantly for keeping tightly that rope everytime that I would find myself 4 meters above the ground, during the climbing courses. I would also like to thank Dr. Micaël Rippert and Mr. Gabriel De Grozals, for your help in the lab and for our scientific conversations, Dr. Florian Trichard, for all the good times outside the lab and the good conversations we have shared, as well as Mr. Nicolas Terrier, for all the help you offered to me in the lab and for training me to be able to work independently at the clean room of the Institut des Nanotechnologies de Lyon.

Finally, I would particularly like to thank Dr. Jérémy Coulm, for all the help you gave me during the last but most challenging part of my experimental work, for happily offering your advice and guidance whenever I would ask for it and for all the interesting scientific conversations we have shared. Most importantly though, I would like to thank you for standing by me through the difficult period of the redaction of the present dissertation, for being patient, trusting that I will get back to normal after the end of it and for believing in me even when I didn't believe in myself anymore.

Last but not least, the greatest thank you of all goes to my family and especially my parents, who have supported me in every possible way they could during my time abroad. I know it's been difficult but thank you for being understanding and for encouraging me to follow my goals, even if that means we get to spend less time together. You are always on my mind and in my heart.

Elena

CONTENTS

RÉSUMÉ……XI
ABSTRACT……...XI
ACKNOWLEDGEMENTS……XIII
CONTENTS……..……XV
ABRREVIATIONS……XVII
LIST OF FIGURES……..……XXIII
LIST OF TABLES……XXIX
GENERAL INTRODUCTION……3
CHAPTER I: BIBLIOGRAPHIC STUDY……5
I.1. Generalities on Biosensors……..……7
I.1.1. Definition and General Working Principle of Biosensors……9
I.1.2. Classification of Biosensors……..……10
I.1.2.1. Classification based on the Biorecognition Element……10
Enzymatic Biosensors……11
Electrochemical Glucose Biosensors- A Special Case ……14
Immunosensors……...16
Nucleic Acid Biosensors……16
Biomimetic Sensors……17
I.1.2.2. Classification based on Transducers……18
I.1.3. Electrochemical Biosensors……...19
I.1.3.1. *Potentiometric Transducers*……..19
I.1.3.2. *Amperometric and Voltammetric Transducers*……19
Generalities……..19
Cyclic Voltammetry (CV)……..……20
I.1.3.3. *Impedimetric Transducers*……...……21
Generalities……..……..21
Electrochemical Impedance Spectroscopy (EIS)……..……..22
I.1.4. Methods for Bioreceptors Immobilization ……..27
Adsorption……..28
Entrapment……29
Cross-linking……..…29
Covalent binding……30
Self-assembled monolayers (SAMs) ……..32
Affinity……33
I. 2. Impact of Nanotechnology on Biosensing-Nanobiosensors……34
I. 2. 1. Nanomaterials for New Biosensing Principles……..……..…35
I.2.1.1. Carbon Nanotubes (CNTs)……..……..……35
Structure, Charasteristics, Synthesis and Functionalization, Applications…...…35

Integration of Carbon Nanotubes in Biosensors……..…37
I.2.1.2. Nanoparticles (NPs)……..…….39
Gold Nanoparticles-A Special Case..…….……40
Integration of Gold Nanoparticles in Biosensors……..……41
I.2.1.3. Polymer Nanostructures……44
I.3. Electrospinning…….……....47
I.3.1. History of Electrospinning ……49
I.3.2. Electrospinning Process…….……51
I.3.3. Effects of Various Parameters on Electrospinning…….58
I.3.3.1. Polymer Solution Parameters……...58
Concentration……..…58
Molecular Weight……...59
Surface Tension……..…59
Solution Viscosity……..…….59
Solution Conductivity……60
I.3.3.2. Processing Parameters……..……60
Applied Voltage……..……60
Feed Rate/ Polymer Flow Rate…….……61
Effect of Collector…….……61
Diameter of Pipette Orifice/Needle……..……..62
Tip to Collector Distance…….……..62
I.3.3.3. Ambient Parameters ……63
I.3.4. Materials Used in Electrospinning ……..……64
I.3.4.1. Natural and Synthetic Polymers……..…….……64
I.3.4.2. Copolymers and Polymer Blends…….…….……64
I.3.4.3. Composites…….……...……65
Electrospun polymer NFs doped with CNTs……..……65
General applications of electrospun NFs with CNTs……...…….65
Electrospun polymer NFs doped with CNTs for electrochemical enzyme-based biosensing……...……67
Electrospun polymer NFs doped with MNPs……70
Electrospun polymer NFs doped with MNPs for electrochemical enzyme-based biosensing…….……72
Electrospun polymer NFs doped with CNTs and MNPs for electrochemical sensing ……...……75
I.4.Nanostructured Conducting Polymers for High Performance Biosensor Applications: Issues and Challenges……76
I.4.1. Importance of Nanostructured Conducting Polymers to Biosensor Applications…76
I.4.2. Conducting Polymers: Characteristics and Synthesis……..77
I.4.3. Challenges of Electrospinning Intrinsically Conducting Polymers……..78

I.4.4. Integration of Nanostructured Conducting Polymers to Sensing Systems……...80
I.5. Conclusion……82

CHAPTER II: ELECTROSPUN WATER-STABLE POLYVINYL ALCOHOL/ POLYETHYLENEIMINE NANOFIBER MATS INCORPORATING ENZYME AND DECORATED WITH GOLD NANOPARTICLES FOR BIOSENSOR APPLICATIONS……85

II.1. Introduction……87
II.2. Apparatus……90
II.2.1. Instrumentation and Experimental Setup for Electrochemical Measurements…...90
II.2.2. Instrumentation and Experimental Setup for Electrospinning Technique……..…91
II.3. Materials……..……92
II.4. Experimental Section……..……96
II.4.1. Preparation of the working electrodes……..……96
II.4.2. Preparation of electrospun solutions……...…….……96
II.4.3. Electrospinning: Fabrication of electrospun PVA-SbQ, PVA-SbQ/MWCNTs-COOH and PVA-SbQ/MWCNTs-COOH/GOx NFs……..……96
II.4.4. Crosslinking of electrospun NFs……..……97
II.4.5. Electrochemical Characterizations……..……97
II.4.5.1.PVA-SbQ NF and PVA-SbQ/MWCNTs-COOH NF modified electrodes…..97
II.4.5.2.PVA-SbQ/MWCNTs-COOH/GOx NF modified electrodes……...……97
II.4.6. Characterization of NFs morphology……...…….……98
II.5. Results and Discussion……98
II.5.1. Optimization study of ES parameters for the fabrication of nanofibrous mats…...98
II.5.1.1. Optimization of PVA-SbQ concentration……..……...…98
II.5.1.2. Influence of MWCNTs-COOH Loading on ES parameters for the fabrication of PVA-SbQ/MWCNTs-COOH NFs……..……...…98
II.5.2. Morphological Characterization of PVA-SbQ, PVA-SbQ/MWCNTs-COOH and PVA-SbQ/MWCNTs-COOH/GOx NFs……...……..…….……...99
II.5.3. Optimization of the post-electrospinning photo-crosslinking step…..…….……102
II.5.4. Electrochemical Characterization of PVA-SbQ and PVA-SbQ/MWCNTs-COOH NFs……..……..……103
II.5.5. BiosensorApplication……..……105
II.5.5.1. Electroanalytical Characterization……..……...……105
II.5.5.2. Analytical performance of the glucose biosensor……...…...……106
II.6. Conclusion and Perspectives……108

CHAPTER III: ELECTROSPUN WATER-STABLE POLYVINYL ALCOHOL /POLYETHYLENEIMINE NANOFIBER MATS INCORPORATING ENZYME AND DECORATED WITH GOLD NANOPARTICLES FOR BIOSENSOR APPLICATIONS……..109

III.1. Introduction…….111
III.2. Materials……...……113
III.3. Experimental Section……..115
III.3.1. Preparation of Working Electrodes…….……**115**
III.3.2. Preparation of electrospun solutions…….……..**115**
III.3.3. Electrospinning: Fabrication of electrospun PVA/PEI and PVA/PEI/GOx nanofibers…….……**115**
III.3.4. Crosslinking of electrospun nanofibers…….……..**116**
III.3.5. Decoration of water-stable electrospun PVA/PEI NFs with AuNPs……..**116**
III.3.6. Electrochemical characterizations……...…...……..**116**
III.3.6.1.PVA/PEI NFs and PVA/PEI/AuNPs NFs modified electrodes……...…..…**116**
III.3.6.2.PVA/PEI/AuNPs NFs/GOx modified electrodes……...……**116**
III.3.7. Characterization of NFs morphology……...……**117**
III.4. Results and Discussion……117
III.4.1. Morphological Characterization of PVA/PEI, PVA/PEI/GOx and PVA/PEI/AuNPs/GOx electrospun NFs……...……**117**
III.4.1.1. Effect of electrospinning parameters on the morphology of PVA/PEI and PVA/PEI/GOx electrospun NFs……...……...……**117**
III.4.1.2. Influence of enzyme on the morphology of the PVA/PEI/GOx electrospun NFs……...……**119**
III.4.2. Crosslinking of electrospun PVA/PEI NFs under GA vapours……..**120**
III.4.3. pH-controlled Decoration of water-stable PVA/PEI NFs with AuNPs……..**120**
III.4.4. Electrochemical Characterization of PVA/PEI NFs and PVA/PEI/AuNPs composite electrospun NFs…….……**122**
III.4.5. Analytical performance of the PVA/PEI/AuNPs/GOx glucose biosensor……..**125**
III.5. Conclusion……128

CHAPTER IV: PREPARATION AND CHARACTERIZATION OF CORE-SHELL POLYPYRROLE NANOFIBERS BY COMBINATION OF ELECTOSPINNING AND VAPOR-PHASE POLYMERIZATION FOR BIOSENSOR APPLICATIONS……129

IV.1. Introduction…….……131
IV.2. Materials and Methods…….……..135
IV.3. Experimental Section…….……138
IV.3.1. Preparation of the working electrodes…….……..……..**138**

IV.3.2. Preparation of electrospun solutions……..…..**138**
IV.3.2.1. Preparation of PAN suspension……...……**138**
IV.3.2.2. Preparation of PAN/FeTos suspensions……...…...**138**
IV.3.3. Electrospinning: Fabrication of electrospun PAN and PAN/FeTos NFs…..…...**138**
IV.3.4. Distillation of Pyrrole……..…...….**139**
IV.3.5. VPP process…..……...……**139**
IV.3.6. Immobilization of GOx on the surface of PPy coated PAN NFs with GA…….**140**
IV.3.7. Covalent immobilization of GOx onto the surface of PPy/P3C coated PAN NFs by using EDC/NHS chemistry……**141**
IV.3.8. Electrical Resistance measurements……..…….……**141**
IV.3.9. Electrochemical Characterizations……..……**142**
IV.3.9.1.PAN NFs, PAN/FeTos/PPy NFs and PAN/FeTos/PPy/PP3C NFs modified electrodes……..……**142**
IV.3.9.2. PAN/FeTos/PPy/GOx NFs and PAN/FeTos/PPy/PP3C/GOx NFs modified electrodes……..……**142**
IV.3.10. Characterization of NFs morphology…….……...**142**
IV.4. Results and discussion……**143**
IV.4.1. Elaboration of electrospun PAN NFs coated with PPy by VVP for glucose detection……..……..……**143**
IV.4.1.1. Effect of electrospinning parameters on the morphology of PAN electrospun NFs……..……**143**
IV.4.1.2. Morphological analysis of coated PAN NFs with PPy……**143**
IV.4.1.3. Electrochemical characterization of PAN/PPy electrospun NFs…….……**145**
IV.4.1.4. Electroanalytical characterization of PAN/PPy/GOx electrospun NFs…...**148**
IV.4.2. Elaboration of electrospun PAN NFs coated with PPy/PP3C by VVP for glucose detection…..……..**148**
IV.4.2.1. First approach: Fabrication of PAN/FeTos composite NFs…….**148**
IV.4.2.2. Second approach: Immersion of PAN NFs into FeTos solutions……**150**
IV.4.2.2.1. Effect of the FeTos concentration on the growth and morphology of PPy/PP3C coating onto core PAN NFs ……...……**150**
IV.4.2.2.2. Effect of Polymerization time on the ICP coating…….……**153**
IV.4.2.2.3. Electroconducting properties……**154**
IV.4.2.2.4. Electrochemical Characterization of PAN/PPy/PP3C core-shell electrospun NFs ……...……**155**
IV.4.2.2.5. Electroanalytical characterization of PAN/PPy/PP3C/GOx electrospun NFs ……..**158**
IV.4.2.2.6. Analytical performance of the glucose biosensor……..**160**
IV.5. Conclusion……**162**

GENERAL CONCLUSION AND PESPECTIVES……...……**165**

ABBREVIATIONS

A	**AACCVD**	Aerosol assisted catalytic chemical vapour deposition
	AC	Alternating current
	AFD	Average fiber diameter
	ATP	4-aminothiophenol
	AuNPs	Gold nanoparticles
B	**BSA**	Bovine serum albumin
C	**CDI**	Carbonyldiimidazole
	CE	Counter electrode
	CNFs	Carbon nanofibers
	CNTs	Carbon nanotubes
	CPE	Constant phase element
	CPs	Conducting polymers
	CV	Cyclic voltammetry
	CVs	Cyclic voltammograms
	CVD	Chemical vapour deposition
D	**DC**	Direct current
	DNA	Deoxyribonucleic acid
E	**EDC**	*N*-(3-Dimethylaminopropyl)-*N*′-ethylcarbodiimide hydrochloride
	EIS	Electrochemical Impedance Spectroscopy
	ELISA	Enzyme Linked Immune Sorbent Assay
	ES	Electrospinning
F	**FAD**	Flavin adenine dinucleotide
	FeTos	Ferric (III) p-toluenesulfonate
	FTIR	Fourier transform infrared spectroscopy
G	**GA**	Glutaraldehyde
	GCE	Glassy carbon electrode
	GOx	Glucose oxidase
H	**HM-PLLA**	High molecular weight poly-L-lactic acid
	HRP	Horseradish peroxidase
I	**ICPs**	Intrinsically conducting polymers
	ISEs	Ion selective electrodes
	ISFETs	Ion-selective field effect transistors
L	**LB**	Langmuir–Blodgett
	LBL	Layer-by-layer
	LOD	Limit of detection
	LSV	Linear scan voltammetry
M	**MIPs**	Molecularly imprinted polymers
	MNPs	Metallic nanoparticles
	MWCNTs	Multiwall carbon nanotubes
N	**NADH**	Nicotinamide adenine dinucleotide
	NFES	Near-field electrospinning
	NFs	Nanofibers
	NFM	Nanofibrous membrane
	NNFs	Nafion nanofibers
	NHS	N-hydroxysuccinimide
	NPs	Nanoparticles
	NW	Nanowire
P	**PAN**	Polyacrylonitrile

	PANI	Polyaniline
	PANCAA	Poly(acrylonitrile-co-acrylic acid)
	PBIBA	Poly-4-(4,7-di(thiophen-2-yl)-1H-benzo[d]imidazol-2-yl)benzaldehyde
	PBS	Phosphate buffer saline
	PCL	Poly (ε-caprolactone)
	P3C	Pyrrole-3-carboxylic acid
	PP3C	Poly(pyrrole-3-carboxylic acid
	PDDA	Poly(diallyldimethylammonium chloride
	PEDOT	Poly(3,4-ethylenedioxythiophene)
	PEI	Polyethyleneimine
	PEO	Poly(ethylene oxide)
	PGA	Polyglycolide
	PLA	Polylactide
	PPVs	Poly(p-phenylenevinylenes)
	PS	Polystyrene
	PThs	Polythiophenes
	PU	Polyurethane
	PVA	Poly(vinyl alcohol)
	PVA-SbQ	Polyvinyl alcohol with styrylpyridinium pendent group
	PVC	Poly(vinyl chloride)
	PVP	Poly(vinyl pyrrolidone)
	Py	Pyrrole
	PPy	Polypyrrole
R	**RE**	Reference electrode
	RNA	Ribonucleic acid
S	**SAMs**	Self-assembled monolayers
	SELEX	Systematic evolution of ligands by exponential enrichment
	SEM	Scanning electron microscopy
	SWCNTs	Single-wall carbon nanotubes
T	**TEM**	Transmission electron microscopy
U	**UV**	Ultaviolet
V	**VPP**	Vapour-phase polymerization
W	**WE**	Working electrode
X	**XRD**	X-ray diffraction analysis

LIST OF FIGURES

CHAPTER I

Figure 1. Multidisciplinary fields of biosensor applications……..**8**
Figure 2. The total biosensors market, showing the world revenue forecast for 2009-2016….**8**
Figure 3. The total biosensors market, showing the percent of revenues by vertical world markets for 2009 and 2016……..……**8**
Figure 4. Schematic representation of the general working principle of biosensors……..…**9**
Figure 5. Schematic representation of biosensors classification based on the biorecognition elemement and/or the transducer……..……**10**
Figure 6. Commonly used bioreceptors used for biosensors……...……**11**
Figure 7. Schematic representation of the active site of an enzyme……**12**
Figure 8. A plot of the reaction velocity (V_0) as a function of the substrate concentration [S] for an enzyme that obeys Michaelis-Menten kinetics shows that the maximal velocity (V_{max}) is approached asymptotically. The Michaelis constant (K_M) is the substrate concentration yielding a velocity of $V_{max}/2$……**13**
Figure 9. a) Effect of temperature on the enzyme activity: heat activation (Zone A), thermal denaturation (Zone B) and b) Effect of pH on enzyme activity……**14**
Figure 10. Schematic representation of working principle of amperometric glucose biosensor based on glucose oxidase……..**15**
Figure 11. General DNA biosensor scheme. Target DNA is captured at the recognition layer (A), and the resulting hybridization is transduced into a measurable electronic signal (B)….**17**
Figure 12. Representation of the working principle of an enzymatic amperometric /voltammetric biosensor……**18**
Figure 13. a) Potential sweep during cyclic voltammetric measurement; E_i is initial value, E_1 and E_2 are two limiting values. b) A typical cyclic voltammogram of a reversible reaction; anodic (a) and cathodic (c) processes, Ep is the potential at the current peak Ip……..…**19**
Figure 14. Nquist plot of EIS……...……**23**
Figure 15. Schematic Faradaic impedance spectra presented in the form of a Nyquist plot for: a) A modified electrode where the impedance is controlled by diffusion of the redox probe (low frequencies) and by the interfacial electron transfer (high frequencies). b) A modified electrode where the impedance is mainly controlled by diffusion of the redox probe. c) A modified electrode where the impedance is controlled by the interfacial electron transfer within the entire range of the applied frequencies. The arrow shows the direction of the frequency increase. Resistance of the electrolyte solution, Rs, and electron transfer resistance, Ret, are shown……...……**24**
Figure 16. Schematic Faradaic impedance spectra presented in the form of a Nyquist plot for: a) A modified electrode where the impedance is controlled by diffusion of the redox probe (low frequencies) and by the interfacial electron transfer (high frequencies). b) A modified electrode where the impedance is mainly controlled by diffusion of the redox probe. c) A modified electrode where the impedance is controlled by the interfacial electron transfer within the entire range of the applied frequen-cies. The arrow shows the direction of the frequency increase. Resistance of the electrolyte solution, Rs, and electron transfer resistance,Rct are shown……...……**25**

Figure 17. Schematic representation of basic methods of biomaterial immobilization on biosensors……..**27**
Figure 18. Interaction between glutaraldehyde and an amino group of a protein……..…..**30**
Figure 19. Common reaction sequences reported for covalent attachment of biomolecules to surfaces. CDI: carbonyldiimidazole, SMCC: succinimidyl 4-(N-maleimidomethyl)cyclohexane-1-carboxylate, EDC: 1-ethyl-3-(3-dimethylaminopropyl)carbodiimide, NHS: N-hydroxysuccinimide……..…**32**
Figure 20. Represenrative self-assembled monolayer of CnH2n+1 alkanethiol on the surface of gold electrode of a DNA sensor……**33**
Figure 21. Schematic representations of a SWCNT and a MWCNT……...…**35**
Figure 22. Assembly of SWCNT electrically contacted glucose oxidase electrode: linking the reconstituted enzyme, on the edge of the FAD-functionalized SWCNT, to the electrode surface……..….**38**
Figure 23. Solutions of gold nanoparticles of various sizes. Nano-Gold colloids exhibit different colours at different sizes and concentrations……..……**40**
Figure 24. Schemes of different GOx biosensors constructed by means of different tailored gold nanoparticle-modified electrode surfaces: (A) GOx/colloidal gold–cysteamine–AuE; (B) GOx/colloidal gold–cysteamine/cysteamine–AuE; (C) GOx/cysteamine–electrodeposited gold nanoparticles–GCE or GOx/3-mercaptopropionic acid (MPA)–electrodeposited gold nanoparticles–GCE……...……**42**
Figure 25. Representative applications of electrospun fibers……..……**48**
Figure 26. Comparison of the annual number of scientific publications with the keywords "electrospinning" and "sensor", as searched by Web of Science……..…**48**
Figure 27. Comparison of the annual number of scientific publications with the keyword "electrospinning" as searched by Web of Science……**51**
Figure 28. Number of patents for applications based on electrospinning in recent years as searched by Google patent……....…**51**
Figure 29. Schematic diagram of typical setups of electrospinning apparatus (a) vertical setup, (b) horizontal set up and c) SEM image of a typical mesh of randomly oriented electro spun nanofibers made of nylon 6,6.……..……**52**
Figure 30. Scheme of a electro-hydrodynamic model of jet elongation, including all the essential elements governing the final fiber diameter……...……**53**
Figure 31. Photograph of a jet of PEO solution during ES……..……**55**
Figure 32. Schematic diagram of advanced electrospinning setup……..……**56**
Figure 33. Different morphologies of electrospun polymer fibers: (a)uniaxially aligned, (b) biaxially oriented, (c) ribbon, (d) porousfibers, (e)Necklace-like, (f) nanowebs, (g) hollow, (h) nanowire-in-microtube,and (i) multichannel tubular……**57**
Figure 34. Schematic representation of parameters that affect the electrospinning process…**58**
Figure 35. A droplet of a 5% solution of poly(ethylene oxide) (PEO) in water, dyed with fluorescein: A) in the absence of an applied voltage and B) at an applied voltage of 20kV, with a let perpendicular to the counter electrode…….……**61**
Figure 36. Collagen structure……...……**64**
Figure 37. Electrospun polymer NFs doped with CNTs: (a) PAN – MWNT, (b) silk fi broin – MWCNT, (c) SWNT bundle (white arrow) embedded in the PS NFs, (d) mesoporous carbon

NF – MWCNT, (e) PAN-g-PDMS –MWCNT, (f) PVP – MWCNT, (g) PEO – MWCNT hybrid NFs with 0.5% MWCNT, (h) PEO – MWCNT hybrid NFs with 3% MWCNT, and (i) PU –MWCNT……..……..67
Figure 38. Electrospun polymer NFs doped with different MNPs: (a) PVA–AuNP, (b) PAN–AgNP, (c) PANi–PtNP; (d) CNF–PdNP, (e) CF–NiNP, (f) CNR–CoNP, (g) ZnO–CuNP, (h) Rh-doped ZrO2 NFs, (i) CNF–$Pd_{30}Ni_{70}$……..……..72
Figure 39. Chemical formulas of the main classes of conductive polymers……78

CHAPTER II
Figure 40. PVA-SbQ entrapment of enzymes……..……88
Figure 41. Photograph of working area, prepresanting the Voltalab 80 PGZ 402 analyzer, the electrochemical cell equipped with a conventional three electrode configuration and the computer used during the electrochemical experiments……...……90
Figure 42. Schematic represantation of the electrochemical cell used throughout the electrochemical experiments, equipped with a conventional three electrode configuration…91
Figure 43. Photograph of the home made electrospinning device used at this work……...…92
Figure 44. Chemical formula of D-glucose……..……92
Figure 45. 3-D structure of GOx……..93
Figure 46. Chemical formula of PVA……..……94
Figure 47. Mechanism of photo-cross-linking of PVA-SbQ……...……94
Figure 48. TEM images of the above synthesized carboxylated multi-walled carbon nanotubes……..……95
Figure 49. To the left: PVA-SbQ solution (6.7 wt%) after stirring for 2h. To the right: PVA-SbQ/MWCNT-COOH mixture containing 5wt% MWCNT-COOH with respect to the polymer mass after 3h of stirring and 2h in ultasonication bath……...……96
Figure 50. Representative SEM images of a) pure PVA-SbQ, b) PVA-SbQ/1MWCNT-COOH, c) PVA-SbQ/5MWCNT-COOH, d)PVA-SbQ/10MWCNT-COOH under optimum conditions and fiber diameter distribution histograms of the above electrospun fibers…..…101
Figure 51. Representative TEM images of a) pure PVA-SbQ, b) PVA-SbQ/1MWCNT-COOH, c) PVA-SbQ/5MWCNT-COOH and d) PVA-SbQ/10MWCNT-COOH under optimum conditions……..……101
Figure 52. Representative SEM images of crosslinked PVA-SbQ/5MWCNT fibers before and after exposure to UV light for 10 min, and after immersion in phosphate buffer solution (0.1M, pH 7.2) for 3h……..……102
Figure 53. Cyclic voltammograms of modified gold electrodes by different electrospun nanofibrous mats (in $[Fe(CN)_6]^{3-/4-}$ aqueous solution, pH 7.2, scan rate 100mV s^{-1})……104
Figure 54. Nyquist plots of impedance spectra obtained at a frequency range between 100 mHz to 100 kHz, at -300 mV, upon increasing concentration of MWCNTs-COOH in the electrospun PVA-SbQ nanofibers. The EIS were recorded in the presence of a 10mM $[Fe(CN)_6]^{3-/4-}$ aqueous solution……...……105
Figure 55. The Randles-Ehrshler model. R_s represents the ohmic resistance of the electrolyte solution, R_{ct} the charge transfer resistance, Z_w the Warburg impedance and CPE the constant phase element……..……105

Figure 56. Influence of glucose concentration on the PVA-SbQ/5MWCNTs-COOH/GOx NFs biosensor response. Cyclic voltammograms recorded in PBS 0.1M, pH 7.2, at a scan rate of 50mV s^{-1}, 10 min after glucose injection**……107**
Figure 57. Calibration curve of the PVA-SbQ/5MWCNT-COOH/GOx NFs biosensor (in PBS 0.1M, pH 7.2). Error bars represent standard deviations obtained from three successive measurements**……..……107**

CHAPTER III
Figure 58. Schematic representation of the working principle of the fabricated biosensor**...112**
Figure 59. Chemical formula of branched PEI used in this work**……..……113**
Figure 60. Chemical formula of 4-aminothiophenol**……..…113**
Figure 61. Chemical formula of glutaraldehyde**……..……..114**
Figure 62. Synthesis of citrate AuNPs according to Turkevich Method**……...……114**
Figure 63. Representative SEM images of electrospun PVA/PEI NFs formed by using a) an applied voltage of 13kV and b) an applied voltage was 25kV. The other electrospinning parameters were set as follows: polymer concentration of 12wt%, flow rate of 0.2mL/h and collection distance of 12cm**……...……..118**
Figure 64. Representative SEM images of electrospun PVA/PEI NFs formed by using a) collection distance of 12cm and b) collection distance of 23cm. The other electrospinning parameters were set as follows: polymer concentration of 12wt%, flow rate of 0.2mL/h and applied voltage of 25kV**……..……118**
Figure 65. Representative SEM images of electrospun PVA/PEI NFs formed by using a) flow rate of 0.2 mL/h and b) flow rate of .0.6 mL/h. The other electrospinning parameters were set as follows: polymer concentration of 12wt%, collection distance of 12cm and applied voltage of 25kV**……...……119**
Figure 66. Representative SEM images of water-stable electrospun PVA/PEI NFs a) after exposure to GA vapors for 30min, b) after immersion in PBS (0.1M, pH 5.0) for 5h and c) after immersion in PBS (0.1M, pH 5.5) for 4 days**……..…120**
Figure 67. a) Representative SEM image of water-stable electrospun PVA/PEI NFs before immersion in the AuNPs solution. b,c,d) Representative SEM images of decorated with citrate AuNPs water-stable electrospun PVA/PEI NFs. Assembly of AuNPs on the NFs after immersion in colloidal solutions with various pH values of b) 7.0, c) 6.0 and d) 5.0**……121**
Figure 68. Cyclic voltammograms of gold modified electrodes by ATP SAMs, ATP SAMs/PVA/PEI water-stable electrospun NFs and ATP SAMs/PVA/PEI/AuNPs water-stable electrospun NFs (in $[Fe(CN)_6]^{3-/4-}$ PBS solution, pH 5.0, scan rate 100mV/s**……...……123**
Figure 69. Nquist plot of impedance spectra obtained for ATP/PVA/PEI water-stable electrospun NFs before immersion in the Au NPs solution. The EIS measurements were performed at -300 mV in the presence of a 10mM $[Fe(CN)_6]^{3-/4-}$ PBS solution by varying frequency in the 100 mHz to 100 kHz range**……..……124**
Figure 70. Nquist plots of impedance spectra obtained for bare gold electrode and for gold electrodes modified with ATP-SAMs and ATP/PVA/PEI/AuNPs water-stable electrospun NFs after immersion in the Au NPs solution pH 5.0. The EIS measurements were performed at -300 mV in the presence of a 10mM $[Fe(CN)_6]^{3-/4-}$ PBS solution by varying frequency in the 100 mHz to 100 kHz range**……...……124**

Figure 71. Nquist plots of impedance spectra obtained for gold electrodes modified with ATP/PVA/PEI/AuNPs/GOx water-stable electrospun NFs upon the increasing concentration of glucose. The EIS measurements were performed at -300 mV in the presence of PBS solution (0.1M, pH 5.0), by varying frequency in the 100 mHz to 100 kHz range**……126**
Figure 72. Calibration curve of the ATP/PVA/PEI/AuNPs/GOx NFs biosensor (in PBS 0.1M, pH 5.0). Error bars represent standard deviations obtained from three successive measurements**……..……127**

CHAPTER IV
Figure 73. Chemical formula of PAN used in this work**……135**
Figure 74. Chemical formula of FeTos used in this work**……..……136**
Figure 75. One-step EDC reaction with carboxyl and amine-containing molecules**…..……136**
Figure 76. Reactions involving EDC, including activation as an NHS ester**…….……137**
Figure 77. Chemical structure of Pyrrole**……..……137**
Figure 78. Chemical structure of P3C used in this work**……...……138**
Figure 79. Distillation setup used for pyrrole**……139**
Figure 80. Two-step, vapor-phase polymerization ICP coating process**……140**
Figure 81. Schematic representation of gold electrodes used for the resistivity measurements**……..141**
Figure 82. To the left: Representative SEM images of electrospun PAN NFs formed by using an applied voltage of 22kV, a polymer concentration of 12wt%, flow rate of 1mL/h and collection distance of 15cm. To the right: TEM images of electrospun PAN NFs fabricated under the above conditions**……..…143**
Figure 83. Different steps of PAN NFs PPy coating during the VPP procedure. a) Uncoated PAN fibers, b) placement of blue mask onto the NFs in order to accurately define the shape and size (height and width) of the conductive area to ensure reproducible resistivity measuremts of the NFs, c)PAN NFs coated with the oxidant after immersion in 20 wt% FeTos solution, d) FeTos coated PAN NFs after annealing at 70°C, d) PPy coated PAN NFs after 15min polymerization time at RT, PPy coated PAN NFs after the removal of protective blue mask**……144**
Figure 84. Representative SEM images of conductive PAN NFs coated with PPy, after exposure to Pyrrole vapos for 15min in ambient conditions**……..……145**
Figure 85. Cyclic voltammograms of gold modified electrodes with PAN NFs and PAN/PPy electrospun NFs by using FeTos solutions of 12, 20 and 40wt% (in $[Fe(CN)_6]^{3-/4-}$ aqueous solution, pH 7.2, scan rate 100mV s^{-1})**……...……146**
Figure 86. Nquist plots of impedance spectra obtained for gold electrodes modified with **PAN/PPy** electrospun NFs by using FeTos solutions of 12, 20 and 40wt%. The EIS measurements were performed at -300 mV in the presence of a 10mM $[Fe(CN)_6]^{3-/4-}$ PBS solution by varying frequency in the 100 mHz to 100 kHz range**…….……147**
Figure 87. Representative SEM images of PAN NFs covered with PPy/PP3C coatings after VPP process and before the cleaning step. The PAN NFs mats were immersed in a) FeTos 12wt%, b) 20wt% and c) 40wt%, respectively**……...……151**

Figure 88. Representative SEM images of PAN NFs covered with PPy/PP3C immersed in a) FeTos 12wt%, b) 20wt% and c) 40wt%, respectively, after ultrasonication for 1min and rinsing with H_2O/MeOH**……..……152**
Figure 89. Representative SEM images of a) uncoated PAN fibers and b) PPy/PP3C coated PAN NFs after rinsing with H_2O/MeOH (polymerization time: 30min, FeTos concentration: 20wt%, PPy/PP3C ratio: 1:2**…….…..153**
Figure 90. Cyclic voltammograms of gold modified electrodes with PAN NFs and PAN/FeTos/PPy/PP3C electrospun NFs by using FeTos concentrations of 12, 20 and 40wt%. The CVs were performed in a 10mM $[Fe(CN)_6]^{3-/4-}$ PBS solution, pH 7.2, at a scan rate of 100mV/s**……..156**
Figure 91. Nquist plots of impedance spectra obtained for gold electrodes modified with PAN NFs by using. The EIS measurements were performed at -300 mV in the presence of a 10mM $[Fe(CN)_6]^{3-/4-}$ PBS solution by varying frequency in the 100 mHz to 100 kHz range**…...…157**
Figure 92. Nquist plots of impedance spectra obtained for gold electrodes modified with PAN/FeTos/PPy/PP3C NFs by using FeTos concentrations of 12, 20 and 40wt%. The EIS measurements were performed at -300 mV in the presence of a 10mM $[Fe(CN)_6]^{3-/4-}$ PBS solution by varying frequency in the 100 mHz to 100 kHz range**……..…157**
Figure 93. Nquist plots of impedance spectra obtained for gold electrodes modified with PAN/FeTos 20wt%/PPy0.05M/PP3C0.1M/GOx electrospun NFs upon the increasing concentration of glucose**…….……159**
Figure 94. Calibration curve of the PAN/FeTos 20wt%/PPy/PP3C/GOx NFs biosensor (in PBS 0.1M, pH 7.2). Error bars represent standard deviations obtained from three successive measurements**……..……160**

LIST OF TABLES

CHAPTER I

Table 1. Advantages and drawbacks of the five basic immobilization methods……..……**28**

Table 2. Different functions of AuNPs in biosensor systems……..……**44**

Table 3a. Comparison of processing techniques for obtaining nanofibers……..…**46**

Table 3b. Advantages and disadvantages of various processing techniques……...……**46**

CHAPTER II

Table 4. Relevant electrochemical enzymatic biosensors based on electrospun polymer nanofibers……..……**89**

Table 5. Optimal electrospinning process parameters for the different MWCNT loadings. 6.7 wt % PVA-SbQ concentration, needle i.d.: 0.644 mm……..……**99**

Table 6. R_{CT} values of PVA-SbQ nanofibrous mats containing 0, 1, 5 and 10% of MWCNTs-COOH respectively……..……**104**

Table 7. Comparison of Amperometric Glucose Biosensors in the Literature……..……**108**

CHAPTER III

Table 8. Fitting parameters obtained from Nquist plots of impedance spectra by using the equivalent Randles-Ehrshler circuit presented in figure 55……**125**

Table 9. Fitting parameters obtained from Nquist plots of impedance spectra by using the equivalent Randles-Ehrshler circuit presented in figure 55 upon the addition of increasing glucose concentration……..……**126**

CHAPTER IV

Table 10. Different approaches employed for the elaboration of impedimetric glucose biosensors, based on the fabrication of conductive NFs through the combination of ES and VPP process……...……**135**

Table 11. Fitting parameters obtained from Nquist plots of impedance spectra by using the equivalent Randles-Ehrshler circuit presented in figure 55……**147**

Table 12. Influence of FeTos solution concentration and polymerization time on AFD of NFs prepared by VPP of Py/P3C (1:2 w/w)……..……..……**154**

Table 13. Results of fitting the Nyquist plots of impedance spectra recorded for gold electrodes modified by PAN NFs and PAN/PPy/PP3C with the equivalent Randles-Ehrshler circuit (figure 55) ……..……..…… **158**

Table 14. Fitting parameters (Randles-Ehrshler model) obtained from Nyquist plots of impedance spectra recorded at increasing glucose concentration for the PAN/PPy/PP3C/GOx NFs biosensor……..……**160**

Table 15. Limit of detection calculated for six electrodes coming from two different batches of VPP process……**161**

GENERAL CONCLUSION AND PESPECTIVES

Table 16. Analytical performances of the developed biosensors……..……..**166**

INTRODUCTION

GENERAL INTRODUCTION

Biosensors are rapid, selective and cost-effective analytical devices exhibiting a wide range of applications in various fields such as health, environment and food. They combine a biologically active element, which selectively recognizes one analyte or a group of analytes, and a physicochemical transducer to deliver complex bioanalytical measurements with simple and easy-to-use formats. Electrochemical biosensors are of particular interest, since they support fast, accurate and inexpensive analytical methods and they offer several distinct advantages such as being easily embedded and integrated into electronics, whilst satisfying the required power demands of decentralized testing, thus indicating great promise for biomedical applications among many others.

Huge efforts have been focused on the miniaturization of electrochemical transducers, resulting in a significant reduction of the amount of the biological entity necessary for the realization of the biosensor, as well as to their easier integration in lab-on-a-chip devices. Despite the benefits associated with reducing the size of the electrodes, the sensitivity of the biosensor will decrease as the specific surface of the electrode, and thus the available immobilization sites for the biorecognition element, decreases. However, this issue can be successfully overcome by efficiently nanoengineering the electrodes' surface through the use of flexible nanostructures.

The design of novel sensing systems integrating nanoscale materials is a rising interdisciplinary topic harnessing the high specific surface area of these materials and their unique electronic, optical, mechanical and catalytic properties. A wide range of nanoscale materials such as nanoparticles, nanotubes of diferent sizes, shapes and compositions have been proved to be very efficient to enhance biosensors performances.

Electrospun fibers in particular, meet many of the requirements to achieve improved performances as a biosensor material since they are featured with very small diameters (ranging from several nm up to some μm), long length, large surface area per unit mass, high surface-to-volume ratio and tunable pore size. Electrospun nanofibers (NFs) have been successfully used in various fields of applications including tissue engineering, textiles, energy storage, catalysis etc but the employment of electrospun nanofibers as immobilization matrices for biosensor elaboration is not yet a very widespread approach. However, the interest in electrospinning technique to fabricate functional nanofibers for biosensing is growing fast due to its many merits such as the simplicity and low cost requirements of the processing system, design flexibility and dimensional stability of the electrospun NFs, easy scaling, high reusability and its versatility. A few research groups have reported the enhanced sensitivity of biosensors based on electrospun nanofibers, when compared to conventional biosensors.

In the present work, we investigated and compared different approaches for the nanoengineering of gold electrodes surface with conductive electrospun nanofibers for the development of enzymatic electrochemical biosensors.

The present manuscript is organized in four chapters. The first chapter is dedicated to a bibliographic review of biosensors and specifically electrochemical biosensors, nanomaterials and their use for biosensors elaboration, electrospinning technique, conducting polymeric nanostructures and their integration into biosensing systems.

The work detailed within chapters II, III and IV describes the development of three pioneering and new electroactive platforms based on electrospun nanofibrous hybrid materials for further application to electrochemical biosensors elaboration, respectively. Glucose oxidase was used as a model enzyme to validate the performance of the developed biosensors and gold electrodes were used as transducers. The first electrobioactive platform to be described involves the easy and rapid one-step fabrication of water-stable electrospun polyvinyl alcohol NFs with styrylpyridinium pendent group (PVA-SbQ) containing carboxylated multiwall carbon nanotubes (MWCNTs-COOH) and glucose oxidase (GOx) for glucose detection. The second electrobioactive surface design to be described involves the modification of gold electrode surfaces with one-step water-stable electrospun polyvinyl alcohol/polyethyleneimine (PVA/PEI) NFs which incorporate glucose oxidase as before and whose surface is uniformly decorated with pH-tunable densities of citrate gold nanoparticles. The third developed electrobioactive platform for biosensing to be described involves the exploitation of conducting core-shell polyacrylonitrile (PAN)/polypyrrole(PPy)/poly(pyrrole-3-carboxylic acid)(PP3C) NFs produced by combination of electrospinning and vapour-phase polymerization method. The carboxylic acid groups expressed on the surface of the PAN/PPy/PP3C nanofibers were used for the covalent immobilization with the amino groups of glucose oxidase (GOx).

A summary of the most significant results will be presented in the conclusion section, where we will try to highlight the advantages and disadvantages of the different approaches employed for the development of biosensors, and to illustrate their possible contribution to the development of new generation biosensing systems with enhanced performance. The present manuscript ends with a brief discussion on the perspectives of the presented work.

CHAPTER I: BIBLIOGRAPHIC STUDY

I.1. Generalities on Biosensors

Bioanalysis is a part of the analytical field essentially based on two broad categories of instrumentation: (a) sophisticated, high-throughput laboratory equipment capable of rapid, accurate and convenient measurement of complex biological interactions and components; (b) biosensors: easy-to-use, portable devices for use by non-specialists for decentralized, in situ or home analysis. The former are expensive and the latter are mass produced and inexpensive.[1]

The basic concept of the biosensor was first stated by Leyland C. Clark in 1962[2], in his seminal description of an ‘‘enzyme electrode’’. Building on his earlier invention of the Clark oxygen electrode, he reasoned that electrochemical detection of oxygen or hydrogen peroxide could be used as the basis for a broad range of bioanalytical instruments, by the incorporation of appropriate immobilized enzymes. The classic example was immobilized glucose oxidase (GOx), which converted a simple platinum electrode into a powerful analytical instrument for the detection of glucose in human samples from people suffering from diabetes. Two decades later, optical transducers were harnessed in conjunction with antibodies to create real-time bioaffinity monitors. These immunosensors laid the foundation for the second major evolutionary line of biosensing instrumentation.

Growth in the field of biosensors has been phenomenal. When the principal journal in the field, Biosensors and Bioelectronics was launched in 1985 by Elsevier, it published about thirty biosensor papers that year out of a total published in the world of approximately one hundred.

Biosensors combine multiple disciplines (figure 1) and they find application in medicine, pharmaceutical, food and process control, environmental monitoring, defence and security, but most of the market of over US$13 billion (figure 2) is driven by medical diagnostics and, in particular, electrochemical glucose biosensors[3] for people with diabetes. The most significant trend likely to impact on biosensors is the emergence of personalized medicine.

The chart presented in figure 3 shows that the percent of revenues from the mentioned markets have grown from 2006 through 2009 and the forecasts up to 2016 suggest that this growth trend will continue.

Hence, such electrochemical devices have come to dominate distributed diagnostics, by providing a simple, inexpensive and yet accurate and sensitive platform for patient diagnosis, whereas optical techniques have found their niche principally in R&D. To complete the picture concerning transduction strategies, advances in acoustic resonance devices are certainly worthy of note, but both thermometric and magnetic transduction have failed to have any serious practical impact to date.[2]

---

[1] A.P.F. Turner, “Biosensors: Sense and Sensibility,” *Chemical Society Reviews* 42, no. 8 (**2013**): 3184.

[2] L.C. Clark and C. Lyons, “Electrode Systems for Continuous Monitoring in Cardiovascular Surgery,” *Annals of the New York Academy of Sciences* 102, no. 1 (**1962**): 29–45.

[3] J.D. Newman and A.P.F. Turner, “Home Blood Glucose Biosensors: A Commercial Perspective,” *Biosensors and Bioelectronics* 20, no. 12 (**2005**): 2435–53.

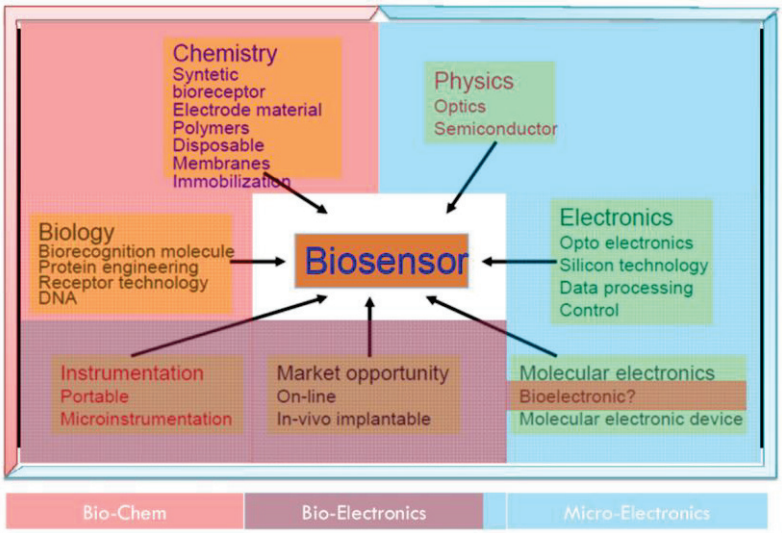

Figure 1. Multidisciplinary fields of biosensor applications.

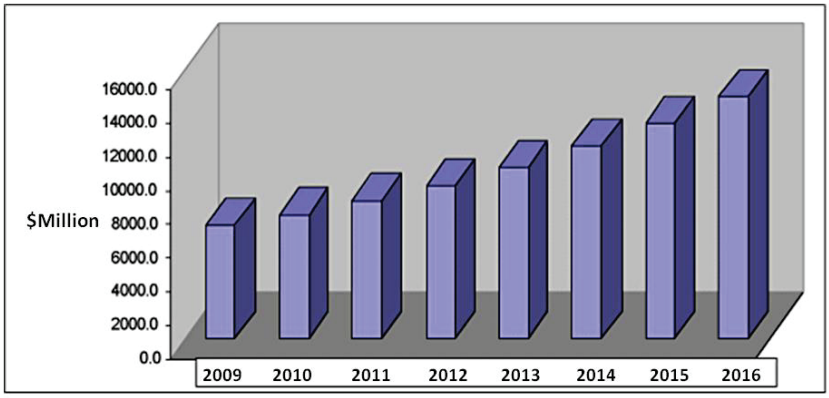

Figure 2. The total biosensors market, showing the world revenue forecast for 2009-2016. http://ww2.frost.com/Frost and Sullivan

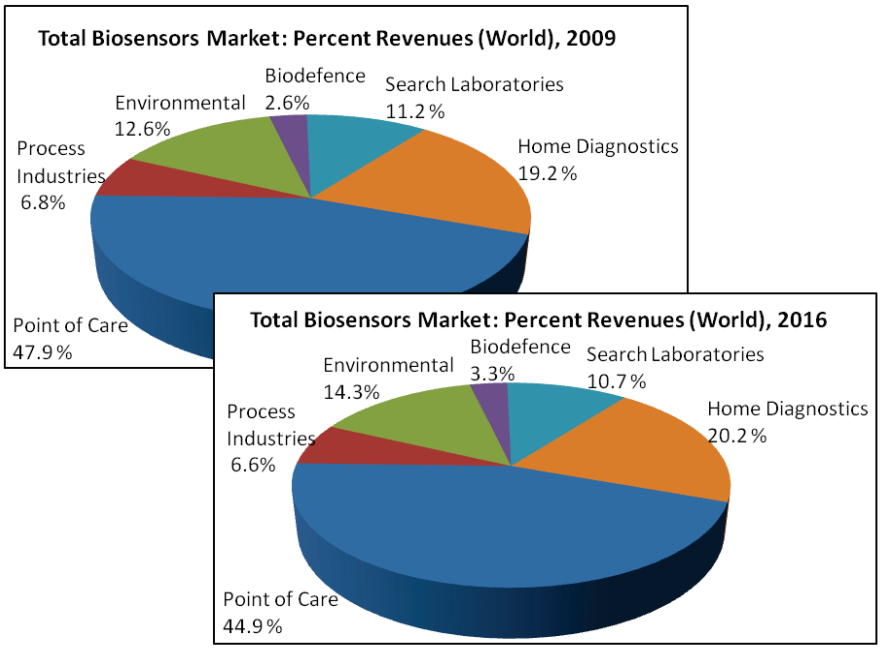

Figure 3. The total biosensors market, showing the percent of revenues by vertical world markets for 2009 and 2016. http://ww2.frost.com/

I.1.1. Definition and General Working Principle of Biosensors

The most widely accepted definition of a biosensor is: "an analytical device which incorporates a biologically active element with an appropriate physical transducer to generate a measurable signal proportional to the concentration of chemical species in any type of sample".[4] Any biosensor consists of the following three basic components: a) a biorecognition element, which is a bioselective membrane involving various biological structures, b) a physical transducer and c) an electronic system for signal amplification and recording and representing the data. The working principle of biosensors is presented in figure 4. A biorecognition element is the basic component of any biosensor. It is due to its recognition element that a sensor can selectively respond to one or several analytes among a large number of other interfering molecules. All types of biological structures (enzymes, antibodies, receptors, nucleic acids, micro-organisms, biological tissues, and even living cells) are used as a recognition element in biosensors. A transducer converts the biological response to a detectable signal, which can be measured electrochemically, optically, acoustically, mechanically, calorimetrically, or electronically, and then correlated with the analyte concentration.

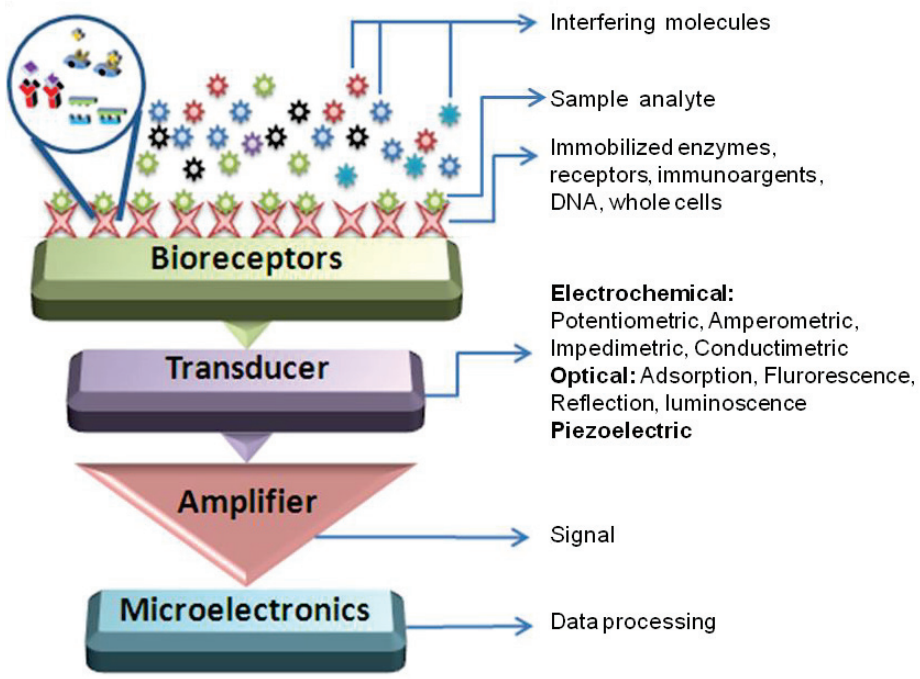

Figure 4. Schematic representation of the general working principle of biosensors.

[4] R.Monošík, M. Streďanský and E. Šturdík, "Biosensors - Classification, Characterization and New Trends," *Acta Chimica Slovaca*, 5, no. 1 (**2012**): 109-120.

I.1.2. Classification of Biosensors

Biosensors can be classified either according to the nature of their biorecognition element or according to the type of signal transduction they employ or, alternatively to a combination of the two.[5] A schematic representation of biosensors classification is illustrated in figure 5:

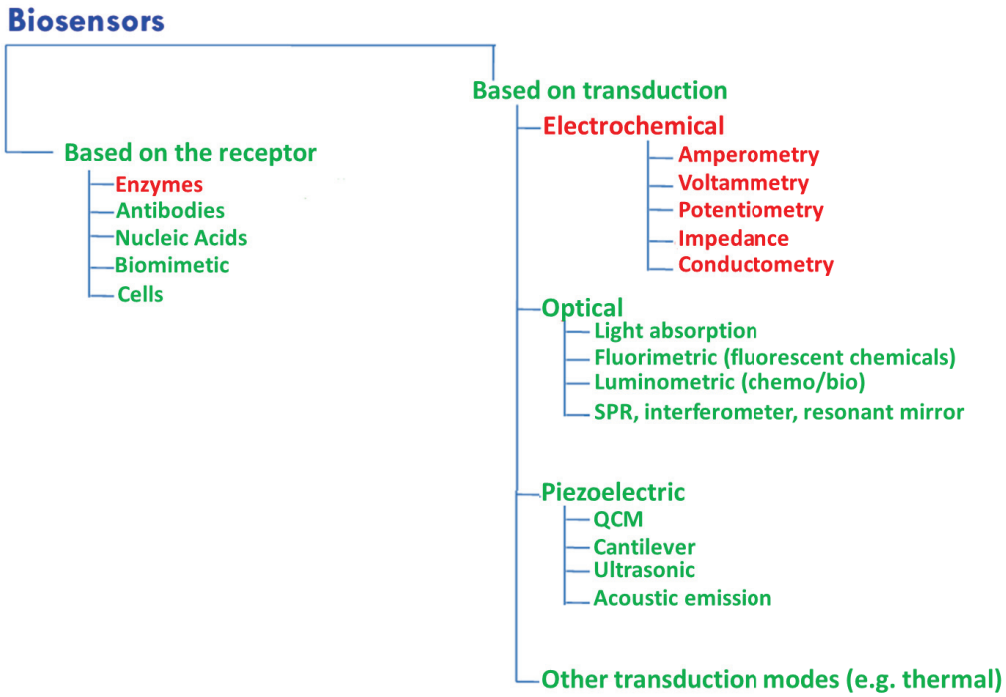

Figure 5. Schematic representation of biosensors classification based on the biorecognition element and/or the transducer.

I.1.2.1. Classification based on the Biorecognition Element

The different bioreceptors that have been used are as numerous as the different analytes that have been monitored using biosensors (**figure 6**). However, bioreceptors can generally be classified into five different major categories. These categories include: 1) enzymes, 2) antibodies, 3) nucleic acids/DNA, 4) cellular structures/cells and 5) biomimetic materials.[4] In the following paragraphs we will more particularly focus on enzyme-based electrochemical biosensors since enzyme electrodes are one of the most common biosensors reported in the literature and have been the topic of our concern in this work. The other categories will be briefly discussed.

[5] D.R. Thévenot et al., "Electrochemical Biosensors: Recommended Definitions and Classification," *Biosensors and Bioelectronics* 16, no. 1 (**2001**): 121–31.

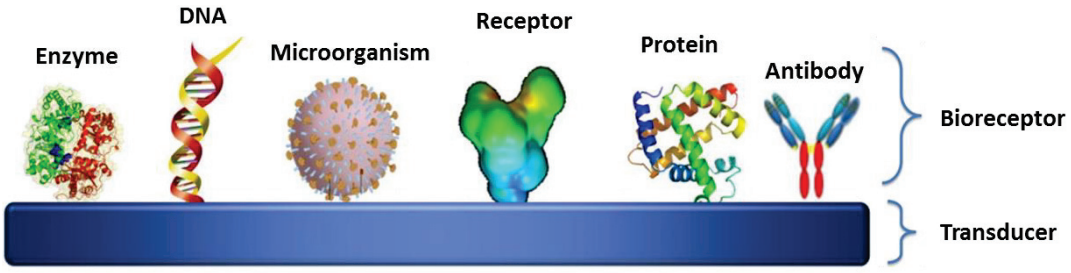

Figure 6. Commonly used bioreceptors used for biosensors.

Enzymatic Biosensors

Enzymes are biological molecules that act as catalysts in specific biochemical reactions. The enzymatic biosensors utilize enzymes which are often chosen as bioreceptors based on their specific binding capabilities as well as their catalytic activity. With the exception of a small group of catalytic ribonucleic acid molecules, all enzymes are proteins. Some enzymes require no chemical groups other than their amino acid residues for activity. Others require an additional chemical component called a cofactor, which may be either one or more inorganic ions, such as Fe^{2+}, Mg^{2+}, Mn^{2+}, or Zn^{2+}, or a more complex organic or metalloorganic molecule called a coenzyme. The catalytic activity of enzymes depends upon the integrity of their native protein conformation. For example, GOx has the FAD cofactor bound to the enzyme in the oxidized form (FAD) or reduced ($FADH_2$).

If an enzyme is denatured, dissociated into its subunits, or broken down into its component amino acids, its catalytic activity is destroyed. In enzymatic reactions, the molecules at the origin of the process, called substrates, are converted into different molecules, called products. In enzymatic electrochemical biosensors, the design is used when the substrate or the product of the enzymatic reaction is electrochemically active, capable of being rapidly and reversibly oxidized or reduced on an electrode upon the application of an appropriate potential. According to their functions, enzymatic sensors are subdivided into substrate and inhibitor ones. Substrate biosensors are used for the determination of specific substrates of enzymatic reactions. The most common biosensors of that type are glucose and urea biosensors,[6,7] which use glucose oxidase and urease as enzymes. Inhibitor sensors are used for the determination of substances reducing the activity of an enzyme.[8] Varieties of enzymes are used for biosensor construction, for example oxidoreductase enzymes are used for lactate, malate, and ascorbate. Extensive review of commercially available biosensors for glucose, cholesterol, lactate, triglycerides and creatinine determination can be found in the review by Monošík et al.[4]

[6] J. Wang, "Electrochemical Glucose Biosensors," *Chemical Reviews* 108, no. 2 (**2008**): 814–25.

[7] C.R. Ispas, G. Grivat and S. Andreescu, "Review: Recent developments in enzyme based biosensors for biomedical analysis," *Analytical Letters* 45, (**2012**): 168–86.

[8] E. Korotkaya, "Biosensors: Design, Classification, and Applications in the Food Industry," *Foods and Raw Materials* 2, no. 2 (**2014**): 161–71.

Active Sites and Enzyme Kinetics

A substrate binds only to a certain region of the enzyme, called the active site, where the catalytic reaction takes place. The active site is a 3D-groove or pocket formed by folding pattern of the protein, lined with amino acid residues.[9] This three-dimensional structure, together with the chemical and electrical properties of the amino acids and cofactors within the active site, permits only a particular substrate to bind to the site, thus determining the specificity of the catalytic reaction. Once the substrate binds to the active site, it is chemically converted to products through a series of steps known as enzymatic mechanism. To understand how enzymes function, we need a kinetic description of their activity. In biochemistry, Michaelis–Menten kinetics is one of the best-known models of enzyme kinetics.[9]

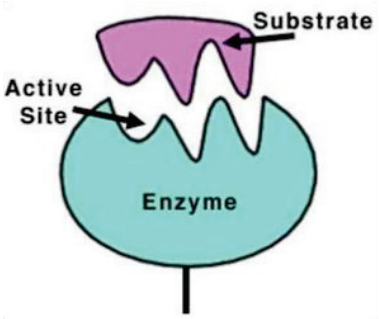

Figure 7. Schematic representation of the active site of an enzyme.

In 1913, Leonor Michaelis and Maud Menten proposed a simple mathematical model for the description of the enzyme kinetics. The model takes the form of an equation describing the rate of enzymatic reactions, by relating reaction rate v to [S], the concentration of a substrate *S*. It involves an enzyme E binding to a substrate S to form a complex ES, which in turn is converted into a product P and the enzyme. This may be represented schematically as:

$$\mathrm{E} + \mathrm{S} \underset{k_{-1}}{\overset{k_1}{\rightleftharpoons}} \mathrm{ES} \xrightarrow{k_2} \mathrm{E} + \mathrm{P}$$

where k_1, k_{-1} and k_2 denote the rate constants for ES formation, the dissociation of ES back to E and S and dissociation of ES to E and P respectively, and the double arrows between S and ES represent the fact that enzyme-substrate binding is a reversible process. Under certain assumptions – such as the enzyme concentration being much less than the substrate concentration – the rate of product formation is given by[10]:

$$v = \frac{d[P]}{dt} = V_{max}\frac{[S]}{K_M + [S]} = k_2[E]_0\frac{[S]}{K_M + [S]}$$

[9] J.M. Berg, J.L. Tymoczko, and L. Stryer, *Biochemistry*, 5th edition, vol. Section 8.4, The Michaelis-Menten Model Accounts for the Kinetic Properties of Many Enzymes. (New York: W H Freeman; **2002**).

where V_{max} represents the maximum rate achieved by the system, at maximum (saturating) substrate concentrations and K_M the Michaelis constant: $V_M = k_2[E]_0$ and $K_M = \frac{k_{-1}+k_2}{k1}$

The reaction rate increases with increasing substrate concentration [S], asymptotically approaching its maximum rate V_{max}, attained when all enzyme is bound to substrate. It also follows that $V_{max}=k_2[E]_0$, where $[E]_0$ is the enzyme concentration, k_2, the turnover number, is the maximum number of substrate molecules converted to product per enzyme molecule per second. The Michaelis constant, K_M, is the substrate concentration at which the reaction rate is at half-maximum, and is an inverse measure of the substrate's affinity for the enzyme—as a small K_M indicates high affinity, meaning that the rate will approach V_{max} more quickly. The value of K_M depends on both the enzyme and the substrate concentration, as well as conditions such as temperature and pH.[9]

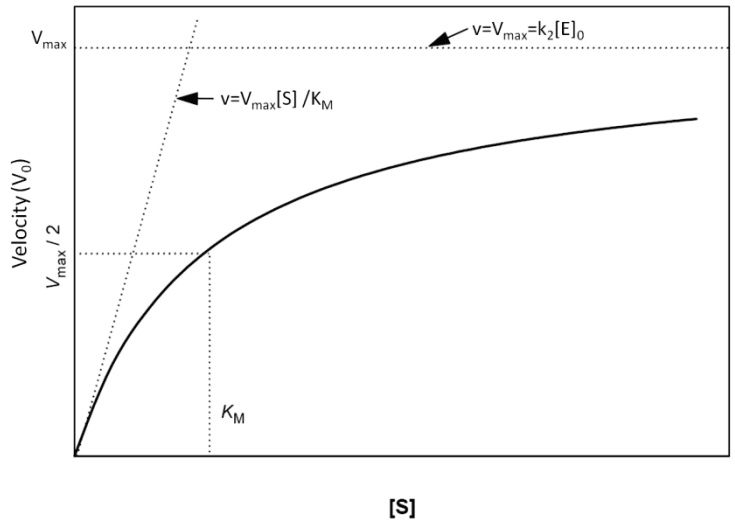

Figure 8. A plot of the reaction velocity (V_0) as a function of the substrate concentration [S] for an enzyme that obeys Michaelis-Menten kinetics shows that the maximal velocity (V_{max}) is approached asymptotically. The Michaelis constant (K_M) is the substrate concentration yielding a velocity of $V_{max}/2$. Extracted from Ref 9.

Parameters Affecting the Rate of an Enzymatic Reaction

Temperature

The rate of chemical reactions generally increases with temperature because the kinetic energy of the molecules is increased, which leads to a higher number of effective collisions resulting to reaction products. However, since enzymes have a tertiary structure which is highly ordered, complex and suitable for the stereospecific binding of the substrate, the elevation of temperature can destroy their structure leading to loss of enzyme activity.[9] The variation of the enzymatic activity in function of the temperature is determined by measuring the changes of the reaction rate as a function of the temperature of the medium (figure 9a). The rate of an enzyme-catalyzed reaction usually increases with increasing temperature up to an optimum point and then it decreases because enzymes are thermosensitive. This optimal temperature allows to obtain a constant speed during the whole duration of the experiment. As

the temperature continues to increase there is a critical point beyond which denaturation of the enzyme occurs. The thermal denaturation of an enzyme also depends on other parameters such as pH, ionic strength and the presence of ligands. Substrate binding generally protects the enzyme. In general, it is advisable to work about 10°C below the denaturation threshold.[9]

pH

Most enzymes are active in a limited pH range. This can be attributed to the stability of the enzyme protein in a certain pH range. The optimum pH is a function of the active site and the affinity of the enzyme for its substrate. Changes in pH can alter the ionization state of the substrate, the ionization state of the catalytic site of the enzyme or the ionization state of a certain number of protein molecules at the active site of the enzyme, so that the conformation and the catalytic activity of the enzyme change. A change in the pH can alter the rates of enzyme-catalyzed reactions, with many enzymes exhibiting a bell-shaped curve when enzyme activity is plotted against pH (figure 9b). The different groups that are present in the active site and can be affected by a change in the pH are: carboxyl α-COOH or amine α-NH_2, NH imidazole of histidine, NH guanidine of arginine, SH sulfydryl of cysteine and phenolic OH of tyrosine, since the pKa value of these groups strongly depends on their polar or non-polar environment.[9]

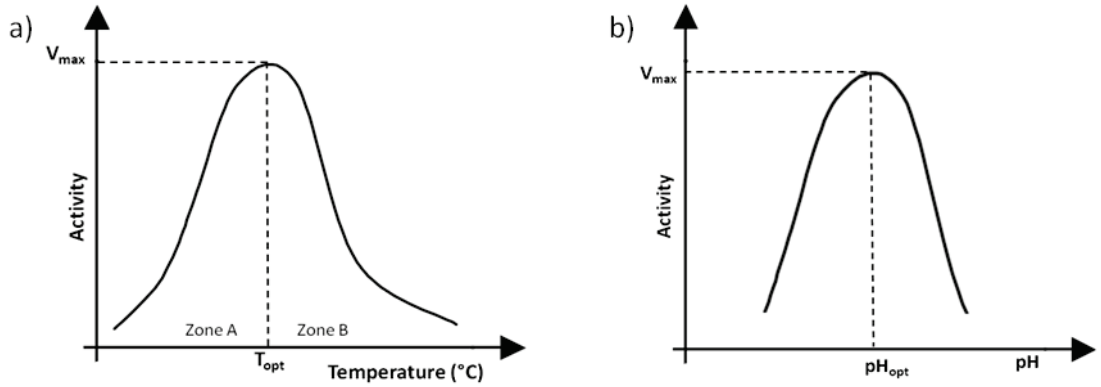

Figure 9. a) Effect of temperature on the enzyme activity: heat activation (Zone A), thermal denaturation (Zone B) and b) Effect of pH on enzyme activity. Extracted from Ref 9.

Electrochemical Glucose Biosensors- A Special Case

As already mentioned, the entire field of biosensors can trace its origin to this original glucose enzyme electrode prepared by Clark[2] in 1962. A wide range of amperometric enzyme electrodes, differing in electrode design or material, immobilization approach, or membrane composition, has been described ever since. The glucose biosensor is the most widely used example of an electrochemical biosensor which is based on a screen-printed amperometric disposable electrode.[6] The working principle of the glucose oxidase based glucose biosensor is illustrated schematically below:

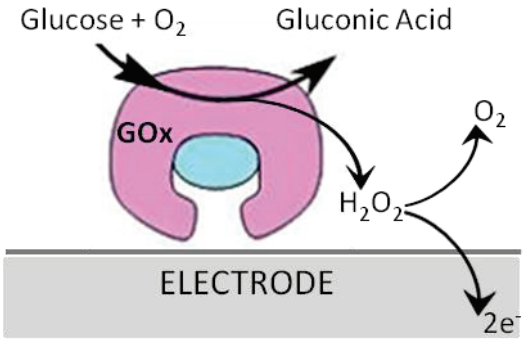

Figure 10. Schematic representation of working principle of amperometric glucose biosensor based on glucose oxidase.

In presence of dissolved oxygen glucose oxidase catalyzes the oxidation of glucose to gluconolactone, which immediately hydrolyzes to gluconic acid. More specifically, the biocatalytic reaction involves the reduction of the flavin group (FAD) in the enzyme by reaction with glucose to give the reduced form of the enzyme (FADH2) followed by re-oxidation of the flavin by molecular oxygen to regenerate the oxidized form of the enzyme GOx(FAD).

$$GOx(FAD) + Glucose \longrightarrow GOx(FADH_2) + Gluconolactone \quad (1)$$

$$GOx(FADH_2) + O_2 \longrightarrow GOx(FAD) + H_2O_2 \quad (2)$$

As it can be seen from reaction (2), hydrogen peroxide is formed as a by-product. The detection of hydrogen peroxide through its oxidation peak, is commonly carried out on a platinum electrode at a moderate anodic potential of around +0.6 V (vs Ag/AgCl):

$$H_2O_2 \longrightarrow O_2 + 2H^+ + 2e^- \quad (3)$$

Measurements of peroxide formation have the advantage of being simple, especially when miniaturized devices are concerned. The intensity of the resulting anodic current from the re-oxidation on the working electrode at applied constant potential is proportional to the glucose concentration.[6]

The above working principle of electrodes for H_2O_2 detection, is now utilized in the most commercially successful glucose biosensors for glucose testing in the home utilizing glucose oxidase or glucose dehydrogenase (GDH).[6] However, the construction of glucose biosensors based on GDH requires a source of NAD^+ and a redox mediator to lower the overvoltage for oxidation of the NADH product.

Immunosensors

Antibodies are immune system-related proteins, also called immunoglobulins, exhibiting very specific binding capabilities for specific structures, called antigens. Each antibody consists of four polypeptides- two heavy chains and two light chains joined to form a "Y" shaped molecule. The amino acid sequence in the tips of the "Y" varies greatly among different antibodies. This variable region, composed of 110-130 amino acids, gives the antibody its specificity for binding the antigen. An antigen-specific antibody "fits" its unique antigen in a highly specific manner. This unique property of antibodies is the key to their usefulness in the development of biosensors. Immunosensors are antibody–antigen based affinity biosensors, in which the detection of antigen as a target analyte is a result of the specific binding of the antigen to particular region of an antibody on the electrode surface.[10, 11]

The specific binding of an antibody to its target antigen in a complex mixture such as serum and plasma provides detection and quantification at levels as low as picograms (pg). Compared with traditional immunoassay methods such as homogeneous competitive assays, heterogeneous competitive and non-competitive assays,[12] with the enzymatic immunoassay ELISA (Enzyme Linked Immune Sorbent Assay) being the most common of them, electrochemical immunosensors are specific, simple and convenient, and can offer multitarget analyses and miniaturization. They can perform in situ, real-time, automation detection.

Nucleic Acid Biosensors

Nucleic acids have received increasing interest as bioreceptors for biosensor and biochip technologies. The complementarity of adenine: thymine (A:T) and cytosine: guanosine (C:G) pairing in DNA forms the basis for the specificity of biorecognition in DNA biosensors, often referred to as genosensors.[13] If the sequence of bases composing a certain part of the DNA molecule is known, then the complementary sequence, often called a probe, can be synthesized and labeled with an optically detectable compound (e.g., a fluorescent label). By unwinding the double-stranded DNA into single strands, adding the probe, and then annealing the strands, the labeled probe will hybridize to its complementary sequence on the target molecule.[8]

DNA biosensors have been successfully used for the detection of cancer sequences[14] and carcinogens[15], pathogenic bacteria[16] and common toxicants and pollutants.[17]

---

[10] E.B. Bahadır and M.K. Sezgintürk, "Applications of Electrochemical Immunosensors for Early Clinical Diagnostics," *Talanta* 132, no. 0 (**2015**): 162–74.

[11] F. Ricci, G.Adornetto and G. Palleschi, "A Review of Experimental Aspects of Electrochemical Immunosensors," *Electrochimica Acta* 84 (**2012**): 74–83.

[12] N. Bojorge Ramírez, A. M. Salgado, and B. Valdman, "The Evolution and Developments of Immunosensors for Health and Environmental Monitoring: Problems and Perspectives," *Brazilian Journal of Chemical Engineering* 26, no. 2 (**2009**): 227–49.

[13] R. Rosario and R. Mutharasan "Nucleic acid electrochemical and electromechanical biosensors: a review of techniques and developments," *Reviews in analytical chemistry* 33, 4 (**2014**): 213-230.

[14] A.A. Ensafi et al., "Sensitive DNA Impedance Biosensor for Detection of Cancer, Chronic Lymphocytic Leukemia, Based on Gold Nanoparticles/gold Modified Electrode," *Electrochimica Acta* 56, no. 24 (**2011**): 8176–83.

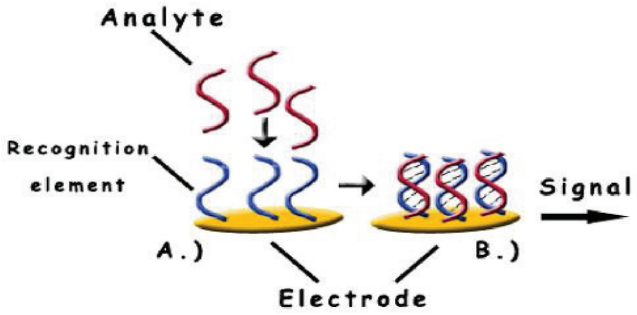

Figure 11. General sDNA biosensor scheme. Target DNA is captured at the recognition layer (A), and the resulting hybridization is transduced into a measurable electronic signal (B). Extracted from Ref 4.

Biomimetic Sensors

An artificial receptor that is fabricated and designed to mimic a bioreceptor is often termed as a biomimetic receptor. Several different methods have been developed over the years for the construction of biomimetic receptors. These methods include: aptamers, artificial membrane fabrication and molecular imprinting. The molecular imprinting technique, which has recently received great interest, is based on the synthesis of a polymeric material endowed with specific recognition sites towards the molecule which must be recognized (template). This objective is accomplished by the addition of the template to a reaction mixture, which is constituted of a functional monomer, a cross-linking agent and a solvent. During the polymerization, the template is incorporated into the polymeric matrix and chemical groups of functional monomers will be arranged according to the shape and chemical properties of the template molecules. The extraction of the template from the obtained polymeric matrix will allow the formation of the template complementary recognition sites with high substrate selectivity and specificity. In this way, selective detection and separation properties are introduced in the nascent polymer.[18]

Another class of biomimetic sensors is based on the use of aptamers as recognition element.[19] Aptamers are artificial oligonucleotides (DNA or RNA) which are also used in DNA sensors. They can bind to a wide variety of entities (e.g. metal ions, small organic molecules, proteins and cells) with high selectivity, specificity, and affinity, equal to or often superior to those of antibodies.[20] These aptamers can be isolated from combinatorial nucleic

---

[15] A.A. Ensafi et al., "A Novel Sensitive DNA–biosensor for Detection of a Carcinogen, Sudan II, Using Electrochemically Treated Pencil Graphite Electrode by Voltammetric Methods," *Talanta* 88 (**2012**): 244–51.
[16] A. Walter et al., "Redox Cycling Amplified Electrochemical Detection of DNA Hybridization: Application to Pathogen E. Coli Bacterial RNA," *Analytica Chimica Acta* 689, no. 1 (**2011**): 29–33.
[17] Q.Zhang, P. Dai and Z. Yang, "Sensitive DNA-Hybridization Biosensors Based on Gold Nanoparticles for Testing DNA Damage by Cd(II) Ions," *Microchimica Acta* 173, no. 3–4 (**2011**): 347–52.
[18] C. Algieri et al., "Bio-Mimetic Sensors Based on Molecularly Imprinted Membranes," *Sensors* 14, no. 8 (**2014**): 13863-13912.
[19] K. Wang et al., "Research and Development of Functionalized Aptamer Based Biosensor," *Chinese Journal of Analytical Chemistry* 42, no. 2 (**2014**): 298–304.
[20] W. Zhou et al., "Aptamer-Based Biosensors for Biomedical Diagnostics," *The Analyst* 139, no. 11 (**2014**): 2627-2640.

acid libraries using in vitro SELEX[21] (Systematic Evolution of Ligands by EXponential enrichment, a combinatorial chemistry technique in molecular biology for selecting oligonucleotides that specifically bind to a target ligand). Synthesizing aptamers is relatively inexpensive, and they can be engineered easily for immobilization purposes. Moreover, unlike proteins, which are irreversibly denatured in unfavorable conditions, aptamers are capable of reversible denaturation. Consequently, by incorporating these aptamers into biosensors, it is possible to subject these sensing elements to repeated use, thereby realizing a device that is potentially recyclable.

I.1.2.2. Classification based on Transducers

Transduction can be accomplished *via* a great variety of methods. Most forms of transduction can be categorized in one of the main three classes:

- Electrochemical transduction: The basic principle for electrochemical biosensors is that chemical reactions between immobilized biomolecule and target analyte produce or consume ions or electrons, which affect measurable electrical properties of the solution, such an electric current or potential.[22] The electrochemical signal produced is then used to relate quantitatively to the amount of analyte present in a sample solution. Therefore, the electrochemical sensors can be further subdivided according to how the electrical measurement is made. They measure the change in voltage (potentiometry), current (amperometry and voltammetry), impedance or conductance resulting from a chemical reaction that either transfers or separates electric charge with reasonable selectivity and sensitivity.[22]
- Optical transduction: this is the most diverse class of transduction because it relies on many different types of spectroscopy, such as absorption, fluorescence, luminescence, phosphorescence, surface plasmon resonance, light scattering spectroscopy, Raman, SERS, refraction, and dispersion spectrometry. These spectroscopic methods can measure different properties, such as energy, polarization, amplitude, decay time, and/or phase. Amplitude is the most commonly measured as it can easily be correlated to the concentration of the analyte of interest.[8]
- Piezoelectric transduction: the piezoelectric sensors employ crystals that undergo elastic deformation under the action of an electric potential. An alternating potential at a certain frequency generates a standing wave in the crystal. Analyte adsorption on the surface of the crystal, which is covered with a biological recognition element, alters the resonance frequency, and this is an indication of binding taking place.[4]

However, new types of transducers are constantly being developed for use in biosensors. Each of the three main classes contains many different subclasses, creating a large number of possible transduction methods or combination of methods.

---

[21] Y.Pu et al., "Using Aptamers to Visualize and Capture Cancer Cells," *Analytical and Bioanalytical Chemistry* 397, no. 8 (**2010**): 3225–33.

[22] D. Wei et al., "Electrochemical Biosensors at the Nanoscale," *Lab on a Chip* 9, no. 15 (**2009**): 2123.

I.1.3. Electrochemical Biosensors

Among these various kinds of biosensors, electrochemical biosensors are a class of the most widespread and successfully commercialized devices of biomolecular electronics.[23] Electrochemical sensors support accurate, fast, and inexpensive analytical methods with the advantages of being easily embedded and integrated into electronics, minimal power demands and having the greatest potential impact in the areas of healthcare, environmental monitoring, food packing and many other applications.[24] In this section we will focus on the electrochemical transduction modes with a particular emphasis on cyclic voltammetry and electrochemical impedance spectroscopy that we have used in our work.

I.1.3.1. Potentiometric Transducers

Potentiometric sensors measure the potential when there is no net current flowing in a system as all the driving forces are in balance. Under these conditions the potential difference between the working electrode and the reference electrode or between two references electrodes separated by a semipermeable membrane shows a linear relationship with the logarithm of the concentration (activity) of the electroactive species (analyte), as given by the Nernst equation. Potentiometry with ion selective electrodes (ISEs) and ion-selective field effect transistors (ISFETs) is an accurate, fast, and inexpensive analytical method.[23] The most widespread potentiometric biosensors employ pH electrodes.

I.1.3.2. Amperometric and Voltammetric Transducers

Generalities

Amperometric biosensors are the most widespread class of electrochemical biosensors.[25] Both amperometric and voltammetric sensors measure the Faradaic current generated during the heterogeneous electron transfer reaction such as the oxidation or reduction of the electroactive analyte species. The current is proportional to the concentration of the analyte. However, in amperometric sensors, the potential is fixed at a constant value and the concentration of the electroactive species is determined by the Faradaic current. Voltammetry is the application of a potential ramp with the subsequent measurement of current as a chemical species reacts at the electrode. Amperometric sensors are usually applied to the measurement of a specific biological component since they are operated at a constant potential.[22, 25] Among voltammetric methods, enzyme based biosensors are the most common electrochemical biosensors.[26] The working electrode is usually a noble metal or

[23] D.W. Kimmel et al., "Electrochemical Sensors and Biosensors," *Analytical Chemistry* 84, no. 2 (**2012**): 685–707.

[24] H. Sharma and R. Mutharasan, "Review of Biosensors for Foodborne Pathogens and Toxins," *Sensors and Actuators B: Chemical* 183, no. 0 (**2013**): 535–49.

[25] Dzyadevych et al., "Amperometric Enzyme Biosensors: Past, Present and Future," *IRBM* 29, no. 2–3 (**2008**): 171–80.

[26] C.N. Kotanen et al., "Implantable Enzyme Amperometric Biosensors," *Biosensors and Bioelectronics* 35, no. 1 (**2012**): 14–26.

screen-printed layer covered by the bioelement. The working principle of enzymatic amperometric/voltammetric biosensors is illustrated schematically below:

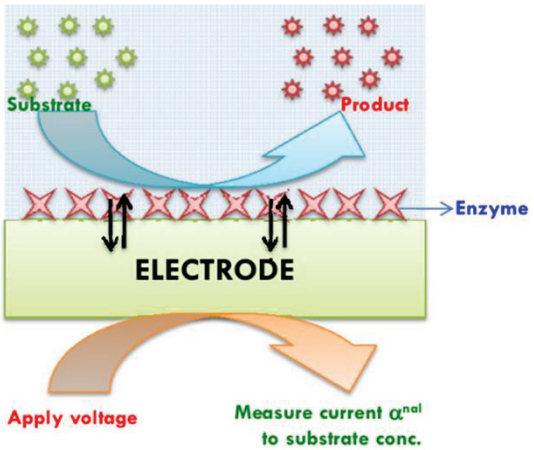

Figure 12. Representation of the working principle of an enzymatic amperometric /voltammetric biosensor.

Cyclic Voltammetry (CV)

Theoretical Background

Cyclic Voltammetry (CV) is the most common electroanalytical technique to obtain preliminary information about an electrochemical process. The basis of voltammetry is the current-voltage relationship exhibited by an indicator electrode immersed in a solution of electroactive species.[27] CV is a modification of linear scan voltammetry (LSV). The cyclic voltammetry can be applied for the study of all electrochemical reactions without limitations. With the help of this method, it is possible to get information about the type of reactions observed in the system and the potentials at which they occur. More specifically, CV has been effectively applied for analytical, mechanistic and kinetic studies of redox reactions, kinetics of heterogeneous electron transfer reactions, coupled chemical reactions, or adsorption processes. It is a simple and direct method of measuring the formal potential of a half reaction, and often it is the first experiment performed in an electroanalytical study. At the same time, this technique is unfortunately not the best one to obtain quantitative data about electrochemical nucleation processes. The current-potential curve obtained is termed cyclic voltammogram. Both oxidized and reduced forms may or may not be stable during the time required to obtain the cyclic voltammogram.[27]

Practical Implementation

The three-electrode method is the most widely used because the electrical potential of reference does not change easily during the measurement. This method uses a reference electrode (RE), working electrode (WE), and a counter electrode (CE) (also called the secondary or auxiliary electrode). Standard CV experiments consist of measuring the current

[27] A.J. Bard and L.R. Faulkner, *Electrochemical Methods: Fundamentals and Applications, 2nd Edition*, vol. 2 (Wiley New York, **2001**).

flowing through the WE during a triangular potential perturbation. The applied potential is measured against the RE, while the CE closes the electrical circuit for the current to flow. The experiments are performed by a potentiostat that effectively controls the voltage between the RE and WE, while measuring the current through the CE (the WE is connected to the ground).[27]

Electrolyte is usually added to the test solution to ensure sufficient conductivity. The combination of the solvent, electrolyte and specific working electrode material determines the range of the potential to be applied.

At the beginning the working electrode is held at some potential, E_i, where no electrode reactions occur. During the measurement, the potential is swept linearly at a rate ν between two limiting potentials E_1 and E_2 (Figure 13a). The same sweep rate is normally chosen for the forward and reverse sweep. The corresponding current is recorded as a function of the varying potential. A theoretical cyclic voltammogram for a reversible system is shown in Figure 13b. For the cathodic scan (applied potential is decreasing) the current has a negative sign, for the anodic scan (applied potential is increasing) the current has a positive sign.[27]

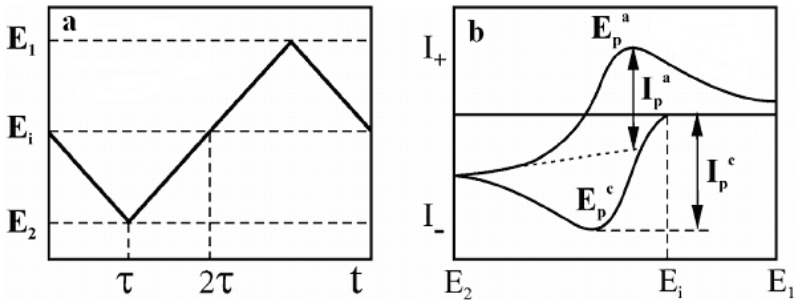

Figure 13. a) Potential sweep during cyclic voltammetric measurement; E_i is initial value, E_1 and E_2 are two limiting values. b) A typical cyclic voltammogram of a reversible reaction; anodic (a) and cathodic (c) processes, Ep is the potential at the current peak Ip. Extracted from Ref 27.

Important parameters in CV:

Cyclic voltammograms are most often characterized by:

a) the location of the forward and reverse peaks on the potential axis (E_p and ΔE_p, allowing the calculation of $E^{0'}$) b) the ratio of currents observed on the reverse and forward scans ($i_{p,rev}$ / $i_{p,\,fwd}$) and c) the dependence of peak currents on the scan rate (i_p vs. $\nu^{1/2}$).

I.1.3.3. Impedimetric Transducers

Generalities

Electrochemical Impedance Spectroscopy (EIS) has proven to be one of the most powerful tools for the investigation of interfacial reaction mechanisms.[28] EIS sensors measure the response (current and its phase) of an electrochemical system to an oscillating potential as

[28] E. Katz and I. Willner, "Probing Biomolecular Interactions at Conductive and Semiconductive Surfaces by Impedance Spectroscopy: Routes to Impedimetric Immunosensors, DNA-Sensors, and Enzyme Biosensors," *Electroanalysis* 15, no. 11 (**2003**): 913–47.

a function of frequency. This approach has been used to study a variety of electrochemical phenomena over a wide frequency range.[28] If the immobilization of biomaterials, e.g., enzymes, antigens/antibodies or DNA on electrodes or semiconductor surfaces alters the capacitance and interfacial electron transfer resistance of the conductive or semiconductive electrodes, EIS can be used to detect that impedance change.

It is proven that impedance spectroscopy allows analysis of interfacial changes originating from biorecognition events at electrode surfaces.[29] Kinetics and mechanisms of electron transfer processes corresponding to biocatalytic reactions occurring at modified electrodes can be also derived from Faradaic impedance spectroscopy. This technique offers several advantages over chronoamperometry and cyclic voltammetry because the effects of solution resistance, double layer charging and currents due to diffusion or to other processes occurring in the monolayer can be observed more explicitly.[27] Moreover, impedance measurement does not require special reagents and is amenable to label-free operation. EIS allows the measurement of several electrochemical reactions that take place at very different rates and provides a more thorough understanding of an electrochemical system than any other electrochemical technique.[22]

Theoretical Background of EIS

An electrochemical reaction at the electrode–electrolyte interface cannot be fully understood by just using traditional electrochemical measurements. Those methods provide only currents made of faradaic and non-faradaic components. A complete description requires impedance measurements made over a broad frequency range at various potentials and determination of all the electrical characteristics of the interface.[30] Impedance biosensors measure the electrical impedance of an interface in AC steady state with constant DC bias conditions. Most often this is accomplished by imposing a small sinusoidal voltage at a particular frequency and measuring the resulting current; the process can be repeated at different frequencies.[28] The impedance is defined as the ratio between the system voltage phasor, U(ω), and the current phasor, I(ω), which are generated by a frequency response analyzer during the experiment (**equation 4**). Either an AC test voltage or AC test current is imposed while the other variable is measured. Mathematically, if the applied voltage is $V_{test}= V_{DC}+ V_{AC}\sin(\omega t)$ and the resulting current is $I_{test}= I_{DC}+ I_{AC}\sin(\omega t - \varphi)$, then the complex-valued impedance Z(ω) has magnitude V_{AC}/I_{AC} and phase φ.

$$Z(\omega) = \frac{U(\omega)}{I(\omega)} = Z_{re}(\omega) + \mathrm{j}Z_{\mathrm{im}}(\omega) \quad (4)$$

[29] A. Bonanni and M.D. Valle, "Use of Nanomaterials for Impedimetric DNA Sensors: A Review," *Analytica Chimica Acta* 678, no. 1 (**2010**): 7–17.
[30] B. Pejcic and R. De Marco, "Impedance Spectroscopy: Over 35 Years of Electrochemical Sensor Optimization," *Electrochimica Acta* 51, no. 28 (**2006**): 6217–29.

Where $\omega=2\pi f$ and ω and f (excitation frequency) have units of $rad \cdot s^{-1}$ and Hz, respectively. Z_{re} and Z_{im} represent the real and imaginary part of Z. The electrode-solution impedance depends on both the bias conditions (V_{DC}) and the measurement frequency (ω). By exciting with a single frequency, a lock-in amplifier can be used to accurately measure the output signal at the same frequency. Voltage excitation is usually employed in EIS because the most troublesome parasitic impedances are in parallel with the measured electrode-solution impedance. In most cases, the measurement process is repeated at different frequencies, yielding $Z(\omega)$.[31] $Z_{re}(\omega)$, and $Z_{im}(\omega)$ components originate mainly from the resistance and capacitance of the interface, respectively. EIS data may be represented in different ways. Figure 14 shows one of the most commonly used, which is the Nyquist plot.

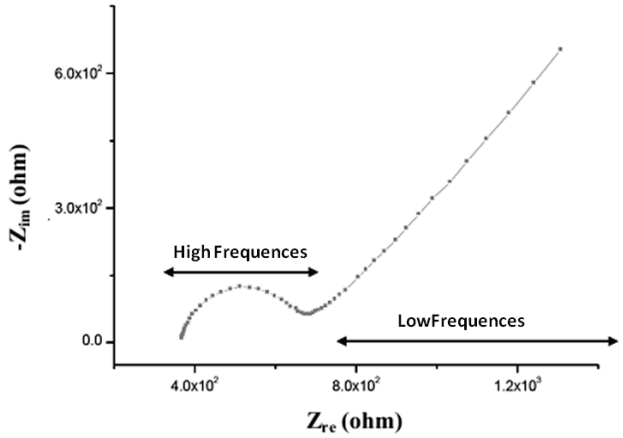

Figure 14. Nyquist plot of EIS.

In impedimetric biosensors, the applied voltage should be quite small – usually 10 mV amplitude or less – for several reasons. First, the current-voltage relationship is often linear only for small perturbations, and only in this situation is impedance strictly defined. A second reason is to avoid disturbing the probe layer. Covalent bond energies are on the order of 1–3 eV but probe-target binding energies can be much lower (and in some cases the probe is not covalently attached to the electrode), and applied voltages will apply a force on charged molecules.[27] This second consideration also applies to DC bias voltages across the electrode-solution interface. Correctly performed, EIS does not damage the biomolecular probe layer, an important advantage over voltammetry or amperometry where more extreme voltages are applied.

Measuring Electrochemical Impedance- Faradaic vs. Nonfaradaic

It is important to distinguish between non faradaic and faradaic biosensors. In electrochemical terminology, a faradaic process is one where charge is transferred across an interface.[28, 31] However, transient currents can flow without charge transfer in nonfaradaic processes (e.g., charging a capacitor). In faradaic EIS a redox species is alternately oxidized

[31] J.S. Daniels and N. Pourmand, "Label-Free Impedance Biosensors: Opportunities and Challenges," *Electroanalysis* 19, no. 12 (**2007**): 1239–57.

and reduced by the transfer of an electron to and from the metal electrode. Thus, faradaic EIS requires the addition of a redox-active species and DC bias conditions such that it is not depleted. In contrast, no additional reagent is required for nonfaradaic impedance spectroscopy, rendering nonfaradaic schemes somewhat more amenable to point-of-care applications. The term capacitive biosensor usually designates a sensor based on a nonfaradaic scheme, usually measured at a single frequency.[28, 31]

A typical shape of a Faradaic impedance spectrum (presented in the form of a Nyquist plot) includes a semicircle region followed by a straight line (figure 15, curve a). The semicircle portion, observed at higher frequencies, corresponds to the electron transfer-limited process, whereas the linear part is characteristic of the lower frequencies range and represents the diffusionally limited electrochemical process. In the case of very fast electron transfer processes, the impedance spectrum could include only the linear part (curve b) whereas a very slow electron-transfer step results in a large semicircle region that is not accompanied by a straight line (curve c).[28] The electron transfer kinetics and diffusional characteristics can be extracted from the spectra. The semicircle diameter equals to the electron transfer resistance, R_{et}. The intercept of the semicircle with the Z_{re}-axis at high frequencies ($\omega \rightarrow \infty$) is equal to the solution resistance, R_s. Extrapolation of the circle to lower frequencies yields an intercept corresponding to R_s+R_{et}. The characteristic frequency, ω_0, given by **equation 5**, has the meaning of the reciprocal of the time constant of the equivalent circuit. The maximum value of the imaginary impedance in the semicircle part corresponds to $Z_{im}=0.5R_{et}$ and is achieved at the characteristic frequency, ω_0.[28]

$$\omega_0 = (C_{dl}R_{et})^{-1} \quad (5)$$

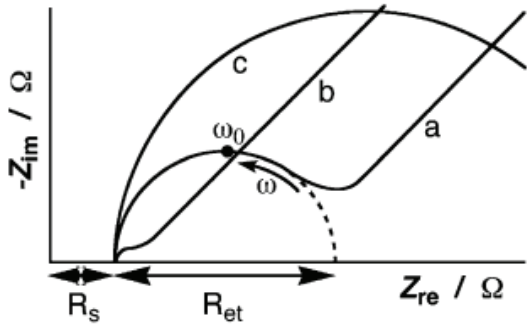

Figure 15. Schematic Faradaic impedance spectra presented in the form of a Nyquist plot for: a) A modified electrode where the impedance is controlled by diffusion of the redox probe (low frequencies) and by the interfacial electron transfer (high frequencies). b) A modified electrode where the impedance is mainly controlled by diffusion of the redox probe. c) A modified electrode where the impedance is controlled by the interfacial electron transfer within the entire range of the applied frequencies. The arrow shows the direction of the frequency increase. Resistance of the electrolyte solution, Rs, and electron transfer resistance, Ret, are shown. Extracted from Ref 28.

One of the most important parameters governing the technique is the applied frequency. At low frequencies (f<1 mHz) the impedance value is basically determined by the DC-conductivity of the electrolyte solution. At very high frequencies (f>100 kHz) inductance of the electrochemical cell and connecting wires could contribute to the impedance spectra. Thus, the analytically meaningful impedance spectra are usually recorded at frequencies where they are mainly controlled by the interfacial properties of the modified electrodes (10 mHz<f<100 kHz).

Data Fitting and Circuit Models

Electrochemical transformations occurring at the electrode/electrolyte interface can be modeled by extracting components of the electronic equivalent circuits that correspond to the experimental impedance spectra. A general electronic equivalent circuit (Randles and Ershler model), which is very often used to model interfacial phenomena, includes the ohmic resistance of the electrolyte solution, Rs, the Warburg impedance, Z_W, resulting from the diffusion of ions from the bulk electrolyte to the electrode interface, the double layer capacitance, C_{dl}, and electron transfer resistance, R_{et}, that exists if a redox probe is present in the electrolyte solution (Figure 16A).[28]

The parallel elements (C_{dl} and Z_W+R_{et}) of the equivalent circuit are introduced since the total current through the working interface is the sum of distinct contributions from the Faradaic process, I_F, and the double-layer charging, I_C. Since all of the current must pass through the uncompensated resistance of the electrolyte solution, R_s, is inserted as a series element in the circuit. The two components of the electronic scheme, R_s and Z_W, represent bulk properties of the electrolyte solution and diffusion features of the redox probe in solution. Therefore, these parameters are not affected by chemical transformations occurring at the electrode surface. The other two components in the scheme, C_{dl} and R_{et}, depend on the dielectric and insulating features at the electrode/electrolyte interface.[28]

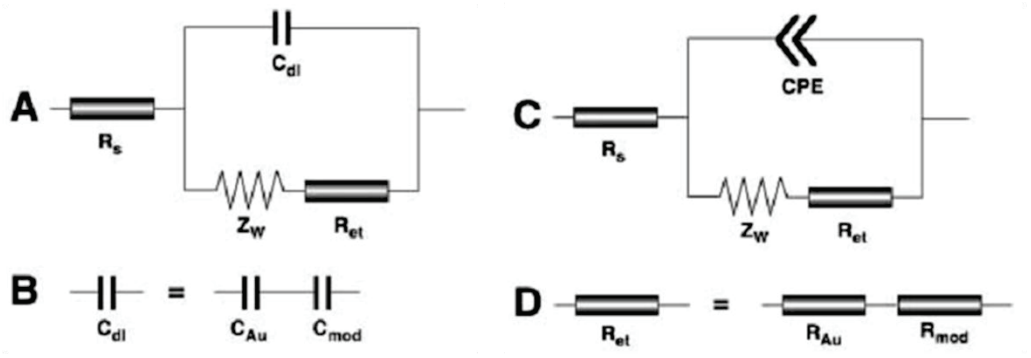

Figure 16. Schematic Faradaic impedance spectra presented in the form of a Nyquist plot for: a) A modified electrode where the impedance is controlled by diffusion of the redox probe (low frequencies) and by the interfacial electron transfer (high frequencies). b) A modified electrode where the impedance is mainly controlled by diffusion of the redox probe. c) A modified electrode where the impedance is controlled by the interfacial electron transfer within the entire range of the applied frequen-cies. The arrow shows the direction of the frequency increase. d) Resistance of the electrolyte solution, Rs, and electron transfer resistance,Ret are shown. Extracted from Ref 28.

The double-layer capacitance depends on the dielectric permittivity introduced into the double-charged layer molecules, ε_{dl}, according to **Equation 6**:

$$C_{dl} = \frac{\varepsilon_{dl} A}{\delta} \quad (6)$$

where $\varepsilon_{dl} = \varepsilon_0 \varepsilon_\rho$ and $\varepsilon_0 = 8.85 \times 10^{-12} Fm^{-1}$ is the dielectric constant of the vacuum, ε_ρ is the effective dielectric constant of the layer separating the ionic charges and the electrode surface, A is the electrode area, and δ is the thickness of the separating layer.

In the equivalent electronic circuit the double-layer capacitance, C_{dl}, can be represented as a sum of a constant capacitance of an unmodified electrode (e.g., for a poly-crystalline Au electrode, $C_{Au} \approx 40 \pm 60 \mu F cm^{-2}$, depending on the applied potential) and a variable capacitance originating from the electrode surface modifier, C_{mod}, connected as series elements, Figure 16B.[28] Any electrode modifier of insulating features decreases the double-layer capacitance as compared to the pure metal electrode. Thus, the double-layer capacitance could be expressed by **Equation 7**.

$$\frac{1}{C_{dl}} = \frac{1}{C_{electr}} + \frac{1}{C_{mod}} \quad (7)$$

Sometimes, particularly when the electrode surface is rough, the electronic properties of the interface cannot be described sufficiently well with a capacitive element, and a constant phase element (CPE), **Equation 8**, should be introduced instead of C_{dl}, Figure 16C. [28]

$$CPE = A^{-1}(j\omega)^{-n} \quad (8)$$

The constant phase element reflects non-homogeneity of the layer, and the extent of the deviation from the Randles and Ershler model is controlled by the parameter n in **Equation 8**. The CPE has meaning of capacitance and the coefficient A becomes equal to the C_{dl} when n=1. The electron transfer resistance, R_{et}, controls the electron transfer kinetics of the redox probe at the electrode interface. Thus, the insulating modifier on the electrode is expected to slow down the interfacial electron transfer kinetics and to increase the electron transfer resistance. The electron transfer resistance at the electrode is given by **Equation 9**, where R_{electr} and R_{mod} are the constant electron transfer resistance of the unmodified electrode and the variable electron transfer resistance introduced by the modifier, in the presence of the solubilized redox probe, respectively. These resistances are also connected as series elements in the equivalent electronic circuit (Figure 16D).[28]

$$R_{et} = R_{electr} + R_{mod} \quad (9)$$

I.1.4. Methods for Bioreceptors Immobilization

To preserve the biological activity of sensing elements, these latter have to be properly immobilized on the transducer surface.[32] The step of sensing elements immobilization onto the transducer is very important because it will govern the overall performance of the biosensor, in terms of response time, specificity, selectivity, sensitivity and reliability. Since the scope of this work is to demonstrate advances in enzymatic electrochemical biosensors, we will mainly focus on the enzyme immobilization methods.[33] Biosensors are usually designed with high enzyme loading to insure sufficient biocatalyst activities, and the enzymes are provided with an appropriate environment to sustain their activities. The local chemical and thermal environment can have profound effects on the enzyme stability. The choice of immobilization method depends on many factors, such as the nature of the enzyme, the type of transducer used, the physicochemical properties of the analyte and the operating conditions in which the biosensor is to function, and overriding all these considerations is necessary for the biological element to exhibit maximum activity in its immobilized microenvironment.[32] In all cases, the immobilization methods must guarantee: (i) the maintenance of the integrity of the conformation of the biological material, in particular the active site; (ii) the access of the analyte to the active site of the biomolecule; (iii) the transportation of the biomolecules through the immobilized biological layer. The main basic methods of immobilizing biomaterials are: adsorption, entrapment, affinity, cross-linking and covalent binding (figure 17). Each immobilization method presents advantages and drawbacks (table 1).

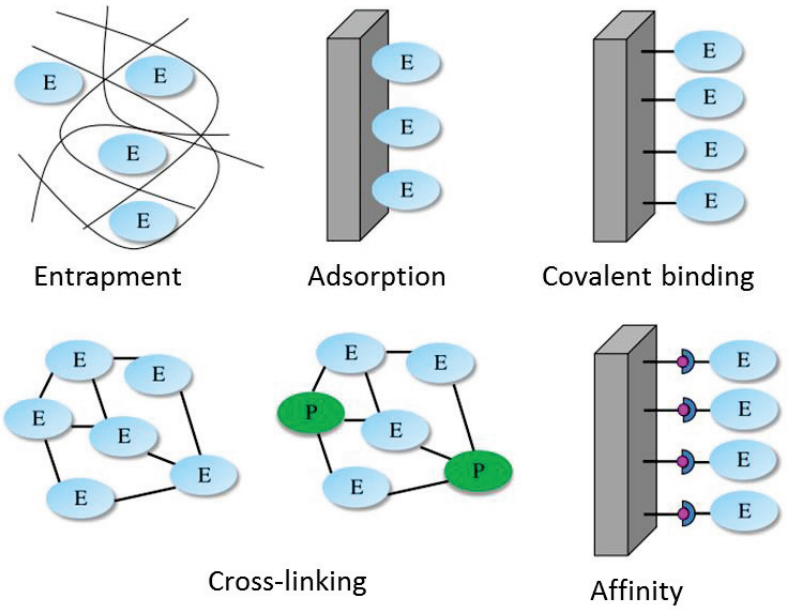

Figure 17. Schematic representation of the basic methods used for biomaterial immobilization on the transducer. Extracted from Ref 32.

[32] A. Sassolas, L. J. Blum and B. D. Leca-Bouvier, "Immobilization Strategies to Develop Enzymatic Biosensors," *Biotechnology Advances* 30, no. 3 (**2012**): 489–511.
[33] S. Datta, L. Rene Christena and Y.R.S. Rajaram, "Enzyme Immobilization: An Overview on Techniques and Support Materials," *3 Biotech* 3, no. 1 (**2013**): 1–9.

Table 1. Advantages and drawbacks of the five basic immobilization methods.[32]

	Binding nature	Advantages	Drawbacks
Adsorption	Weak bonds	- Simple and easy - Limited loss of enzyme activity	- Desorption -Non-specific adsorption
Entrapment	Incorporation of the enzyme within a gel or a polymer	- Several types of enzymes can be immobilized within the same polymer - No chemical reaction between the monomer and the enzyme that could affect the activity	- High concentrations of monomer and enzyme needed for electropolymerization -Diffusion barrier -Enzyme leakage
Cross-linking	Bond between enzyme/cross-linker /inert molecule	- Simple	- High enzyme activity loss
Covalent binding	Chemical binding between functional groups of the enzyme and those on the support	- No diffusion barrier - Stable - Short response time - High enzyme activity loss	- Matrix not regenerable - Coupling with toxic product
Affinity	Affinity bonds between a functional group (e.g. avidin) on a support and affinity tag (e.g. biotin) on a protein sequence	- Controlled and oriented immobilization	- Need of the presence of specific groups on enzyme (e.g. His, biotin)

Adsorption: It is the simplest and fastest way to physically immobilize enzymes onto solid supports and it does not need any substantial pretreatment of the sensor components or use of special-purpose chemicals. Enzyme is dissolved in solution and the solid support is placed in contact with the enzyme solution for a fixed period of time. The unadsorbed enzyme is then removed by washing with buffer. Adsorption can be subdivided into mainy catagories based on physical adsorption, electrostatic interactions (layer by layer deposition, electrochemical doping and pre-immobilization on ion-exchanger beads) and retention in a lipidic microenvironment (Langmuir- Blodgett, LB, technique). However, the main two classes are: physical adsorption and chemical adsorption (chemisorption). Physical adsorption is weak and occurs mainly via Van der Waals, Coulomb, ionic interactions or hydrogen bonding. Many substances adsorb enzymes on their surfaces, eg. alumina, charcoal, clay, cellulose, kaolin, silica gel, glass and collagen.[32] The result of adsorptive immobilization is largely determined by the properties of the transducer surface, including its charge, the presence of polar groups, its redox potential, and its energetic uniformity. Adsorption does not always afford a high concentration of a biological component. In order to increase the amount of enzyme adsorbed, the transducer is pretreated so as to generate charged or polar groups

enhancing biomaterial adsorption. This is done by using various methods of oxidation and surface modification with polymers or functionalizing reagents. For example, the oxidation of gold and carbon electrodes increases their protein, nucleic acid, and microorganism adsorption capacity.This technique is generally non-destructive for enzyme activity. Although this immobilization method causes little or no enzyme inactivation, this technique presents drawbacks: enzymes are loosely bound to the support and desorption of the enzyme resulting from changes in temperature, pH and ionic strength, appears to be the main problem. Thus, biosensors based on adsorbed enzyme suffer from poor operational and storage stability. Another drawback is the non-specific adsorption of other proteins or substances.[32]

Entrapment: Biomaterial inclusion into a forming polymer matrix is actually a universal method applicable to various types of recognition elements. Enzymes can be immobilized in three-dimensional matrices such as an electropolymerized film, an amphiphilic network composed of polydimethylsiloxane (PDMS), a photo-cross-linkable polymer, a silica gel, a polysaccharide gel or a carbon paste.[32] This immobilization technique is easy to perform. Enzyme, mediators and additives can be simultaneously deposited in the same sensing layer. Biosensors based on physically entrapped enzymes are often characterized by increased operational and storage stability. Another obvious advantage of this method is its universality. However, its drawback is that the network may impede diffusion of substrate and hampers analyte permeation. In addition, if the molecules included into the network are not chemically bonded to it, they can be washed away resulting in a loss of activity. Such limitations can restrict the performances of the systems.[32]

Cross-linking: Immobilization of enzymes by cross-linking with glutaraldehyde or other bifunctional agents such as glyoxal or hexamethylenediamine is another well-known approach to develop biosensors to chemically bond the biomaterial onto solid supports or gels. The enzyme can be either cross-linked with each other or in the presence of a functionally inert protein such as bovine serum albumin. The technique of crosslinking or co-crosslinking is based on the interaction between a protein/enzyme and a bifunctional agent in order to form a network. An example of such cross-linking is the action of glutaraldehyde[34], which forms Schiff bases with amino, hydroxyl, and thiol groups of proteins and nucleic acids (figure18). This method is attractive due to its simplicity and the strong chemical binding achieved between biomolecules. The main drawback is the possibility of activity losses due to the distortion of the active enzyme conformation and the chemical alterations of the active site during cross-linking.

[34] O. Barbosa et al., "Glutaraldehyde in Bio-Catalysts Design: A Useful Crosslinker and a Versatile Tool in Enzyme Immobilization," *RSC Adv.* 4, no. 4 (**2014**): 1583–1600.

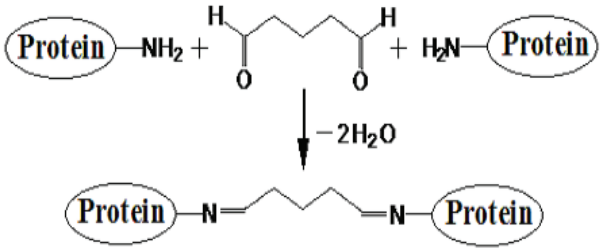

Figure 18. Interaction between glutaraldehyde and an amino group of a protein. Extracted from Ref 8.

Covalent binding: Covalent bonding is likely the most widespread immobilization method of enzymes used to develop enzymatic biosensors. The sensor surface is modified to acquire a reactive group, for example by the use of SAMs, to which a functional group of the biomaterial can be attached by forming a covalent bond. In the case of enzymatic biosensors, the enzyme is covalently bonded to the support matrix through a functional group which is not essential for its catalytic activity.[4] It requires mild conditions under which reactions are performed, such as low temperature, low ionic strength and pH in the physiological range. The choice of chemicals to be used in this immobilization method depends on the molecules to be bonded and on the support material.

Covalent bonding is usually carried out in three steps: the first step is purification of the support and functionalization of its surface with the necessary groups, the second step is biomaterial immobilization, and the third one is removal of weakly bound molecules with a pure solvent. Obviously, the sequence of chemical reactions should be chosen so that the bonds formed at the early stages persist at the later stages.[8]

Covalent immobilization method improves the uniformity, density and distribution of the bioelements, as well as reproducibility and homogeneity of the surfaces. It may decrease or eliminate some common problems such as instability, diffusion and aggregation, or inactivation of biomolecules since it ensures strong biomaterial–support binding and prevents biomaterial loss. Moreover it provides means to produce sensors with a long service life.[32] In the case of enzymes, it is always necessary to investigate the efficiency of binding by each method. In particular, it is necessary to compare the activity of an enzyme in solution and the activity of the same enzyme in the immobilized state.

The carrier support material can either be an inorganic material (e.g. controlled pore glass), a natural (e.g. cellulose) or synthetic polymer (e.g. nylon). Covalent immobilization can be performed directly onto the transducer surface or onto a thin membrane fixed onto the transducer.

Numerous protocols for employing different conjugation chemistries are available once a particular surface (e.g., gold, silicate, polymers) has been functionalized with an “active” outer layer. The choice of surface functionalization strategy is dependent on what types of functional groups linked to biomolecules are available. Usually, nucleophilic functional groups present in amino acid side chains of proteins are used for coupling. However, since most biomolecules have amino, carboxylic, thiol, or hydroxyl groups, which limit the type of

chemistry that can be used for conjugation to these functional groups, the basic conjugation schemes are based on activation of carboxylic groups, activation of amino groups and chemisorption (-SH groups).[32] For these purposes the reagents such as carbodiimide, succinimide esters and maleinimides are often used for covalent binding of the enzymes onto support materials bearing $–NH_2$, –SH, or –COOH groups on their surface.

These conjugation strategies use one or more of the reaction pathways summarized in figure 19, which only shows a subset of all possible conjugation chemistries available.[35] Hydroxylated surfaces are first modified with carbonyldiimidazole (CDI) to form a reactive intermediate, which forms a stable carbamate bond to an amino-terminated biomolecule group (figure 19a) Amine-terminated surfaces provide several options for biomolecule attachment. For example, a surface amine group can be modified with glutaraldehyde, which forms an imine bond (sometimes referred to as a Schiff's base) with an aldehyde, leaving the other aldehyde free for repeating this chemistry with an amino-terminated biomolecule group (figure 19b). Symmetrical diisothiocyanates have also been used as bifunctional linkers for attachment of amine-functionalized surfaces to either thiol-terminated or amine-terminated biomolecules (figure 19c). Finally, a widely used method to covalently immobilize enzymes onto carboxylated surfaces through their anino groups is the 1-ethyl-3-(3-dimethylaminopropyl)carbodiimide (EDC)/ N-hydroxysuccinimide (NHS) coupling (Scheme 19e).

[35] S. Balamurugan et al., "Surface Immobilization Methods for Aptamer Diagnostic Applications," *Analytical and Bioanalytical Chemistry* 390, no. 4 (**2008**): 1009–21.

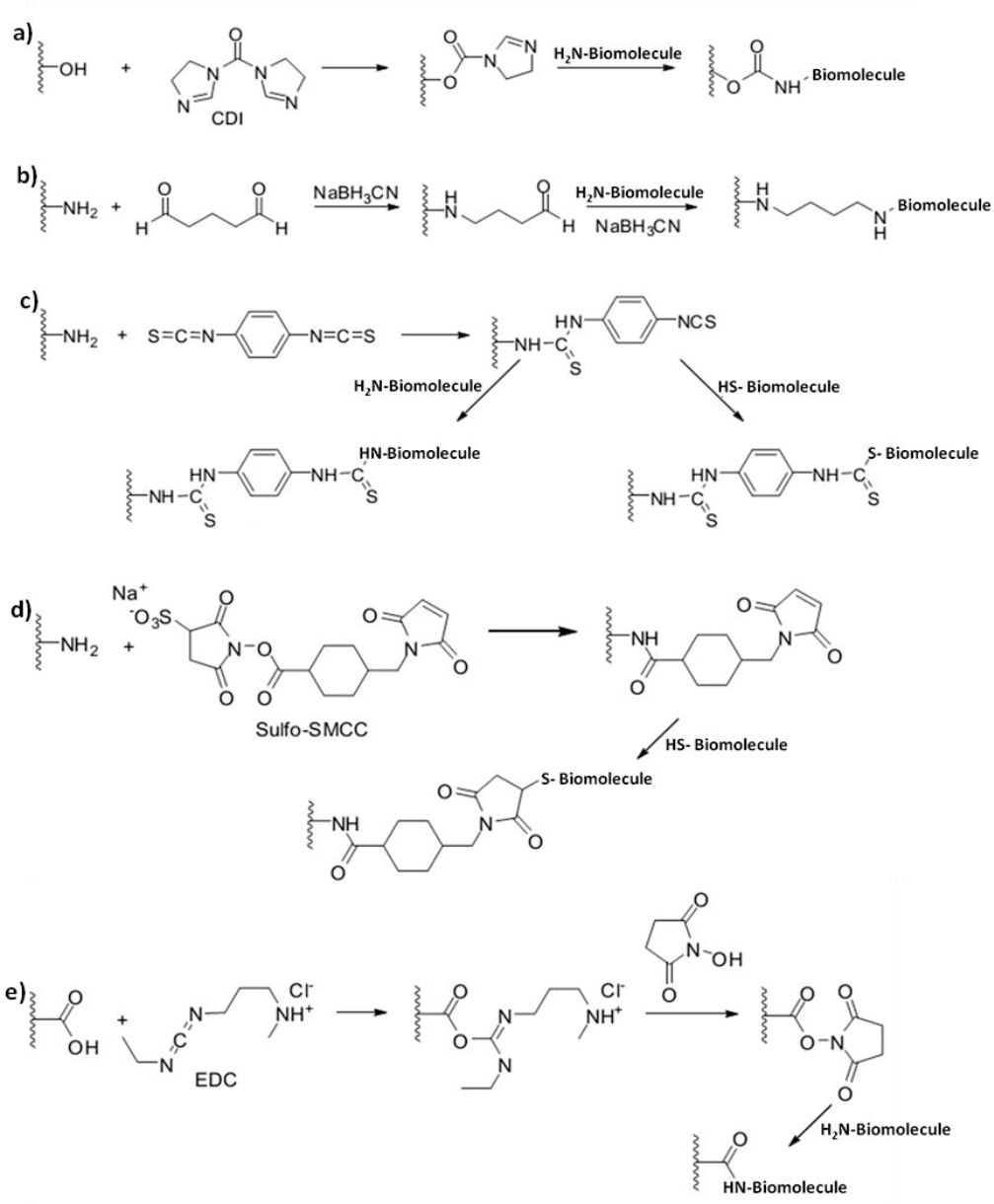

Figure 19. Common reaction sequences reported for covalent attachment of biomolecules to surfaces. CDI: carbonyldiimidazole, SMCC: succinimidyl 4-(N-maleimidomethyl)cyclohexane-1-carboxylate, EDC: 1-ethyl-3-(3-dimethylaminopropyl)carbodiimide, NHS: N-hydroxysuccinimide. Extracted from Ref 35.

Alkanethiol self-assembled monolayers (SAMs)

An easy way to introduce all the above functional groups onto gold surfaces is the functionalization of the latter with SAMs, for subsequent conjugation to biomolecules. A tremendous advantage of this method is that the underlying monolayer can be devised to prevent nonspecific adsorption of biomolecule to the gold surface. Monolayer formation begins with the interaction between the polar moiety (head) of separate molecules and the support surface (figure 20). The subsequent ordering of the molecules in the monolayer plane, or layer self-assembling, is due to the Van der Waals interaction between the hydrophobic

moieties (tails) of the molecules. Various materials, including silicon, metals, and oxides, can serve as the support. SAMs are usable as a matrix for inclusion of biopolymers and hydrophobic non macromolecular compounds.[4]

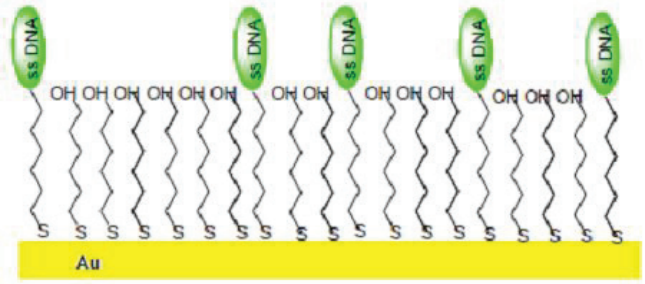

Figure 20. Representative self-assembled monolayer of C_nH_{2n+1} alkanethiol on the surface of gold electrode of a DNA sensor. Extracted from Ref 8.

Afinity: Efforts have been achieved in order to develop biosensors based on oriented and site-specific immobilization of enzymes. A strategy is to create (bio)affinity bonds between an activated support (e.g.with lectin, avidin, metal chelates) and a specific group (a tag) of the protein sequence (e.g. carbohydrate residue, biotin, histidine). This method allows to control the biomolecule orientation in order to avoid enzyme deactivation and/or active site blocking. Several affinity methods have been described to immobilize enzymes through (strept)avidin-biotin, lectin-carbohydrate and metal cation–chelator interactions. An enzyme can contain affinity tags in its sequence (e.g. a sugar moiety) but, in some cases, the affinity tag (e.g. biotin) needs to be attached to the protein sequence by genetic engineering methods such as site-directed mutagenesis, protein fusion technology and post-transcriptional modification.[32]

I.2. Impact of Nanotechnology on Biosensing

Recent trends in nanotechnology have brought new possibilities for developing novel electrochemical biosensors of improved sensitivity, specificity, speed, and cost.[36, 37] The miniaturization of sensors[38] within nanometer dimensions provides great versatility for incorporation into multiplexed, portable, wearable, and even implantable medical devices. Nanomaterials or matrices with at least one of their dimensions ranging in scale from 1 to 100 nm, have also acquired an important impact on the development of electrochemical biosensors.[39]

Since the fundamental processes of life occur at the nanoscale considering that most biological systems including viruses, membranes and protein complexes are naturally nanostructured materials, biosensors exploiting nanomaterials can leverage principles and materials common to biological systems.[37] Owing to their similar dimensions with redox proteins, such nanoscale materials have been used to achieve direct electrical wiring of redox enzymes to electrode surface, to promote electrochemical reaction, to impose nanobarcode for biomaterials and to amplify the signal of biorecognition event.[36] Nanomaterials such as metal nanoparticles, carbon nanotubes or nanowires, polymeric nanofibers, magnetic nanoparticles and quantum dots have been actively investigated for their applications in biosensors[40, 41], which have become a new interdisciplinary frontier between biological detection and material science. In the past years, research groups have started to explore an integrated approach combining electronics and biology to build biosensors on the nanoscale. Devices based on nanowires and nanofibers are emerging as powerful platforms for the direct detection of biological and chemical species, including determining low concentrations of proteins and viruses.[42]

There are different strategies for creating next generations of nanobiosensor devices: 1) the use of a completely new class of nanomaterial for sensing purposes, 2) new immobilization strategies, and 3) the new nanotechnological approaches.

---

[36] A. Hayat, G. Catanante and J. Marty, "Current Trends in Nanomaterial-Based Amperometric Biosensors," *Sensors* 14, no. 12 (**2014**): 23439–61.

[37] K.B. Cederquist and S.O. Kelley, "Nanostructured biomolecular detectors: pushing performance at nanoscale," Current Opinion in Chemical Biology 16, no.3-4 (**2012**):415-421.

[38] M. Kuphal et al., "Polymer-Based Technology Platform for Robust Electrochemical Sensing Using Gold Microelectrodes," *Sensors and Actuators B: Chemical* 161, no. 1 (**2012**): 279–84.

[39] S.H. Lee, J.H. Sung and T.H. Park, "Nanomaterial-Based Biosensor as an Emerging Tool for Biomedical Applications," *Annals of Biomedical Engineering* 40, no. 6 (**2012**): 1384–97.

[40] B.J. Sanghavi et al., "Nanomaterial-Based Electrochemical Sensing of Neurological Drugs and Neurotransmitters," *Microchimica Acta* 182, no. 1–2 (**2015**): 1–41.

[41] W. Zhang et al., "Nanomaterial-Based Biosensors for Environmental and Biological Monitoring of Organophosphorus Pesticides and Nerve Agents," *TrAC Trends in Analytical Chemistry* 54 (**2014**): 1–10.

[42] X.R. Gan and H.M. Zhao, "A review: Nanomaterials Applied in Graphene-Based Electrochemical Biosensors," *Sensors and Materials* 27, no.2 (**2015**): 191-215.

I.2.1. Nanomaterials for New Biosensing Principles

A wide variety of nanostructures have been reported in the literature for interesting analytical applications. Among these, organic and inorganic nanotubes, nanoparticles, and metal oxide nanowires have provided promising building blocks for the realization of nanoscale electrochemical biosensors due to their biocompatibility and the important combination of properties, such as high surface area, good electrical properties, and chemical stability. In particular, the ability to tailor the size and structure and hence the properties of nanomaterials offers excellent prospects for designing novel sensing systems and enhancing the performance of the bioanalytical assay. In this section, we will summarize the progress made in the integration of nanomaterials such as i) **carbon nanotubes** (CNTs), ii) **nanoparticles** (NPs), and iii) **polymer nanostructures**, such as **nanofibers**, in electrochemical biosensing systems and in the following chapters we will offer a fully detailed description of the main principles and applications of these nanomaterial-based biosensing systems.

I.2.1.1. Carbon Nanotubes (CNTs)

Structure, Charasteristics, Synthesis and Functionalization, Applications

Since their discovery in 1991[43], CNTs have attracted great attention from researchers. Through the amazing mechanical and structure-dependent electronic properties, these nanosized cylindrical structures promote many application areas of materials science such as nanoelectronic devices, capacitors, superconducters, and nanocomposites. In particular, fast electron transfer ability, high aspect ratio, electrochemical stability, and biocompatibility properties of CNTs have generated great interest for possible applications in electrochemical biosensing.[44, 45]

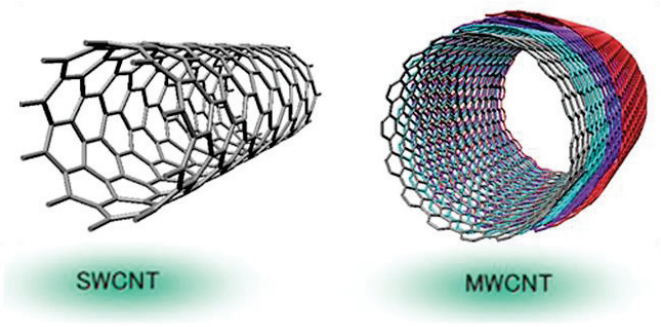

Figure 21. Schematic representations of a SWCNT and a MWCNT.

[43] S. Iijima, "Helical Microtubules of Graphitic Carbon," *Nature,* 354, (**1991**): 56–58.
[44] Z. Wang and Z. Dai, "Carbon Nanomaterial-Based Electrochemical Biosensors: An Overview," *Nanoscale* 7, no. 15 (**2015**): 6420–31.
[45] S. Demirci Uzun et al., "Bioactive Surface Design Based on Functional Composite Electrospun Nanofibers for Biomolecule Immobilization and Biosensor Applications," *ACS Applied Materials & Interfaces* 6, no. 7 (**2014**): 5235–43.

CNTs are fullerene - like structures (Figure 21) that can be single-walled (SWCNTs) or multiwalled (MWNTs).[44] SWNTs are cylindrical graphite sheets of 0.5–1 nm diameter capped by hemispherical ends, while MWNTs comprise several concentric cylinders of these graphitic shells with a layer spacing of 0.3 – 0.4 nm. MWCNTs tend to have diameters in the 2 – 100 nm range. CNTs can be produced by arc discharge methods[46], laser ablation[47], or chemical vapour deposition (CVD)[48], which has the advantage of allowing the control of the location and alignment of synthesized nanostructures. CNTs can be functionalized with different chemical groups using covalent and non-covalent procedures.[51]

Functionalized CNTs are then conjugated to different recognition molecules for bioanalytical applications. Various target analytes can be oxidized by CNTs at low potentials with minimal surface fouling, an appealing feature for the development of electrochemical sensors with high selectivity and reusability.[49] In a SWNT every atom is on the surface and exposed to the environment. Moreover, charge transfer or small changes in the charge environment of a nanotube can cause drastic changes to its electrical properties. The electrocatalytic activity of CNTs has been related to the "topological defects" characteristic of their particular structure. The presence of pentagonal domains in the hemispherical ends or in defects along the graphite cylinder produces regions with charge density higher than in the regular hexagonal network, thus increasing the electroactivity of CNTs.[50] Thus due to their unique electric, electrocatalytic and mechanical properties CNTs have found wide application as electrode materials and a huge number of electrochemical biosensors have been described employing CNTs as a platform for biomolecule immobilization as well as for electrochemical transduction. The only limitation can be their highly stable and closed structure, which does not allow a high degree of functionalization.[49] Adsorption or covalent immobilization can only be achieved at the open end of functionalized nanotubes, after a proper oxidative pretreatment.[51]

[46] S. Iijima and T. Ichihashi, "Single-shell carbon nanotubes of 1-nm diameter", *Nature*, 363, (**1993**): 603-605.
[47] T. Guo et al., "Catalytic Growth of Single-Walled Manotubes by Laser Vaporization," *Chemical Physics Letters* 243, no. 1–2 (**1995**): 49–54.
[48] G. Che et al., "Chemical Vapor Deposition Based Synthesis of Carbon Nanotubes and Nanofibers Using a Template Method," *Chemistry of Materials* 10, no. 1 (**1998**): 260–67.
[49] S.K. Vashist et al., "Advances in Carbon Nanotube Based Electrochemical Sensors for Bioanalytical Applications," *Biotechnology Advances,* 29, 2 (**2011**): 169–88.
[50] G. Rivas et al., "Carbon Nanotubes for Electrochemical Biosensing," *Talanta* 74, no. 3 (**2007**): 291–307.
[51] J.Wang and Y.Lin, "Functionalized Carbon Nanotubes and Nanofibers for Biosensing Applications," *TrAC Trends in Analytical Chemistry* 27, no. 7 (**2008**): 619–26.

Integration of Carbon Nanotubes in Biosensors

One of the first new nanomaterials to impact on amperometric biosensors were **carbon nanotubes** (CNTs), which were blended into a number of formulations to improve current densities and overall performance of enzyme electrodes and enzyme-labelled immunosensors.[52, 53, 54] An extremely important challenge in electrochemical enzyme-based biosensors is the establishment of satisfactory electrical communication between the active site of the enzyme and the electrode surface. Moreover, most electroactive sites of enzymes are electrically insulated by a protein shell. Thus, to fabricate effective enzyme-based biosensors, research on CNT-based biosensors has been focused on two issues: (i) improving the electron-transfer reactions between enzyme and electrodes and, (ii) enhancing the electrochemical reactivity of enzymatic products.[55]

Nevertheless, for biological applications the lack of dispersibility of CNTs in aqueous media has been a major technical barrier. Great efforts have been devoted to finding cost-effective approaches to functionalize CNTs for attachment of biomolecules, such as proteins (e.g., enzymes, anti-bodies), DNA and aptamers. In general, to achieve maximum attachment of biomolecules and keep the activity of the biomolecules on the CNTs, the choice of methods for treating CNTs and the method for attaching biomolecules are very critical for the performance of the biosensors.

According to the orientation of CNTs on the electrode surface, two approaches are generally used for immobilizing CNTs on electrodes: (i) non-aligned and (ii) aligned. In the non-aligned approach, CNTs are randomly immobilized on the electrode surface by physical adsorption (e.g., casting or spin casting) and composite entrapment using polymers and sol-gel. On the other hand, several approaches have been developed to achieve density-controlled, aligned CNTs. Both approaches are widely used for biosensor developments. The adsorption of CNTs on an electrode surface is a simple approach, while aligned CNTs on the electrode surface make electron transfer easier due to the high conductance of the edge plane of CNTs. Moreover, aligned CNTs can be prepared in parallel for fabricating CNT arrays on a substrate.[52]

Vertically aligned CNTs act as molecular wires (‘nanoconnectors’) to facilitate direct electron transfer between the underlying electrode and the redox centers of enzymes.[6] For instance, Willner’s group[56] demonstrated that aligned reconstituted glucose oxidase (GOx) on the edge of SWCNT can be linked to an electrode surface (figure 22). Such enzyme

[52] Z. Zhu et al., “A Critical Review of Glucose Biosensors Based on Carbon Nanomaterials: Carbon Nanotubes and Graphene,” *Sensors* 12, no. 12 (**2012**): 5996–6022.

[53] C.B. Jacobs, M. Jennifer Peairs, and B. Jill Venton, “Review: Carbon Nanotube Based Electrochemical Sensors for Biomolecules,” *Analytica Chimica Acta* 662, no. 2 (**2010**): 105–27.

[54] L. Agüí, P. Yáñez-Sedeño and J.M. Pingarrón, “Role of Carbon Nanotubes in Electroanalytical Chemistry,” *Analytica Chimica Acta* 622, no. 1–2 (**2008**): 11–47.

[55] J. Filip, P. Kasak and J. Tkac, “Graphene as signal amplifier for preparation of ultrasonic electrochemical biosensors,” *Chemical papers* 69, no.1 (**2015**): 112-133.

[56] F. Patolsky, Y. Weizmann, and I. Willner, “Long-Range Electrical Contacting of Redox Enzymes by SWCNT Connectors,” *Angewandte Chemie International Edition* 43, no. 16 (**2004**): 2113–17.

reconstitution on the end of CNT represents an extremely efficient approach for 'plugging' an electrode into GOx. Electrons were thus transported along distances higher than 150 nm with the length of the SWCNT controlling the rate of electron transport. An interfacial electron transfer rate constant of 42 s^{-1} was estimated for 50 nm long SWCNT. Efficient direct electrical connection to GOx was reported also by Gooding's group[57] in connection to aligned SWCNT arrays.

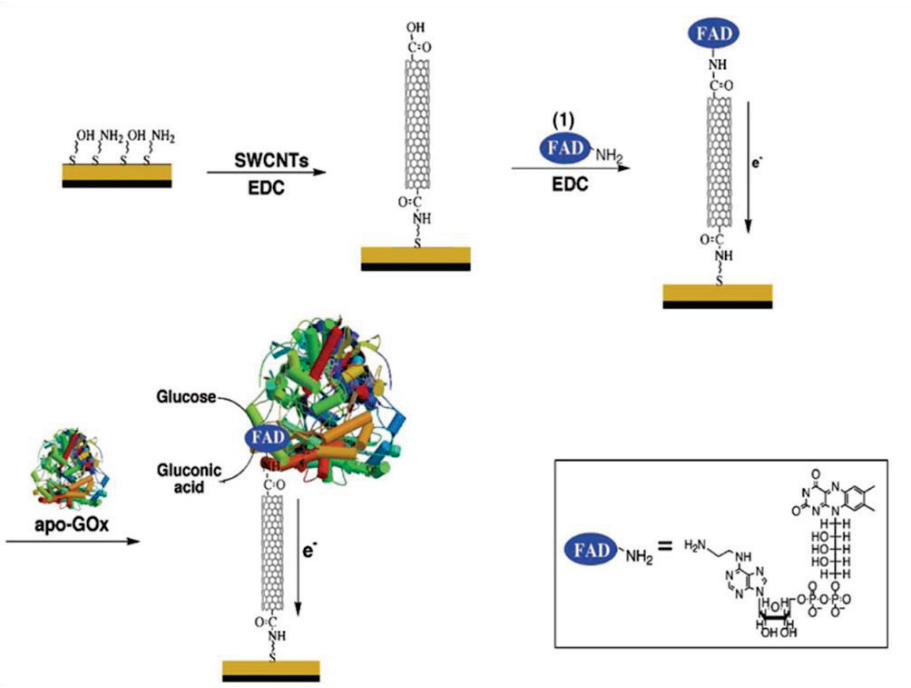

Figure 22. Assembly of SWCNT electrically contacted glucose oxidase electrode: linking the reconstituted enzyme, on the edge of the FAD-functionalized SWCNT, to the electrode surface. Extracted from Ref 56.

Nanowire biosensors are a class of nanobiosensors, of which the major sensing components are made of nanowires coated by biological molecules such as DNA molecules, proteins/enzymes, etc. The nanomaterials transduce the chemical binding event on their surface into a change in the conductance of the nanowire in an extremely sensitive, real time and quantitative fashion. In particular, the use of carbon nanowires for biosensor development has grown in recent years because of their physical and chemical properties (e.g., conductivity, surface area, inherent and induced chemical functionalities, and biocompatibility). Recent activity on carbon nanowire-based biosensors has focused on functionalization of the carbon nanowires for biosensing DNA and proteins.[51] The functionalization of carbon nanowires is critical for utilizing their specific properties for biosensor development. Some approaches to biochemical functionalization of synthetic carbon nanowires have been studied, including physical adsorption and covalent bonding. Electrochemical techniques are often used to produce functional groups on the surface of

[57] J.J. Gooding et al., "Protein Electrochemistry Using Aligned Carbon Nanotube Arrays," *Journal of the American Chemical Society* 125, no. 30 (**2003**): 9006–7.

carbon nanowires for further modifications. Vamvakaki et al.[58] reported a glucose biosensor based on highly-activated carbon nanowires with direct enzyme immobilization. This is a highly efficient method for developing very sensitive, stable, reproducible electrochemical biosensors. Wu and co-workers[59] reported a carbon nanowire-based amperometric glucose sensor, which showed excellent catalytic activity of soluble carbon nanowires. It was obtained with a simple nitric-acid treatment, with electro-reduction of dissolved oxygen at a low operating potential. The carbon nanowire membrane showed good stability and provided fast response to dissolved oxygen. The use of a low operating potential (-0.3 V) and a Nafion membrane also produced good selectivity toward glucose detection.

To sum up, the above studies and many more performed by a great number of research groups have demonstrated that CNT enhance the electrochemical reactivity of important biomolecules and promote the electron-transfer reactions of proteins (including those where the redox center is embedded deep within the glycoprotein shell). In addition to enhanced electrochemical reactivity, CNT-modified electrodes have been shown useful to accumulate important biomolecules (e.g., nucleic acids) and to alleviate surface fouling effects (such as those involved in the NADH oxidation process). The remarkable sensitivity of CNT conductivity to the surface adsorbates permits the use of CNT as highly sensitive nanoscale sensors. The above mentioned properties make CNT extremely attractive for a wide range of electrochemical biosensors applications, ranging from amperometric enzyme electrodes to DNA hybridization biosensors.

I.2.1.2. Nanoparticles (NPs)

One of the most versatile classes of nanomaterials is **nanoparticles**. Depending on their composition (metal, semiconductor, magnetic), nanosize particles (or beads) exemplify different functions in electroanalytical applications. Nanoparticles (NPs), especially nobel metallic nanoparticles (MNPs), have unique electrical, optical, magnetic, and catalytic properties in addition to their pronounced biocompatibility, thus their potential applications in the fields of nanotechnology, materials science, biomedical engineering, tissue engineering and biosensing have been an area of intense scientific interest.[81] Metal nanoparticles provide three main functions: enhancement of electrical contact between biomolecules and electrode surface, catalytic effects, and, together with semiconductor ones, labeling and signal amplification.[60, 61]They are typically obtained by chemical reduction of corresponding transition metal salts in the presence of a stabilizer (self-assembled monolayers, microemulsions, polymers matrixes), which give the surface stability and proper

[58] V.Vamvakaki, K. Tsagaraki and N.Chaniotakis, "Carbon Nanofiber-Based Glucose Biosensor," *Analytical Chemistry* 78, no. 15 (**2006**): 5538–42.

[59] L. Wu, X. Zhang and H. Ju, "Amperometric Glucose Sensor Based on Catalytic Reduction of Dissolved Oxygen at Soluble Carbon Nanofiber," *Biosensors and Bioelectronics* 23, no. 4 (**2007**): 479–84.

[60] L. Ding et al., "Utilization of Nanoparticle Labels for Signal Amplification in Ultrasensitive Electrochemical Affinity Biosensors: A Review," *Analytica Chimica Acta* 797 (**2013**): 1–12.

[61] L. Wang et al., "Nanoparticle-Based Environmental Sensors," *Materials Science and Engineering: R: Reports* 70, no. 3–6 (**2010**): 265–74.

functionalization, in order to modulate charge and solubility properties.[62] Among them, the most widely used for biosensing applications have been gold nanoparticles (AuNPs) because of their unique biocompatibility, structural, electronic, and catalytic properties.

Gold Nanoparticles-A Special Case

The unique ability of gold nanoparticles to provide a suitable microenvironment for biomolecules immobilization retaining their biological activity is a major advantage for the preparation of biosensors. Furthermore, gold nanoparticles permit direct electron transfer between redox proteins and bulk electrode materials[63], thus allowing electrochemical sensing to be performed with no need for electron transfer mediators. Characteristics of gold nanoparticles such as high surface-to-volume ratio, high surface energy, ability to decrease proteins–metal particles distance, and the functioning as electron-conducting pathways between prosthetic groups and the electrode surface, have been claimed as reasons to facilitate electron transfer between redox proteins and electrode surfaces. Gold nanoparticles have also demonstrate to constitute useful interfaces for the electrocatalysis of redox processes of molecules such as H_2O_2, O_2 or NADH involved in many significant biochemical reactions.[64, 65]

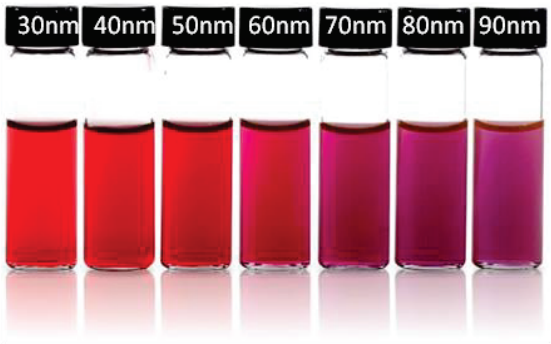

Figure 23. Solutions of gold nanoparticles of various sizes. Nano-Gold colloids exhibit different colours at different sizes and concentrations.

[62] S. Guo and Erkang Wang, "Synthesis and Electrochemical Applications of Gold Nanoparticles," *Analytica Chimica Acta* 598, no. 2 (**2007**): 181–92.
[63] Y. Xiao et al., "'Plugging into Enzymes': Nanowiring of Redox Enzymes by a Gold Nanoparticle," *Science*, **2003**, 299 edition.
[64] E. Hutter and Dusica Maysinger, "Gold-Nanoparticle-Based Biosensors for Detection of Enzyme Activity," *Trends in Pharmacological Sciences* 34, no. 9 (**2013**): 497–507.
[65] Y. Li, Hermann, J. Schluesener and S. Xu, "Gold Nanoparticle-Based Biosensors," *Gold Bulletin* 43, no. 1 (**2010**): 29–41.

Integration of Gold Nanoparticles in Biosensors

The electrodes are usually modified by AuNPs in different ways to improve the performance of the biosensor.[66, 67, 68] Among the various strategies followed, a useful and simple way consists on the direct deposition of nanoparticles onto the electrode surface. For example, tyrosinase immobilization by cross-linking onto a GCE modified with electrodeposited gold nanoparticles was used to prepare a biosensor which showed a high activity towards various phenolic compounds.[69] Also, gold electrodes can be modified by attachement of AuNPs *via* covalent bond. A glucose biosensor was prepared by covalent attachment of GOx to a gold nanoparticle monolayer-modified Au electrode.[70] The so prepared biosensor exhibited a wide linear range of glucose response, high sensitivity, good reproducibility and stability.

Generally, modification of electrode surfaces with self-assembled mono-layers (SAMs) of thiols provides a simple way to design tailored materials that can be further used as functionalized sites to immobilize gold nanoparticles and enzymes. A comparison of the analytical performance of different GOx biosensor designs based on several SAM-modified electrodes showed that a configuration involving colloidal gold bound to cysteamine monolayers self-assembled on a gold disk electrode exhibited a high sensitivity and a long biosensor lifetime in comparison with other GOx biosensors. Schemes displaying the different strategies for GOx biosensors preparation using tailored gold nanoparticle-modified electrodes are shown in Figure 24. Multilayer films of GOx/gold nanoparticles on the Au electrode surface using cysteamine as a covalent attachment cross-linker were prepared by layer-by-layer (LBL) technique, which has attracted much attention because of its simplicity and wide choice of methods. The bioelectrocatalytic response was directly correlated to the number of deposited bilayers, to the amount of active enzyme immobilized on the Au electrode surface.[71]

---

[66] S. Zeng et al., "A Review on Functionalized Gold Nanoparticles for Biosensing Applications," *Plasmonics* 6, no. 3 (**2011**): 491–506.

[67] J.F. Rusling, "Nanomaterials-Based Electrochemical Immunosensors for Proteins," *The Chemical Record* 12, no. 1 (**2012**): 164–76.

[68] M. Hasanzadeh et al., "Dendrimer-Encapsulated and Cored Metal Nanoparticles for Electrochemical Nanobiosensing," *TrAC Trends in Analytical Chemistry* 53 (**2014**): 137–49.

[69] J.M. Pingarrón, P. Yáñez-Sedeño and A. González-Cortés, "Gold Nanoparticle-Based Electrochemical Biosensors," *Electrochimica Acta* 53, no. 19 (**2008**): 5848–66.

[70] N.D. Dimcheva and E.G. Horozova, "Electrochemical Enzymatic Biosensors Based on Metal Micro-/nanoparticles-Modified Electrodes: A Review," *Chemical Papers* 69, no. 1 (**2015**): 17-26.

[71] A.A. Saei et al., "Electrochemical Biosensors for Glucose Based on Metal Nanoparticles," *TrAC Trends in Analytical Chemistry* 42, no. 0 (**2013**): 216–27.

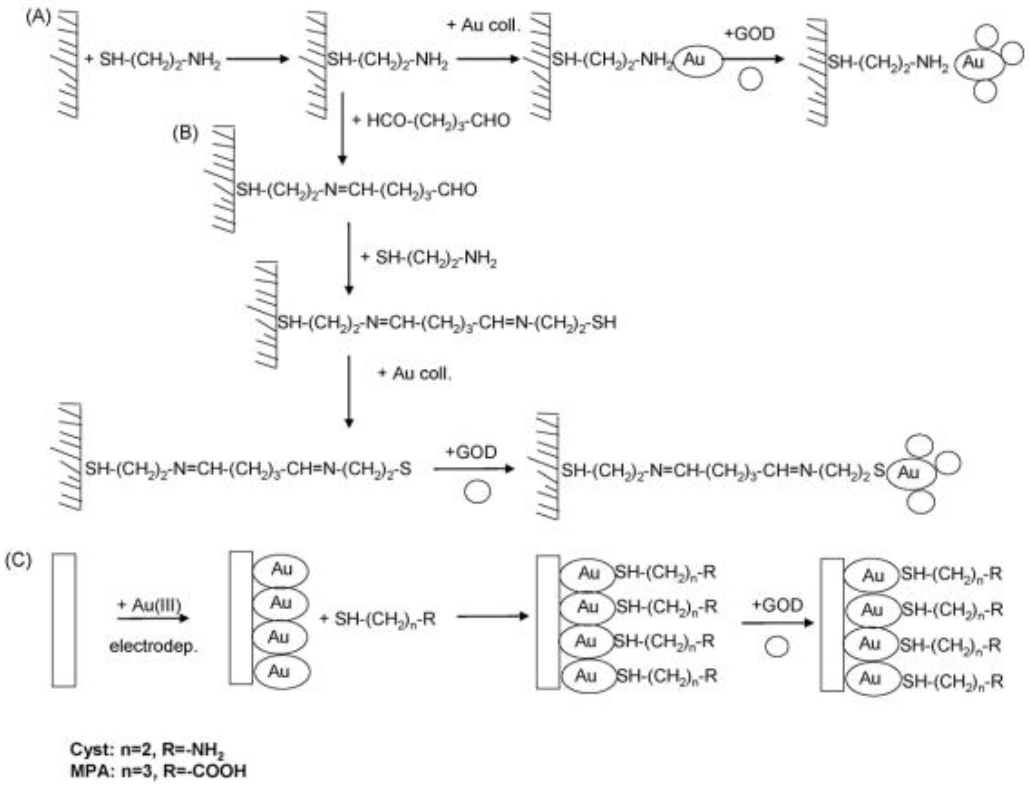

Figure 24. Schemes of different GOx biosensors constructed by means of different tailored gold nanoparticle-modified electrode surfaces: (A) GOx/colloidal gold–cysteamine–AuE; (B) GOx/colloidal gold–cysteamine/cysteamine–AuE; (C) GOx/cysteamine–electrodeposited gold nanoparticles–GCE or GOx/3-mercaptopropionic acid (MPA)–electrodeposited gold nanoparticles–GCE. Extracted from Ref 69.

AuNPs/enzyme hybrid systems have been widely investigated by Willner's group[72, 73] in order to overcome the lack of electrical communication often observed between redox enzymes and an electrode surface. When it was realized that the spatial separation between the active site and the electrode is due to the isulating protein shell, AuNPs were used as nanoconnectors to shorten electron transfer distances and mediate charge transport. Biocatalytic electrodes were prepared by conjugation of ap-GOx (apoprotein form) with AuNPs functionalized with a flavin adenine dinucleotide cofactor unit extracted from active GOx and self-assembled on a dithiol-modified gold electrode. In this way, nanoparticles were implanted in intimate contact with the active site of the enzyme, thus forming a hybrid architecture that facilitated the electrocatalytic oxidation of glucose, thanks to highly efficient electron transport.

[72] Y.M. Yan et al., "Biocatalytic Growth of Au Nanoparticles Immobilized on Glucose Oxidase Enhances the Ferrocene-Mediated Bioelectrocatalytic Oxidation of Glucose," *Advanced Materials* 20, no. 12 (**2008**): 2365–70.
[73] I. Willner, Bernhard Basnar, and Bilha Willner, "Nanoparticle-Enzyme Hybrid Systems for Nanobiotechnology: Nanoparticle-Enzyme Hybrid Systems," *FEBS Journal* 274, no. 2 (**2007**): 302–9.

Orozco et al.[74] demonstrated the role of AuNPs in enhancing the voltammetric performance of ultra -microelectrodes based biosensors through a comparative study of bare and nanoparticle modified surfaces using HRP as a model recognition element. HRP was covalently immobilized by means of a thiol self-assembled monolayer used for the amperometric detection of catechol. The use of AuNPs increased the sensitivity of the developed biosensor 3-fold with respect to bare microelectrodes.

Conjugation of gold nanoparticles with other nanomaterials and biomolecules is another useful strategy for the preparation of enzyme biosensors with improved analytical performance. These devices exhibit the characteristics of the involved nanomaterials and also the advantages of composite electrodes, such as low background currents, a great versatility because it is possible to incorporate different substances into the bulk of the electrode matrix, and an easy surface regeneration. In this context, hybrid nanoparticles/nanotubes materials have shown to possess interesting properties, which can be profited for the development of electrochemical biosensors. A colloidal gold–CNT composite electrode using Teflon as the non-conducting binding material showed significantly improved responses to H_2O_2 when compared with other carbon composite electrodes, including those based on CNTs. The incorporation of GOx into the new composite matrix allowed the preparation of a mediatorless glucose biosensor with a remarkably higher sensitivity than that from other GOx–CNT bioelectrodes.[75] Hybrid composites can be also prepared by selective attachment of gold nanoparticles to carbon nanotubes surfaces. This requires previous CNTs functionalization to immobilize gold nanoparticles. So, cationic polyethyleneamine or anionic citrate used as dispersants can change the surface properties of CNTs yielding acidic or basic surfaces. Then, CNTs could be successfully coated with gold nanoparticles by electrostatic interaction.

In another configuration, a direct electrochemical biosensing platform was fabricated by covalent incorporation of CNTs and gold nanoparticles onto a GCE modified with electropolymerized poly(thionine). The synergic effects of the composite nanomaterials together with the excellent mediating ability of the redox polymer, allowed faster electron transfer and higher enzyme immobilization efficiency than the designed based on CNTs or gold nanoparticles, as it was demonstrated using HRP as a test enzyme model. Furthermore, in enzyme biosensors based on hybrid AuNPs-polymer materials, the presence of gold nanoparticles in the conductive polymer matrix provides enhanced electrochemical activity/conductivity and restricts enzyme leaking while allowing rapid diffusion of substrate and product using small amount of enzyme. To sum up, in table 2 we present the various roles that AuNPs have played in the development of biosensing systems.[65]

[74] J. Orozco, C. Jiménez-Jorquera and C. Fernández-Sánchez, "Gold Nanoparticle-Modified Ultramicroelectrode Arrays for Biosensing: A Comparative Assessment," *Bioelectrochemistry* 75, no. 2 (**2009**): 176–81.

[75] J. Manso et al., "Electrochemical Biosensors Based on Colloidal Gold–carbon Nanotubes Composite Electrodes," *Journal of Electroanalytical Chemistry* 603, no. 1 (**2007**): 1–7.

Table 2. Different functions of AuNPs in electrochemical biosensor systems.

Principle of detection	Functions of AuNPs	Properties used	Sensor advantages
Changes in electrical characteristics	Immobilization platform	Biocompatibility, large surface area	Improved sensitivity and stability
	Catalysis of reactions/ Enhancement of electron transfer	High surface energy, interface-dominated properties	Improved sensitivity and stability

I.2.1.3. Polymer Nanostructures

Another class of nanomaterials that exhibit appealing properties for sensor applications are polymeric nanostructures.

Fabrication of Polymer Nanostructures

Technologies based on polymer nanostructures have been restricted in deploying on a commercial scale, mainly due to a lack of reliable and reproducible synthetic techniques. Therefore, the development of synthetic routes to polymer nanomaterials is a subject of great interest in contemporary nanoscopic research.[76, 77] The synthetic strategies for obtaining polymer nanomaterials can be classified into hard-template synthesis, soft-template synthesis, and template-free synthesis.[78]

The hard template approach involves a synthesis of nanostructured polymers within the pores or channels of membranes. Hard-template synthesis is advantageous in tailoring the dimensions of nanomaterials.[79, 80] It has been widely implemented in the preparation of highly oriented and ordered one-dimensional nanostructures such as: core/shell nanoparticles, nanocapsules, nanorods, nanotubes, nanowires, and nanofibers.[81] However, these approaches suffer from disadvantages such as complicated synthetic process, etching away the template material after the formation of the polymer nanostructures, limited production capacity, and comparatively high cost. The soft-template approach has appeared as an alternative strategy to effectively fabricate polymer nanomaterials in a simpler and less expensive way because it

[76] J. Jang et al., "Dual-Functionalized Polymer Nanotubes as Substrates for Molecular-Probe and DNA-Carrier Applications," *Advanced Functional Materials* 16, no. 6 (**2006**): 754–59.
[77] H. Yoon, et al., "Charge-Transport Behavior in Shape-Controlled Poly(3,4-Ethylenedioxythiophene) Nanomaterials: Intrinsic and Extrinsic Factors," *Small* 3, no. 10 (**2007**): 1774–83.
[78] J. Jang, "Conducting Polymer Nanomaterials and Their Applications," in *Emissive Materials Nanomaterials*, vol. 199, Advances in Polymer Science (**2006**), 189–260.
[79] Satyanarayana V.N.T. Kuchibhatla et al., "One Dimensional Nanostructured Materials," *Progress in Materials Science* 52, no. 5 (**2007**): 699–913.
[80] S.I. Cho and S.B. Lee, "Fast Electrochemistry of Conductive Polymer Nanotubes: Synthesis, Mechanism, and Application," *Accounts of Chemical Research* 41, no. 6 (**2008**): 699–707.
[81] K. Jackowska, A.T. Bieguński and M. Tagowska, "Hard Template Synthesis of Conducting Polymers: A Route to Achieve Nanostructures," *Journal of Solid State Electrochemistry* 12, no. 4 (**2008**): 437–43.

eliminates the use of the solid template and postsynthesis etching procedure.[82] Soft template synthesis requires the presence of the structure-directing molecules such as surfactants, block copolymers, polyelectrolytes, liquid crystals, and biomolecules.[83] In addition to the template approach, the polymer nanostructures can be formed by no-template techniques, such as radiolytic, sonochemical, electrochemical techniques, rapid mixing reactions, and interfacial polymerization. Template-free synthesis is very straightforward without using specific sacrificial templates. However, this approach is limited to particular precursor materials.

The aforementioned approaches require post-synthetic process for incorporating the nanomaterials into sensing systems, during which the soft structures may be damaged or obtained in the form of aggregates. Moreover, precise control on manipulation and positioning of the nanomaterials is rather difficult and one must employ some pick-and-place technique to capture the nanostructures and to position them at the point of use, fact that often results in low device yield and irreproducible sensor response. Accordingly, there has been some effort to directly fabricate nanomaterials-integrated sensing systems such as nanowire electrode junctions using electrochemical and lithographic techniques.[84] Although such methods yield controlled conducting polymer microstructures, they also possess limitations for creating structures with sub-100-nm dimensions on a large scale. It still remains a challenge to discover efficient, scalable, and site-specific methods for integrating the nanomaterials into sensing systems.[85]

Among the various existing synthetic strategies for obtaining nanostructures, such as template synthesis methods, soft lithography, drawing, phase separation, self-assembly etc., electrospinning technique was chosen in this work for the fabrication of nanofibers in view of electrochemical biosensor fabrication.[86] Electrospinning is a broadly used technology for electrostatic fiber formation which utilizes electrical forces to produce polymer fibers with diameters ranging from 2 nm to several micrometers using polymer solutions.[87] A comparison of the various issues relating to these processing methods is displayed in Table 3a and 3b.[88] The electrospinning technique offers many benefits, such as the simplicity and versatility and low cost requirements of the processing system, positioning of the nanostructures to the point of use, no need of post-synthetic treatment for incorporating the nanomaterials into biosensing

[82] J. Chen et al., "The Design, Synthesis and Characterization of Polyaniline Nanophase Materials," *Comptes Rendus Chimie* 11, no. 1–2 (January 2008): 84–89, doi:10.1016/j.crci.2007.06.008.
[83] G. Cao and D. Liu, "Template-Based Synthesis of Nanorod, Nanowire, and Nanotube Arrays," *Advances in Colloid and Interface Science* 136, no. 1–2 (**2008**): 45–64.
[84] A. Pimpin and W. Srituravanich, "Review on Micro- and Nanolithography Techniques and Their Applications," *Engineering Journal* 16, no. 1 (**2012**): 37–56.
[85] H. Yoon and J. Jang, "Conducting-Polymer Nanomaterials for High-Performance Sensor Applications: Issues and Challenges," *Advanced Functional Materials* 19, no. 10 (**2009**): 1567–76.
[86] S. Ramakrishna et al., "Electrospun Nanofibers: Solving Global Issues," *Materials Today* 9, no. 3 (**2006**): 40–50.
[87] N.Bhardwaj and S.C. Kundu, "Electrospinning: A Fascinating Fiber Fabrication Technique," *Biotechnology Advances* 28, no. 3 (**2010**): 325–47.
[88] S. Ramakrishna, *An Introduction to Electrospinning and Nanofibers* (Singapore; Hackensack, NJ: World Scientific, **2005**).

systems. Furthermore, ES is superior in production and construction of ordered or more complex nanofibrous assemblies

In the following sections we will only focus on the electrospinning technique and its application to biosensors since it was the technique which was used to fabricate nanofibers in this work.

Table 3a. Comparison of processing techniques for obtaining nanofibers.[88]

Process	Technological advances	Can the process be scaled?	Repeatability	Convenient to process?	Control on fiber dimensions
Drawing	Laboratory	✖	✓	✓	✖
Template Synthesis	Laboratory	✖	✓	✓	✓
Phase Separation	Laboratory	✖	✓	✓	✖
Self-Assembly	Laboratory	✖	✓	✖	✖
Electrospinning	Laboratory (with potential for industrial processing)	✓	✓	✓	✓

Table 3b. Advantages and disadvantages of various processing techniques. [88]

Process	Advantages	Disadvantages
Drawing	Minimum equipment requirement	Discontinuous process
Template Synthesis	Easy creation of fibers of different diameters by using different templates	Complicated synthetic process, Required post-synthetic process
Phase Separation	Minimum equipment requirement. Process can directly fabricate a nanofiber matrix. Batch-to-batch consistency is achieved easily. Mechanical properties of the matrix can be tailored by adjusting polymer concentration.	Limited to specific polymers
Self-Assembly	Good for obtaining smaller nanofibers	Complex process
Electrospinning	Low cost requirements, production of long, continuous nanofibers	Jet instability

I.3. Electrospinning

With the emergence of nanotechnology, researchers become more interested in studying the unique properties of nanoscale materials. Electrospinning is an electrostatic nanofiber fabrication technique which has attracted more interest in recent years due to its versatility and potential for applications in diverse fields. It produces polymer fibers with diameters ranging from 2nm to several micrometers. Besides traditional two-dimensional (2D) nanofibrous structures, electrospinning is powerful in fabrication of three-dimensional (3D) fibrous macrostructures.[89, 90] Electrospun fibers have notable applications including tissue engineering,[91] sensors/ biosensors, [89, 92, 93] electronics,[94] catalysis,[95] textiles, filters, actuators,[96] energy storage,[97, 98] protective clothing, drug delivery, wound dressings and wound healing[99] and enzyme immobilization.[100] The most representative applications of electrospinning are depicted in figure 25.

[89] Z. Su, J. Ding, and G.Wei, "Electrospinning: A Facile Technique for Fabricating Polymeric Nanofibers Doped with Carbon Nanotubes and Metallic Nanoparticles for Sensor Applications," *RSC Adv.* 4, no. 94 (**2014**): 52598–610.

[90] B. Sun, Y.Z. Long, H.D. Zhang, M.M Li, J.L. Duvail, X.Y. Jiang and H.L. Yin, "Advances in Three-Dimensional Nanofibrous Macrostructures via Electrospinning," *Progress in Polymer Science* 39, no. 5 (**2014**): 862–90.

[91] Xuegang Zhou et al., "In Vitro Hydrolytic and Enzymatic Degradation of Nestlike-Patterned Electrospun poly(D,L-Lactide-Co-Glycolide) Scaffolds," *Journal of Biomedical Materials Research Part A* 95A, no. 3 (**2010**): 755–65.

[92] M. Scampicchio, A. Bulbarello, A. Arecchi, M. S. Cosio, S. Benedetti, S. Mannino, "Electrospun Nonwoven Nanofibrous Membranes for Sensors and Biosensors," *Electroanalysis* 24, no. 4 (**2012**): 719–25.

[93] S. Agarwal, J.H. Wendorff, and A. Greiner, "Use of Electrospinning Technique for Biomedical Applications," *Polymer* 49, no. 26 (**2008**): 5603–21.

[94] A. Luzio, E.V. Canesi, C. Bertarelli, M. Caironi, "Electrospun Polymer Fibers for Electronic Applications," *Materials* 7, no. 2 (**2014**): 906–47.

[95] A. Both Engel, Y. Holande, S. Tingry, A. Cherifi, D. Cornu, K. Servat, T. Napporn and K. B. Kokoh, "Electrospun Carbon Fibers: Promising Electrode Material for Abiotic and Enzymatic Catalysis," *The Journal of Physical Chemistry C*, June 11, **2015**, doi:10.1021/acs.jpcc.5b04352.

[96] L. Zhang, A. Aboagye, A. Kelkar, C. Lai, and H. Fong, "A Review: Carbon Nanofibers from Electrospun Polyacrylonitrile and Their Applications," *Journal of Materials Science* 49, no. 2 (**2014**): 463–80.

[97] A. Both Engel, A. Cherifi, S. Tingry, D. Cornu, A. Peigney and C. Laurent, "Enhanced Performance of Electrospun Carbon Fibers Modified with Carbon Nanotubes: Promising Electrodes for Enzymatic Biofuel Cells," *Nanotechnology* 24, no. 24 (**2013**): 245402.

[98] A. Both Engel, A. Cherifi, M. Bechelany, S. Tingry and D. Cornu, "Control of Spatial Organization of Electrospun Fibers in a Carbon Felt for Enhanced Bioelectrode Performance," *ChemPlusChem* 80, no. 3 (**2015**): 494–502.

[99] Y. Liu, Y. Sun, H. Yan, X. Liu, W. Zhang, Z. Wang and X. Jiang ., "Electrospun Fiber Template for Replica Molding of Microtopographical Neural Growth Guidance," *Small* 8, no. 5 (**2012**): 676–81.

[100] W.Chen, S. He, W. Pan, Y. Jin, W. Zhang and X. Jiang, "Strategy for the Modification of Electrospun Fibers That Allows Diverse Functional Groups for Biomolecular Entrapment," *Chemistry of Materials* 22, no. 23 (**2010**): 6212–14.

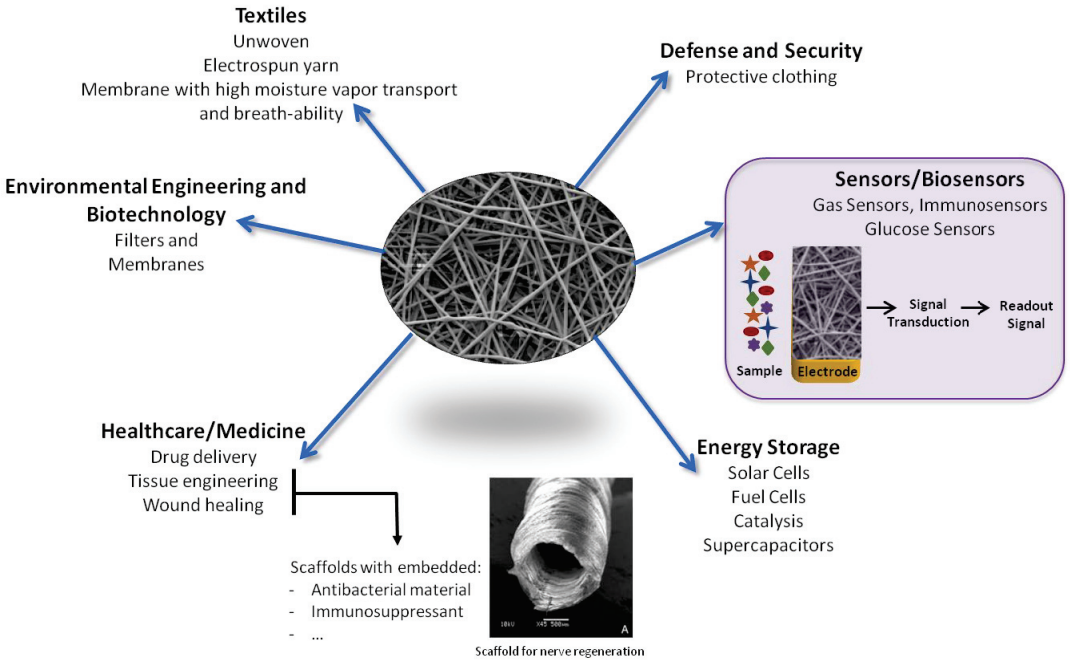

Figure 25. Representative applications of electrospun fibers.

The interest in ES technique to fabricate functional nanomaterials for sensing is growing fast. A survey of open publications related with "electrospinning" and "sensor" in the past 10 years with Web of Science was performed and the result is shown in Figure 26. Meanwhile, the applications of the electrospun nanomaterials for fabricating electrochemical sensors and biosensors are still at an early but promising stage.

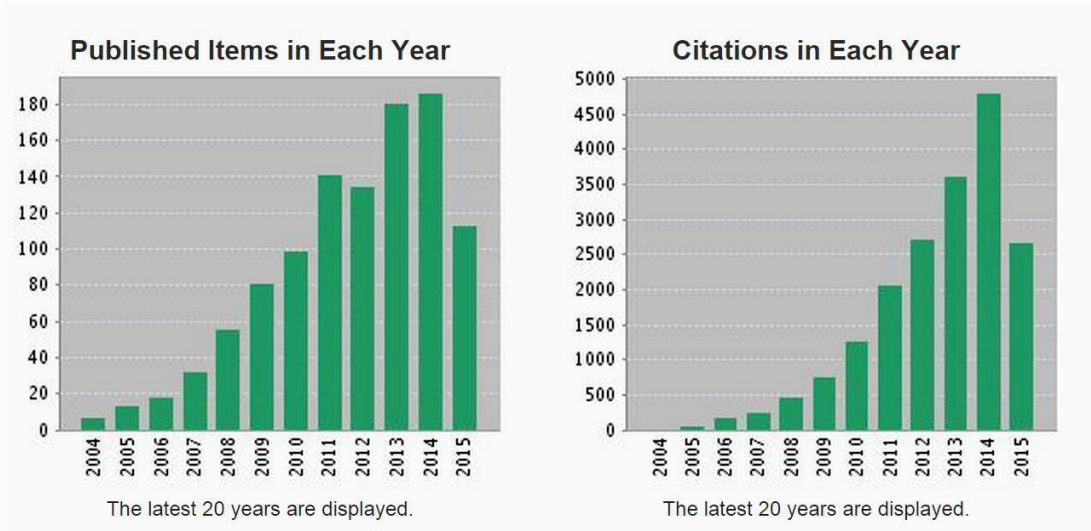

Figure 26. Comparison of the annual number of scientific publications with the keywords "electrospinning" and "sensor", as searched by Web of Science.

The sub-micron range spun fibers produced by ES, offer various advantages such as high surface area to volume ratio, tunable porosity, malleability to conform to a wide variety of sizes and shapes and the ability to control nanofiber composition in order to get desired properties and functionality that is otherwise difficult to achieve by using standard mechanical fiber-spinning techniques. Apart from the huge success and advantages of electrospinning method and spun nanofibers, there are still some challenges that need proper consideration. The limitation of the relatively low production rate of nanofibers has been a bottleneck problem that limits their application. To increase the production rate of the spun fibers, several groups have proposed different ways of producing multiple jets instead of a single one which leads to enhanced performances.

Over the years, more than 200 polymers have been electropun and the number is still increasing gradually with time. In the following sections the electrospinning technique with its promising advantages and potential applications will be described. The electrospinning theory and process, spinnable polymers, polymer solution parameters, processing conditions, ambient parameters and solvent properties will be discussed.[87, 88]

I.3.1. History of Electrospinning

Electrospinning is an old technique, however it was forgotten and rediscovered in the 1990s.[87] The neglect of this technique by researchers is ascribed to two possible reasons. One reason is that the high-voltage electrostatic generation technique was not very mature in the earlier years, and the other is that the small-size effect of the electrospun NFs had not been understood before the development of nanotechnology. The interaction between an electrical field and a polymer solution was first observed in 1897 by Rayleigh and in 1914 Zeleny [101] performed a detailed study on electrospraying. Electrospraying is a method of ionizing delicate macromolecules for mass spectroscopy analysis[102]. To this point, to avoid any confusion, it should be mentioned that electrospinning and electrospraying are two similar technologies which differ mainly in the structure of produced materials. Final products of electrospinning are nanofibers, however the electrospraying results are spherical microparticles.

From 1934 to 1944, Formhals published a series of patents on electrospinning, describing an experimental setup for the production of polymer filaments using an electrostatic force.[103] The first patent (US Patent Number: 2116942) on electrospinning was issued for the fabrication of textile yarns and a voltage of 57 kV was used for electrospinning cellulose acetate using acetone and monomethyl ether of ethylene glycol as solvents. This

[101] J. Zeleny, "The Electrical Discharge from Liquid Points, and a Hydrostatic Method of Measuring the Electric Intensity at Their Surfaces," *Phys. Rev.* 3, no. 2 (**1914**): 69–91.

[102] J. Kameoka et al., "An Electrospray Ionization Source for Integration with Microfluidics," *Analytical Chemistry* 74, no. 22 (**2002**): 5897–5901.

[103] Z.M. Huang et al., "A Review on Polymer Nanofibers by Electrospinning and Their Applications in Nanocomposites," *Composites Science and Technology* 63, no. 15 (**2003**): 2223–53.

process was patented by Antonin Formhals[104] in 1934 and also later granted related patents (U.S. Patents 2116942, 2160962 and 2187306) in 1938, 1939, and 1940.[105] Formhals's spinning process consists of a movable thread collecting device to collect threads in a stretched condition, like that of a spinning drum in conventional spinning.[106] About 50 patents for electrospinning polymer melts and solutions have been filed in the past 60 years.[107] Simons in 1966[108] patented an apparatus for the production of non-woven fabrics that were ultra thin and very light in weight with different patterns using electrical spinning. However, the work of Taylor [109] in 1969, on electrically driven jets has laid the groundwork for electrospinning. In 1971, Baumgarten[110] made an apparatus to electrospin acrylic fibers with diameters in the range of 0.05–1.1 μm.

The term "electrospinning", derived from "electro-static spinning", has been used relatively recently (in around 1994), but its origin can be traced back to more than 60 years ago. With the help of nanotechnology, ES technique was recovered by Reneker et al.[111] in 1996, who found that it is a very simple and powerful technique to generate ultrafine polymeric fibers with diameters ranging from micrometer to nanometer. Since then ES technique has been widely utilized for academic research and industrial applications.[89] The popularity of the ES process can be realized by the fact that over 200 universities and research institutes worldwide are studying various aspects of the electrospinning process and the fiber it produces and also the number of patents for applications based on electrospinning has grown in recent years (Figures 27 and 28). Some companies such as eSpin Technologies, NanoTechnics, and KATO Tech are actively engaged in reaping the benefits of the unique advantages offered by electrospinning, while companies such as Donaldson Company and Freudenberg have been using this process for the last two decades in their air filtration products.[86]

---

[104] A. Formhals, "Process and Apparatus for Preparing Artificial Threads," no. 1975504 (**1934**), http://www.google.de/patents?hl=de&lr=&vid=USPAT1975504&id=_X5oAAAAEBAJ&oi=fnd&dq=formhals&printsec=abstract#v=onepage&q=formhals&f=false.

[105] K. J. Pawlowski et al., "Biomedical Nanoscience: Electrospinning Basic Concepts, Applications, and Classroom Demonstration," *MRS Online Proceedings Library* 827 (**2004**): 17-28.

[106] T. Subbiah et al., "Electrospinning of Nanofibers," *Journal of Applied Polymer Science* 96, no. 2 (**2005**): 557–69.

[107] D. Li and Y. Xia, "Electrospinning of Nanofibers: Reinventing the Wheel?," *Advanced Materials* 16, no. 14 (**2004**): 1151–70.

[108] H.L. Simons, *Process and Apparatus for Producing Patterned Non-Woven Fabrics* (Google Patents, **1966**), http://www.google.com/patents/US3280229.

[109] G. Taylor, "Electrically Driven Jets," *Proceedings of the Royal Society of London. A. Mathematical and Physical Sciences* 313, no. 1515 (**1969**): 453–75.

[110] P.K. Baumgarten, "Electrostatic Spinning of Acrylic Microfibers," *Journal of Colloid and Interface Science* 36, no. 1 (**1971**): 71–79.

[111] D.H. Reneker and I. Chun, "Nanometre Diameter Fibres of Polymer, Produced by Electrospinning," *Nanotechnology* 7, no. 3 (**1996**): 216.

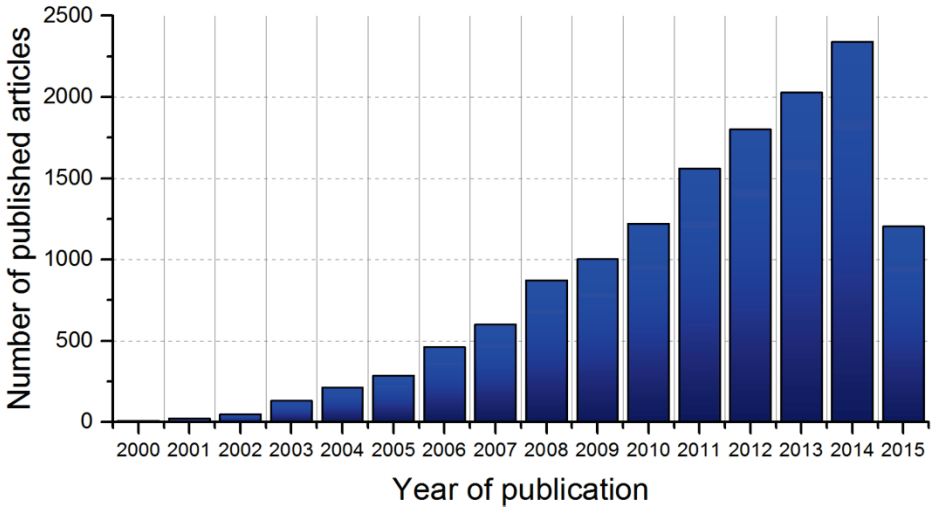

Figure 27. Comparison of the annual number of scientific publications with the keyword "electrospinning" as searched by Web of Science.

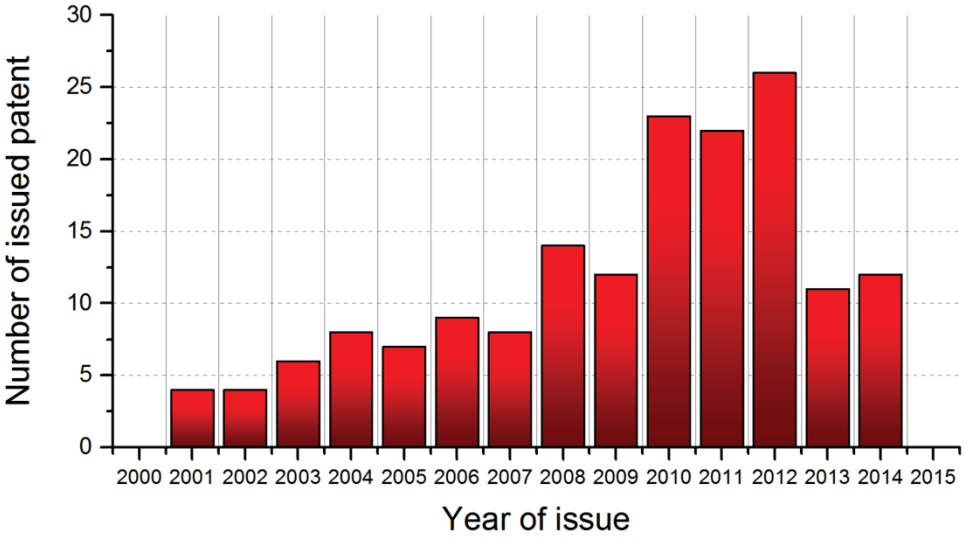

Figure 28. Number of patents for applications based on electrospinning in recent years as searched by Google patent.

I.3.2. Electrospinning Process

Electrospinning is conducted at room temperature with atmosphere conditions. Currently, there are two standard electrospinning setups, vertical and horizontal[87] (figure 29a and b). The ES standard setup consists of four major components: a high-voltage power supply, a spinneret with a metallic needle, a syringe pump and a grounded collector, as shown in Fig. 29a, b. However, some solvents used for the preparation of the electrospun mixture may emit unpleasant or even harmful smells, so the process should be conducted within chambers having a ventilation system.

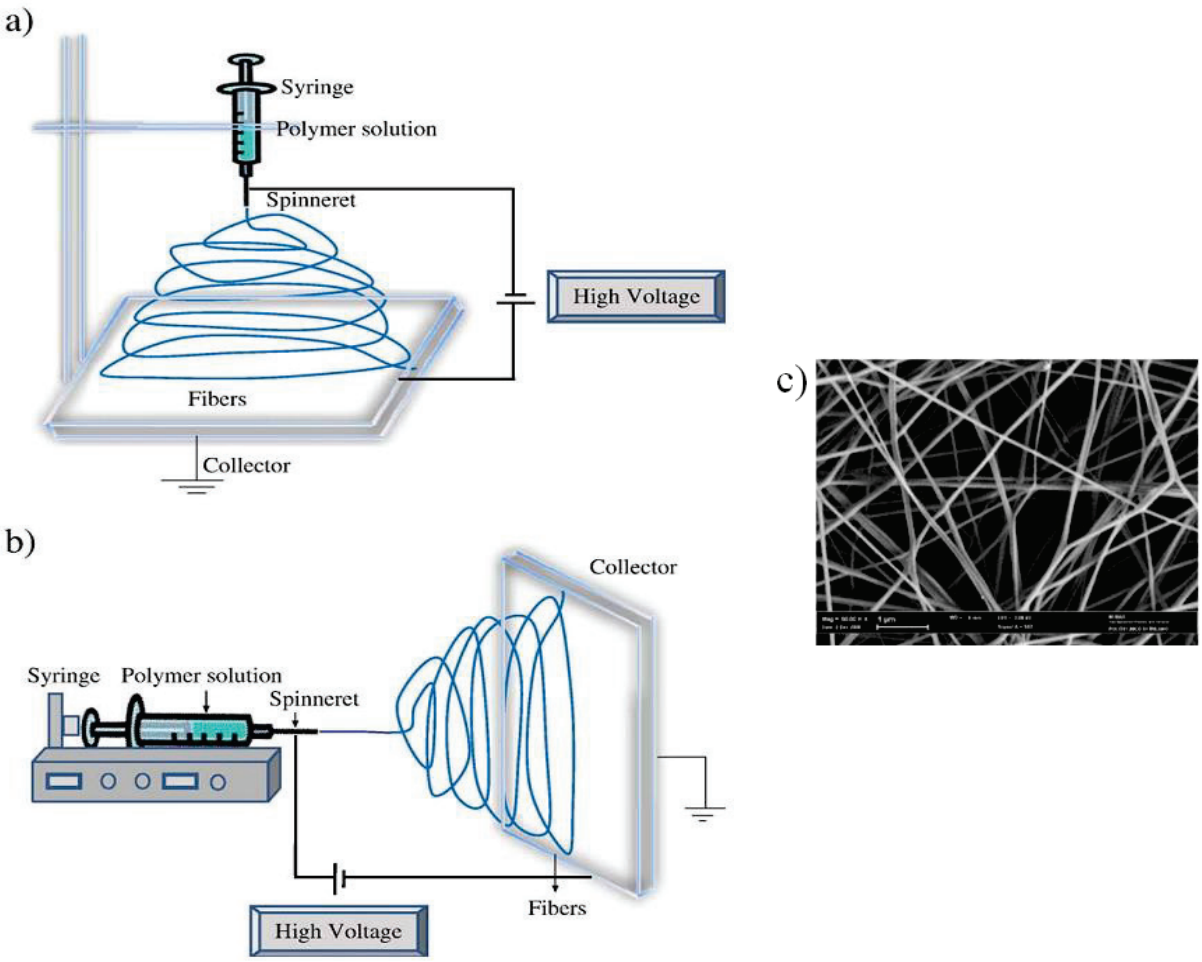

Figure 29. Schematic diagram of typical setups of electrospinning apparatus (a) vertical setup and (b) horizontal set up. c) SEM image of a typical mesh of randomly oriented electro spun nanofibers made of nylon 6,6. Reformed from Ref 87.

Most of the polymers are dissolved in solvents before electrospinning, and then the solution of the polymer, or composite is loaded into the syringe and this viscous liquid is driven to the needle tip by a syringe pump, forming a droplet at the tip.[112, 113, 114]

During the electrospinning process, a polymer solution held by its surface tension at the end of a capillary tube is subjected to an electric field and an electric charge is induced on the liquid surface due to this electric field. The droplet is first stretched into a structure called Taylor cone. When the electric field applied reaches a critical value, the repulsive electrical forces overcome the surface tension forces.[87] Eventually, an electrified jet of the solution is ejected from the tip of the Taylor cone. The jet is then elongated and whipped continuously by

[112] L. Cao et al., "Fabrication of Multiwalled Carbon Nanotube/Polypropylene Conductive Fibrous Membranes by Melt Electrospinning," *Industrial & Engineering Chemistry Research* 53, no. 6 (**2014**): 2308–17.
[113] L. Cao et al., "Morphology, Crystallization Behavior and Tensile Properties of B-Nucleated Isotactic Polypropylene Fibrous Membranes Prepared by Melt Electrospinning," *Chinese Journal of Polymer Science* 32, no. 9 (**2014**): 1167–75.
[114] C. Wang et al., "How to Manipulate the Electrospinning Jet with Controlled Properties to Obtain Uniform Fibers with the Smallest Diameter?—a Brief Discussion of Solution Electrospinning Process," *Journal of Polymer Research* 18, no. 1 (**2011**): 111–23.

electrostatic repulsion until it is deposited onto the collector. The elongation with unstable bending results in the formation of NFs.

Nevertheless, the electrospinning process presents an electrified fluid dynamics related problem. In order to control the morphology, structure, and mass production of the electrospun nanofibers, it is necessary to understand quantitatively how the electrospinning process transforms the fluid solution through a millimeter diameter capillary tube into solid micro/nanofibers which are four to five orders of magnitude smaller in diameter. Recent theoretical and experimental studies have demonstrated that the jet thinning process can be divided into three stages as depicted in figure 30: (1) jet initiation and elongation of the charged jet along a straight line; (2) growth of electrical bending instability -also known as whipping instability- and further elongation of the jet, which may or may not be accompanied with the jet branching and/or splitting; (3) solidification of the jet into micro/nanofibers and deposition on collector.[90]

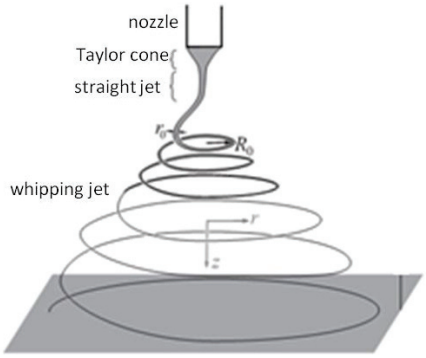

Figure 30. Scheme of a electro-hydrodynamic model of jet elongation, including all the essential elements governing the final fiber diameter. Extracted from Ref 125.

Since for each specific application, a narrow range of NF diameters is generally required to optimize the performance, fiber diameter control is essential. However, even though a significant amount of empirical knowledge has been accumulated over the past two decades[114] given the lack of predictive models, the correct diameter range is often attained by trail-and-error. For this reason several research teams tried to develop comprehensive theoretical models that would allow predicting how the NF diameter depends on the solution and processing parameters. One of the first models of electrospinning was proposed by Yarin et al.[115] and it is based on a bead-spring simulation of a jet-flow of a charged fluid between the electrodes. Although quite comprehensive in nature, it has found a rather limited acceptance by experimentalists due to its fully numerical nature and the absence of a simple analytical relationship for the terminal fiber diameter, e.g., in a scaling form, which could be used in an everyday practice. Reneker and coworkers [116, 117], Shin et al. [118, 119] and Hohman et al.[120, 121] investigated mathematical

[115] A.L. Yarin, S. Koombhongse, and D. H. Reneker, "Bending Instability in Electrospinning of Nanofibers," *Journal of Applied Physics* 89, no. 5 (**2001**): 3018-26.
[116] D.H. Reneker et al., "Bending Instability of Electrically Charged Liquid Jets of Polymer Solutions in Electrospinning," *Journal of Applied Physics* 87, no. 9 (**2000**): 4531–47.
[117] D.H. Reneker and Alexander L. Yarin, "Electrospinning Jets and Polymer Nanofibers," *Polymer* 49, no. 10 (**2008**): 2387–2425.
[118] Y.M. Shin et al., "Electrospinning: A Whipping Fluid Jet Generates Submicron Polymer Fibers," *Applied Physics Letters* 78, no. 8 (**2001**): 1149-51.
[119] Y.M. Shin et al., "Experimental Characterization of Electrospinning: The Electrically Forced Jet and Instabilities," *Polymer* 42, no. 25 (**2001**): 09955–67.
[120] M.M. Hohman et al., "Electrospinning and Electrically Forced Jets. I. Stability Theory," *Physics of Fluids* 13, no. 8 (**2001**): 2201-20.

expositions and asymptotic analyses to model the instabilities due to which the jet loses its stability against radial distortion[118] leading to bending and almost horizontal orientation of the fiber in the whipping jet zone. Reneker and coworkers[116, 117] described the path of the jet as a straight segment followed by a series of successively smaller electrically driven bending coils, with each bending coil having turns of increasing radius. They proposed that the elongation of each segment by the electrical forces is caused by the charge carried with the jet continues.

More specifically, an alternative model which also zooms into the so called whipping part of the electrospinning jet was developed at MIT by Fridrikh et al.[122] is built around an assumption that the terminal fiber diameter is determined by an equlibrium between the Coulombic repulsion between the charges on the jet's surface and the liquid's surface tension.[108] Such an argumentation yields for the fiber diameter d_f, up to a numerical prefactor,

$$d_f \sim \left(\gamma \frac{Q^2}{I^2}\right)^{1/3} w_p{}^{1/2} \qquad (10)$$

Where γ is the surface tension of the polymer solution, w_p is the polymer volume fraction, Q is the flow rate, and I is the electric current in the system, so that *I/Q* corresponds to the electric charge per unit volume of the jet. Interestingly, experiments[122] on polycaprolactone solutions showed a perfect agreement with the predicted $(Q/I)^{2/3}$ power law. However, there is a serious deficiency in formula (10) as it states that the terminal fiber diameter is independent of liquid viscosity and evaporation conditions, in contradiction to the common experience.[123, 124]

Very recently, Stepanyan et al.[125] presented a simple electro-hydrodynamic model of the jet elongation, which includes all the essential elements governing the final fiber diameter. They showed that, in contrast to the predictions of Eq.(10), it is the kinetics of elongation and evaporation, which governs the NF diameter, rather than the equilibrium between the Coulombic repulsion between the charges on the jet's surface and the liquid's surface tension. The viscosity of the polymer solution entered the quantitative model and was proven to have a profound influence on the diameter. Such an argumentation lead to a scaling formula for the fiber's terminal radius:

$$r_f \sim (k\rho_s \eta_0)^{1/3} \left(\frac{Q}{I}\right)^{2/3} \qquad (11)$$

---

[121] M.M. Hohman et al., "Electrospinning and Electrically Forced Jets. II. Applications," *Physics of Fluids* 13, no. 8 (**2001**): 2221-36.

[122] S. Fridrikh et al., "Controlling the Fiber Diameter during Electrospinning," *Physical Review Letters* 90, no. 14 (**2003**): 144502/1-4.

[123] Y. Cai and M. Gevelber, "The Effect of Relative Humidity and Evaporation Rate on Electrospinning: Fiber Diameter and Measurement for Control Implications," *Journal of Materials Science* 48, no. 22 (**2013**): 7812–26.

[124] S.Y. Tsou, H.S. Lin and C. Wang, "Studies on the Electrospun Nylon 6 Nanofibers from Polyelectrolyte Solutions: 1. Effects of Solution Concentration and Temperature," *Polymer* 52, no. 14 (**2011**): 3127–36.

[125] R. Stepanyan et al., "Fiber Diameter Control in Electrospinning," *Applied Physics Letters* 105, no. 17 (**2014**): 173105.

An interesting point is that although Equation (11) was derived by completely different arguments than those used by Fridrikh et al. to derive Equation (10), it features the same dependency on the ratio Q/I. Additionally, Equation 11 states that the final fiber diameter is dependent on the evaporation rate k and the solution viscosity η_0 with a power law exponent 1/3. Finally, it was proven that the predicted scaling laws from Stepanyan et al. were very well supported by the experiments, both their own and available in the literature.[122, 123]

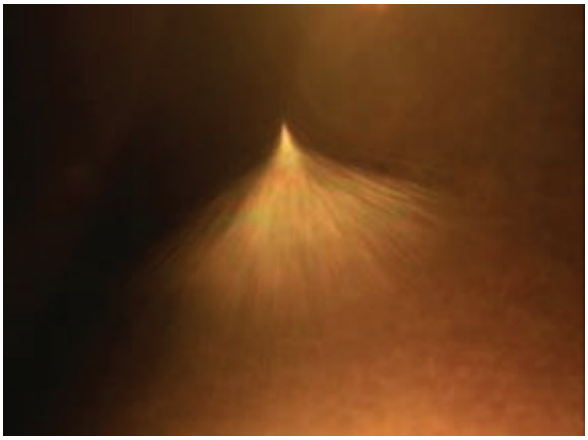

Figure 31. Photograph of a jet of PEO solution during ES. Extracted from Ref 127.

With the expansion of this technology, several research groups have developed more sophisticated systems that can fabricate more complex nanofibrous structures in a more controlled and efficient manner. [89, 126, 127, 128] Since during a conventional ES process, the polymer jet exhibits bending instabilities due to the repulsive forces between the charges carried within the jet, the electrospun fibers always result in a random orientation, which restricts the applications of ES technique for preparing new functional materials. To overcome this restriction Su et al.[89] developed a more advanced ES setup by adding a pair of parallel auxiliary electrodes between the spinneret and drum collector and replaced the common rotating drum collector with a high speed one (figure 32) to get not only well-oriented NF alignment but also controllable NF placement in the large-scale NF mats for extensive applications in electrochemical sensing.[129, 130, 131, 132] The two symmetric, rectangular, and

[126] S. Kidoaki, I.K. Kwon and T. Matsuda, "Mesoscopic Spatial Designs of Nano- and Microfiber Meshes for Tissue-Engineering Matrix and Scaffold Based on Newly Devised Multilayering and Mixing Electrospinning Techniques," *Biomaterials* 26, no. 1 (**2005**): 37–46.

[127] A. Greiner and J.H. Wendorff, "Electrospinning: A Fascinating Method for the Preparation of Ultrathin Fibers," *Angewandte Chemie International Edition* 46, no. 30 (**2007**): 5670–5703.

[128] A. Rogina, "Electrospinning Process: Versatile Preparation Method for Biodegradable and Natural Polymers and Biocomposite Systems Applied in Tissue Engineering and Drug Delivery," *Applied Surface Science* 296 (**2014**): 221–30.

[129] Z. Su et al., "Chain Conformation, Crystallization Behavior, Electrical and Mechanical Properties of Electrospun Polymer-Carbon Nanotube Hybrid Nanofibers with Different Orientations," *Carbon* 50, no. 15 (**2012**): 5605–17.

[130] Z. Su et al., "Biomimetic 3D Hydroxyapatite Architectures with Interconnected Pores Based on Electrospun Biaxially Orientated PCL Nanofibers," *RSC Adv.* 4, no. 29 (**2014**): 14833–39.

auxiliary aluminum electrodes were operated at a high voltage of the same polarity as the needle but with an adjustable potential controlled by another independent high-voltage power supply. The alignment of polymeric NFs can be improved by constraining the bending instability, which is thought to be the main reason to cause random orientation.

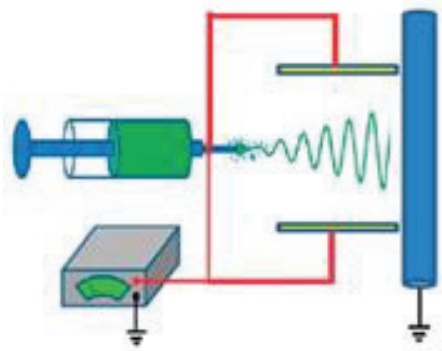

Figure 32. Schematic diagram of advanced electrospinning setup. Extracted from Ref 89.

NF structures with different morphologies e.g., parallel and crossed fiber arrays, helical or wavy fibers, twisted fiber yarns, patterned fiber web, and 3D fibrous stacks, fabricated with the modified ES technique[130, 133, 134, 135, 136, 137] are depicted in Figure 33.

[131] Z. Ouyang et al., "Fabrication, Characterization and Sensor Application of Electrospun Polyurethane Nanofibers Filled with Carbon Nanotubes and Silver Nanoparticles," *Journal of Materials Chemistry B*, 2013.
[132] P. Zhang et al., "Electrospun Doping of Carbon Nanotubes and Platinum Nanoparticles into the B-Phase Polyvinylidene Difluoride Nanofibrous Membrane for Biosensor and Catalysis Applications," *ACS Applied Materials & Interfaces*, April 10, 2014.
[133] M.B. Bazbouz and G.K. Stylios, "Novel Mechanism for Spinning Continuous Twisted Composite Nanofiber Yarns," *European Polymer Journal* 44, no. 1 (**2008**): 1–12.
[134] Q. Du, D.R. Harding and H. Yang, "Helical Peanut-Shaped Poly(vinyl Pyrrolidone) Ribbons Generated by Electrospinning," *Polymer* 54, no. 25 (**2013**): 6752–6759.
[135] J. Yu et al., "Production of Aligned Helical Polymer Nanofibers by Electrospinning," *European Polymer Journal* 44, no. 9 (**2008**): 2838–44.
[136] S. Soliman et al., "Multiscale Three-Dimensional Scaffolds for Soft Tissue Engineering via Multimodal Electrospinning," *Acta Biomaterialia* 6, no. 4 (**2010**): 1227–37.
[137] F.L. Zhou et al., "Jet Deposition in near-Field Electrospinning of Patterned Polycaprolactone and Sugar-Polycaprolactone Core–shell Fibres," *Polymer* 52, no. 16 (**2011**): 3603–10.

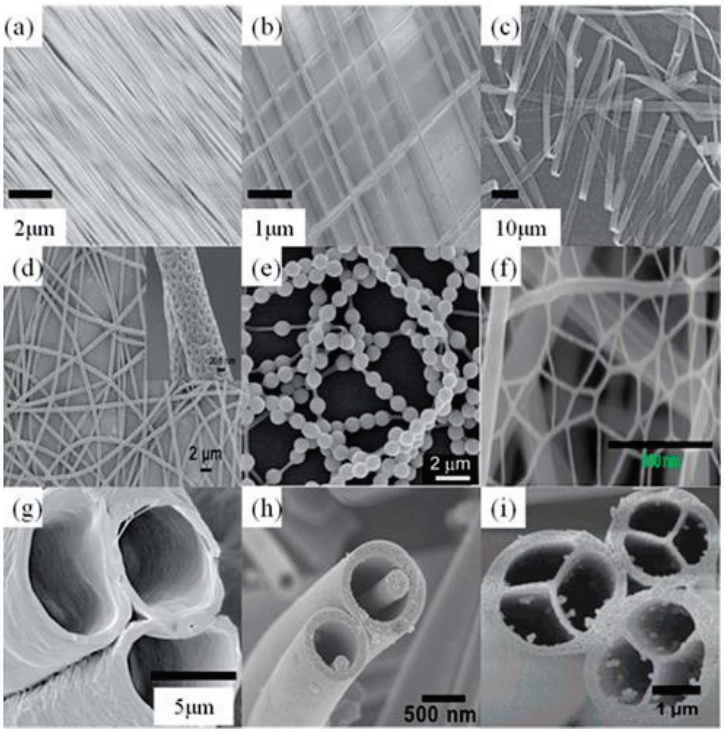

Figure 33. Different morphologies of electrospun polymer fibers: (a)uniaxially aligned, (b) biaxially oriented, (c) ribbon, (d) porousfibers, (e)Necklace-like, (f) nanowebs, (g) hollow, (h) nanowire-in-microtube,and (i) multichannel tubular. Extracted from Ref 89.

Although the alignment of nanofibers has been accomplished through the use of a rotating drum collector and by using electrical fiels manipulation, precise 2D and 3D patterning is still very difficult to achieve with far-field electrospinning. Recent results on a variant of electrospinning called near-field electrospinning[138] (NFES) produced some encouraging initial results, opening up a possibility of achieving scalable precision patterning with polymeric nanofibers.

[138] G.S. Bisht et al., "Controlled Continuous Patterning of Polymeric Nanofibers on Three-Dimensional Substrates Using Low-Voltage Near-Field Electrospinning," *Nano Letters* 11, no. 4 (**2011**): 1831–37.

I.3.3. Effects of Various Parameters on Electrospinning

The electrospinning process is governed by many parameters, classified broadly into solution parameters, processing parameters, and ambient parameters which are summarized in figure 34. Among them, the most important parameters that have a great influence on the electrospinning process are the following four: applied voltage, surface tension, molecular weight and viscosity.

The minimal requirement to perform electrospinning is to find the proper equilibrium between these four parameters to get a continuous jet, while avoiding Plateau-Rayleigh instability. Commonly, this is relatively easily achieved by tuning only the polymer concentration and the molecular weight, thus classifying these two parameters as the primary ones. However, it is highly probable that the tunning of only these two parameters is not sufficient to provide a solution that satisfies the requirements needed for the electrospinning process. Moreover, if a well-defined fiber diameter is the objective of a study, then a much more complex equilibrium, than the initial one, among all the other electrospinning parameters depicted in figure 34 much be achieved. In the following paragraphs a brief description of all ES parameters will be presented.

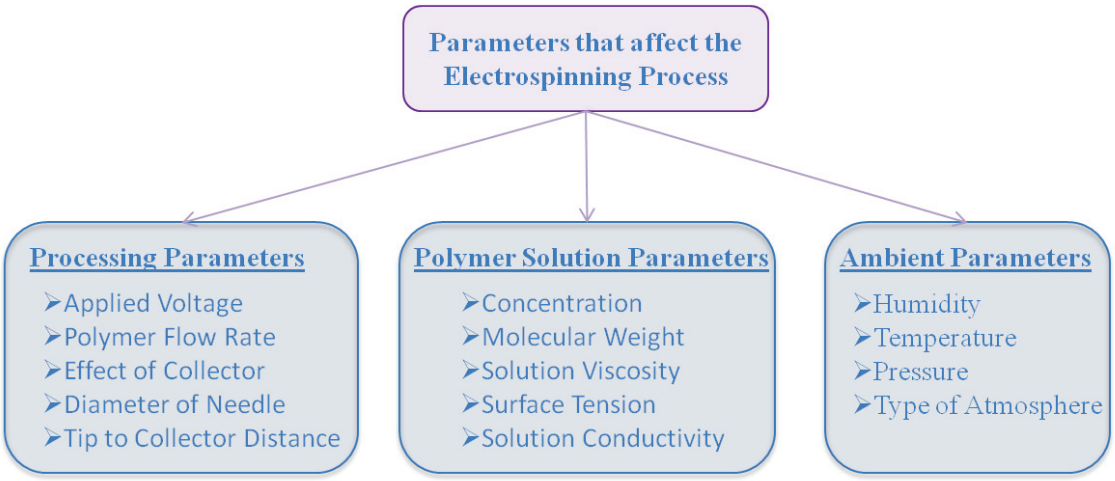

Figure 34. Schematic representation of parameters that affect the electrospinning

I.3.3.1. Polymer Solution Parameters

Concentration

The concentration of polymer solution is an important parameter affecting the fiber morphology, thus it was studied for a variety of synthetic and natural polymers-solvent systems.[128] It has been found that at low polymer solution concentration, a mixture of beads and fibers is obtained and as the solution concentration increases, the shape of the beads changes from spherical to spindle-like and finally uniform fibers with increased diameters are formed because of the higher viscosity resistance.[87, 139]

[139] A.K. Haghi and M. Akbari, "Trends in Electrospinning of Natural Nanofibers," *Physica Status Solidi (a)* 204, no. 6 (**2007**): 1830–34.

Molecular Weight

The molecular weight of the polymer has a significant effect on rheological and electrical properties such as viscosity, surface tension, conductivity and dielectric strength.[89] It is the source of the elastic component of the solution rheology and it reflects the entanglement of the molecules and their ability to stretch. It provides a higher cohesion of the jet which subsequently permits the imposition of a higher stretching of the later without breaking it. Thanks to the molecular weight, it is possible to stretch the jet in order to overcome the surface tension and also to avoid the formation of beads before spraying occurs.

Generally, high molecular weight polymer solutions have been used in electrospinning as they provide the desired viscosity for the fiber generation. It has been observed that a significantly low molecular weight solution tends to form beads rather than fibers and a high molecular weight solution gives fibers with larger average diameters.[93] However, in some cases even when the polymer concentration is low, the polymer can maintain enough number of entanglements of the polymer chains, thus ensuring high cohesion of the jet and restraining the effects of surface tension, which plays a significant role in beads formation on electrospun nanofibers.[140] Nevertheless, it has been observed that high molecular weights are not always essential for the electrospinning process if sufficient intermolecular interactions can provide a substitute for the interchain connectivity obtained through chain entanglements.

Surface Tension

The initiation of electrospinning requires the coulomb repulsion to overcome the surface tension, with the latter one determining the onset of the jet explusion. It is the source of the Plateau-Rayleigh instability along the still liquid jet which could lead to beads formation if the stretching is too weak.

Surface tension is more related to the nature of the solvent rather than to the polymer. Different solvents may contribute different surface tensions. Generally, the high surface tension of a solution inhibits the ES process because of instability of the jet and the generation of sprayed droplets .The formation of droplets, bead and fibers depends on the surface tension of solution and a lower surface tension of the spinning solution helps electrospinning to occur at a lower electric field.[87] However, a lower surface tension of a solvent will not always be more suitable for electrospinning. Basically, surface tension determines the upper and lower boundaries of the electrospinning window if all other variables are held constant.

Solution Viscosity

It is the result of the dissipative component of the solution's rheology, it derives from the dissipated energy by the slipping of the molecules and it plays an important role in determining the fiber size and morphology during spinning of polymeric fibers. Higher viscocity tends to reduce the bending instability since a part of the energy is dissipated inside

[140] S.H. Tan et al., "Systematic Parameter Study for Ultra-Fine Fiber Fabrication via Electrospinning Process," *Polymer* 46, no. 16 (**2005**): 6128–34.

the jet, thus imposing a reduction of the stretching. It results in lower probability to fracture the ejected jet into droplets, thus it is reducing the risk of electrospraying but it can possibly increase the diameter of the final fiber.

It has been found that with very low viscosity there is no continuous fiber formation and that with very high viscosity there is difficulty in the ejection of jets from polymer solution, thus there is a requirement of optimal viscosity for electrospinning. Viscosity, polymer concentration and molecular weight of polymer are strongly correlated to each other.[87] For solution of low viscosities, surface tension is the dominant factor and just beads or beaded fibers are formed, while above a critical concentration a continuous fibrous structure is obtained and its morphology is affected by the concentration of the solution.

Solution Conductivity

ES involves stretching of the solution caused by repulsion of the charges at its surface. Thus, if the conductivity of the solution is increased, more charges can be carried by the electrospinning jet. Solution conductivity is mainly determined by the polymer type, solvent used, and the availability of ionisable salts. The increase of the electrical conductivity of a solution, significantly decreases the diameter of the electrospun NFs due to the increase in electric charges carried by the jet and thud tensile force in the presence of an electric field.[87] On the contrary, with low conductivity of the solution, insufficient elongation of a jet occurs which leads to the formation of fibers and beads. Moreover, Hayati et al.[141] have shown that highly conductive solutions are extremely unstable in the presence of strong electric fields, which results in a dramatic bending instability as well as a broad diameter distribution.

I.3.3.2. Processing Parameters

Applied Voltage

A crucial element in electrospinning is the application of a high voltage to the solution. The high voltage induces the necessary charges on the solution and together with the electric field, initiates the ES when the electrostatic force in the solution overcomes the surface tension of the solution. Researchers have suggested that when higher voltages are applied, there is more polymer ejection and this facilitates the formation of a larger diameter fiber.[142] Other authors have reported that an increase in the applied voltage (i.e., by increasing the electric field strength), increases the electrostatic repulsive force on the fluid jet which ultimately favors the narrowing of fiber diameter. In most cases, a higher voltage causes greater stretching of the solution due to the greater columbic forces in the jet as well as a stronger electric field and these effects lead to reduction in the fiber diameter and also rapid evaporation of solvent from the fibers results. Furthermore, at a higher voltage there is greater

[141] I. Hayati et al., "Investigations into the Mechanisms of Electrohydrodynamic Spraying of Liquids: I. Effect of Electric Field and the Environment on Pendant Drops and Factors Affecting the Formation of Stable Jets and Atomization," *Journal of Colloid and Interface Science* 117, no. 1 (**1987**): 205–21.

[142] C. Zhang et al., "Study on Morphology of Electrospun Poly(vinyl Alcohol) Mats," *European Polymer Journal* 41, no. 3 (**2005**): 423–32.

probability of beads formation. The effect of high voltage is not only on the physical appearance of the fibers, but it also affects the crystallinity of the polymeric fiber. The electrostatic field may cause the polymer molecules to be more ordered during the electrospinning thus it induces a great crystallinity in the fiber. [88, 143]

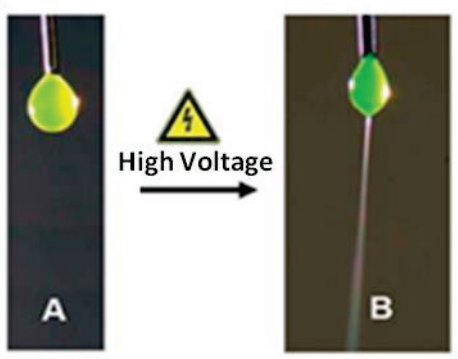

Figure 35. A droplet of a 5% solution of poly(ethylene oxide) (PEO) in water, dyed with fluorescein: A) in the absence of an applied voltage and B) at an applied voltage of 20kV, with a let perpendicular to the counter electrode. Extracted from Ref 127.

Feed Rate/ Polymer Flow Rate

Flow rate of the polymer solution is an important process parameter as it influences the material transfer rate. For a given voltage the feed rate must be carefully tuned to maintain a stable Taylor cone. A lower feed rate is basically more desirable to obtain thinner fibers.[144] When the feed rate is significantly increased, there is a corresponding increase in the fiber diameter and sometimes it could result to the collection of still wet fibers due to unavailability of proper drying time prior to reaching the collector.

Effect of Collector

In most ES setups, the collector plate is made out of a conductive material such as aluminum foil which is electrically grounded so that there is a stable potential difference between the source and the collector. However, other collectors such as conductive paper, conductive cloth, wire mesh[145], pin[146], parallel or grided bars[147], rotating rod, rotating wheel/cylinder[148], liquid non solvent such as methanol coagulation bath[149] are also used.

---

[143] S. Zhao et al., "Electrospinning of Ethyl–cyanoethyl Cellulose/tetrahydrofuran Solutions," *Journal of Applied Polymer Science* 91, no. 1 (**2004**): 242–46.

[144] X. Yuan et al., "Morphology of Ultrafine Polysulfone Fibers Prepared by Electrospinning," *Polymer International* 53, no. 11 (**2004**): 1704–10.

[145] X. Wang et al., "Formation of Water-Resistant Hyaluronic Acid Nanofibers by Blowing-Assisted Electro-Spinning and Non-Toxic Post Treatments," *Polymer* 46, no. 13 (**2005**): 4853–67.

[146] B. Sundaray et al., "Electrospinning of Continuous Aligned Polymer Fibers," *Applied Physics Letters* 84, no. 7 (**2004**): 1222–24.

[147] D. Li, Y. Wang and Y. Xia, "Electrospinning Nanofibers as Uniaxially Aligned Arrays and Layer-by-Layer Stacked Films," *Advanced Materials* 16, no. 4 (**2004**): 361–66.

[148] C.Y. Xu et al., "Aligned Biodegradable Nanofibrous Structure: A Potential Scaffold for Blood Vessel Engineering," *Biomaterials* 25, no. 5 (**2004**): 877–86.

Several research groups have demonstrated the use of a rotating drum or a rotating wheel-like bobbin or metal frame as the collector, for getting aligned electrospun fibers more or less parallel to each other.[150] Several types of split electrodes have been used for getting aligned nanofibers and typically such collectors consist of two conductive substrates separated by a void gap where aligned nanofibers are deposited.

Diameter of Pipette Orifice/Needle

The internal diameter of the needle or the pipette orifice has a certain effect on the ES process. A smaller internal diameter was found to reduce the clogging as well as the amount of beads on the electrospun fibers. Decrease in the internal diameter of the orifice was also found to cause a reduction in the diameter of the electrospun fibers. When the size of the droplet at the tip of the orifice is decreased, such as in the case of a smaller internal diameter of the orifice, the surface tension of the droplet increases. For the same voltage supplied, a greater columbic force is required to cause jet initiation.[87] As a result, the acceleration of the jet decreases and this allows more time for the solution to be stretched and elongated before it is collected. However, if the diameter of the orifice is too small, it may not be possible to extrude a droplet of solution at the tip of the orifice.[143]

Tip to Collector Distance

The time of flight as well as the electric field strength may also affect the ES process and the resultant fibers. Varying the distance between the tip and the collector has a direct influence on both these factors. A minimum distance is required to give the fibers sufficient time to dry before reaching the collector, otherwise with distances that are either too close or too far, beads have been observed. Depending on the solution property, the effect of varying the distance may or may not have a significant effect on the fibers morphology. One important physical aspect of the electrospinning nanofibers is their dryness from the solvent used to dissolve the polymer.[151] Thus, there should be optimum distance between the tip and collector which favors the evaporation of solvent from the nanofibers.

---

[149] C.S. Ki et al., "Electrospun Three-Dimensional Silk Fibroin Nanofibrous Scaffold," *Journal of Applied Polymer Science* 106, no. 6 (**2007**): 3922–28.

[150] J.M. Deitzel et al., "The Effect of Processing Variables on the Morphology of Electrospun Nanofibers and Textiles," *Polymer* 42, no. 1 (**2001**): 261–72.

[151] R. Jalili, Seyed Abdolkarim Hosseini, and Mohammad Morshed, "The Effects of Operating Parameters on the Morphology of Electrospun Polyacrilonitrile Nanofibres," *Iranian Polymer Journal* 14, no. 12 (**2005**): 1074-81.

I.3.3.3. Ambient Parameters

Apart from solution and processing parameters, ambient parameters encompass the humidity, temperature, pressure and the type of atmosphere that surround the jet, significantly affect the ES process. Since there is an inverse relationship between temperature and viscosity, it is apparent that every time that the temperature changes, the viscosity of the solution also changes.

The variation in humidity has been studied and it was shown that by increasing humidity there is an appearance of small circular pores on the surface of the fibers, fabricated from polymers mainly dissolved in organic solvents. Further increasing the humidity leads to the pores coalescing.[152] It has been found that at very low humidity, a volatile solvent may dry rapidly as the evaporation of the solvent is faster. Sometimes the evaporation rate is so fast than compared to the removal of the solvent from the tip of the needle and this would create a problem with electrospinning. As a result, the electrospinning process may only be carried out for a few minutes before the needle tip is clogged. It has also been suggested that the high humidity can help the discharge of the electrospun fibers.[147, 153]

Air composition in the ES environment also has an effect on the ES process. Different gases have different behavior under electrostatic field. For example, helium breaks down under high electrostatic field and thus electrospinning is not possible.

[152] C.L. Casper et al., "Controlling Surface Morphology of Electrospun Polystyrene Fibers: Effect of Humidity and Molecular Weight in the Electrospinning Process," *Macromolecules* 37, no. 2 (**2004**): 573–78.
[153] M. Li et al., "Electrospun Protein Fibers as Matrices for Tissue Engineering," *Biomaterials* 26, no. 30 (**2005**): 5999–6008.

I.3.4. Materials Used in Electrospinning

Electrospun nanofibers may be fabricated from a remarkably wide range of inorganic[154, 155, 156] and organic materials.[97, 157] These latter include synthetic polymers, natural polymers, copolymers, polymer blends including proteins, nucleic acids, enzymes and even polysaccharides and composites. The specific physical and chemical properties of the created fibers make them very versatile for different applications such as optoelectronics, sensors and biosensors, catalysis, textiles, filters, fiber reinforcement, tissue engineering, drug delivery, and wound healing.

I.3.4.1. Natural and Synthetic Polymers

It is not surprising that one of the greatest potential of electrospun fibers is their application in the area of bioengineering[128] since the sub-micron dimension of the fibers resembles that of a natural extracellular matrix. Naturally occurring polymers normally exhibit better biocompatibility and low immunogenicity, compared to synthetic polymers, when used in biomedical applications. Typical natural polymers include collagen, silk protein, fibrinogen, chitosan, gelatin, casein, cellulose acetate, hyaluronic acid, chitin etc. Scaffolds fabricated from natural polymers promise better clinical functionality.[87] However, partial denaturation of natural polymers has been reported in recent years that demands concern.

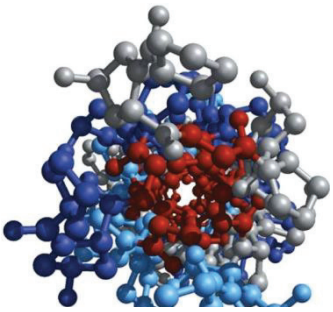

Figure 36. Collagen structure.

Synthetic polymers often offer many advantages over natural polymers as they can be tailored to give a wider range of properties such as, necessary mechanical properties (viscoelasticity and strength), and desired degradation rate.[158] Typical polymers used in biomedical applications are hydrophobic biodegradable polyesters, such as polyglycolide (PGA), polylactide (PLA), poly (ε-caprolactone) (PCL) and polyurethane (PU), which have all been electrospun into nanofibrous scaffolds. Other typical synthetic polymers that have been successfully electrospun are: poly(ethylene oxide) (PEO), polyacrylonitrile (PAN), poly(vinyl alcohol) (PVA), polystyrene, polyurethane, poly(vinyl chloride) (PVC), poly(vinyl pyrrolidone) (PVP).

---

[154] Y. Dai, W. Liu, E. Formo, Y. Sun and Y. Xia, "Ceramic Nanofibers Fabricated by Electrospinning and Their Applications in Catalysis, Environmental Science, and Energy Technology," *Polymers for Advanced Technologies* 22, no. 3 (**2011**): 326–38.

[155] Y. Zhao, L. Sun, M. Xi, Q. Feng, C. Jiang and H. Fong, "Electrospun TiO_2 Nanofelt Surface-Decorated with Ag Nanoparticles as Sensitive and UV-Cleanable Substrate for Surface Enhanced Raman Scattering," *ACS Applied Materials & Interfaces* 6, no. 8 (**2014**): 5759–67.

[156] S. Chattopadhyay, J. Saha and G. De, "Electrospun Anatase TiO_2 Nanofibers with Ordered Mesoporosity," *J. Mater. Chem. A* 2, no. 44 (**2014**): 19029–35.

[157] M. Bourourou, M. Holzinger, K. Elouarzaki, A. Le Goff, F. Bossard, C. Rossignol, E. Djurado, V. Martin, D. Curtil, D. Chaussy, A. Maaref and S. Cosnier "Laccase Wiring on Free-Standing Electrospun Carbon Nanofibres Using a Mediator Plug," *Chem. Commun.*, **2015**, doi:10.1039/C5CC03906A.

[158] M. Hakkarainen, "Aliphatic Polyesters: Abiotic and Biotic Degradation and Degradation Products," in *Degradable Aliphatic Polyesters*, vol. 157, Advances in Polymer Science (**2002**): 113–38.

I.3.4.2. Copolymers and Polymer Blends

Sometimes, it is beneficial to obtain a structure that combines the properties of two or more polymers. This can be achieved either through polymerization of two different monomers to form a copolymer or by physical mixing of two or more polymers to form a blend. Electrospinning with copolymers offers property enhancement of polymeric materials, including tailoring of thermal stability, mechanical strength and barrier properties, or improving cell affinity and has therefore been often pursued for engineering structural applications through methods as copolymerization, melt-blending and incorporation of inorganic fillers.[159]

I.3.4.3. Composites

Composites are combination of two distinct material phases, a bulk phase-the matrix- and a second phase- the reinforcement phase- which gives to the composite its additional and superior properties that are not available in any single conventional material. Both phases can be metal, ceramic or polymer. In most cases, composites are designed for load-bearing applications and the second component of the composite acts as a reinforcement phase. However, other classes of composites have been developed and used for their interesting electrical, thermal or magnetic properties.[88] For biosensor applications, that constitute the aim of the present work, the fabrication of conductive fibers is required. In the following sections we will focus on composites based on polymer NFs incorporating conductive nanomaterials such as carbon nanotubes and metallic nanoparticles (MNPs).

Electrospun polymer NFs doped with CNTs

It is well known that the filling of CNTs into the electrospun polymeric NFs can greatly influence the mechanical, electrical, and thermal properties of NFs. To maximize the reinforcement of CNTs in polymer composites, the alignment and dispersion of CNTs in NFs are two important factors that should be considered but are not easy to achieve.

General applications of electrospun NFs with CNTs

In 2004, Reneker's group[160] for the first time found that the orientation of MWCNTs within the electrospun NFs was much higher than that within the polyacrylonitrile (PAN) polymer crystal matrix (Fig. 37a). This finding suggests that not only the surface tension and jet elongation but also the slow relaxation of MWCNTs in NFs are the key factors for the orientation of MWCNTs. As a result of the highly anisotropic orientation of MWCNTS in the polymer NFs, the fabricated PAN–MWCNT nanofibrous mats possessed enhanced properties like electrical conductivity, mechanical strength, thermal stability, and dimensional stability.

---

[159] M. Wang et al., "Electrospinning of poly(MMA-Co-MAA) Copolymers and Their Layered Silicate Nanocomposites for Improved Thermal Properties," *Polymer* 46, no. 10 (**2005**): 3407–18.

[160] J.J. Ge et al., "Assembly of Well-Aligned Multiwalled Carbon Nanotubes in Confined Polyacrylonitrile Environments: Electrospun Composite Nanofiber Sheets," *Journal of the American Chemical Society* 126, no. 48 (**2004**): 15754–61.

With natural polymer, Jin's group prepared silk fibroin fibers[161], where MWCNTs were embedded and well aligned (Fig. 37b). Meanwhile, Haddon's group[162] studied SWCNT reinforced polymer composite membranes using ES technique. NFs with diameters in the range of 50–100 nm were obtained by spinning SWCNTs filled PS composites. TEM observations revealed that the incorporation of small bundles of SWCNTs orient parallel to the NF axis (Fig. 37c).

By using a post-treatment process, Lee's group[163] prepared the mesoporous CNT-embedded carbon NFs (Fig. 37d). ES can also be used to fabricate NFs with multi-component polymer matrix. Shim's group[164] fabricated copolymer NFs doped with MWCNTs by ES and utilized the fabricated NFs as a chemiresistor to detect the aromatic volatile organic compounds (Fig. 37f).

Su's group[89] has also reported that both the alignment of MWCNTs in the electrospun PEO NFs and the orientation of electrospun PEO–MWCNT hybrid NFs can be controlled by an advanced ES technique. The embedding and alignment of MWCNTs in PEO NFs were confirmed by TEM, as shown in Fig. 37g and 37h. By increasing the content of MWCNTs in the electrospun NFs, MWCNTs were tended to align closely in a line, forming an ideal structure that can best express the unique anisotropic properties of CNTs. In a next study, they further investigated the preparation of polyurethane (PU) NFs filled with MWCNTs and created a novel PU – MWCNT conductive fibrous membrane with ES technique (Fig. 37i).

Throughout these studies it was clearly shown that the use of CNTs to reinforce and enhance the performance of polymer – CNT hybrid NFs can produce a new generation of composite materials. The above introduction highlights the fact that the intrinsic crystalline quality and the straightness of the embedded CNTs are significant factors influencing the reinforcement capability.

[161] M. Kang, P. Chen and H.J. Jin, "Preparation of Multiwalled Carbon Nanotubes Incorporated Silk Fibroin Nanofibers by Electrospinning," *Current Applied Physics* 9, no. 1 (**2009**): S95–97.

[162] R.Sen et al., "Preparation of Single-Walled Carbon Nanotube Reinforced Polystyrene and Polyurethane Nanofibers and Membranes by Electrospinning," *Nano Letters* 4, no. 3 (**2004**): 459–64.

[163] S.H. Park et al., "MWCNT/mesoporous Carbon Nanofibers Composites Prepared by Electrospinning and Silica Template as Counter Electrodes for Dye-Sensitized Solar Cells," *Journal of Photochemistry and Photobiology A: Chemistry* 246 (**2012**): 45–49.

[164] J. Choi, D.W. Park and S.E. Shim, "Electrospun PEDOT: PSS/carbon nanotubes/PVP Nanofibers as Chemiresistors for Aromatic Volatile Organic Compounds," *Synthetic Metals* 162, no. 17–18 (**2012**): 1513–18.

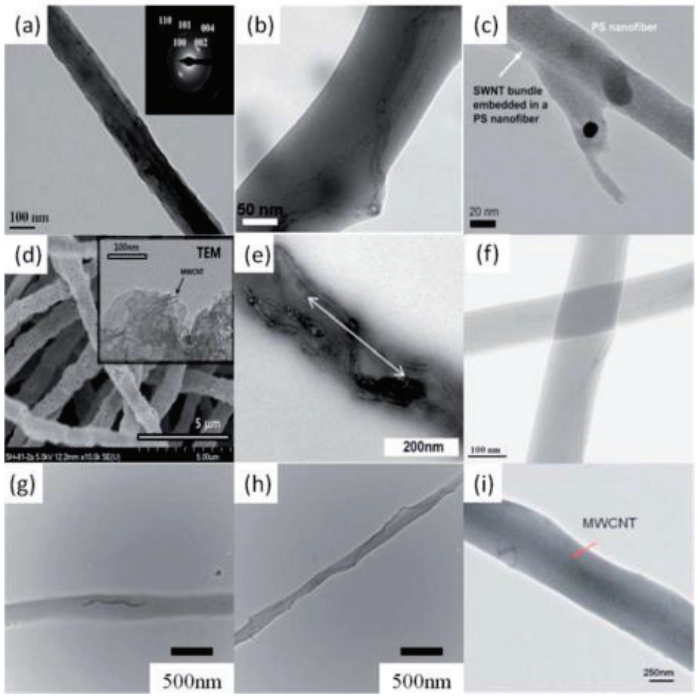

Figure 37. Electrospun polymer NFs doped with CNTs: (a) PAN – MWNT, (b) silk fibroin – MWCNT, (c) SWNT bundle (white arrow) embedded in the PS NFs, (d) mesoporous carbon NF – MWCNT, (e) PAN-g-PDMS –MWCNT, (f) PVP – MWCNT, (g) PEO – MWCNT hybrid NFs with 0.5% MWCNT, (h) PEO – MWCNT hybrid NFs with 3% MWCNT, and (i) PU –MWCNT. Extracted from Ref 89.

Electrospun polymer NFs doped with CNTs for electrochemical enzyme-based biosensing

CNT-NFs composites are also very attractive for biosensor applications and in particular for the elaboration of enzyme-based electrochemical biosensors. As already mentioned, electrospun NFs meet many of the requirements to achieve improved performances as a biosensor material since they are featured with very small diameters, long length, large surface area per unit mass, high surface-to-volume ratio and tunable pore size.[89]

NFs-CNTs composite materials seems to be very promising for the development of new generation biosensing systems with improved sensitivity and superior performance compared to the existing biosensors. In the electrospun polymer–CNT composites, polymers not only act as the matrix for the uniform distributions of CNTs and the formation of a sensing layer, but also play a significant role in enhancing the electrochemical characteristics by means of their interactions with CNTs. The applications of electrospun NFs-CNTs composites for fabricating new generation electrochemical enzyme nanobiosensors are still at an early but promising stage. A real challenge lies in the possibility to produce a three-component composite (NFs/CNTs/enzyme) of maximal electrochemical and biological sensing properties.

Different strategies have been proposed to produce enzyme-loaded electrospun NFs.[165] One of the most common methods consists in immobilizing the enzymes onto hydrophobic

[165] Z.G. Wang et al., "Enzyme Immobilization on Electrospun Polymer Nanofibers: An Overview," *Journal of Molecular Catalysis B: Enzymatic* 56, no. 4 (**2009**): 189–95.

NFs (e.g. carbon[97], Nylon 6,6[45], polyacrylonitrile[166]), which generally requires the modification of NFs surface to improve its biocompatibility.

Following this approach, Im et al.[167] constructed CNT-doped PAN porous NFs by ES technique and further modified the NFs with glucose oxidase, GOx, for electrochemical sensing of glucose. CNTs were embedded as an electrically conductive additive to improve the electrical property of the porous CNFs. The effects of CNT addition and oxyfluorination on the performance of the fabricated glucose sensor were investigated with cyclic voltammetry (CV). The current peak intensity in the CVs increased due to the effect of CNT additive and oxyfluorination treatment. This result was attributed to efficient GOx immobilization and the improved affinity between GOx and the surface resulting from the introduced hydrophilic functional groups on carbon surface and the efficient electron transfer. When glucose was freshly injected to achieve higher glucose concentrations, the stabilization time of the current was approximately 7s at every step. This rapid stabilization of current is attributed to the enhanced effect of CNTs on the electrical properties of electrode.

In another study, Lee et al.[168] fabricated another glucose sensor by immobilizing GOx onto electrospun polymer [poly(diallyldimethylammonium chloride) (PDDA) and PMMA]–MWCNT nanofibrous membranes. The fabricated PMMA(PDDA)–MWCNT/GOx exhibits excellent electrocatalytic activity towards hydrogen peroxide (H_2O_2) with a pronounced oxidation current at +100 mV. Glucose was amperometrically detected at +100 mV in 0.1 M phosphate buffer solution (PBS, pH 7). The linear response for glucose detection is in the range of 20 μM to 15 mM with a detection limit of 1 mM and a response time of 4 s. The superior performance of this kind of sensors is due to the wrapping of PDDA over MWCNTs that bound with GOx.

Uzun et al.[45] fabricated a glucose sensor by preparing nylon 6,6 NFs incorporating MWCNTs via ES technique, which were further coated with a conducting polymer named PBIBA [poly-4-(4,7-di(thiophen-2-yl)-1H-benzo[d]imidazol-2-yl)benzaldehyde] to covalently attach GOx on the surface of the fibers due to the free aldehyde groups of the CP. The resulting novel glucose biosensor revealed good stability and promising I max values (16.67 μA) and long shelf life (44 days). The linear response for glucose detection is in the range of 0.01 mM to 2 mM with a detection limit of 9 μA.

Wang et al.[169] constructed CNT-doped poly(acrylonitrile-co-acrylic acid) (PANCAA) NFs by ES technique and further modified the NFs with glucose oxidase, by covalently

---

[166] R. Xu et al., "Laccase–Polyacrylonitrile Nanofibrous Membrane: Highly Immobilized, Stable, Reusable, and Efficacious for 2,4,6-Trichlorophenol Removal," *ACS Applied Materials & Interfaces* 5, no. 23 (**2013**): 12554–60.

[167] J.S. Im et al., "The Effects of Carbon Nanotube Addition and Oxyfluorination on the Glucose-Sensing Capabilities of Glucose Oxidase-Coated Carbon Fiber Electrodes," *Applied Surface Science* 258, no. 7 (**2012**): 2219–25.

[168] K.M. Manesh et al., "A Novel Glucose Biosensor Based on Immobilization of Glucose Oxidase into Multiwall Carbon Nanotubes–polyelectrolyte-Loaded Electrospun Nanofibrous Membrane," *Biosensors and Bioelectronics* 23, no. 6, 18 (**2008**): 771–79.

[169] Z.G. Wang et al., "Carbon Nanotube-Filled Nanofibrous Membranes Electrospun from Poly(acrylonitrile- *co* -Acrylic Acid) for Glucose Biosensor," *The Journal of Physical Chemistry C* 113, no. 7 (**2009**): 2955–60.

immobilizing GOx on the membranes through the activation of carboxyl groups on the PANCAA nanofiber surface. The electrochemical properties of enzyme electrodes were characterized by chronoamperometric measurements, which showed that MWCNT filling enhances the electrode current and sensitivity. Combined with the results of kinetic studies, it was concluded that the interactions between MWCNT and FAD play a significant role in enhancing the electroactivity of the immobilized GOx, even though the secondary structure of the immobilized GOx is disturbed in the presence of MWCNT.

However, when enzymes are attached to NFs after electrospinning, only the external surface of the NFs may be used for further enzyme immobilization, without taking full advantage of the internal volume of fibers that can protect enzyme molecules from harsh conditions. Enzyme loading is therefore rather limited. Therefore another way to proceed consists in electrospinning a blend of enzymes and water-soluble polymer. Encapsulation of enzymes into polymer NFs helps preserving their biological activity.[231] Electrospun composites of CNTs with water-soluble polymers (e.g. PVA) are of particular interest for these applications, since they provide a suitable environment for the incorporation of biomolecules within the mixture, thus leading to one-step fabrication techniques of novel electroactive surfaces for biosensing.

Recently, Ford's[170] and Ding's group[171] reported the successful fabrication of PVA-SWCNTs nanofibers and PVA-MWCNTs nanofibers respectively. The hybrid nanofibers exhibited electrical conductivity of $1.8x10^{-4}$ S/cm. Shortly afterwards, Ford's team[172] fabricated SWCNT/poly(vinyl alcohol)**(**PVA**)/** Bovine Serum Albumin **(**BSA**)** nanofibers by ES technique in order to study their role in the chemical deactivation of threat agents by means of enzymatic proteins. It was proven that protein loading and the surface chemistry of hybrid nanofibers influenced the efficacy by which embedded enzymes could digest the substrate of interest and most importantly that the activity of BSA was not compromised because of its incorporation within the nanofiber. Most importantly, active proteins remained accessible to the substrate regardless of its affinity with the host polymer. This study confirms that the polymeric nanofibrous platform modulated by SWNTs can be a viable approach to the engineering of enzyme catalytic biosensors.

Su at al.[173] developed a novel biosensing platform for glucose detection, by electrospinning a solution of poly(vinylalcohol) (PVA)/chitosan/graphene oxides (GO) and glucose oxidase (GOx) to fabricate to NFs. After ES, the modified electrode with electrospun PVA/chitosan/GOD/GO NFs was placed in glutaraldehyde vapor for crosslinking to form

---

[170] E.N. J. Ford et al., "Influence of SWNTs on the Preferential Alignment of Molecular Moieties in PVA Fibers," *Macromolecular Chemistry and Physics* 213, no. 6 (**2012**): 617–26.

[171] Ding et al., "Self-Assembled Transparent Conductive Composite Films of Carboxylated Multi-Walled Carbon Nanotubes/poly(vinyl Alcohol) Electrospun Nanofiber Mats", *Material Letters* 128, (**2014**):310-313.

[172] E.N.J. Ford et al., "Role of Single-Walled Carbon Nanotubes on Ester Hydrolysis and Topography of Electrospun Bovine Serum Albumin/Poly(vinyl Alcohol) Membranes," *ACS Applied Materials & Interfaces* 6, no. 14 (**2014**): 11741–48.

[173] X. Su et al., "A Novel Platform for Enhanced Biosensing Based on the Synergy Effects of Electrospun Polymer Nanofibers and Graphene Oxides," *The Analyst* 138, no. 5 (**2013**): 1459.

water-insoluble nanofibers. Then, a thin layer of Nafion was deposited on the surface of the matrix, the prepared electrode was used for glucose amperometric detection. The electrode exhibited high sensitivity 11.98 μA cm^{-1} mM^{-1}, good stability, low detection limit (5μM) and wide linear range of 5 μM–4 mM.

Finally, a mixture of PVA and enzyme was already electrospun by Tang et al.[174] and after intensive enzymatic studies it was proven that by using this enzyme immobilization approach the enzyme still remains very active after the electrospinning process.

Electrospun polymer NFs doped with MNPs

As already mentioned, the electrochemical properties of MNPs are extremely sensitive to their sizes, shape, and dispersion. A high dispersion of MNPs in functional materials is important to present high electrochemical activity, while the associated tendency of MNPs to aggregate would lower their catalytic activity and reuse life-time. Therefore, how to design and prepare MNP-based materials with long-term dispersion stability and high catalytic efficiency is a primary challenge for their wide applications.[175] Several strategies have been utilized to synthesize and immobilize MNPs into electrospun polymer NFs. For instance, polymer–MNP hybrid NFs can be prepared by mixing MNPs into a polymer solution and spinning subsequently.[176] MNPs can also be directly deposited onto electrospun polymer NFs via surface modication. Alternatively, MNPs can be synthesized on the surface of electrospun polymer NFs through thermal and chemical reduction of metallic precursor ions.[177]

Zhang et al.[178] prepared PAN NFs decorated with AgNPs by ES technique. AgNPs were created on the PAN NFs with a seed-mediated electroless plating. A typical TEM image is shown in Fig. 38b, in which numerous AgNPs were attached onto PAN NFs. The AgNPs were roughly spherical in shape and were randomly distributed on the surface of the NFs with a moderate density. The size distribution of AgNPs is 23 $\pm$5 nm. Lei and co-workers[179] reported the successful preparation of polyaniline (PANI) NFs with integrated Pt nanoflowers. PANi was prepared by in situ polymerization of aniline on an electrospun NF template in an acidic solution with ammonium persulfate as the oxidant. Pt nanoflowers were further electro-deposited onto the PANi NF backbone by CV, resulting in novel functionalized hybrid NFs (Fig. 38c).

---

[174] C. Tang et al., "Cross-Linked Polymer Nanofibers for Hyperthermophilic Enzyme Immobilization: Approaches to Improve Enzyme Performance," *ACS Applied Materials & Interfaces* 6, no. 15 (**2014**): 11899–906.

[175] H. Zhu et al., "Facile and Green Fabrication of Small, Mono-Disperse and Size-Controlled Noble Metal Nanoparticles Embedded in Water-Stable Polyvinyl Alcohol Nanofibers: High Sensitive, Flexible and Reliable Materials for Biosensors," *Sensors and Actuators B: Chemical* 185 (**2013**): 608–19.

[176] J. Song et al., "Safe and Effective Ag Nanoparticles Immobilized Antimicrobial NanoNonwovens," *Advanced Engineering Materials* 14, no. 5 (**2012**): B240–46.

[177] T. Zhang et al., "Biotemplated Synthesis of Gold Nanoparticle-Bacteria Cellulose Nanofiber Nanocomposites and Their Application in Biosensing," *Advanced Functional Materials* 20, no. 7 (**2010**): 1152–60.

[178] L. Zhang et al., "Electrospun Nanofibrous Membranes Surface-Decorated with Silver Nanoparticles as Flexible and Active/Sensitive Substrates for Surface-Enhanced Raman Scattering," *Langmuir* 28, no. 40 (**2012**): 14433–40.

[179] W. Jia, L. Su and Y. Lei, "Pt Nanoflower/polyaniline Composite Nanofibers Based Urea Biosensor," *Biosensors and Bioelectronics* 30, no. 1 (**2011**): 158–64.

You's group prepared PdNP-modified CNFs by ES and subsequent thermal treatments.[180] Figure 38d shows the SEM image of the electrospun CNF–PdNP hybrid. The surface of CNFs is coarse and the diameter is in the 200–500 nm range. The spherical PdNPs with a mean diameter of about 75 nm can be observed on the surface of CNFs. Meanwhile, they also prepared NiNP-loaded CNFs (CNF–NiNP) by combination of ES technique and thermal treatment.[181] The TEM image illustrates that the NiNPs with a diameter of about 50 nm are embedded in the CNF matrix (Fig. 38e). Shanmugam et al. fabricated CoNP-doped porous carbon nanorods (CNR–CoNP) by an easy and versatile ES technique and followed by one-step carbonization at 900 °C in Ar.[182] FE-TEM analysis clearly shows that the CoNPs are actually embedded in the CNRs (Fig. 38f). The size of CoNPs ranges from 20 nm to 100 nm. Wang's group synthesized Cu-doped ZnO NFs via ES technique.[183] The SEM image of the as-synthesized Cu-doped ZnO NFs is shown in Fig. 38g.

Xia's group reported a simple method for functionalizing the surface of ZrO_2 nanofibrous membranes with RhNPs.[89] The ZrO_2 membranes were fabricated in the form of nonwoven mats by ES with a solution of polyvinylpyrrolidone (PVP) and zirconium acetylacetonate, followed by calcination in air at 550 °C to yield the tetragonal phase. The fibrous mats were then immersed in a polyol reduction bath to coat the surface of the NFs with RhNPs of 2–5 nm in size.

[180] H. Zhang et al., "Electrochemical Detection of Hydrazine Based on Electrospun Palladium Nanoparticle/Carbon Nanofibers," *Electroanalysis* 21, no. 16 (**2009**): 1869–74.

[181] Y.L. et al., "Nonenzymatic Glucose Sensor Based on Renewable Electrospun Ni Nanoparticle-Loaded Carbon Nanofiber Paste Electrode," *Biosensors and Bioelectronics* 24, no. 11 (**2009**): 3329–34.

[182] P. Ramakrishnan and S. Shanmugam, "Electrochemical Performance of Carbon Nanorods with Embedded Cobalt Metal Nanoparticles as an Electrode Material for Electrochemical Capacitors," *Electrochimica Acta* 125 (**2014**): 232–40.

[183] M. Zhao et al., "Electrospun Cu-Doped ZnO Nanofibers for H2S Sensing," *Sensors and Actuators B: Chemical* 156, no. 2 (**2011**): 588–92.

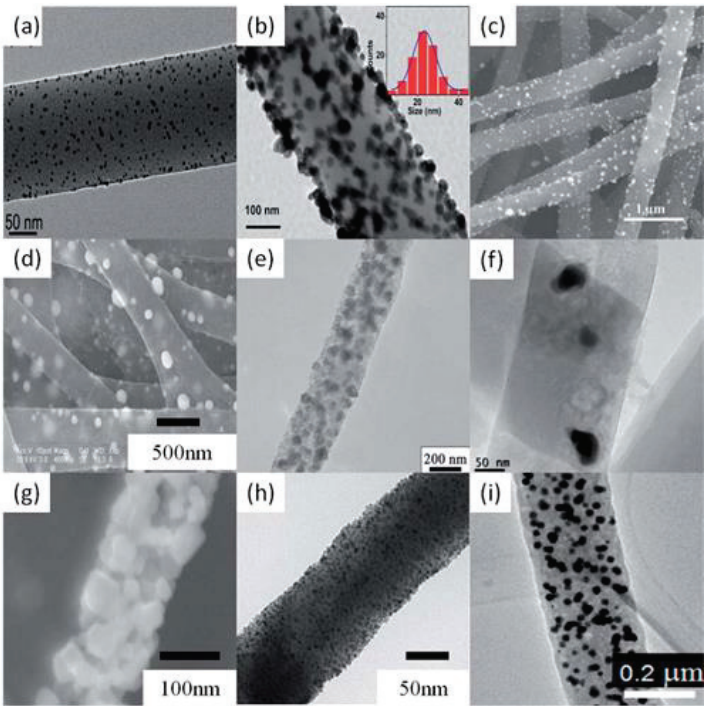

Figure 38. Electrospun polymer NFs doped with different MNPs: (a) PVA–AuNP, (b) PAN–AgNP, (c) PANi–PtNP, (d) CNF–PdNP, (e) CF–NiNP, (f) CNR–CoNP, (g) ZnO–CuNP, (h) Rh-doped ZrO2 NFs, (i) CNF–$Pd_{30}Ni_{70}$. Extracted from Ref 89.

Electrospun polymer NFs doped with MNPs for electrochemical enzyme-based biosensing

Recently, the synthesis and immobilization of noble metal nanoparticles (MNPs) into and onto electrospun nanofibers[184, 185, 186] for producing functional nanocomposites in sensing have attractred much attention. By introducing a small amount of MNP, in/on the electrospun polymeric NFs, the mechanical strength and conductivity of the final NF-MNP composites can be obviously improved compared to those of pristine polymeric fibers. ES technique has been used to prepare MNP–CNF composites for electrochemical sensing applications by spinning metal precursor-containing polymer NFs, followed by a thermal treatment.[187] The advantages of this method include the uniform dispersion of MNPs within the framework of CNF, the high electrical conductivity of CNF, and the highly porous and mechanically strong network structure of the resulting composite, which contribute to a high electrochemical

[184] X. Fang et al., "Facile Immobilization of Gold Nanoparticles into Electrospun Polyethyleneimine/polyvinyl Alcohol Nanofibers for Catalytic Applications," *Journal of Materials Chemistry* 21, no. 12 (**2011**): 4493.

[185] H. Zhu et al., "Self-Assembly of Various Au Nanocrystals on Functionalized Water-Stable PVA/PEI Nanofibers: A Highly Efficient Surface-Enhanced Raman Scattering Substrates with High Density of 'hot' Spots," *Biosensors and Bioelectronics* 54 (**2014**): 91–101.

[186] J. Bai et al., "A Simple and Effective Route for the Preparation of Poly(vinylalcohol) (PVA) Nanofibers Containing Gold Nanoparticles by Electrospinning Method," *Solid State Communications* 141, no. 5 (**2007**): 292–95.

[187] J. Huang et al., "Simultaneous Electrochemical Determination of Dopamine, Uric Acid and Ascorbic Acid Using Palladium Nanoparticle-Loaded Carbon Nanofibers Modified Electrode," *Biosensors and Bioelectronics* 24, no. 4 (**2008**): 632–37.

activity by providing a larger active surface area, preventing MNPs from detachment and agglomeration, and facilitating electron and mass transfer within the system.

Guo et al.[188] successfully prepared Pd–Ni alloy NP-doped carbon NFs (CNF–PdNi) composites by a simple method involving ES of precursor PAN/$Pd(acac)_2$/$Ni(acac)_2$ NFs, followed by a thermal process to reduce metals and carbonize PAN (**figure 38i**). CV studies showed that the CNF–PdNi-based electrodes reveal enhanced redox properties compared to the Ni-metal electrode and show significantly improved electrocatalytic activity to sugars (e.g., glucose, fructose, sucrose, and maltose) oxidation. The application potential of CNF–PdNi-based electrodes in flow systems for sugar detection was explored. A very low limit of detection for sugar (e.g.,7–20 nM), high resistance to surface fouling, excellent signal stability and reproducibility, and a very wide detection linear range (e.g., 0.03–800mM) were revealed for this new type of CNF–PdNi composite as the detecting electrode.

Hou and co-workers[189] synthesized PdNP-loaded CNFs (CNF–PdNP) by the combination of ES and thermal treatment processes. The CNF–PdNP-modified carbon paste electrode (CNF–PdNP/CPE) demonstrated direct and mediatorless responses to H_2O_2 at low potentials. The results of CVs suggested a faster electron transfer rate and higher electrocatalytic activity toward the reduction of H_2O_2 at the CNF–PdNP/CPE when compared to AgNP-modified glassy carbon electrode (GCE). The sensor achieved 95% of the steady-state current within 5 s. The CNF–PdNP/CPE displayed a wider linear range from 0.2 mM to 20 mM and a slope of 4.15 μAmM^{-1}.

Liu et al.[190] produced a novel PtNP-loaded carbon NF (CNF–PtNP) electrode with ES technique, and further applied the electrode for sensing of H_2O_2. When applied to the electrochemical detection of H_2O_2, the CNF–PtNP electrode exhibited low over-potential, fast response, and high sensitivity. In addition, the CNF–PtNP electrode showed good selectivity for H_2O_2 detection in the presence of ascorbic acid, acetaminophenol and uric acid under physiological pH condition. The electrode exhibited strong and fast response to each injection of analyte, attributing to the high electrocatalytic efficiency of the well-dispersed PtNPs. With this electrospun electrode, a detection limit of 0.6 μM with a linear range of 1–800 μM was obtained.

To produce electrochemical enzymatic biosensors of enhanced sensitivity, NFs/AuNPs/enzyme composites can be elaborated. Devadoss's group[191] reported the electrochemical application of AuNP-decorated Nafion NFs (NNF–AuNP) using a facile ES technique. Owing to the uniform distribution of the AuNPs and the large surface area of the NNFs, the NNF–AuNPS-modified electrodes gave rise to greatly improved electrochemical

[188] Q. Guo et al., "Pd–Ni Alloy Nanoparticle/Carbon Nanofiber Composites: Preparation, Structure, and Superior Electrocatalytic Properties for Sugar Analysis," *Analytical Chemistry* 86, no. 12 (**2014**): 5898–5905.
[189] J. Huang et al., "Electrospun Palladium Nanoparticle-Loaded Carbon Nanofibers and Their Electrocatalytic Activities towards Hydrogen Peroxide and NADH," *Advanced Functional Materials* 18, no. 3 (**2008**): 441–48.
[190] Y. Liu et al., "A Novel and Simple Route to Prepare a Pt Nanoparticle-Loaded Carbon Nanofiber Electrode for Hydrogen Peroxide Sensing," *Biosensors and Bioelectronics* 26, no. 11 (**2011**): 4585–90,.
[191] A. Devadoss et al., "Gold Nanoparticle-Composite Nanofibers for Enzymatic Electrochemical Sensing of Hydrogen Peroxide," *The Analyst* 138, no. 17 (**2013**): 5025.

properties compared to AuNP-free electrodes. When they were employed as reservoirs for immobilizing horseradish peroxidase (HRP), sensitive electrochemical detection by the enzyme reaction was achieved. The detection sensitivity for H_2O_2 was determined to be as low as 38 Nm. To determine the electrochemical response to H_2O_2, CV was performed in the absence and presence of 0.01 mM H_2O_2, where HRP-immobilized NNFs and NNF–AuNP-modified electrodes were compared. Upon the addition of 0.01 mM H_2O_2, the most noticeable change in the current was observed for the NNF–AuNP electrode. The current density of NNF–AuNP/HRP-modified electrodes was almost 2.4-fold greater than that of NNF/HRP-modified electrodes. This result clearly indicates that the AuNPs play a critical role in H_2O_2 reduction through catalyzing HRP enzyme on the composite electrode. Furthermore, the NNF–AuNP-modified electrode in the absence of HRP did not show the distinct redox peak even at high concentrations of H_2O_2 indicating that the reduction of H_2O_2 at the electrode surface is predominantly catalyzed by the immobilized HRP. This kind of H_2O_2 sensor has a good linear range from as 0.06 to 0.08 μM with a current sensitivity of 0.3242 $\mu A \mu M^{-1}$.

Nevertheless, to have the surface of the polymeric fibers effectively covered with MNPs, which is essential in applications where the amount of accessible sites is important (i.e their catalytic performance in biosensing), a large ratio of MNPs relative to the polymeric NFs is usually incorporated into the polymer solution leading to an increase in the cost. So, alternatively, MNPs can be directly deposited onto electrospun polymer NFs via surface modication.[192, 193, 194] Dong et al.[192] demonstrated the successful assembly of MNPs (Ag, Au, Pt) onto electrospun nylon 6 NFs by controlling the interfacial hydrogen-bonding interactions.

Recently, Zhu et al.[175] reported the fabrication of water stable PVA/MNPs fibers for biosensors. They prepared highly uniform and monodisperse noble MNPs (Ag, Au, and Pt) in polyvinyl alcohol (PVA) NFs by combining electrospinning (a mixture of MNPs and PVA) and an in situ reduction technique (crosslinking under GA vapors), which were used as efficient biosensor for the detection of H_2O_2. The fabricated AgNPs/PVA NFs functionalized electrodes exhibited remarkably increased electrochemical catalysis toward H_2O_2 and excellent stability, reusability, high sensitivity and broad linear range (10μM to 560 μM). The rapid electrode response to the change of the H_2O_2 concentration is attributed to the fast diffusion of the H_2O_2 onto the surface of small AgNPs through the porous nanofibers structures.

Wang et al.[194] reported a facile route to fabricate water stable AuNP–poly(vinyl alcohol) (PVA/AuNPs) hybrid nanofibrous mats with tunable densities of AuNPs and further demonstrated the potential application of as-prepared PVA/AuNPs NFs as efficient H_2O_2

[192] H.Dong et al., "Assembly of Metal Nanoparticles on Electrospun Nylon 6 Nanofibers by Control of Interfacial Hydrogen-Bonding Interactions," *Chemistry of Materials* 20, no. 21 (**2008**): 6627–32.

[193] L. Ouyang et al., "Catalytic Hollow Fiber Membranes Prepared Using Layer-by-Layer Adsorption of Polyelectrolytes and Metal Nanoparticles," *Catalysis Today* 156, no. 3–4 (**2010**): 100–106,.

[194] J. Wang et al., "Facile Fabrication of Gold Nanoparticles-Poly(vinyl Alcohol) Electrospun Water-Stable Nanofibrous Mats: Efficient Substrate Materials for Biosensors," *ACS Applied Materials & Interfaces* 4, no. 4 (**2012**): 1963–71.

biosensor substrate materials. The PVA NFs were rendered water stable through the designed in situ cross-linkage in co-electrospun PVA/glutaraldehyde NFs. The electrospun water stable NFs were covered with MPTES, which triggered homogeneous decoration with AuPs through gold-sulfur bonding. Finally, the PVA/AuNPs NFs embedded with horseradish peroxidase (HRP) by electrostatic interactions were used as biosensor substrate materials for H_2O_2 detection. The fabricated PVA/AuNPs/HRP biosensor showed a highly sensitivity with a detection limit of 0.5 μM.

Chowdhury[195] et al. reported the fabrication of a biosensing platform by covalent attachment of biomolecules on PANI nanowire (NW) decorated with gold nanoparticles (AuNP) for the detection of glucose, complementary DNA strand and Lamin A protein. The lower detection limit (1μM), higher sensitivity (14.63 $\mu AmM^{-1}cm^{-2}$), wide dynamic range (1μM to 20mM), greater stability and the excellent specificity demonstrates the sensors enhanced performance compared to other glucose sensors.

Electrospun polymer NFs doped with CNTs and MNPs for electrochemical sensing

One of the latest trends in the development of new generation electrochemical sensors is the use of electrospun fibers doped with both CNTs and MNPs.[196, 197] Considering the good electrocatalytic performance of AgNPs and the excellent conductivity of MWCNTs, Ouyang et al.[198] reported the electrospun preparation of PU NFs filled with MWCNTs and AgNPs (PU–MWCNT–AgNP) for the fabrication of electrochemical sensors. The prepared PU–MWCNT–AgNP hybrid NFs are expected to have better performance than either PU–MWCNT or PU–AgNP NFs. By simply blending the suspension of modified MWCNTs and commercialized AgNPs with PU solution and then performing ES, PU–MWCNT–AgNP hybrid NFs were directly electrospun onto the surface of a polished GCE and the performance of the NF-modified GCE for H_2O_2 sensing was investigated. The presented CV results indicated that the PU/MWCNT/AgNPs-modified GCE has better electrocatalytic activity than either PU/MWCNT or PU/AgNPs modified GCE toward the reduction of H_2O_2, which confirms the synergistic effect of MWCNTs and AgNPs. PU–MWCNT–AgNP-modified GCE reveals a linear response to H_2O_2. The sensor has a linear detection range from 0.5 to 30 mM, and possesses a detection limit of 18.6μM (S/N=3) with a sensitivity of 160.6 $\mu AmM^{-1}cm^{-2}$.

---

[195] A.D.Chowdhury, R. Gangopadhyay and A. De, "Highly Sensitive Electrochemical Biosensor for Glucose, DNA and Protein Using Gold-Polyaniline Nanocomposites as a Common Matrix," *Sensors and Actuators B: Chemical* 190 (**2014**): 348–56.

[196] S. Hwang et al., "Formation of Electrically Conducting, Transparent Films Using Silver Nanoparticles Connected by Carbon Nanotubes," *Thin Solid Films* 562 (**2014**): 445-450.

[197] S. Xiao et al., "Fabrication of Multiwalled Carbon Nanotube-Reinforced Electrospun Polymer Nanofibers Containing Zero-Valent Iron Nanoparticles for Environmental Applications," *Journal of Materials Chemistry* 20, no. 27 (**2010**): 5700-5708.

[198] Ouyang et al., "Fabrication, Characterization and Sensor Application of Electrospun Polyurethane Nanofibers Filled with Carbon Nanotubes and Silver Nanoparticles," *Journal of Materials Chemistry B* 1 (**2013**):2415-2424.

In a further study, Zhang et al.[199] fabricated PVDF/MWCNT/PtNPs nanofibrous membrane by ES and utilized the membrane for sensors of H_2O_2 and glucose. The nonenzymatic amperometric biosensor has highly stable and sensitive, and selective detection of H_2O_2 and glucose.

I.4. Nanostructured Conducting Polymers for High Performance Biosensor Applications: Issues and Challenges

Another very interesting class of materials for the production of electrospun NFs for biosensor applications is the one of conducting polymers. Except for the advantages that they have to offer in the biosensors field, in the following sections we will describe the challenges that are encountered during the electrospinning of such materials, while demonstrating alternative ways to overcome this issue.

I.4.1. Importance of Nanostructured Conducting Polymers to Biosensor Applications

Conducting polymers (CPs) are multifunctional materials of particular interest that can be employed as receptors as well as transducers or immobilization matrices in electrochemical biosensing due to their unique electrical properties.[200, 201] They possess fascinating chemical and physical properties, such as intrinsic conductivity, derived from their conjugated π-electron system and so they have been used to enhance the speed, sensitivity and versatility of biosensors.[202, 203] CPs have a variety of advantages such as facile synthesis, structural diversity and flexibility, light weight, and cost effectiveness.

From the viewpoint of sensor applications, the most distinguishing properties of CPs are as follows: i) conducting polymers can be readily prepared by electrochemical and chemical polymerization. The electrochemical synthesis allows the direct deposition of the polymer on the electrode surface, with simultaneous entrapment of protein molecules. It is thus possible to control the spatial distribution of the immobilized enzymes, the film thickness and modulate the enzyme activity by changing the state of the polymer, ii) they are highly sensitive to a broad range of analytes at ambient temperature; iii) an amplified response is expected from their inherent transport properties (e.g., electrical conductivity and rapid electron transfer), iv) the polymer structure is conveniently modified or functionalized to display selective responses toward specific analytes, v) a sensor array can be fabricated through electrochemical deposition or solution casting, which allows miniaturization and mass

[199] Zhang et al., "Electrospun Doping of Carbon Nanotubes and Platinum Nanoparticles into the B-Phase Polyvinylidene Difluoride Nanofibrous Membrane for Biosensor and Catalysis Applications" *ACS Applied Materials & Interfaces* 1 (**2014**):7563-7571.

[200] A. J. Heeger, "Semiconducting and Metallic Polymers: The Fourth Generation of Polymeric Materials (**Nobel** Lecture)," *Angewandte Chemie International Edition* 40, no. 14 (**2001**): 2591–2611.

[201] A.G. MacDiarmid, "'Synthetic Metals': A Novel Role for Organic Polymers (**Nobel** Lecture)," *Angewandte Chemie International Edition* 40, no. 14 (**2001**): 2581–90.

[202] M. Singh et al., "Polypyrrole Based Amperometric Glucose Biosensors," *Sensors and Actuators B: Chemical* 143, no. 1 (**2009**): 430–43.

[203] H. Shirakawa, "The Discovery of Polyacetylene Film: The Dawning of an Era of Conducting Polymers (**Nobel** Lecture)," *Angewandte Chemie International Edition* 40, no. 14 (**2001**): 2574–80.

production of sensor devices. These features make it highly attractive to use conducting polymers for sensor applications.[85] Most conducting polymer sensors rely on electrochemical detection techniques using amperometric, potentiometric, and conductometric methods. The response mechanisms of conducting polymers comprise oxidation/reduction, swelling, conformational changes, charge transfer, and so forth.

Nevertheless, only limited progress had been made in conducting-polymer-based biosensors until nanostructured CPs, such as nanofibers, nantubes, nanorodes, etc., have emerged as promising candidates for high-performance signal transducer applications. Significant advances in the synthesis of conducting-polymer nanomaterials have been recently reported, with enhanced sensitivity relative to their bulk counterparts. More specifically, when formed as nanostructures, CPs inherit the fascinating properties from their bulky counterparts and possess further appealing properties such as high surface area, ease of preparation by chemical or electrochemical methods, considerable signal amplification due to their electrical conductivity, and fast electron transfer rate. By virtue of the high surface-to-volume ratio, CP nanomaterials are capable of yielding excellent sensitivity via enhanced interaction between the conducting polymers and a wide range analytes. The nanostructured materials permit rapid adsorption/desorption kinetics for analytes, leading to fast response/recovery time even at room temperature. Moreover, they allow easy chemical functionalization of their structure in order to obtain high specificity towards different compounds, and are amenable to fabrication procedures that greatly facilitate miniaturization and array production.[85]

I.4.2. Conducting Polymers: Characteristics and Synthesis

As mentioned, CPs are characterized by an extended π-conjugation along the polymer backbone which promotes their unusual electronic properties such as intrinsic conductivity,[204] low energy optical transitions, low ionization potential and high electron affinity. This extended π -conjugated system of the conducting polymers have single and double bonds alternating along the polymer chain. The higher values of the electrical conductivity obtained in such organic polymers have led to the name 'synthetic metals'.[205] Their electrical conductivity results from the formation of charge carriers ("doping") upon oxidizing (p - doping) or reducing (n-doping) their conjugated backbone.[206] In this way they assume the electrical properties of metals, while having the characteristics of organic polymers, such as light weight, resistance to corrosion, flexibility, and ease of fabrication.[207] The main classes of conductive polymers are shown in figure 39.

---

[204] G. Bidan, "Electroconducting Conjugated Polymers: New Sensitive Matrices to Build up Chemical or Electrochemical Sensors. A Review," *Sensors and Actuators B: Chemical* 6, no. 1–3 (**1992**): 45–56.

[205] M. Gerard et al., "Application of Conducting Polymers to Biosensors," *Biosensors and Bioelectronics* 17, no. 5 (**2002**): 345–59.

[206] U. Lange et al., "Conducting Polymers in Chemical Sensors and Arrays," *Analytica Chimica Acta* 614, no. 1 (**2008**): 1–26.

[207] S. Palaniappan and Amalraj John, "Polyaniline Materials by Emulsion Polymerization Pathway," *Progress in Polymer Science* 33, no. 7 (**2008**): 732–58.

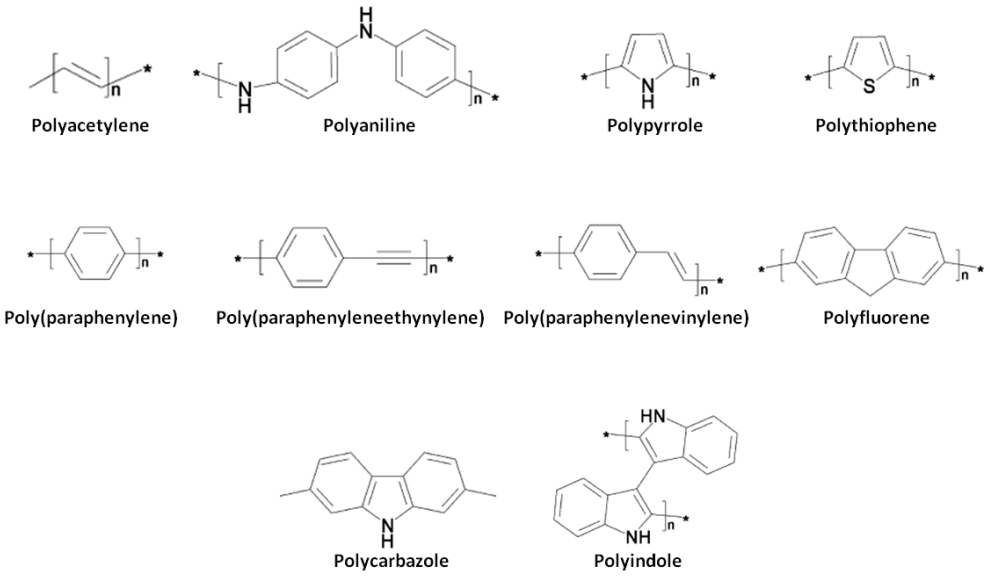

Figure 39. Chemical formulas of the main classes of conductive polymers.

Various methods are available for the synthesis of conducting polymers. The polymers can be synthesized either by addition of an external agent (this approach is often referred as "chemical synthesis" of CP) or by electrochemical reaction. A widely used technique is the oxidative coupling involving the oxidation of monomers to form a cation radical followed by coupling to form dications and the repetition leads to the polymer.[205] Chemical synthesis of CP is usually performed by such oxidants as $(NH_4)_2S_2O_7$ or $FeCl_3$ and is commonly used for the preparation of CP solutions, while electrochemical deposition is used mainly for deposition of CP films on conducting substrates. An advantage of this method is the possibility to control the film thickness by varying either the potential or current with time during the film growth. Other popular techniques for depositing thin films on various substrates are spin coating by a solution of a chemically synthesized CP, the deposition of one or more monomolecular layers of CP by Langmuir–Blodgett technique, or coating of substrates by bilayers of CP and opposed charged polymers by the layer-by-layer technique.[206]

I.4.3. Challenges of Electrospinning Intrinsically Conducting Polymers

Electrospinning is capable of producing conductive fibrous membranes with high specific area, high porosity and tunable fiber diameters, which further broadened conductive polymers applicability in a wide range of applications.[208] However, processing intrinsically conducting polymers (ICPs) has always represented a challenge. Indeed, most of them are insoluble and infusible due to the stiffness of their all-conjugated aromatic backbone structures[103], which renders them hardly electrospinnable. Therefore to overcome this issue, different approaches maybe used which allow the fabrication of conductive NFs. These

[208] J. Wang et al., "Electrospun Porous Conductive Polymer Membranes," ed. Nakhiah C. Goulbourne and Zoubeida Ounaies, (**2012**): 83420F – 83420F – 13.

techniques include: a) the addition of a spinnable polymer used as a carrier to the ICP[209, 210, 211, 212] to improve the spinability of the latter. Nevertheless, the electroactive properties of ICPs can be significantly reduced when blended with conventional polymers. b) the dispersion of a conductive load such as carbon nanotubes or metal nanoparticles into a non-conducting polymer matrix[129, 213, 214, 215, 216, 217] as it has already been described in details in the previous section, c) the use of polymer precursors by subsequent conversion into conducting polymer in the second step[218], and d) the use of a core-shell coaxial electrospinning by subsequent removal of the non-conductive core or shell.[219, 220]

Recently, an interesting processing technique has been developed and optimized to fabricate conductive fibers on electrospun non-conductive fibers: the Vapour-Phase Polymerization technique (VPP)[221, 222]. The method was originally described by Mohammadi et al.[223] as a chemical vapour deposition (CVD) process using $FeCl_3$ or H_2O_2 as oxidizing agents for polymerization of PPy films. VPP is a two-step in situ polymerization process: (1) the oxidant is deposited from solution onto a substrate by a usual coating method (spin-coating, screen-printing, inkjet printing, etc.) and annealed in order to remove the solvent; (2) the coated substrate is then placed in a reactor kept in dry conditions and filled with the

[209] K. Low et al., "Composition-Dependent Sensing Mechanism of Electrospun Conductive Polymer Composite Nanofibers," *Sensors and Actuators B: Chemical* 207 (**2015**): 235–42.

[210] Mohammad Rezaul Karim, "Fabrication of Electrospun Aligned Nanofibers from Conducting Polyaniline Copolymer/polyvinyl Alcohol/chitosan Oligossacaride in Aqueous Solutions," *Synthetic Metals* 178 (**2013**): 34–37.

[211] E. Zampetti et al., "Biomimetic Sensing Layer Based on Electrospun Conductive Polymer Webs," *Biosensors and Bioelectronics* 26, no. 5 (**2011**): 2460–65.

[212] I.S. Chronakis, "Conductive Polypyrrole Nanofibers via Electrospinning: Electrical and Morphological Properties," I S Chronakis, "Conductive Polypyrrole Nanofibers via Electrospinning: Electrical and Morphological Properties," *Polymer* 47 (**2006**): 1597-1603.

[213] K. Ketpang and Jun Seo Park, "Electrospinning PVDF/PPy/MWCNTs Conducting Composites," *Synthetic Metals* 160, no. 15–16 (**2010**): 1603–1608.

[214] S. Mazinani, Abdellah Ajji, and Charles Dubois, "Morphology, Structure and Properties of Conductive PS/CNT Nanocomposite Electrospun Mat," *Polymer* 50, no. 14 (**2009**): 3329–42.

[215] Z. Ding et al., "Self-Assembled Transparent Conductive Composite Films of Carboxylated Multi-Walled Carbon Nanotubes/poly(vinyl Alcohol) Electrospun Nanofiber Mats," *Materials Letters* 128 (**2014**): 310–13.

[216] Y. Sharma et al., "Fabrication of Conducting Electrospun Nanofibers Scaffold for Three-Dimensional Cells Culture," *International Journal of Biological Macromolecules* 51, no. 4 (**2012**): 627–31.

[217] S. Shao et al., "Osteoblast Function on Electrically Conductive Electrospun PLA/MWCNTs Nanofibers," *Biomaterials* 32, no. 11 (**2011**): 2821–33.

[218] D.Y. Youn et al., "Facile Synthesis of Highly Conductive RuO2-Mn3O4 Composite Nanofibers via Electrospinning and Their Electrochemical Properties," *Journal of The Electrochemical Society* 158, no. 8 (**2011**): A970.

[219] J.C. Dias et al., "Electrical Properties of Intrinsically Conductive Core–shell Polypyrrole/poly(vinylidene Fluoride) Electrospun Fibers," *Synthetic Metals* 197 (**2014**): 198–203.

[220] Minoru Miyauchi et al., "Conductive Cable Fibers with Insulating Surface Prepared by Coaxial Electrospinning of Multiwalled Nanotubes and Cellulose," *Biomacromolecules* 11, no. 9 (**2010**): 2440–45.

[221] J.P. Lock, S.Gap Im and K. K. Gleason, "Oxidative Chemical Vapor Deposition of Electrically Conducting Poly(3,4-Ethylenedioxythiophene) Films," *Macromolecules* 39, no. 16 (**2006**): 5326–29..

[222] B. Winther-Jensen and K. West, "Vapor-Phase Polymerization of 3,4-Ethylenedioxythiophene: A Route to Highly Conducting Polymer Surface Layers," *Macromolecules* 37, no. 12 (**2004**): 4538–43.

[223] A. Mohammadi et al., "Chemical Vapour Deposition (CVD) of Conducting Polymers: Polypyrrole," *Synthetic Metals* 14, no. 3 (**1986**): 189–97.

monomer vapours. When the vapours come into contact with the oxidant, they polymerize at the exact same place where the oxidant was coated. This latter step is a solvent-free process where the oxidant is thought to play a templating role that leads to particularly ordered polymers and sometimes crystalline ones.

Different studies demonstrated that this high molecular order resulted in polymers with significantly higher charge conductivities (better interchain π-π stacking resulting in enhanced charge mobility in the polymer).[224] For example, thin films of vapour-phase polymerized polypyrrole (PPy) have reached conductivities of 200 S/cm.[225] Moreover since it is a flexible and solventless method it simplifies the coating process on a variety of organic and inorganic materials because it does not depend on evenly wetting the substrate surface and also it enables conformal coatings on high-area-surface morphologies, like fibers and pores, important for higher device efficiencies.[221] The VPP technique was successfully used to coat electrospun nanofibers of conventional polymers with an ICP[226, 227, 228] and the electrical properties observed for these polymeric porous nanostructured materials are very promising.

The VPP technique is generally used to achieve highly ordered thin films of ICPs and as metallic electrode replacement in organic electronic devices, such as photovoltaics, field-effect transistors, or light-emitting devices.[224] Bai et al.[227] reported the fabrication of a gas sensor based on polypyrrole (PPy)/PMMA composite fibers for sensing ammonia or chloroform vapour, prepared by combining electrospinning and vapor-phase polymerization, which exhibited greatly improved performances comparing with those of the device based on a PPy flat film.

I.4.4. Integration of Electrospun Conducting Polymers to Sensing and Biosensing Systems

Electrospun conductive polymeric NFs, mainly produced by mixing a conductive and a non conductive polymer and by the dispersion of a conductive loading into a non-conducting polymer matrix, have been employed to detect diverse analytes such as toxic gases, volatile organic compounds, and biological species. It has been proven that the utilization of conducting electrospun polymeric NFs[229], such as polyaniline NFs (PANI),[230] polypyrrole

---

[224] A.Laforgue and Lucie Robitaille, "Production of Conductive PEDOT Nanofibers by the Combination of Electrospinning and Vapor-Phase Polymerization," *Macromolecules* 43, no. 9 (**2010**): 4194–4200.

[225] P. Subramanian, N. B. Clark, L. Spiccia, D. R. MacFarlane, B Winther-Jensen and C. Forsyth, "Vapour Phase Polymerisation of Pyrrole Induced by iron(III) Alkylbenzenesulfonate Salt Oxidising Agents," *Synthetic Metals* 158, no. 17–18 (**2008**): 704–11.

[226] F. Granato, A. Bianco, C. Bertarelli and G. Zerbi, "Composite Polyamide 6/Polypyrrole Conductive Nanofibers," *Macromolecular Rapid Communications* 30, no. 6 (**2009**): 453–58.

[227] H. Bai, L. Zhao, C. Lu, C. Li and G. Shi, "Composite Nanofibers of Conducting Polymers and Hydrophobic Insulating Polymers: Preparation and Sensing Applications," *Polymer* 50, no. 14 (**2009**): 3292–3301.

[228] S. Nair, S. Natarajan and S. H. Kim, "Fabrication of Electrically Conducting Polypyrrole-Poly(ethylene Oxide) Composite Nanofibers," *Macromolecular Rapid Communications* 26, no. 20 (**2005**): 1599–1603.

[229] Y. Long et al., "Recent Advances in Synthesis, Physical Properties and Applications of Conducting Polymer Nanotubes and Nanofibers," *Progress in Polymer Science* 36, no. 10 (**2011**): 1415–42.

[230] M. Zhao et al., "Polyaniline Nanofibers: Synthesis, Characterization, and Application to Direct Electron Transfer of Glucose Oxidase," *The Journal of Physical Chemistry C* 113, no. 12 (**2009**): 4987–96.

(PPy) NFs,[202, 231, 232, 233] and poly(3,4-ethylenedioxythiophene) (PEDOT) NFs,[234] as biomolecule immobilization matrices for the fabrication of sensors provides high surface area for loading and that in this way it is possible to generate reproducible, highly sensitive and long time stable biosensors.

Suitable surface functionalization of the NFs can lead to a significant improvement of properties relevant to their sensor applications. Covalent and non-covalent approaches have been commonly used to functionalize conducting-polymer nanomaterials. From the viewpoint of covalent approaches, CP nanotubes/nanofibers can be easily modified by grafting functional groups on the polymer backbone or by employing inherently functionalized monomers during polymerization. On the other hand, the non-covalent approaches take advantage of the incorporation of appropriate counter ions into the polymer during synthesis and the electrostatic adsorption of guest molecules on the nanomaterial surface.

Compared with non-covalent approaches, covalent approaches offer more stable and robust functionalities that can withstand further handling and modification steps. In addition, covalent approaches may allow control over the surface functionality in both qualitative and quantitative aspects. A notable example involves chemical derivatization of pyrrole monomer for PPy functionalization.[76] The pyrrole monomer has been modified by chemical substitution predominantly at the nitrogen and 3-position. The N and 3 substitutions ensure that the pyrrole rings are bonded *via* the a,a' linkages. While N-substituted PPy tends to have poor conductivity due the disruption in π-electron conjugation, 3-substituted PPy shows electrochemical properties equivalent to those of non-substituted PPy. Various functional groups such as amino, carboxyl, and alkyl groups have been successfully incorporated into the PPy backbone for specific functionalities, including hydrophobicity/hydrophilicity, adhesion, lubrication, and biocompatibility. For example, the surface carboxyl groups of the nanotubes have been coupled with various functional materials such as organic dyes, DNA, protein, and even nanoparticles.[231, 232, 235]

The above stated support the fact that conducting polymer NFs may be excellent candidates for fabricating high-performance sensors. However, to realize next-generation high-performance sensors based on conducting-polymer NFs, there are still several technological challenges to be solved for practical (bio)sensor applications.[85]

---

[231] H. Yoon et al., "A Novel Sensor Platform Based on Aptamer-Conjugated Polypyrrole Nanotubes for Label-Free Electrochemical Protein Detection," *ChemBioChem* 9, no. 4 (**2008**): 634–41.

[232] H. Yoon et al., "Field-Effect-Transistor Sensor Based on Enzyme-Functionalized Polypyrrole Nanotubes for Glucose Detection," *The Journal of Physical Chemistry B* 112, no. 32 (**2008**): 9992–97.

[233] J.P. Lellouche et al., "Polydipyrrole- and Polydicarbazole-Nanorods as New Nanosized Supports for DNA Hybridization," *Chemical Communications*, no. 34 (**2005**): 4357.

[234] J. Jang et al., "Chemical Sensors Based on Highly Conductive Poly(3,4 Ethylenedioxythiophene) Nanorods," *Advanced Materials* 17, no. 13 (**2005**): 1616–20.

[235] S. Ko and J. Jang, "A Highly Efficient Palladium Nanocatalyst Anchored on a Magnetically Functionalized Polymer-Nanotube Support," *Angewandte Chemie International Edition* 45, no. 45 (**2006**): 7564–67.

I.5. Conclusion

The presented bibliographic study illustrated that the development of innovative and efficient electrochemical biosensors has been the subject of many studies in the recent decades. Since electrochemical sensing is essentially a surface phenomenon, subsequently the surface morphology and electrical properties of the working electrode are critical parameters which determine the sensor performance. In order to enhance both sensitivity and selectivity, the surface topology must be engineered at the nanoscale in order to maximize the contact surface between the sensor and the solution to be analyzed. This surface must also be chemically modified in order to promote specific interaction between the latter and the target molecules. Finally, the surface must be conductive enough, in order to get a sensor with a low electronic transfer resistance.

In this context, nanofibers meet many of the requirements to achieve improved biosensor performances, mainly because they can significantly increase the specific area of the electrode. More specifically, it was highlighted that NFs produced by employing the electrospinning technique are of particular interest due to the advantages that this technique has to offer over other techniques, such as the simplicity and versatility of the processing system and the design flexibility of the electrospun NFs without the need of post-synthetic treatments of the electrospun NFs.

In this chapter, we have shown that the coupling of non conductive electrospun NFs with other classes of nanomaterials such as metallic nanoparticles and carbon nanotubes, leads to a great variety of different pioneering nanostructures that offer great prospects in the development of a whole new generation of biosensing systems.

The above concept is validated through the comparison of a great variety of conventional biosensors reported in the literature and those few based on composite electrospun nanofibers, with the latter exhibiting superior advantages in terms of sensitivity, stability and fast response. However, the employment of such nanostructures as immobilization platforms for the development of new generation biosensors with enhanced performance is still in an early stage. Therefore, there are still limitations to be overcome and improvements to be done in areas such as the simplicity and rapidity of the synthetic method employed for the construction of the biosensor and the reproducibility of the novel biosensors.

Furthermore, in this chapter we have cited another approach to produce conductive electrospun NFs, by coating non-conductive electrospun NFs with a layer of conducting polymer through the VVP process. However, to the best of our knowledge, the combination of the electrospinning technique with the VPP process has not been employed for the elaboration of enzyme-based electrochemical biosesnors.

Through our work we have tried to address the above issues and to contribute in a more simple, easy and rapid way, towards the fabrication of highly senstitive and stable electroactive platforms for electrochemical enzyme biosensors based on conductive electrospun NFs. In chapters II and III, the one-step synthesis of composite CNTs/polymer/enzyme NFs and AuNPs/polymer/enzyme NFs for biosensor elaboration will

be demonstrated respectively. Finally, in chapter IV we will demonstrate the fabrication of an original and highly sensitive electrochemical biosensor based on conductive NFs through the combination of the electrospinning technique and VPP process.

CHAPTER II: ONE-STEP FABRICATION OF ELECTROSPUN PHOTOCROSSLINKABLE POLYVINYL ALCOHOL NANOFIBER MATS INCORPORATING CARBOXYLATED MULTIWALL CARBON NANOTUBES AND ENZYME FOR BIOSENSOR APPLICATIONS

II.1. Introduction

Among the different approaches already reported in the literature for the elaboration of NF-based enzymatic electrochemical biosensors, in this chapter we focused on the technique that consists of the one-step electrospinning of polymer/enzyme/conductive nanomaterial blends.

To do so, among a wide spectrum of polymers we had to strategically select one which would satisfy the following requirements 1) good processability/electrospinnability, 2) biocompatibility (especially in terms of solvent compatibility with the biomolecule since the biomolecule is mixed with the polymer) and 3) high conductivity. Glucose oxidase (GOx) was used as a model enzyme for the detection of glucose. Poly(vinyl alcohol) (PVA), a nontoxic, water soluble synthetic polymer[236], was a great candidate due to its many advantageous properties, e.g., its hydrophilicity, good physical properties, processability, high biocompatibility,[237, 238, 239] good chemical resistance and facile modification of its pendant hydroxyl groups. More specifically, its high water content and minimal diffusion restrictions provide the immobilized enzyme a microenvironment close to that of the soluble enzyme. However, its high hydrophilicity contributes to the fast dissolution of PVA nanofibers (NFs) in aqueous solution, which limits its applications in biosensing. It has been shown that this issue can be overcome by a crosslinking step,[240, 241, 242] generally performed by exposure to glutaraldehyde solutions[250] or vapours.[173] This step is time-consuming and requires careful optimization to preserve enzyme conformation and activity. For this reason, it was decided to work with a PVA derivative with pendent styrylpyridinium groups (SbQ), PVA-SbQ, which has been extensively used as a photocrosslinkable material due to its water stability, high photosensitivity and good storage stability.[243] PVA-SbQ was been widely used in the development of enzymatic biosensors[244] and the PVA-SbQ entrapment of enzymes is schematically represented in figure 40.

---

[236] M. A.P. Nunes, P.C.B. Fernandes and M.H.L. Ribeiro, "High-Affinity Water-Soluble System for Efficient Naringinase Immobilization in Polyvinyl Alcohol-Dimethyl Sulfoxide Lens-Shaped Particles: High-affinity water system for efficient naringinase immobilization," *Journal of Molecular Recognition* 25, no. 11 (**2012**): 580–94.

[237] C. Tang et al., "Effect of pH on Protein Distribution in Electrospun PVA/BSA Composite Nanofibers," *Biomacromolecules* 13, no. 5 (**2012**): 1269–78.

[238] T. Kowalczyk et al., "Electrospinning of Bovine Serum Albumin. Optimization and the Use for Production of Biosensors.," *Biomacromolecules* 9, no. 7 (**2008**): 2087–90.

[239] J.J. Won et al., "Electrospun Core–shell Nanofibers from Homogeneous Solution of Poly(vinyl Alcohol)/bovine Serum Albumin," *International Journal of Biological Macromolecules* 50, no. 5 (**2012**): 1292–98.

[240] E. Yang, X. Qin and S. Wang, "Electrospun Crosslinked Polyvinyl Alcohol Membrane," *Materials Letters* 62, no. 20 (**2008**): 3555–57.

[241] J.M. Gohil, A. Bhattacharya, and P. Ray, "Studies On The Crosslinking Of Poly (Vinyl Alcohol)," *Journal of Polymer Research* 13, no. 2 (**2006**): 161–69.

[242] J. Zeng et al., "Photo-Induced Solid-State Crosslinking of Electrospun Poly(vinyl Alcohol) Fibers," *Macromolecular Rapid Communications* 26, no. 19 (**2005**): 1557–62.

[243] K. Ichimura, "Photocrosslinkable Poly(vinyl alcohols): Preparation, Properties and Application," H*eterogeneous chemistry reviews, 3* **(1996)**: 419-441.

[244] J.M. Guisan, ed., *Immobilization of Enzymes and Cells*, vol. 1051, Methods in Molecular Biology (Totowa, NJ: Humana Press, **2013**).

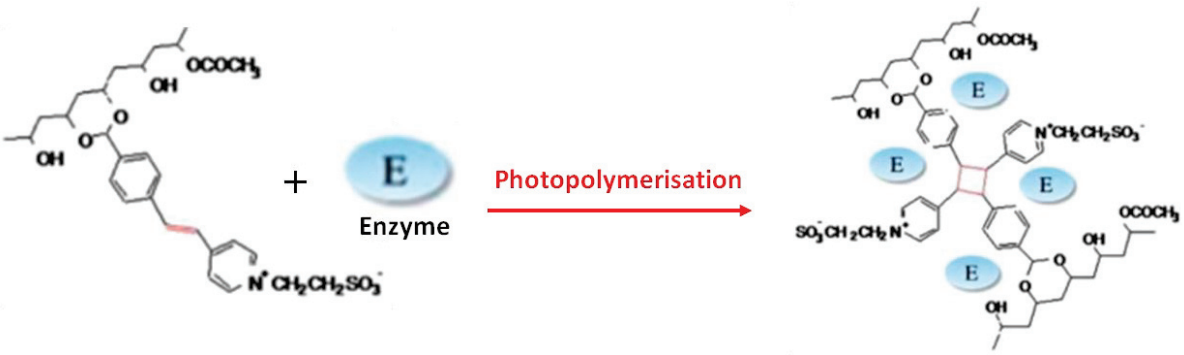

Figure 40. PVA-SbQ entrapment of enzymes. Extracted from Ref 32.

The photocrosslinking behaviour and mechanism of PVA-SbQ have been systematically investigated.[243, 245, 246, 247]Y. Liu et al.[247] were the first to prepare water-insoluble electrospun PVA-SbQ fibers.

Despite their many merits, PVA-SbQ nanofibers still did not satisfy the third and very crucial parameter of electrical conductivity. To improve the conductivity of the polymeric NFs, we proceeded to the addition of carboxylated multiwall carbon nanotubes as conductive fillers into the PVA-SbQ matrix. Nevertheless, the lack of solubility of CNTs in aqueous media has been a technical barrier for many groups in the past. For this reason, herein we decided to work with MWCNTfunctionalized with carboxylic groups (MWCNTs-COOH), to improve their dispersibility in PVA and PVA/GOx aqueous solutions.[248]

Electrospun PVA fibers filled with nanomaterials such as graphene, graphene oxide or carbon nanotubes have already been used for the elaboration of enzymatic electrochemical biosensors as it is illustrated in Table 4. The enzyme was either encapsulated in polymer, when PVA matrix is used, or immobilized after electrospinning, when other types of matrices were used (carbon, nylon 6,6, chitosan or polyacrylonitrile). The interest of the encapsulation of enzyme in polymer nanofibers is the preservation of its activity.[174] The objective of this study was the fabrication of an efficient bioactive surface design for biosensing, by modifying gold electrode surfaces with one-step electrospun PVA-SbQ/MWCNT-COOH/GOx nanofibers. This configuration has never been tested until now (Table 4). Furthermore, MWCNTs-COOH have never been used as conductive fillers in PVA-SbQ NFs for any kind of application.

---

[245] E.S. Cockburn, R.Stephen Davidson, and Julie E. Pratt, "The Photocrosslinking of Styrylpyridinium Salts via a [2 + 2]-Cycloaddition Reaction," *Journal of Photochemistry and Photobiology A: Chemistry* 94, no. 1 (**1996**): 83–88.

[246] Y. Shindo, et al., "Reactivities and Thermal Mechanical Properties of Polyvinyl alcohol and Poly(vinyl-b-acrylic acid) with Pendant Styrylpyridinium Groups," Journal of Photopolymer Science and Technology, 15 (**2002**):153-158.

[247] Y. Liu et al., "Water Resistance of Photocrosslinked Polyvinyl Alcohol Based Fibers," *Materials Letters* 63, no. 3–4 (**2009**): 419–21.

[248] Jeongwoo Lee et al., "Measurement of the Dispersion Stability of Pristine and Surface-Modified Multiwalled Carbon Nanotubes in Various Nonpolar and Polar Solvents," *Measurement Science and Technology* 18, no. 12 (**2007**): 3707–12.

Table 4. Relevant amperometric enzymatic biosensors based on electrospun polymer nanofibers.

Polymer	Enzyme	Nanomaterials	Electrode	Dynamic range	LOD	Ref
Encapsulation of enzyme in the polymer before electrospinning						
PVA Reticulation with GA	GOx	None	Au	1mM – 10 mM	50 µM	[249]
PVA Reticulation with GA	GOx	Graphene (20 ppm)	Pt	0 – 15 mM	NR	[250]
PVA/chitosan/ Nafion layer	GOx	Graphene oxide	Pt	5 µM – 3.5 mM	5 µM	[173]
Silica-PVA	Tyrosinase encapsulated	None	ITO	0 – 100 mM	10 µM	[251]
Immobilization of enzyme after electrospinning						
Carbon	GOx	None	SPE	0 – 20 mM	NR	[252]
Nylon 6,6/PBIBA	GOX	MWCNTs	Graphite	0.01 mM – 2 mM	10 µM	[45]
Chitosan/CNTs	Uricase	CNTs	Au modified with AgNPs	1µM – 0.4 mM	1 µM	[253]
polyacrylonitrile	Polyphenol oxidase	CNTs	PPO modified PAN–NH_2–CNT fibers	0 – 1 mM	0.9 µM	[254]

In this chapter, PVA bearing UV cross-linkable pendent styrylpyridinium groups (PVA-SbQ) was used as polymer matrix to enable a fast, easy and soft cross-linking step without any added chemicals. Different electrospinning parameters including flow rate, applied voltage, distance between tip and collector, polymer concentration were tailored to produce PVA-SbQ/MWCNT-COOH nanofibers (NFs) with minimal beading. The electrochemical properties of electrospun PVA-SbQ/MWCNT-COOH nanofibrous mats were characterized by cyclic voltammetry and electrochemical impedance spectroscopy. Scanning electron

[249] Guanglei Ren et al., "Electrospun Poly(vinyl Alcohol)/glucose Oxidase Biocomposite Membranes for Biosensor Applications," *Reactive and Functional Polymers* 66, no. 12 (**2006**): 1559–64.
[250] C. M. Wu, "Graphene Modified Electrospun Poly(vinyl Alcohol) Nanofibrous Membranes for Glucose Oxidase Immobilization," *Express Polymer Letters* 8, no. 8 (**2014**): 565–73.
[251] Dennis A. Oriero et al., "Electrospun Biocatalytic Hybrid silica–PVA-Tyrosinase Fiber Mats for Electrochemical Detection of Phenols," *Microchemical Journal* 118 (**2015**): 166–75.
[252] Tae-Sung Bae et al., "Effects of Carbon Structure Orientation on the Performance of Glucose Sensors Fabricated from Electrospun Carbon Fibers," *Journal of Non-Crystalline Solids* 358, no. 3 (**2012**): 544–49.
[253] Apon Numnuam, Panote Thavarungkul, and Proespichaya Kanatharana, "An Amperometric Uric Acid Biosensor Based on Chitosan-Carbon Nanotubes Electrospun Nanofiber on Silver Nanoparticles," *Analytical and Bioanalytical Chemistry* 406, no. 15 (**2014**): 3763–72.
[254] Mariem Bourourou et al., "Chemically Reduced Electrospun Polyacrilonitrile–carbon Nanotube Nanofibers Hydrogels as Electrode Material for Bioelectrochemical Applications," *Carbon* 87 (**2015**): 233–38.

microscopy (SEM) and transmission electron microscopy (TEM) were used to characterize the morphology of the nanofibers. The obtained biosensor enabled successful detection of glucose by cyclic voltammetry.

II.2. Apparatus

II.2.1. Instrumentation and Experimental Setup for Electrochemical Measurements

During all electrochemical experiments, cyclic voltammetry and electrochemical impedance spectroscopy were carried out using Voltalab 80 PGZ 402 analyzer (Hach Lange, France) in a 5 mL cell equipped with a conventional three electrode configuration as seen in figure 41. The analyzer was controlled by a software named "Voltamaster".

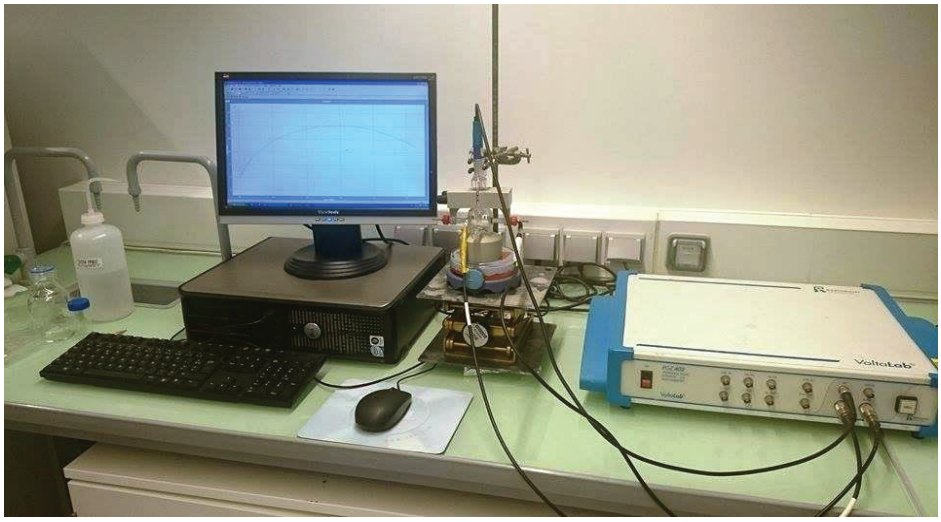

Figure 41. Photograph of working area, presenting the Voltalab 80 PGZ 402 analyzer, the electrochemical cell equipped with a conventional three electrode configuration and the computer used during the electrochemical experiments.

Electrochemical Cell

Cyclic voltammetry and impedimetric measurements were carried out by using a glass electrochemical cell with a conventional three electrode configuration: a working electrode (WE), a reference electrode (RE) and a counter electrode (CE) (figure 42). The geometry of the cell allows a well defined arrangement of three electrodes. As a matter of fact it is important to ensure a homogeneous current density at the working electrode and minimize the phenomenon of ohmic drop, maintaining the working electrode as close as possible to the counter electrode. The **Working Electrode** used for the electrochemical experiments was a macroelectrode consisted of a gold layer of thickness 300 nm, deposited by evaporation onto substrates of Si / SiO_2 using an adhesion layer of 30 nm of titanium (Ti). The gold electrodes were fabricated by the French RENATECH network (Laboratoire d'Analyse et d'Architecture des Systèmes-LAAS, CNRS Toulouse). The active surface of the working electrode was 0.07 cm^2. The **Reference Electrode** used was a silver chloride electrode Ag/AgCl. A platinum

electrode was used as **Counter Electrode**. The active surface of the counter electrode was 0.29 cm^2.

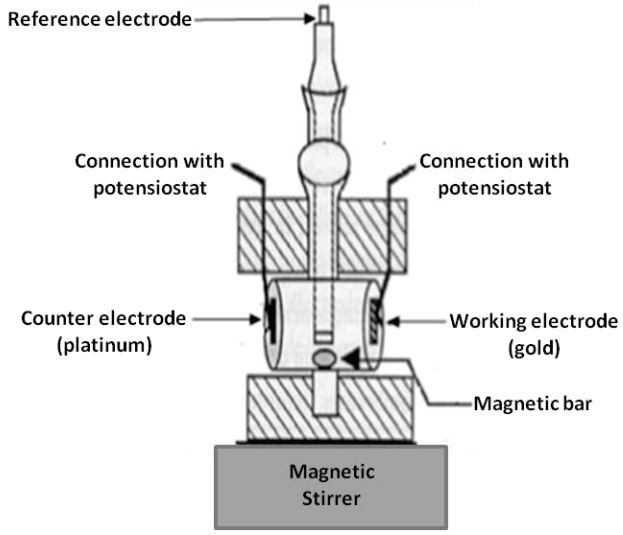

Figure 42. Schematic representation of the electrochemical cell used throughout the electrochemical experiments, equipped with a conventional three electrode configuration.

II.2.2. Instrumentation and Experimental Setup for Electrospinning Technique

In this study, PVA-SbQ, PVA-SbQ/ MWCTNs-COOH and PVA-SbQ/ MWCTNs-COOH/GOx nanofibers were fabricated by using the electrospinning technique. The NFs were fabricated by a home-made electrospinning device at the Institute of Nanotechnology of Lyon (INL) which is represented in figure 43.

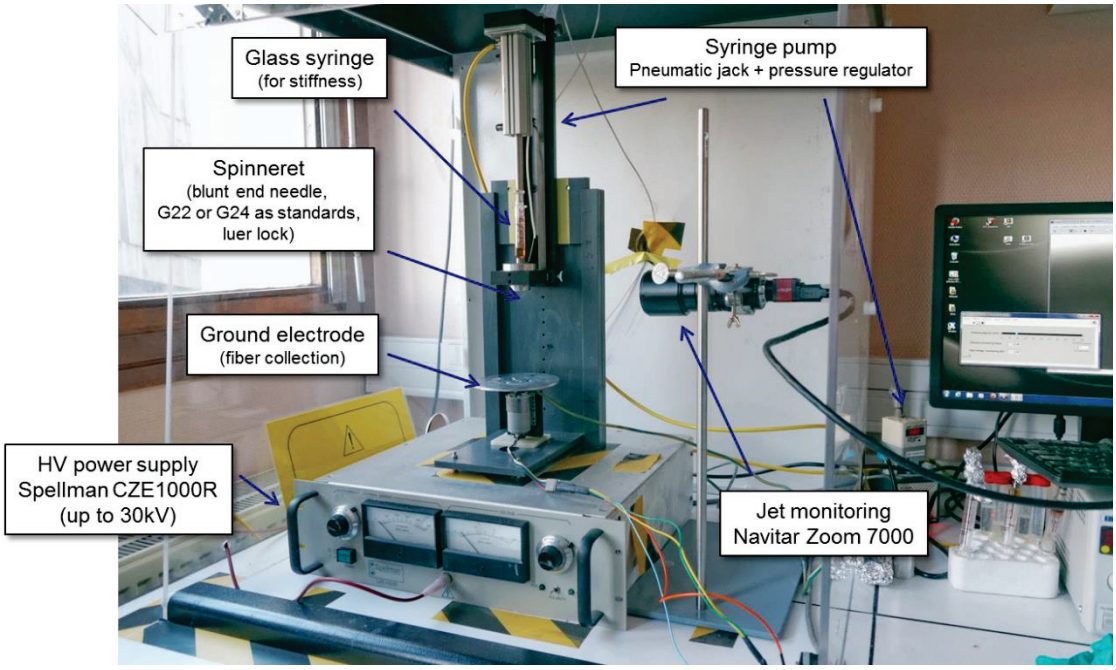

Figure 43. Photograph of the home made electrospinning device used at this work.

The spinneret was made of a glass syringe equipped with a luer lock port to connect blunt-end needles (22 gauge). To control the feed rate of the polymer solution with no induced fluctuations, a pneumatic jack driven by an electro-pneumatic regulator (ITV 1030, SMC) and controlled through a LabView interface was used. The electrical field was produced by a high voltage power supply (Spellman CZE1000R) delivering up to 30kV.

II.3. Materials

Polyvinyl alcohol with styrylpyridinium pendent groups (PVA-SbQ SPP-H-13: degree of polymerization 1700, degree of saponification 88, betaine SbQ 1.3 mol%, solid content 13.35wt%, pH 6.2) was purchased from Toyo Gesei, Glucose and Glucose Oxidase, GOx, from *Aspergillus niger* was purchased from Sigma-Aldrich (Saint-Quentin-Fallavier, France). Carboxylated multi-walled carbon nanotubes (MWCNT-COOH, O.D. x L 100<nm x 5-10μm, purity >95%) were synthesized by Dr.Madjid Arab at Université du Sud Toulon Var – Institut Matériaux Microélectronique et Nanosciences de Provence, France. The multiwall carbon nanotubes were dispersed in aqueous solution (C=0.2 mg/mL) containing 2% (m/v) of SDS. All reagents were used without further purification. Phosphate saline buffer solutions were prepared with mono and dibasic phosphate (pH 7.2, 0.1M).

Glucose, is a sugar with the molecular formula $C_6H_{12}O_6$ and molecular weight of 180.16 g/mol. α-D-glucose is one of the 16 aldose stereoisomers. The D-isomer (figure 44) occurs widely in nature, but the L-isomer does not. Glucose is produced during photosynthesis from water and carbon dioxide, using energy from sunlight. The reverse of the photosynthesis reaction, which releases this energy, is a very important source of power for cellular respiration.

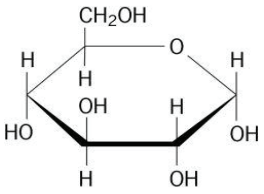

Figure 44. Chemical formula of D-glucose.

GOx enzyme is an oxido-reductase that catalyses the oxidation of of β-D-glucose to D-glucono-1,5-lactone, which then hydrolyzes to gluconic acid. It is often extracted from *Aspergillus niger*.

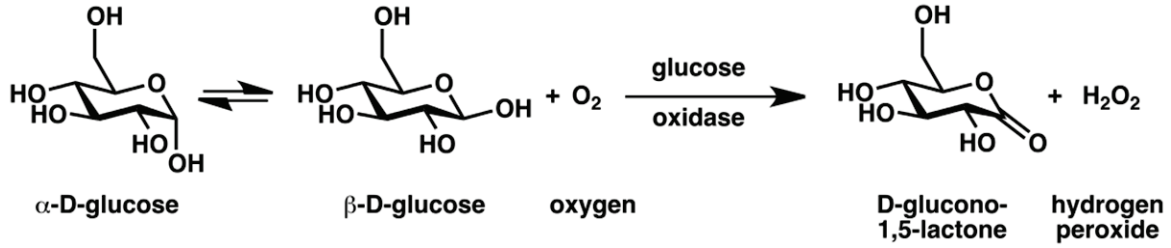

GOx from *Aspergillus Niger* is a dimeric protein consisting of 2 equal subunits each with a molecular weight of 80 kDa. Each subunit contains one mole of flavin adenine dinucleotide and one mole of iron. The enzyme is a glycoprotein containing approximately 16% neutral sugar and 2% amino sugar. The enzyme also contains 3 cysteine residues and 8 potential sites for N-linked glycosylation. The oxidation reaction is performed by the FAD cofactors bound deep inside the enzyme, shown in red. The active site where glucose binds is just above the FAD, in a deep pocket shown with a star. Notice that the enzyme, like many proteins that act outside of cells, is covered with carbohydrate chains, shown in green. Some other characteristics may be found below:

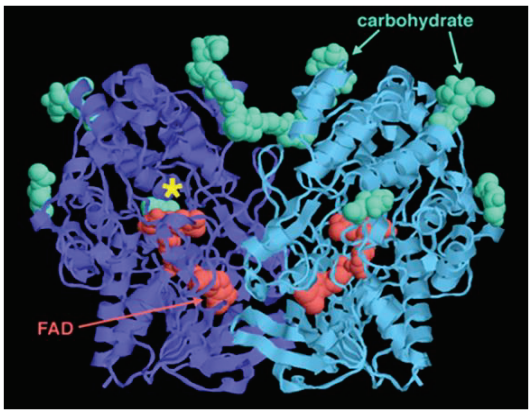

Figure 45. 3-D structure of GOx. Extracted from RCSB PDB-101 (Protein Data Bank).

Molecular weight: 160 kDa (gel filtration)
Extinction coefficient: $E^{1\%}$= 16.7 (280 nm)
Isoelectric point: 4.2
Optimal pH: 5.5 (broad activity range of pH 4-7)
Inhibitors: Ag^{+}, Hg^{2+}, and Cu^{2+} ions, phenylmercuric acetate and p-chloromercuribenzoate inhibit glucose oxidase. Non metallic sulfhydryl reagents, such as N-ethylmaleimide, iodoacetate, and iodoacetamide, are not inhibitors.
Substrates: Glucose oxidase is relatively specific for b-D-glucose (K_M of 33-110 mM). It also oxidizes D-aldohexoses, monodeoxy-D-glucoses, and methyl- D-glucoses at varying rates. The following substrates are listed in decreasing order of oxidation rate: D-glucose, 2-deoxy-D-glucose, 4-O-methyl-D-glucose, 6-deoxy-D-glucose, 4-deoxy-D-glucose, 3-deoxyD-glucose, 3-O-methyl-D-glucose.

Polyvinyl alcohol, PVA, is a water soluble synthetic polymer, white and odorless with chemical formula $[CH_2CH(OH)]_n$ (figure 46). Unlike most vinyl polymers, PVA is not prepared by polymerization of the corresponding monomer. The monomer, vinyl alcohol, is unstable with respect to acetaldehyde. PVA is prepared by first polymerizing vinyl acetate, and the resulting poly(vinyl acetate) is converted to the PVA. The final properties of PVA mainly depend on the properties of its parent polymer, i.e., poly(vinyl acetate), its polymerization conditions and degree of hydrolysis.[241]

All multifunctional compounds capable of reacting with the hydroxyl group may be used as a cross linker of PVA, such as dialdehydes, dicarboxylic acids, dianhydrides, etc.[240]

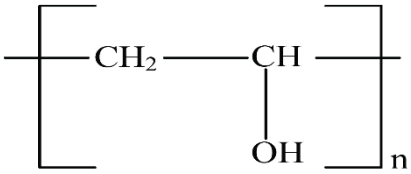

Figure 46. Chemical formula of PVA.

As already mentioned the photocrosslinking behaviour and mechanism of PVA-SbQ have been systematically investigated by Ichimura et al.[243], Shindo et al.[246], Cockburn et al. [245] and Liu et al.[247] The SbQ pendant groups undergo [2+2]-cycloaddition reactions which crosslink the PVA backbones (Figure 47).

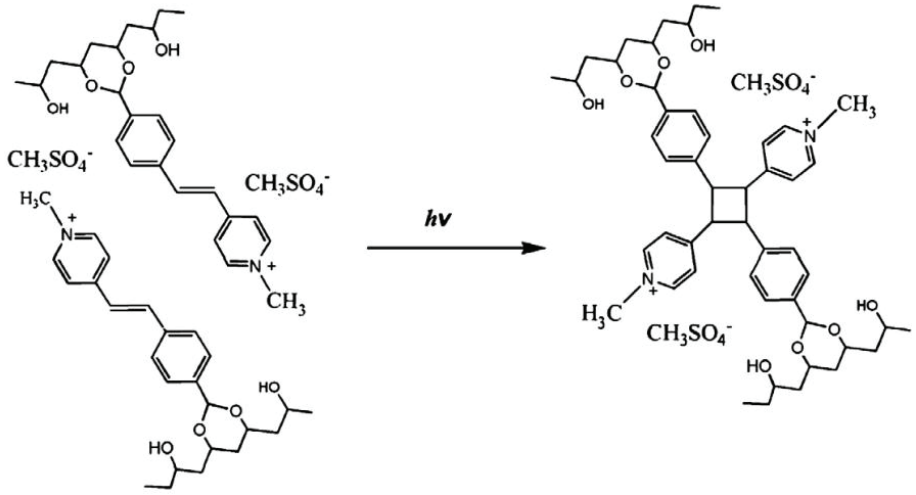

Figure 47. Mechanism of photo-cross-linking of PVA-SbQ. Extrected from Ref 247.

MWCNTs-COOH- Synthesis and functionalization

MWCNTs were produced by aerosol-assisted catalytic chemical vapor deposition (AACCVD). The growth approach was based on the catalytic decomposition of liquid hydrocarbons by pyrolysing mixed aerosols containing both the hydrocarbon and the metallic source which simultaneously and continuously filled the reactor volume.[255] The solution was prepared by dissolving 5 wt% of ferrocene in toluene. The experimental setup was composed of four different parts: an aerosol generator, a ceramic multi-piezoelectric generator, a quartz reactor placed in a furnace and a gas system inlet. The above solution was placed inside the ultrasonic aerosol generator which was connected to the reactor and an air flow of 400 mL min^{-1} was flushed inside the reactor. The temperature of the tubular furnace is then raised up to 820 °C in 1 h. As soon as the synthesis temperature was reached, the argon flow was increased to 1 L min^{-1}. The piezoelectric ceramic, operating at 850 KHz, of the ultrasonic generator was then activated creating an aerosol at the gas-liquid interface which was carried by the argon flow through the heated quartz reactor. At the end of the experiment, the samples were then slowly collected and cooled down to room temperature.

In this study, the obtained multi-walled carbon nanotubes (MWCNTs) were used after being chemically surface-modified in mixed solvents of nitric and sulfuric acid (3:1 molar ratio) at 90 °C for 10 min, followed by high-energy sonication in ethanol for two hours.[256] In this way the MWCNTs were functionalized with (-COOH) and hydroxylic (-COH) groups. Finally, the functionalized MWCNTs were collected by filtration, then washed with distilled water and dried in an oven at a temperature of 80 °C. They were finally dispersed in a 2% (m/v) SDS aqueous solution to achieve a 0.2 mg/mL concentration.

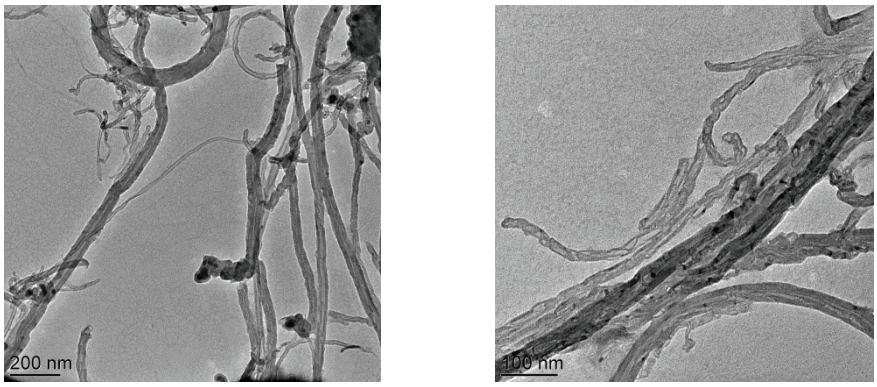

Figure 48. TEM images of the above synthesized carboxylated multi-walled carbon nanotubes.

[255] M. David et al., "Carbon Nanotubes/ceria Composite Layers Deposited on Surface Acoustic Wave Devices for Gas Detection at Room Temperature," *Thin Solid Films* 520, no. 14 (**2012**): 4786–91.

[256] Jae Whan Cho et al., "Electroactive Shape-Memory Polyurethane Composites Incorporating Carbon Nanotubes," *Macromolecular Rapid Communications* 26, no. 5 (**2005**): 412–16.

II.4. Experimental Section

II.4.1. Preparation of the working electrodes

As mentioned in II.2.1., gold electrodes were used as working electrodes. Before functionalization, the gold electrodes were cleaned in an ultrasonic bath for 10 min in acetone and dried under a N_2 flow, then dipped for 2 min at room temperature into a piranha solution, and then rinsed with ethanol. Between and after these treatments, the gold electrodes were rinsed thoroughly with ultrapure water.

II.4.2. Preparation of electrospun solutions

For the fabrication of pure PVA-SbQ NFs, PVA-SbQ solutions (1.5, 5.3, 6.7 and 8 wt%) were prepared by appropriate dilutions of the 13.3 wt% commercial solution in ultrapure water. Transparent and homogeneous solutions were obtained by stirring for 2h at room temperature. For the fabrication of PVA-SbQ/MWCNTs-COOH nanofibers, three PVA-SbQ/ MWCNT-COOH suspensions containing 1, 5 and 10wt% of MWCNT-COOH with respect to the polymer mass were prepared. To do so, MWCNT-COOH at different concentrations (1, 5 and 10 wt% respectively) were added to PVA-SbQ solutions individually and the resulting PVA-SbQ/MWCNT-COOH suspensions were mechanically stirred for 3h and sonicated for 2h at ambient conditions to obtain homogeneous solutions. For the fabrication of PVA-SbQ/MWCNTs-COOH/GOx nanofibers, glucose oxidase (GOx) powder was added to each of the above mixtures (15mg enzyme per mL of polymer solution) and the resulting composites were stirred for another half an hour.

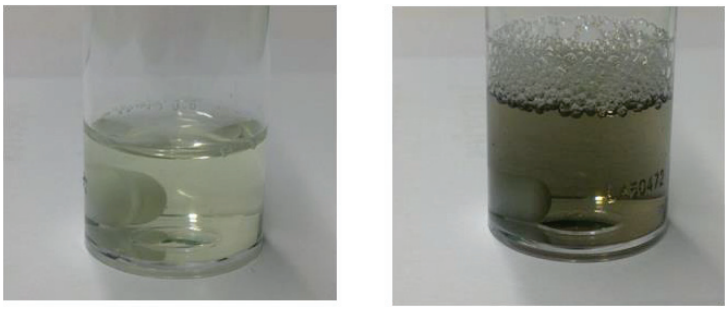

Figure 49. To the left: PVA-SbQ solution (6.7 wt%) after stirring for 2h. To the right: PVA-SbQ/MWCNT-COOH mixture containing 5wt% MWCNT-COOH with respect to the polymer mass after 3h of stirring and 2h in ultasonication bath.

II.4.3. Electrospinning: Fabrication of electrospun PVA-SbQ, PVA-SbQ/MWCNTs-COOH and PVA-SbQ/MWCNTs-COOH/GOx NFs

PVA-SbQ, PVA-SbQ/MWCNTs-COOH and PVA-SbQ/MWCNTs-COOH/GOx suspensions were loaded immediately after preparation into a glass syringe fitted with a stainless needle (0.644 mm I.D.), the cleaned working gold electrodes were placed on the collector inside the ES chamber and fibers were spun at room room temperature (23±2 °C) in

the dark in order to avoid photocrosslinking. The nanofibers were directly deposited on the surface of the electrodes. Since solution viscosity and conductivity varies with MWCNTs-COOH concentration, electrospinning parameters (e.g. applied voltage, feed rate and collection distance) had to be adjusted in each experiment to limit bead formation. Optimal values found for the different MWCNTs-COOH loading are summarized in table at section II.5.1.2. These values were not significantly affected by the addition of GOx in the PVA-SbQ/MWCNTs-COOH composite.

II.4.4. Crosslinking of electrospun NFs

The electrospun NFs were irradiated for 10 min at 365nm in a Bio-link BLX UV- cross-linker (Vilbert Lourmat) equipped with one 100 W UV lamp. All the treated mats were immersed into phosphate saline buffer (pH 7.2) to examine their water stability.

II.4.5. Electrochemical Characterizations

Cyclic voltammetry (CV) and electrochemical impedance spectroscopy (EIS) characterizations were all performed at room temperature. A Voltalab 80 PGZ 402 analyzer and a 5 mL cell equipped with a conventional three electrode configuration were employed, as described in section II.2.1.

II.4.5.1. PVA-SbQ NF and PVA-SbQ/MWCNTs-COOH NF modified electrodes

EIS characterization of PVA-SbQ NF and PVA-SbQ/MWCNTs-COOH NF modified electrodes were carried out in 0.1 M phosphate saline buffer (PBS) pH 7.2 containing 10 mM $K_3Fe(CN)_6^{3-}$ and $K_4Fe(CN)_6^{4-}$, varying the frequency in the 100mHz to 100kHz range and acquiring 5 points per decade. An excitation voltage of 10mV was superimposed on a dc potential of -300mV. Impedance data were fitted to equivalent electrical circuits by means of the ZView2 software (Scribner Associates Inc, Southern Pines, USA). The same electrodes were also characterized by CV, the potential being cycled from -400 and +600 mV (versus Ag/AgCl) with a scan speed of 100 mV/s. 0.1M PBS buffer pH 7.2 containing 10 mM $K_3Fe(CN)_6^{3-}$ and $K_4Fe(CN)_6^{4-}$ was chosen as electrolyte. After each measurement, the electrolyte solution was refreshed, and the electrodes were washed with distilled water to remove any residues.

II.4.5.2. PVA-SbQ/MWCNTs-COOH/GOx NF modified electrodes

Biosensing experiments were performed by injecting glucose from mother solution into the 4 mL electrochemical cell containing the PVA-SbQ/MWCNT-COOH/GOx NF modified electrodes and 0.1 M PBS pH 7.2 as electrolyte. After 5 min reaction, CV was perfomed at 50mV/s in the 0-800 mV range for the specific detection of hydrogen peroxide. Three replicates were performed for each glucose concentration and related standard deviations were calculated.

II.4.6. Characterization of NFs morphology

Fiber mats were characterized by transmission electron microscopy (TEM) using a Philips CM120 instrument operating at an accelerating voltage of 120 kV and by scanning electron microscopy with a TESCAN MIRA3 FEG-SEM microscope after sample metallization (2 nm Pt or Cr).

II.5. Results and Discussion

II.5.1. Optimization study of ES parameters for the fabrication of nanofibrous mats

It is known that surface morphology of electrospun NFs may be affected by different parameters, which may be divided into three main categories: i) solution parameters, i.e. concentration and molecular weight of the polymer, viscosity, conductivity and surface tension, ii) processing parameters, i.e. applied voltage, collection distance, feed rate, iii) ambient parameters, i.e. humidity, temperature.[87] In our study, temperature was regulated at 23±2 °C and all the processing parameters were carefully adjusted in each experiment to produce smooth and uniform fibers without beads and drops.

II.5.1.1. Optimization of PVA-SbQ concentration

The influence of PVA-SbQ concentration on NFs morphology was first investigated by pure polymer solutions. Four concentrations, 1.5, 5.3, 6.7 and 8 wt% of PVA-SbQ were tested. We observed that it was not possible to produce NFs at the lowest polymer concentration due to the insufficient viscocity of the solution for ES. At 5.3 wt% concentration value, polymer chain entanglements were still insufficient to achieve complete stabilization of the jet but the jet was produced and the contraction of its diameter driven by the surface tension caused the solution to form beads. Increasing PVA-SbQ concentration from 5.3 up to 6.7 and finally 8 wt%, helped solving this issue and pure fibers were generated. However, the 8wt% PVA-SbQ solutions supplemented with carbon nanotubes appeared as hardly electrospinnable due to the very high viscocity that the blend exhibited. The 6.7 wt% concentration was therefore selected for further experiments.

II.5.1.2. Influence of MWCNTs-COOH loading on ES parameters for the fabrication of PVA-SbQ/ MWCNTs-COOH NFs

Since PVA-SbQ solution viscosity and conductivity varies with MWCNTs-COOH concentration, electrospinning parameters (e.g. applied voltage, feed rate and collection distance) had to be adjusted in each experiment to limit bead formation during the fabrication of PVA-SbQ/ MWCNTs-COOH NFs. To do so, a wide range of applied voltage (10-18kV), tip-to-collector distance (9-23cm) and feed rate (1-3 mL/h) were tested in order to find the optimal conditions. Optimal values found for the different MWCNTs-COOH loadings are

summarized in Table 5. These values were not significantly affected by the presence of GOx in the polymer composite during the fabrication of PVA-SbQ/ MWCNTs-COOH/GOx NFs.

Table 5. Optimal electrospinning process parameters for the different MWCNT loadings. 6.7 wt % PVA-SbQ concentration, needle i.d.: 0.644 mm, deposition time : 1 min.

Polymer Matrix (wt%)	MWCNT-COOH loading (wt%)	Feed Rate (mL/h)	Distance from Collector (cm)	Applied Voltage (kV)
6.7	1	2.0	10	10
	5	1.0	10	12
	10	3.0	15	14

II.5.2. Morphological Characterization of PVA-SbQ, PVA-SbQ/MWCNTs-COOH NFs and PVA-SbQ/MWCNTs-COOH/GOx NFs

PVA-SbQ/MWCNT-COOH nanofibers obtained from the 6.7 wt% PVA-SbQ solution containing 1%, 5% and 10% MWCNTs are named as PVA-SbQ/1MWCNT, PVA-SbQ/5MWCNT, and PVA-SbQ/10MWCNT, respectively. SEM and TEM images of the pure PVA-SbQ NFs revealed a perfectly smooth fiber surface (figures 50a and 51a) with average diameter (AFD) of 350±20nm. PVA-SbQ/MWCNTs-COOH NFs containing 1 and 5wt% MWCNTs-COOH with respect to the polymer mass were also bead free and slightly less uniform than pure PVA-SbQ NFs, with an AFD of 250±50nm for both MWCNT-COOHs concentrations. They exhibited a slighty smaller diameter and a narrowest distribution, when compared to pure PVA-SbQ NFs.

Thus, it was concluded that the incorporation of nanotubes reduces the average diameter of the NFs (figures 50b and 50c). The observed decrease of the AFD with the increase of CNTs concentration in the composite, is in good agreement with results generally reported in the literature[257, 258, 259, 260, 261] for PVA polymeric matrices and for Nylon matrix.[45] It is known that incorporation of CNTs has a significant impact on both the electrospinnability of polymer solutions and the morphological and electrical properties of the produced NFs.[254, 262] The reduced fiber diameter for the MWCNT/PVA NFs is presumably due to increased stretching

[257] O. Koysuren, "Preparation and Characterization of Polyvinyl Alcohol/carbon Nanotube (PVA/CNT) Conductive Nanofibers," *Journal of Polymer Engineering* 32, no. 6–7 (**2012**): 407–13.
[258] G.R. Rakesh, "A Facile Route for Controlled Alignment of Carbon Nanotube-Reinforced, Electrospun Nanofibers Using Slotted Collector Plates," *Express Polymer Letters* 9, no. 2 (**2014**): 105–18.
[259] M. Naebe et al., "Electrospun Single-Walled Carbon Nanotube/polyvinyl Alcohol Composite Nanofibers: Structure–property Relationships," *Nanotechnology* 19, no. 30 (**2008**): 305702.
[260] N. Diouri and M. Baitoul, "Effect of Carbon Nanotubes Dispersion on Morphology, Internal Structure and Thermal Stability of Electrospun Poly(vinyl Alcohol)/carbon Nanotubes Nanofibers," *Optical and Quantum Electronics* 46, no. 1 (**2014**): 259–69.
[261] K.K.H. Wong et al., "The Effect of Carbon Nanotube Aspect Ratio and Loading on the Elastic Modulus of Electrospun Poly(vinyl Alcohol)-Carbon Nanotube Hybrid Fibers," *Carbon* 47, no. 11 (**2009**): 2571–78.
[262] N. Ning et al., "Dramatically Improved Dielectric Properties of Polymer Composites by Controlling the Alignment of Carbon Nanotubes in Matrix," *RSC Adv.* 4, no. 9 (**2014**): 4543–51.

of the fiber diameter during ES, as a result of increased charge when the conductive CNTs were present in the polymer solution. Therefore, CNTs act as lubricant in electrospinning solution and thereby induce homogenization and shrinkage of composite nanofibers.

Embedded nanotubes, well dispersed in the polymer matrix and some aligned along the NFs direction, were detected by TEM after the study of PVA-SbQ/MWCNTs-COOH NFs containing 1 and 5 wt% MWCNTs-COOH with respect to the polymer mass. (figures 51b and 51c). The hydrogen bonding interactions between the hydroxyl groups present in PVA-SbQ and carboxyl groups present on the acid treated MWCNTs can also contribute to the reduction in PVA-SbQ/MWCNT-COOH NFs diameter and alignment by favouring MWCNT-COOHs dispersion into the PVA-SbQ solution.[258, 263]

On the contrary, the formation of beads could not be avoided at the highest MWCNT-COOH concentration tested (10wt%) and a significant increase of AFD which corresponds to 450 $\pm$100 nm was observed (figure 50d**)**. The significant increase in fibers diameter and the non uniformity of fiber shape for PVA-SbQ/10MWCNT-COOH could be the result of poor alignment of MWCNT inside the fibers and the formation of MWCNT-COOH agglomerates. This speculation was supported by TEM images showing the presence of clusters of coiled/ bundles CNTs inside the fibers (figure 51d). It is reported by Wong et al.[261] that once the CNT loading reach a certain level, the CNTs inevitably form bundles and clusters and distribute non uniformly within the fibers.

All and all, it is important to say that since in this study voltage and feed rate were adjusted during the fabrication process each time to reduce bead formation, the diameter of the obtained fibers is not only dependent of MWCNT-COOH concentration as reported in literature, but also to the ES parameters.

Finally, the morphology of PVA-SbQ/MWCNT-COOH fibers was further investigated after the incorporation of GOx in the electrospun mixture. The proportion of added enzyme was 30 wt% with respect to the polymer mass. It was observed that the addition of GOx in the mixture which was electrospun did not affect the electrospinning parameters, since voltage, feed rate and collection distance were the same in the presence and in the absence of GOx. Furthermore, in this work it was shown that after the incorporation of GOx inside the fibers no obvious change had been recorded in the diameter of PVA-SbQ/5MWCNT-COOH/GOx fibers comparing to PVA-SbQ/5MWCNT-COOH fibers, which is in good agreement with what has been reported in the literature for protein concentration lower than 50%. [237, 249, 264, 265] In addition, smooth fiber surfaces, along with the uniformly distributed fiber sizes, suggest that PVA and enzymes are well mixed due to polar interactions between PVA and enzyme.

---

[263] S. Sarkar et al., "Polymer-Derived Ceramic Composite Fibers with Aligned Pristine Multiwalled Carbon Nanotubes," *ACS Applied Materials & Interfaces* 2, no. 4 (**2010**): 1150–56.

[264] Y. Wang and Y.L. Hsieh, "Immobilization of Lipase Enzyme in Polyvinyl Alcohol (PVA) Nanofibrous Membranes," *Journal of Membrane Science* 309, no. 1–2 (**2008**): 73–81.

[265] A. Moradzadegan et al., "Immobilization of Acetylcholinesterase in Nanofibrous PVA/BSA Membranes by Electrospinning," *Engineering in Life Sciences* 10, no. 1 (**2010**): 57–64.

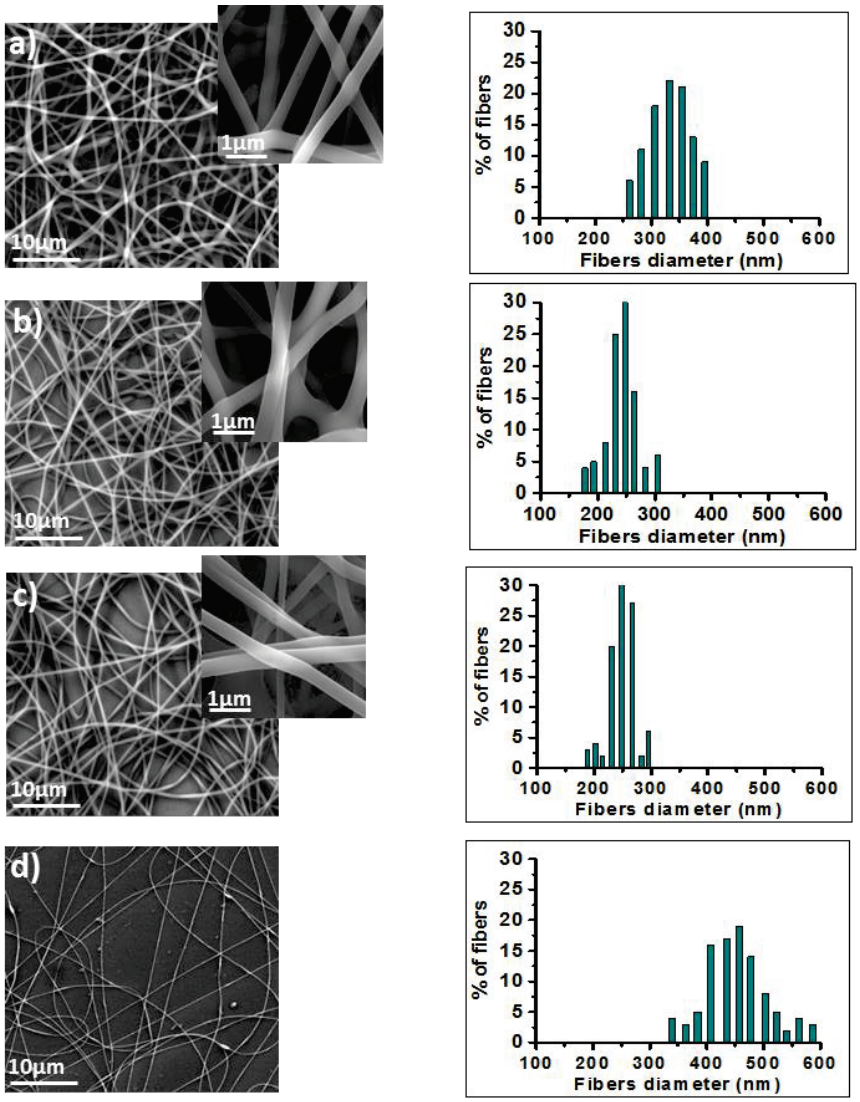

Figure 50. Representative SEM images of a) pure PVA-SbQ, b) PVA-SbQ/1MWCNT-COOH, c) PVA-SbQ/5MWCNT-COOH, d)PVA-SbQ/10MWCNT-COOH under optimum conditions and fiber diameter distribution histograms of the above electrospun fibers.

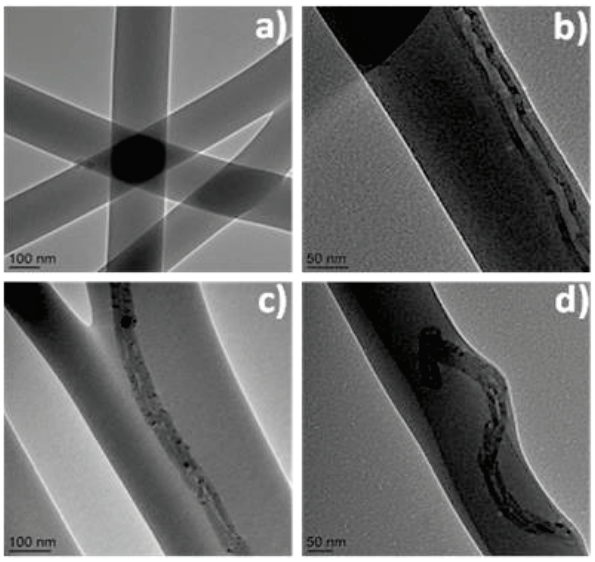

Figure 51. Representative TEM images of a) pure PVA-SbQ, b) PVA-SbQ/1MWCNT-COOH, c) PVA-SbQ/5MWCNT-COOH and d) PVA-SbQ/10MWCNT-COOH under optimum conditions.

II.5.3. Optimization of the post-electrospinning photo-crosslinking step

Since the PVA-SbQ used for electrospinning is a water-soluble polymer, the formed electrospun PVA-SbQ and PVA-SbQ/MWCNT-COOH/GOx NFs dissolve immediately upon coming into contact with aqueous solutions. To retain their water stability a crosslinking step was necessary. For this purpose, the NFs were irradiated by a 100-W UV lamp. Different exposure times (from 0 to 30 min) were tested. The morphology of cross-linked NFs, as observed by SEM, was compared to the one observed after soaking in PBS for various times in the 0-14h range. As expected, the nanofibrous mats dissolved immediately after immersion in PBS in absence of irradiation. Setting irradiation time to 10 or 30 min helped preventing NFs dissolution by inducing cross-linking reaction. Immersion into PBS resulted in a slight swelling of the NFs, but the overall morphology was retained, even after 14h of contact. It was observed that swelling was maximal after 1h, whatever the irradiation time. Figure 52 shows the effect of immersion on the cross-linked NFs morphology. However, 10-min cross-linking time was finally selected since it was proven that after irradiation of the PVA-SbQ/MWCNTs-COOH/GOx NFs for 10 min a CV signal was recorded proving that the enzyme retains its activity, whereas after irradiation for 30 min no CV signal could be further detected demonstrating a loss of enzyme activity.

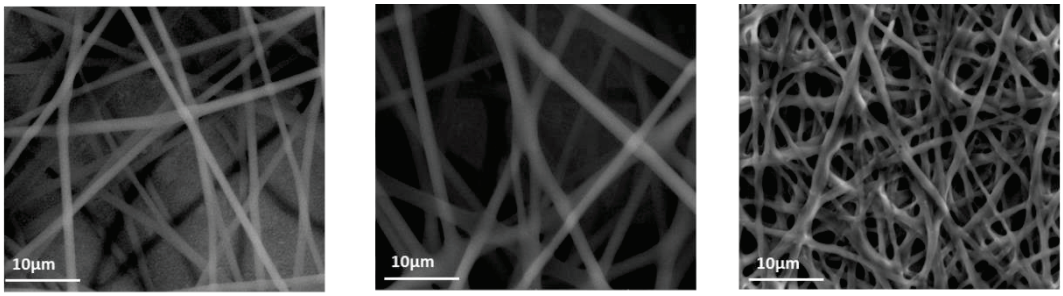

Figure 52. SEM images of crosslinked PVA-SbQ/5MWCNT fibers before and after exposure to UV light for 10 min, and after immersion in phosphate buffer solution (0.1M, pH 7.2) for 3h.

II.5.4. Electrochemical Characterization of PVA-SbQ and PVA-SbQ/MWCNTs-COOH NFs

In order to confirm the influence of carbon nanotubes loading on the electrical properties of nanofibrous mats, cyclic voltammetry and electrochemical impedance spectroscopy were employed. CVs were recorded in 10mM at pH 7.2 at scan rate 100mV/s using $Fe(CN)_6^{3-}/Fe(CN)_6^{4-}$ couple as a redox probe. The potential was repetitively cycled until several consecutive curves were superimposed. Cyclic voltagrammograms were recorded before and after the functionalization of the electrode surface with the nanofibrous mats. Potential separation of redox peaks and current density of peak maximum in CVs can be correlated to the electron transfer properties of the NF mat modified gold electrodes.

As seen in figure 53, both oxidation and reduction peaks of the $Fe(CN)_6^{3-}/Fe(CN)_6^{4-}$ couple could be clearly detected before the modification of the gold electrode with NF mats. The separation between anodic and cathodic peak potentials ($\Delta E_p=E_{pa}-E_{pc}$) was 155mV. A large increase of ΔE_p up to 510mV was observed together with a drastic decrease of the anodic peak intensity (I_{pa}) from 1150 to 25 $\mu A \cdot cm^{-2}$ following the modification of the gold electrode surface with pure PVA-SbQ NFs. This result could be attributed to the electrical insulating properties of PVA-SbQ polymer.

Further incorporation of MWCNTs-COOH into the fibers led to a significant improvement of the charge transfer efficiency through the mat. I_{pa} intensities reached 137, 204 and 398 $\mu A \cdot cm^{-2}$ for 1%, 5% and 10% of MWCNTs-COOH respectively. This result is consistent with the larger electroactive surface exhibited by PVA/MWCNTs modified electrodes.[266] Electrons may be transfered through the insulating polymer layers that separate CNTs by a tunneling mechanism during conduction. The size of CNT agglomerates could be reduced by using an ultrasonic bath for dispersion into SDS/water mixture. Owing to the excellent conductivity of CNTs, electrical resistivity decreases with increasing content of the conductive nanoobjects. Alignment of the nanotubes plays an important role in the conductive properties of the NFs, as observed by several authors.[257, 262]

The electronic transfer properties of the bare, pure PVA-SbQ and PVA-SQ/MWCNTs-COOH modified gold electrodes were also characterized by EIS by varying the frequency in the 100mHz to 100 kHz range at a constant potential of -300mV. The Nyquist plots were repetitively cycled until several consecutive plots were superimposed. EIS is a very powerful technique to explore metal electrode/aqueous electrolyte interfaces and it has been extensively used.[267] Nyquist plots of bare and modified electrodes presented in Figure 54, were satisfactorily fitted ($\chi^2 = 6x10^{-3}$) with a Randles-Ehrshler equivalent electrical circuit which comprised the ohmic resistance of the bulk electrolyte (R_s) in series with a parallel

[266] Y.C. Tsai and J.D. Huang, "Poly(vinyl Alcohol)-Assisted Dispersion of Multiwalled Carbon Nanotubes in Aqueous Solution for Electroanalysis," *Electrochemistry Communications* 8, no. 6 (**2006**): 956–60.
[267] E.P. Randviir and C.E. Banks, "Electrochemical Impedance Spectroscopy: An Overview of Bioanalytical Applications," *Analytical Methods* 5, no. 5 (**2013**): 1098.

combination of the constant phase element (CPE) as non-ideal capacitor and the Warburg resistance, Z_w, resulting from ion diffusion from the bulk electrolyte to the electrode interface, in series with the interfacial charge resistance resistance (R_{ct}) (figure 55) Due to the surface heterogeneity, the impedance $Z(\omega)$ of such an non-ideal layer can be expressed as $Z(\omega)=CPE^{-1}(j\omega)^{-n}$, where ω is a circular frequency and n parameter varies from 0 to 1.[267]

From the Nquist plots fitting, it was concluded that CPE behave as capacitance since values of n (=0.9) were close to 1. A value of 43.8 $\mu F/cm^2$ was obtained for PVA-SbQ NF modified electrode and this value increased by 10% in presence of 1% of MWCNTs, showing that the dielectric constant of the composite was increased. As it can be seen in table 6**,** the incorporation of 1, 5 and 10% of MWCNT-COOH into PVA-SbQ NFs induced a 11, 30 and 60% decrease of R_{CT} value. These results are consistent with those obtained by cyclic voltammetry: the decrease of charge transfer resistance reflects the enhancement of the charge transfer, due to the increase of the conductivity of the PVA-SbQ/ MWCNTs-COOH NFs.

Table 6. R_{CT} values of PVA-SbQ nanofibrous mats containing 0, 1, 5 and 10% of MWCNTs-COOH respectively.

Nanofibrous Mat	Pure PVA-SbQ	PVA-SbQ/1 MWCNT-COOH	PVA-SbQ/5 MWCNT-COOH	PVA-SbQ/10 MWCNT-COOH
R_{CT} ($k\Omega \cdot cm^{-2}$)	14.89	13.21	10.41	5.86

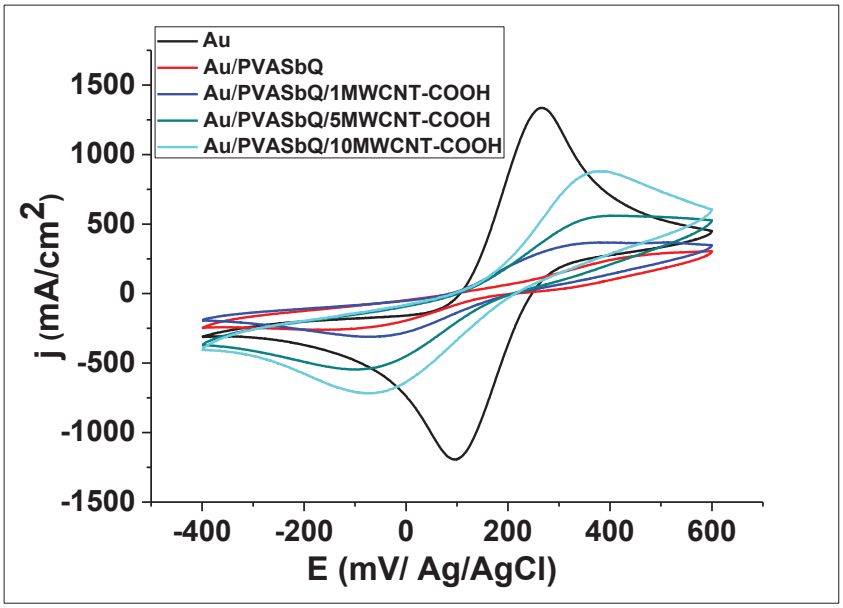

Figure 53. Cyclic voltammograms of modified gold electrodes by different electrospun nanofibrous mats (in $[Fe(CN)_6]^{3-/4-}$ aqueous solution, pH 7.2, scan rate 100mV s^{-1}).

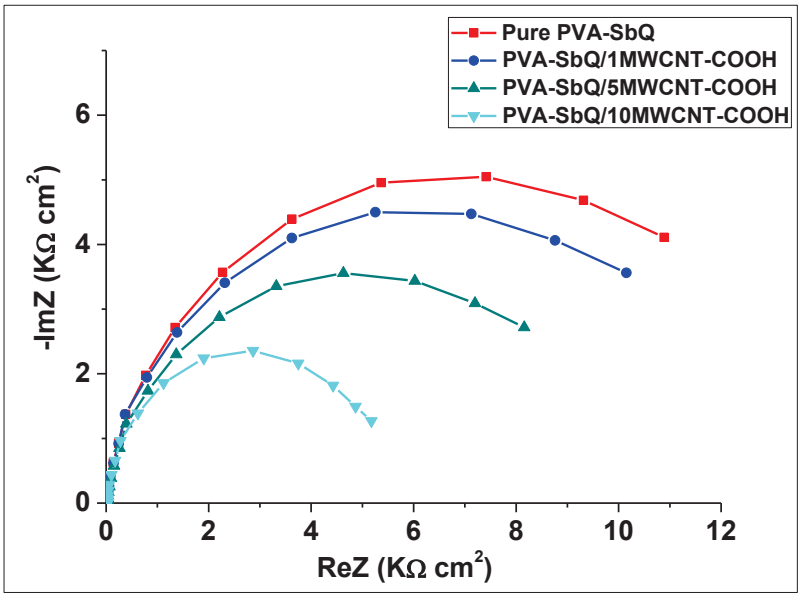

Figure 54. Nyquist plots of impedance spectra obtained at a frequency range between 100 mHz to 100 kHz, at -300 mV, upon increasing concentration of MWCNTs-COOH in the electrospun PVA-SbQ nanofibers. The EIS were recorded in the presence of a 10mM $[Fe(CN)_6]^{3-/4-}$ aqueous solution.

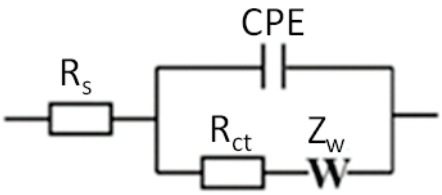

Figure 55. The Randles-Ehrshler model. R_s represents the ohmic resistance of the electrolyte solution, R_{ct} the charge transfer resistance, Z_w the Warburg impedance and CPE the constant phase element.

Therefore, based on the results of the morphological and electrochemical characterizations we have selected to work with PVA-SbQ/5MWCNT NFs for the elaboration of the biosensor because they satisfied both the requirements of smooth, bead-free morphology and enhanced electrical properties.

II.5.5. Biosensor Application

II.5.5.1. Electroanalytical Characterization

The electroanalytic characterization of the glucose biosensors was performed by using CV as the detection technique (Figure 56), recording the current density at the PVA-SbQ/5MWCNT-COOH/GOx NFs modified electrode at different concentrations of GOx substrate (glucose) after 10 min of contact. This time was sufficient to achieve a stable signal for each injected concentration.

As seen in Figure 56, the biosensor signal increased with glucose concentration in the 0-4 mM range. No peak could be detected in the same conditions in the absence of GOx (i.e.

with the PVA-SbQ/5MWCNT-COOH NFs control electrode) independently on the added glucose concentration up to 4 mM, demonstrating that CV signal recorded for the PVA-SbQ/5MWCNT-COOH NFs biosensor is only due to glucose oxidation catalyzed by the immobilized GOx inside the fibers. In presence of dissolved oxygen, this reaction produces gluconic acid and hydrogen peroxide according to equation: Glucose + O_2 ⇒ Gluconic acid + H_2O_2. The current density measured by CV (Figure 56) corresponds to hydrogen peroxide oxidation at the electrode: $H_2O_2 \Rightarrow O_2 + 2H^+ + 2e^-$. The hydrogen peroxide is detected through its oxidation peak, which was recorded at 527 mV/Ag/Ag/AgCl.The oxidation of H_2O_2 at conventional solid electrodes needs a high overpotential as high as +900mV/ Ag/Ag/AgCl, but wiring of enzyme with conductive nanomaterials is known to decrease this potential value until +300mV/ Ag/Ag/AgCl.[75] In the present study, the favorable hydrophilic environment of GOx preserves its catalytic activity and the vicinity of GOx with MWCNTs allows a better electron transfer rate and a rather low potential value is required for H_2O_2 oxidation: 527 mV/ Ag/Ag/AgCl.

II.5.5.2. Analytical performance of the glucose biosensor

Figure 57 shows the calibration curve obtained by plotting current density versus log(glucose concentration) for the PVA-SbQ/5MWCNT-COOH/GOx NFs biosensor. The biosensor signal was linear up to 4mM range and the resulting calibration curve had an R-squared value of 0.984. The limit of detection (LOD), calculated as the concentration of glucose giving a signal equal to three times the standard deviation on the blank (i.e. in absence of glucose) was 2µM. As seen in Table 7, the proposed biosensor exhibited a wide linear range and a LOD lower than most of the amperometric glucose biosensors based on electrospun NFs already reported in the literature. It offers the advantage to be easy and more rapid to prepare.

The relative standard deviations calculated from three consecutive measurements on one single biosensor were lower than 5% in the 5µM-4mM range, showing an excellent repeatability of the proposed biosensor. Inter-sensor reproducibility of the method was also rather good as the relative standard deviation, calculated from the analysis of the 5 µM glucose solution using five different biosensors, was 12%.

Additionally, operational and storage stabilities were determined. There exists no decrease of the PVA-SbQ/5MWCNT-COOH/GOx biosensor response subsequent after 10 measurements of the 2mM glucose solution, performed the same day. In the same way, CV signal remained stable for 5 days when the biosensor was tested once a day at the 2 mM glucose concentration and the biosensor was kept at 4°C between two measurements. These results demonstrate the good operational and storage stabilities of the PVA-SbQ/5MWCNT-COOH/GOx NFs biosensor.

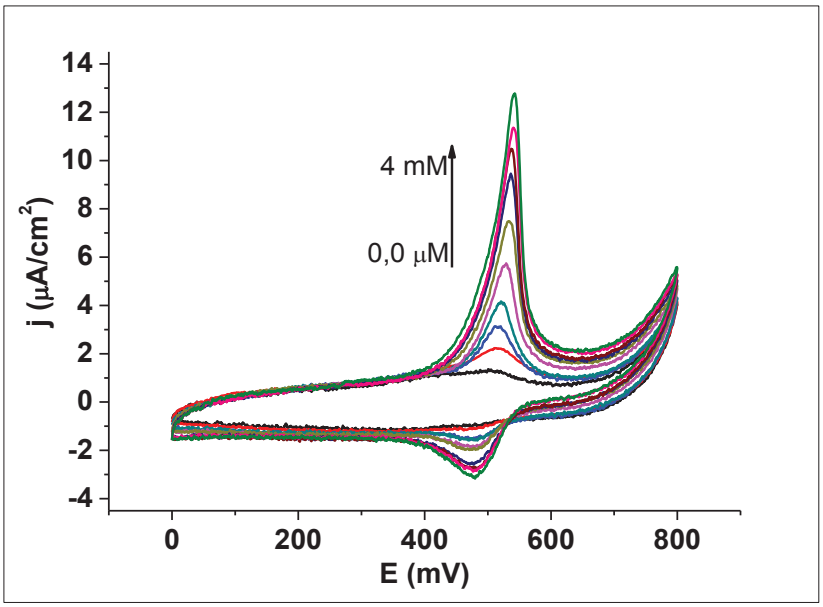

Figure 56. Influence of glucose concentration on the PVA-SbQ/5MWCNTs-COOH/GOx NFs biosensor response. Cyclic voltammograms recorded in PBS 0.1M, pH 7.2, at a scan rate of 50mV s^{-1}, 10 min after glucose injection.

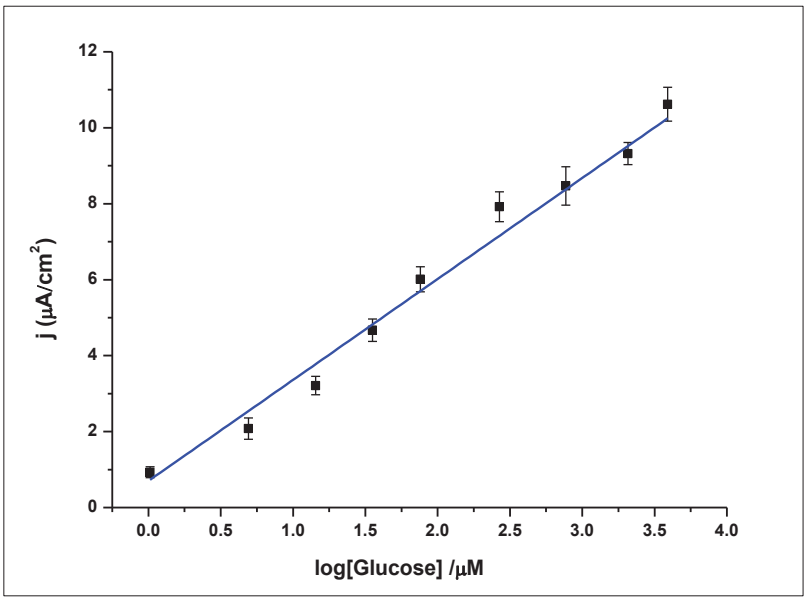

Figure 57. Calibration curve of the PVA-SbQ/5MWCNT-COOH/GOx NFs biosensor (in PBS 0.1M, pH 7.2). Error bars represent standard deviations obtained from three successive measurements.

Table 7. Comparison of proposed biosensor with amperometric glucose biosensors in the literature based on GOx and electrospun NFs.

Immobilization Matrix	Detection Limit (μM)	Linear Range	Reference
Nylon 6.6/PBIBA fibers/GOx NFs	18	0.02-2 mM	Uzun 2014 [45]
Nylon 6.6/4MWCNT/PBIBA NFs	9	0.01-2 mM	Uzun 2014 [45]
Mn_2O_3-Ag NFs	1.73	up to 1.1 mM	Huang 2011[268]
PANCAA /MWCNT/ GOx	670	0.67-7 mM	Wang 2009 [169]
Nafion/PVA/Chitosan/GOx/GO NFs	5	0.005-3.5 mM	Su 2013 [173]
CS/AuNPs/ GOx NFs	2	0.01-2 mM	Huang 2012[269]
PVA-SbQ/5MWCNT-COOH/GOx NFs	2	0.001-4 mM	this work

II.6. Conclusion and Perspectives

In the present study, a one-step elaboration of PVA-SbQ/MWCNT-COOH/GOx electrospun nanofibrous mats followed by a rapid and facile photochemical cross-linking step was proposed and these electroactive surfaces were further evaluated for electrochemical biosensor application. The combination of MWCNTs and PVA-SbQ polymer improved the electron transfer ability of the generated nanofibrous mats and preserved enzyme activity.

The resulting glucose biosensor exhibited high $I_{max,}$ was linear in a wide range of glucose concentration (up to 4mM) and a very low LOD value (2μM) was achieved. This approach of blending enzyme, MWCNTs-COOH, and water-soluble polymers offers a simple method to produce biologically active electrospun fibers and thus fabricating novel electroactive platforms for enzyme immobilization in one-step synthesis. Most importantly, enzymes remained active and accessible to the substrate regardless its affinity to the host polymer. This study paves the way for the engineering of new generation biosensing systems with improved sensitivity and superior performance compared to existing biosensors. This novel nanofiber based platform is not only limited to enzymatic biosensor and it could also be used for the development of immunobiosensors, nucleic acid biosensor, etc.

[268] S.Huang et al., "Glucose Biosensor Using Glucose Oxidase and Electrospun Mn2O3-Ag Nanofibers," *Electroanalysis* 23, no. 8 (**2011**): 1912–20.
[269] Y. Huang et al., "Fabrication of a Chitosan/glucose Oxidase–poly (anilineboronic acid)–Au nano/Au-Plated Au Electrode for Biosensor and Biofuel Cell," *Biosensors and Bioelectronics* 31, no. 1 (**2012**): 357–62.

CHAPTER III: ELECTROSPUN WATER-STABLE POLYVINYL ALCOHOL/POLYETHYLENEIMINE NANOFIBER MATS INCORPORATING ENZYME AND DECORATED WITH GOLD NANOPARTICLES FOR BIOSENSOR APPLICATIONS

III.1. Introduction

In the previous chapter, we demonstrated that electrospun PVA NFs nanofibers may act as a suitable immobilization matrix for GOx and may be used for the elaboration of very performing electrochemical biosensors for glucose detection, the enzyme remaining active and accessible to the substrate. NFs were produced by electrospinning GOx/PVA solutions containing dispersed carboxylated CNTs. Herein, a second approach was evaluated, which consists in immobilizing GOx in electrospun NFs and decorating them with gold nanoparticles. PVA/ polyethyleneimine (PEI) blend solutions were investigated for the elaboration of the NFs. PEI is a polycationic water soluble polymer bearing ionized amino groups able to interact with anionic groups located at proteins surface and constitutes a good matrix for enzyme stabilization.[270] It has already been used for tissue engineering scaffolds,[271] catalytic[184] and biosensor applications.[272] However, electrospinning of PEI itself in aqueous solutions does not generate ultra-fine fibers due to the strong polarity and hydrophilicity[273] of the polymer and the formation of intermolecular hydrogen bondings.

Blending PEI and PVA produces flexible networks of high porosity with enhanced mechanical strength and thermal stability due to the formation of strong hydrogen bondings between amino groups of the PEI chain and hydroxyl groups of the PVA chain[274] and it was shown that electrospinning of the blend[275] could result in ultrafine PEI/PVA NFs of enhanced mechanical properties, thus making them promising candidates for biosensing.[275] The fast dissolution of PVA/PEI nanofibers (NFs) in aqueous solution, as observed for PVA alone, could be overcomed by a crosslinking step.[276]

In this chapter we report the fabrication of a highly sensitive, stable and efficient bioactive surface design for biosensing, by modifying the gold electrode surfaces with one-step water-stable electrospun polyvinyl alcohol/polyethyleneimine (PVA/PEI) nanofibers incorporating glucose oxidase (PVA/PEI/GOx NFs), followed by their uniform decoration with pH-tunable densities of citrate AuNPs. In spite of the attractive properties of PVA/PEI blends and their abundant use for the production of functional membranes, they have been

---

[270] J.M. Bolivar et al., "Coating of Soluble and Immobilized Enzymes with Ionic Polymers: Full Stabilization of the Quaternary Structure of Multimeric Enzymes," *Biomacromolecules* 10, no. 4 (**2009**): 742–47.

[271] N. Khanam et al., "Electrospun Linear Polyethyleneimine Scaffolds for Cell Growth," *Acta Biomaterialia* 3, no. 6 (**2007**): 1050–59.

[272] S. Kurunczi et al., "Polyethylene Imine-Based Receptor Immobilization for Label Free Bioassays," *Sensors and Actuators B: Chemical* 181 (May 2013): 71–76.

[273] C. Dong et al., "Preparation of PVA/PEI Ultra-Fine Fibers and Their Composite Membrane with PLA by Electrospinning," *Journal of Biomaterials Science, Polymer Edition* 17, no. 6 (**2006**): 631–43.

[274] Sua Choi, Duck Kun Hwang, and Heon Sang Lee, "Thermal Properties in Strong Hydrogen Bonding Systems Composed of Poly(vinyl Alcohol), Polyethyleneimine, and Graphene Oxide," *Carbon Letters* 15, no. 4 (**2014**): 282–89.

[275] X. Fang et al., "Fabrication and Characterization of Water-Stable Electrospun Polyethyleneimine/polyvinyl Alcohol Nanofibers with Super Dyesorption Capability," *New J. Chem.* 35, no. 2 (**2011**): 360–68.

[276] C. Tang et al., "In Situ Cross-Linking of Electrospun Poly(vinyl Alcohol) Nanofibers," *Macromolecules* 43, no. 2 (**2010**): 630–37.

rarely exploited for the elaboration of biosensors[175] and this is the first time that cross-linked PVA/PEI/GOx NFs decorated with Au nanoparticles are proposed for this purpose.

Firstly, adhesion improvement of the electrospun PVA/PEI/GOx NFs onto the gold electrode surface by modifying the surface with a conductive self-assembled monolayer (SAM) was investigated. For the formation of the SAMs, 4-aminothiophenol was used, bearing thiol groups for covalent bonding to the gold surface and amine groups which reacted with the amine groups of PEI in a following crosslinking step.

Then, different electrospinning parameters including flow rate, applied voltage, distance between tip and collector, polymer concentration were tailored to produce PVA/PEI NFs with minimal beading. The NFs were rendered water insoluble via exposure to glutaraldehyde vapours and their conductive properties were significantly improved by pH-tunable decoration with AuNPs. The effect of pH of Au colloidal solutions on the assembly of AuNPs on water-stable PVA/PEI nanofibers was investigated.

The electrochemical properties of electrospun PVA/PEI and PVA/PEI/AuNPs nanofibrous mats were characterized by cyclic voltammetry and electrochemical impedance spectroscopy. Scanning electron microscopy (SEM) was used to characterize the morphology of the NFs. GOx, used as model enzyme, was further incorporated into the PVA/PEI mixture, before electrospinning, resulting to the fabrication of PVA/PEI/GOx NFs. The analytical performances of the produced NFs were finally determined.

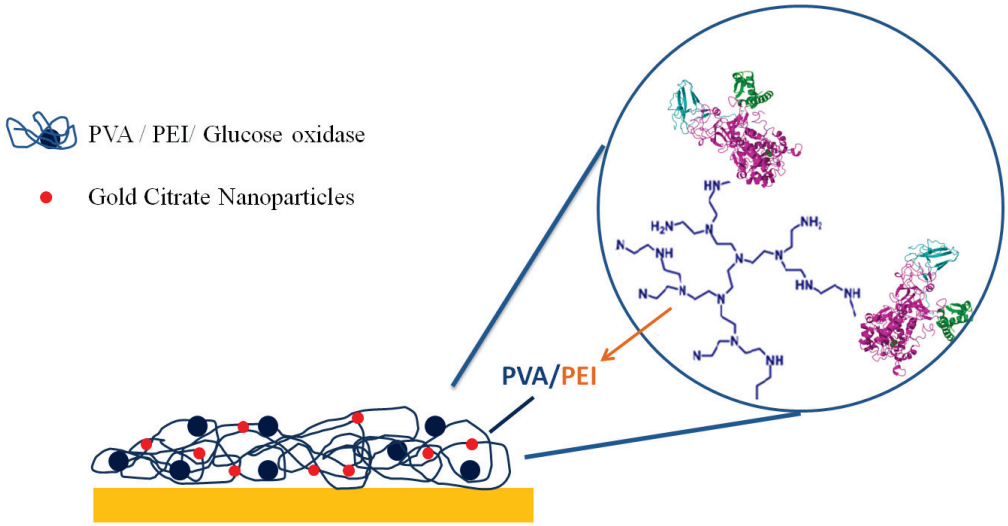

Figure 58. Schematic representation of the working principle of the fabricated biosensor.

III.2. Materials

Polyvinyl alcohol powder (PVA, average M_w:85,000-124,000, 87-89% hydrolyzed), Polyethyleneimine (PEI, , average M_n~60,000 by GPC, average M_w~750,000 by LS, 50wt% in H_2O), 4-aminothiophenol (ATP), Glutaraldehyde (GA, 25wt% aqueous solution), Glucose and GOx, from *Aspergillus niger* was purchased from Sigma-Aldrich (Saint-Quentin-Fallavier, France). Citrate gold nanoparticles (diameter: 23±5 nm) were synthesized in the Laboratoire Hubert Curien (University Jean Monnet, Saint-Etienne, France). All reagents were used without further purification. Phosphate saline buffer solutions were prepared using monopotassic and dibasic phosphate, sodium and potassium chloride from Sigma-Aldrich (pH adjuste at 5.0 with HCl, 0.1M).

A detail description of the characteristics of GOx, glucose and PVA was made in section II.3.

Polyethyleneimine, PEI, is a water-soluble synthetic polymer, colorless to light yellow and odorless with repeating unit composed of the amine group and two carbon aliphatic CH_2CH_2 spacer. Linear polyethyleneimines contain all secondary amines, in contrast to branched PEIs which contain primary, secondary and tertiary amino groups. Totally branched, dendrimeric forms are also reported. The linear PEIs are solids at RT, where branched PEIs are liquids at all molecular weights. Branched PEI can be synthesized by the ring opening polymerization of aziridine. Depending on the reaction conditions different degrees of branching can be achieved.

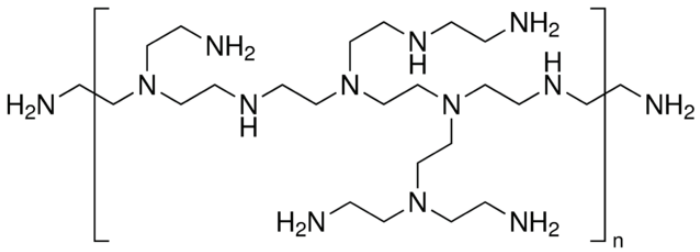

Figure 59. Chemical formula of branched PEI used in this work.

4-aminothiophenol, ATP, is an aromatic thiol, white to yellow solid, with a molecular weight of 125.19 g/mol.

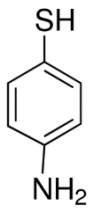

Figure 60. Chemical formula of ATP.

Glutaraldehyde, GA, is a bifunctional agent used extensively for cross-linking, with molecular formula $C_5H_8O_2$ and molecular weight 100.1 g/mol (anhydrous product). The density of the 25% solution at 20°C is 1.06 g/mL.

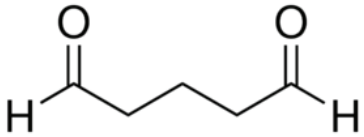

Figure 61. Chemical formula of glutaraldehyde.

Citrate-Stabilized AuNPs

Gold nanoparticles were synthetized according to the following procedure (Turkevich and Frens method): tetrachloroauric(III) acid trihydrate (11.6 mg, 2.9×10^{-5}mol) was dissolved in pure water (21 mL) in a 100 mL round bottomed flask equipped with a condenser. Then this solution was heated to reflux. In another 100 mL round bottomed flask, sodium citrate dihydrate (27.4 mg, 9.3×10^{-5} mol) was dissolved in pure water (7 mL) and then added to the first flask. During the addition, the yellow gold chloride solution turned red, indicating the formation of gold clusters (Figure 62). The mixture was moderately stirred, refluxed for 30 min under continuous stirring and cooled to room temperature under continuous stirring to yield the nanoparticle solution. Laser granulometer measurements (Malvern Zetasizer 1000 HSA laser granulometer) showed the absence of aggregates and a nanoparticle size of around 23 nm with a standard deviation of 5 nm was determined by TEM analysis. From the UV-Vis spectrum recorded at room temperature on a Perkin Elmer Lambda 900 UV/Vis/NIR spectrophotometer, the plasmon band was measured at around 527 nm.[277, 278]

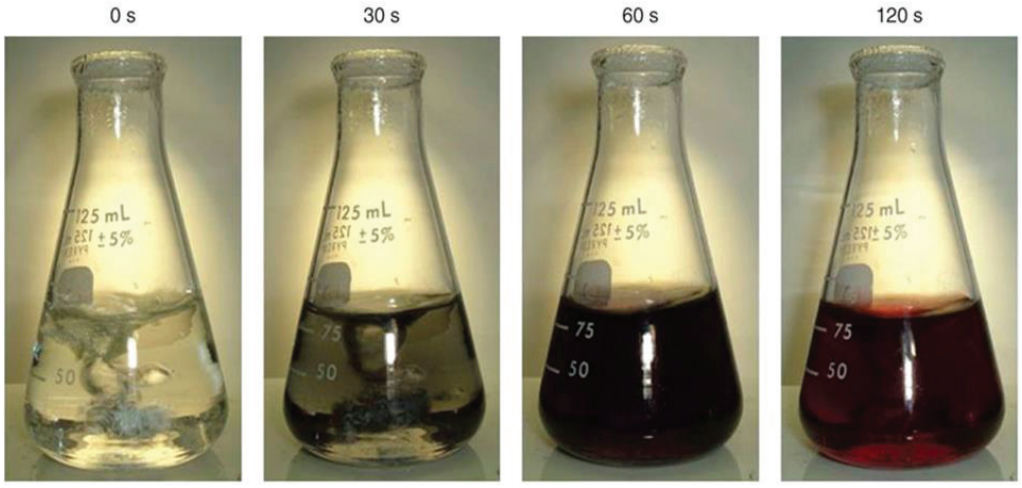

Figure 62. Synthesis of citrate AuNPs according to Turkevich Method.

[277] W. Nouira, A. Maaref, H. Elaissari, F. Vocanson, M. Siadat and N. Jaffrezic-Renault, "Comparative Study of Conductometric Glucose Biosensor Based on Gold and on Magnetic Nanoparticles," *Materials Science and Engineering: C* 33, no. 1 (**2013**): 298–303.

[278] W. Nouira, A. Maaref, A. Elaissari, F. Vocanson, M. Siadat and N. Jaffrezic-Renault, "Enhanced Response of a Proteinase K-Based Conductometric Biosensor Using Nanoparticles," *Sensors* 14, no. 7 (**2014**): 13298–307.

III.3. Experimental Section

III.3.1. Preparation of Working Electrodes

Working electrodes used in this work were the same as the ones used in chapter 2 and described in section II.2.1. (300-nm gold/30-nm titanium on silicon substrate). Before functionalization, the gold electrodes were cleaned in an ultrasonic bath for 10 min in acetone and dried under a N_2 flow, then dipped for 2 min at room temperature into a H_2O_2:H_2SO_4 (3:7 v/v) piranha solution and rinsed with ethanol. Between and after these treatments, the gold electrodes were rinsed thoroughly with ultrapure water. Subsequently, the electrodes were incubated in an 10 mM ATP solution (6.75 mg of ATP in 1mL of ethanol) for 12 h in order to spontaneously formulate the SAMs. After the formation, the electrodes were rinsed with ethanol and PBS (pH 5.0, 0.1M).

III.3.2. Preparation of electrospun solutions

Two concentrated PVA and PEI solutions (12 wt%) were first prepared. The first one was obtained by dissolving PVA powder into water at 80 C° for 3 h under magnetic stirring, and then cooling it down to room temperature. PEI solution was obtained by simple dilution of the commercial 50 wt% solution in water. Adequate volumes of both solutions were further mixed under magnetic stirring overnight to achieve a homogeneous solution with a PVA/PEI weight ratio of 3:1.[274, 275] For the fabrication of PVA/PEI/GOx NFs, GOx powder was added to the above mixture (15mg enzyme per mL of polymer solution) and the resulting composites were stirred for another half an hour.

III.3.3. Electrospinning: Fabrication of electrospun PVA/PEI and PVA/PEI/GOx NFs

NFs were fabricated using a home-made electrospinning device descrided in section II.2.2. PVA/PEI and PVA/PEI/GOx suspensions were loaded immediately after preparation into a glass syringe fitted with a stainless needle (0.644 mm I.D.), the cleaned working gold electrodes were placed on the collector inside the ES chamber and fibers were spun at room room temperature (23±2 °C). The NFs were directly deposited on the surface of the gold electrodes. Electrospinning parameters (e.g. applied voltage, feed rate and collection distance) ranging from 10-25kV for the applied voltage, 9-23 cm for the tip-to-collector distance and 0.1-0.5mL/h for the polymer flow rate, had to be adjusted to limit bead formation. Optimal values found for electrospinning parameters are given in details in section III.4.1. These values were not significantly affected by the addition of GOx in the PVA/PEI mixture.

III.3.4. Crosslinking of electrospun NFs

Gold electrodes modified with PVA/PEI electrospun NFs were exposed to GA vapours for 30 min. All the treated mats were immersed into phosphate saline buffer (pH 5.0) to examine their water stability.

III.3.5. Decoration of water-stable electrospun PVA/PEI NFs with AuNPs

For pH-controlled assembly of AuNPs on water-stable PVA/PEI NFs and PEI/PVA/GOx NFs, the pH values of the solution of AuNPs was adjusted to 5.0, 6.0, 7.0, respectively, from the original pH 8.9 using a 1 M HCl solution. Immediately after pH adjustment, the electrospun NF mats, were immersed into the pH-adjusted solutions. After a 3 h immersion, the mats were taken out, thoroughly rinsed in deionized water and N_2-dried.

III.3.6. Electrochemical characterizations

Cyclic voltammetry (CV) and electrochemical impedance spectroscopy (EIS) characterizations were all performed at room temperature in a Faraday cage. A Voltalab 80 PGZ 402 analyzer (Hach Lange, France) and a 5 mL electrochemical cell equipped with a conventional three electrode configuration were employed as described in section II.2.1.

III.3.6.1. PVA/PEI NFs and PVA/PEI/AuNPs NFs modified electrodes

EIS characterization of PVA/PEI NFs and PVA/PEI NFs modified electrodes were carried out in 0.1 M phosphate buffer saline buffer (PBS) pH 5.0 containing 10 mM $K_3Fe(CN)_6^{3-}$ and $K_4Fe(CN)_6^{4-}$, varying the frequency in the 100 mHz to 100 kHz range and acquiring 5 points per decade. An excitation voltage of 10 mV was superimposed on a dc potential of -300 mV. Impedance data were fitted to equivalent electrical circuits by means of the ZView2 software (Scribner Associates Inc, Southern Pines, USA). The same electrodes were also characterized by CV, the potential being cycled from −400 and +600 mV (versus Ag/AgCl) with a scan speed of 100 mV/s. 0.1 M PBS buffer pH 5.0 containing 10 mM $K_3Fe(CN)_6^{3-}$ and $K_4Fe(CN)_6^{4-}$ was chosen as electrolyte. After each measurement, the electrolyte solution was refreshed, and the electrodes were washed with distilled water to remove any residues.

III.3.6.2. PVA/PEI/AuNPs/GOx NF modified electrodes

Biosensing experiments were performed by injecting glucose from a mother solution into the 4 mL electrochemical cell containing the PVA/PEI/AuNPs/GOx NF modified electrodes and 0.1 M PBS pH 5.0 as electrolyte. EIS measurements were performed by varying the frequency in the 100 mHz to 100 kHz range and acquiring 5 points per decade, on a dc potential of -300 mV. Three replicates were performed for each glucose concentration and related standard deviations were calculated.

III.3.7. Characterization of NFs morphology

Fiber mats were characterized by scanning electron microscopy with a TESCAN MIRA3 FEG-SEM microscope after sample metallization (2 nm Pt or Cr).

III.4. Results and Discussion

III.4.1. Morphological Characterization of PVA/PEI, PVA/PEI/GOx and PVA/PEI/AuNPs/GOx electrospun NFs

III.4.1.1.Effect of electrospinning parameters on the morphology of PVA/PEI and PVA/PEI/GOx electrospun NFs

PVA exhibits good viscosity for ES and the addition of PVA into other polymer solutions can significantly improve the spinnability of the polymers.[279, 274] Therefore, in this study, we selected the PEI/PVA mixture to obtain uniform, polymer NFs with abundant amine groups on the fiber surfaces. It has been mentioned that surface morphology of electrospun NFs may be affected by various parameters (Section I.3.3.).[87] In our study, temperature was regulated at 23±2 °C and key processing parameters such as flow rate, applied voltage, tip-to-collector distance were systematically optimized to produce smooth and uniform fibers without beads and drops.

The influence of applied voltage on nanofibers morphology was first investigated. The polymer concentration was set at 12 wt% and kept steady throughout the whole ES procedure according to the literature.[275] Figure 63 shows the SEM images of the electrospun PVA/PEI NFs fabricated by using an applied voltage of a) 13kV and b) 25kV, whilst the other ES parameters were set as follows: a polymer flow rate of 0.2 mL/h and tip-to-collector distance of 12 cm. SEM images revealed a perfectly smooth fiber surface with an average diameter (AFD) of 360±20nm at an applied voltage of 13kV (figure 63a). Significantly thinner (AFD: 240±20nm) but also bead free fibers were obtained when the applied voltage was 25kV (figure 63b). The observed decrease of AFD upon the increasing values of applied voltage is in good agreement with results generally reported in the literature.[275, 280] Higher voltage can cause greater stretching of the solution due to greater columbic forces in the jet as well as stronger electric field, leading to reduction in the fiber diameter. In a next step, applied voltage of 25kV was selected to further optimize the other ES parameters, to fabricate uniform PVA/PEI nanofibers.

[279] S. Xiao et al., "Immobilization of Zerovalent Iron Nanoparticles into Electrospun Polymer Nanofibers: Synthesis, Characterization, and Potential Environmental Applications," *The Journal of Physical Chemistry C* 113, no. 42 (**2009**): 18062–68,.

[280] W. Zuo et al., "Experimental Study on Relationship between Jet Instability and Formation of Beaded Fibers during Electrospinning," *Polymer Engineering & Science* 45, no. 5 (**2005**): 704-709.

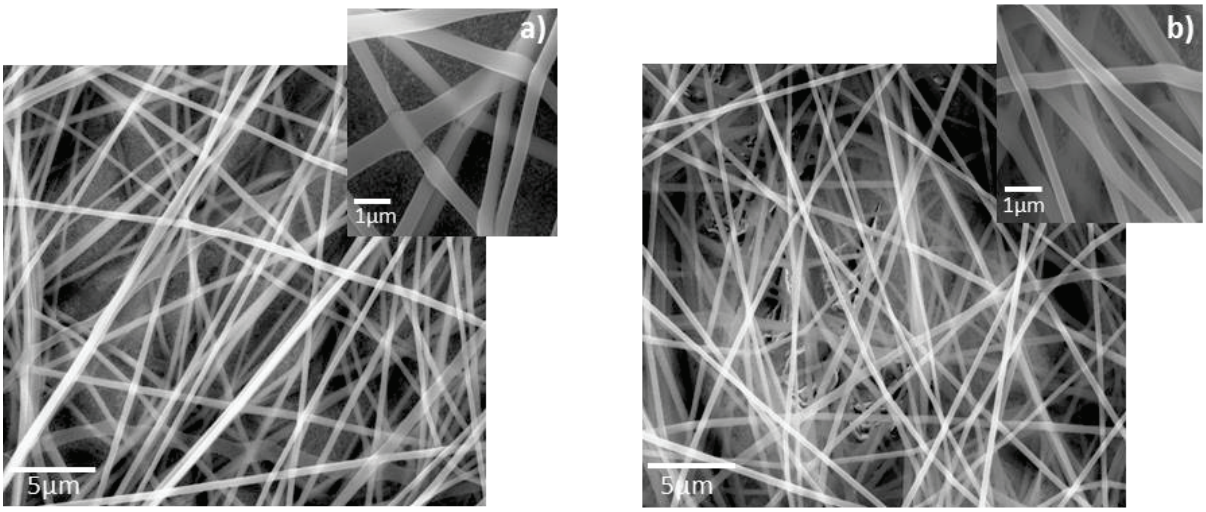

Figure 63. Representative SEM images of electrospun PVA/PEI NFs formed by using a) an applied voltage of 13kV and b) an applied voltage was 25kV. The other electrospinning parameters were set as follows: polymer concentration of 12 wt%, flow rate of 0.2 mL/h and collection distance of 12 cm.

Afterwards, the tip-to-collector distance was increased from 12 cm to 23 cm, whilst the flow rate was kept at 0.2 mL/h. Generally, increasing the collection distance is beneficial for solvent evaporation and solidification of the nanofibers.[281] The electrospun PVA/PEI NFs obtained at both collection distances revealed a uniform and smooth surface free of beads (figure 64). It was clear that the morphology of the NFs did not significantly change at the selected two collection distances. Electrospun NFs fabricated at 12 cm tip-to-collector distance exhibited smaller AFD (270± 30nm) (figure 64a) when compared to NFs fabricated at 23 cm tip-to-collector distance (AFD: 380±20nm). (figure 64b)

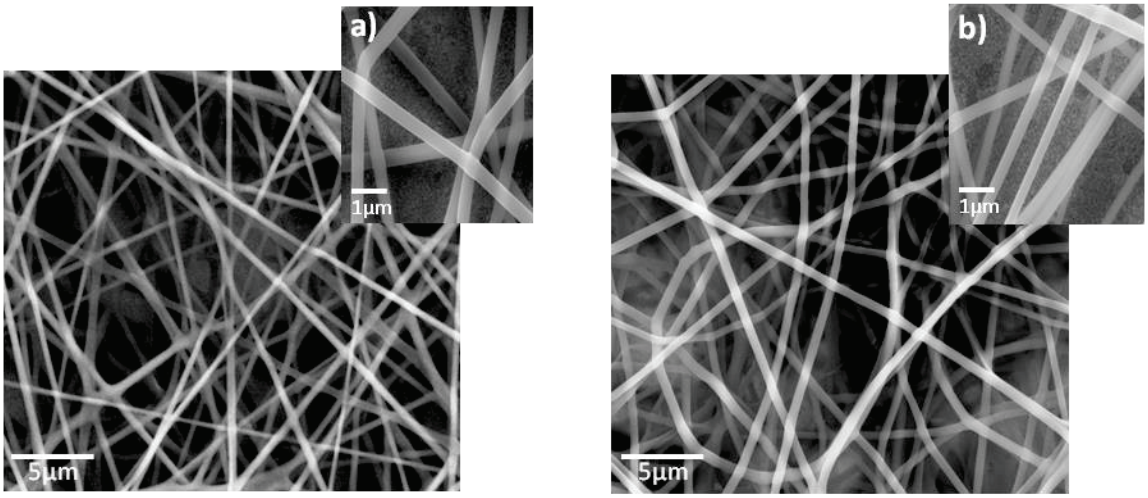

Figure 64. Representative SEM images of electrospun PVA/PEI NFs formed by using a) collection distance of 12cm and b) collection distance of 23cm. The other electrospinning parameters were set as follows: polymer concentration of 12 wt%, flow rate of 0.2 mL/h and applied voltage of 25 kV.

[281] S. Megelski et al., "Micro- and Nanostructured Surface Morphology on Electrospun Polymer Fibers," *Macromolecules* 35, no. 22 (**2002**): 8456–66.

Finally, the influence of the polymer flow rate on the fibers morphology was investigated. To do so, the applied voltage was set at 25 kV and the tip-to-collector distance at 12cm, whilst ranging the polymer flow rate from 0.2 to 0.6 mL/h. SEM images of PVA/PEI NFs at a flow rate of 0.2 mL/h revealed a perfectly smooth surface with an AFD of 220±30nm (figure 65a), whereas beaded structures along the NFs where observed when the flow rate was 0.6 mL/h, with AFD of 310±30nm. (figure 65b) At higher flow rates, the Taylor cone was unstable and droplets were frequently spouting out.

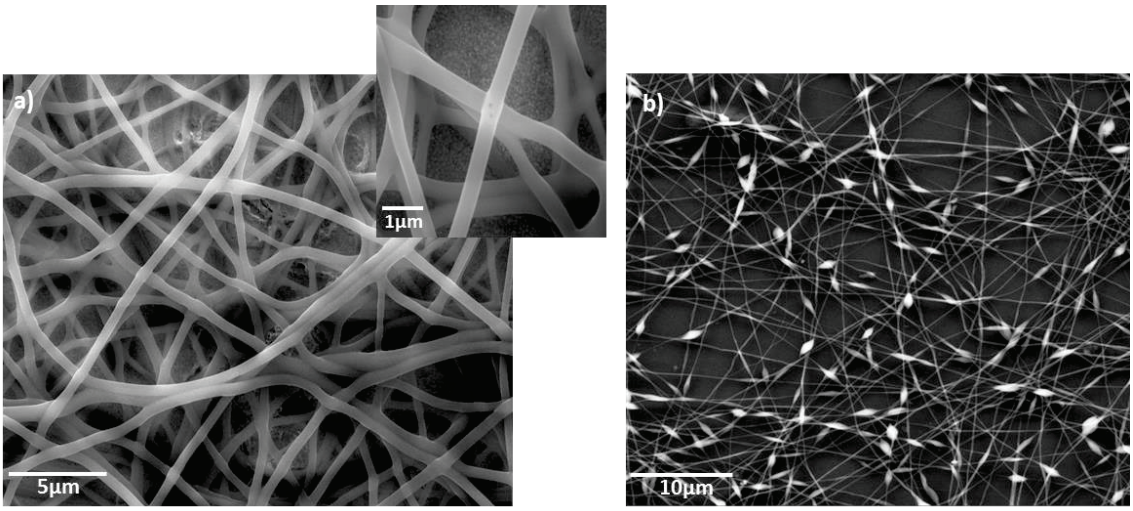

Figure 65. Representative SEM images of electrospun PVA/PEI NFs formed by using a) flow rate of 0.2 mL/h and b) flow rate of 0.6 mL/h. The other electrospinning parameters were set as follows: polymer concentration of 12 wt%, collection distance of 12 cm and applied voltage of 25 kV.

III.4.1.2.Influence of enzyme on the morphology of the PVA/PEI/GOx electrospun NFs

The proportion of added enzyme was 30 wt% with respect to the polymer mass. Morphology of PVA/PEI fibers was further investigated after the incorporation of GOx in the electrospun mixture. It was observed, as for the PVA-SbQ/MWCNT/GOX NFs described in the previous chapter, that the addition of GOx in the mixture which was electrospun did not affect the electrospinning parameters, since voltage, feed rate and collection distance were the same in the presence and in the absence of GOx. Furthermore, in this work, it was shown that after the incorporation of GOx inside the fibers no obvious change had been recorded in the diameter of PVA/PEI/GOx fibers comparing to PVA/PEI fibers. In addition, smooth fiber surfaces, along with the uniformly distributed fiber sizes, suggest that PVA/PEI and enzymes are well mixed due to polar interactions between enzyme and both PVA and PEI.

Thus the electrospinning parameters of PEI/PVA NFs were optimized at a concentration of 12 wt% (PEI/PVA= 1:3), flow rate of 0.2 mL/h, applied voltage of 25 kV and tip-to-collector distance of 12 cm.

III.4.2. Crosslinking of electrospun PVA/PEI NFs under GA vapours-Water insolubility

Since both PEI and PVA used for electrospinning are water-soluble polymers, a crosslinking step was necessary. For this purpose, the NFs were exposed to GA vapours for times varying from 0 to 30 min. Different exposure times (from 0 to 30 min) were tested. As expected, it was observed that without exposure of the NFs to GA vapours, the nanofibrous mats were totally dissolved upon immersion in phosphate saline buffer (0.1M, pH 5.0). On the contrary, after exposure from 15 to 30 min to GA vapours, the NFs became water-insoluble and the morphology of the fibers was retained, suggesting the successful crosslinking reaction induced by glutaraldehyde vapours, during which the hydroxyl groups of the PVA and the amine groups of PEI react with the aldehyde groups of GA to form aldimine linkages.[34, 282] Furthermore, upon exposure to GA vapours, the amine groups which were introduced onto the surface of the gold electrodes by modifying with the ATP conductive self-assembled monolayer, reacted with the amine groups along the backbone of PEI NFs, thus resulting to adhesion improvement of the electrospun PVA/PEI/GOx NFs onto the gold electrode surface. After immersion in PBS (0.1M, pH 5.0), ranging from 5h to 4 days, the nanofibrous structure was still preserved (figure 66). The AFD of the GA cross-linked NFs (350±30nm) was slightly larger than the one of non-crosslinked NFs (270±30), possibly due to the swelling of the NFs during the GA vapour cross-linking step. These results are in good agreement with results reported in the literature.[275]

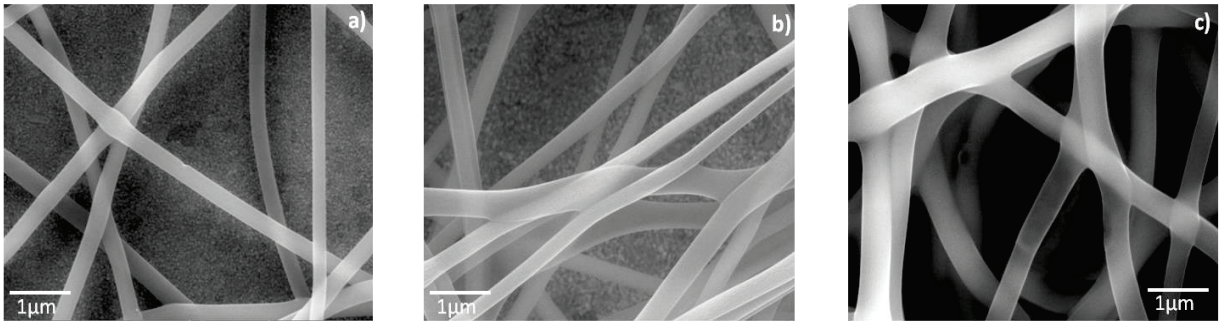

Figure 66. Representative SEM images of water-stable electrospun PVA/PEI NFs a) after exposure to GA vapors for 30min, b) after immersion in PBS (0.1M, pH 5.0) for 5h and c) after immersion in PBS (0.1M, pH 5.5) for 4 days.

III.4.3. pH-controlled Decoration of water-stable PVA/PEI NFs with AuNPs

The initial Au-colloidal solution exhibited a deep red wine colour and had a pH of 8.9. The citrate ions, weakly bounded on the NPs surface, imparted negative charges to the metal NPs and prevented their aggregation.[192, 283, 284] The electrospun water-stable PVA/PEI NFs

[282] Y.Z. Zhang et al., "Crosslinking of the Electrospun Gelatin Nanofibers," *Polymer* 47, no. 8 (**2006**): 2911–17.
[283] A. Henglein and M. Giersig, "Formation of Colloidal Silver Nanoparticles: Capping Action of Citrate," *The Journal of Physical Chemistry B* 103, no. 44 (**1999**): 9533–39.

and PVA/PEI/GOx NFs modified gold electrodes were immersed into pH-adjusted solutions of AuNPs, with pH values of 5.0, 6.0 and 7.0. The pH values ranging from 5.0 to 7.0 were carefully selected, by taking into consideration that GOx is active on a specific pH range (4-7) with an optimum at 5.5. The colour of the nanofibrous mats evolved from white into dark red after they were immersed for 3h in AuNPs solutions of pH 5.0 and 6.0 and into light red after immersion for 3h in solutions of pH 7.0. Aggregates of NPs were observed in the solutions with pH ranging from 5.0 to 7.0 after the solutions stood overnight. After removing the PVA/PEI/AuNPs NFs modified electrodes from the AuNPs solutions, the NFs were rinsed with distilled water and dried with N_2. Figure 67 shows SEM images of water-stable PVA/PEI/AuNPs NFs as a function of pH values of the AuNPs solutions. At pH 5.0 we observed that AuNPs distribute uniformly and in a high coverage density on the surface of water-stable NFs (figure 67d), whereas when the pH value increased to 6.0 and then to 7.0, the coverage density of AuNPs on the surface decreased (figure 67b, 67c).

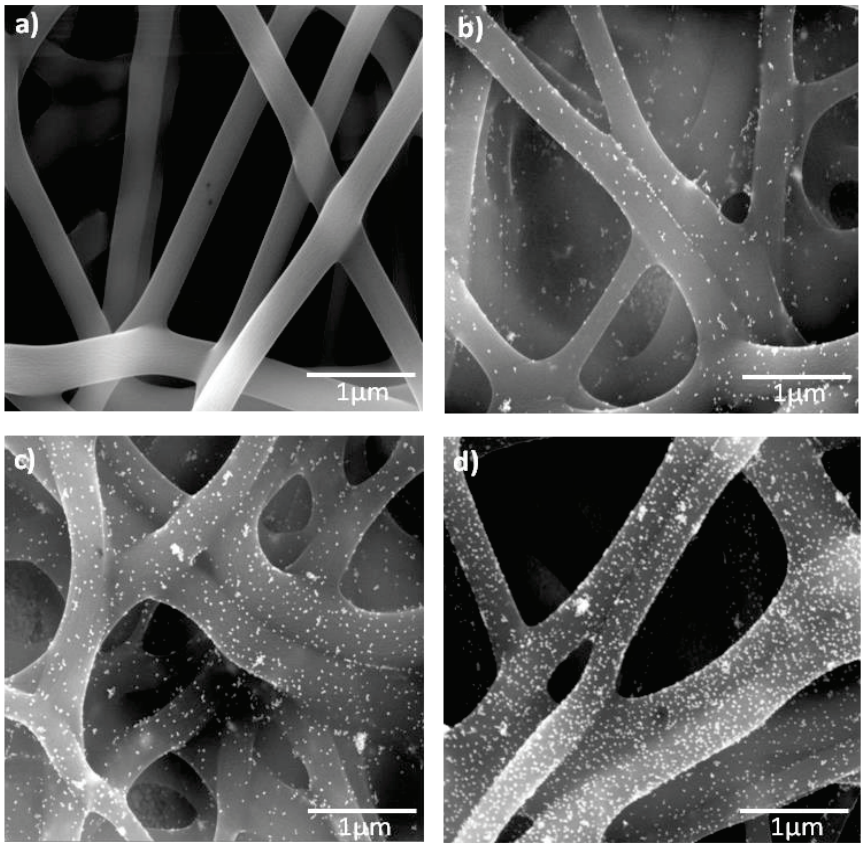

Figure 67. a) Representative SEM image of water-stable electrospun PVA/PEI NFs before immersion in the AuNPs solution. b, c, d) Representative SEM images of decorated with citrate AuNPs water-stable electrospun PVA/PEI NFs. Assembly of AuNPs on the NFs after immersion in colloidal solutions with various pH values of b) 7.0, c) 6.0 and d) 5.0.

[284] C. Li et al., "Facile Synthesis of Concentrated Gold Nanoparticles with Low Size-Distribution in Water: Temperature and pH Controls," *Nanoscale Research Letters* 6, no. 1 (**2011**): 1–10.

The assembly mechanism for citrate AuNPs on the electrospun water-stable PVA/PEI NFs could be explained on the basis of hydrogen bonding interactions between the amine groups along the PEI backbone and the carbonyl in the carboxylate groups capped on the surface of citrate AuNPs. Similar results were reported from Dong et al.[192] while decorating nylon NFs with AgNPs. Furthermore, in our study, taking into account that the pKa values of branched PEI are 4.5 for primary, 6.7 for secondary and 11.6 for tertiary amine groups,[285] it is obvious that at pH regions ranging from 5.0 to 6.7 PEI exists in a highly (but not fully) protonated form, facilitating the electrostatic interactions with the citrate ions bound to the AuNPs surface. The results are in good agreement with what has been generally reported in the literature.[286, 287] It is important to mention that uniform dispersion and immobilization of AuNPs on the PVA/PEI/GOx NFs surface was performed in an aqueous environment, thus eliminating the need of an extra step of coating the NFs with organic solvents (such as mercaptopropyltrimethoxysilane) for covalent binding of MNPs on the NFs surface[185, 194] which led to a facile and green approach for the fabrication of electroactive nanofibrous novel platforms for enzyme immobilization.

III.4.4. Electrochemical Characterization of PVA/PEI NFs and PVA/PEI/AuNPs composite electrospun NFs

In order to confirm the influence of AuNPs loading on the electrical properties of nanofibrous mats, CV and EIS were employed. CVs were recorded in 10 mM PBS at pH 5.0 at a scan rate of 100mV/s using $Fe(CN)_6^{3-}/Fe(CN)_6^{4-}$ couple as redox probe. The potential was repetitively cycled until several consecutive curves were superimposed. Cyclic voltagrammograms were recorded before and after the functionalization of the electrode surface with the ATP SAMs and with the nanofibrous mats.

As seen in Figure 68, both oxidation and reduction peaks (I_{pa}=1194 $\mu A \cdot cm^{-2}$) of the $Fe(CN)_6^{3-}/Fe(CN)_6^{4-}$ couple could be clearly detected before the gold electrode modification with NF mats. The separation between anodic and cathodic peak potentials ($\Delta E_p = E_{pa} - E_{pc}$) was 161 mV. After the modification of the gold electrode surface with SAMs formed from 4-ATP molecules, only a slight decrease of the anodic current peak was induced (I_{pa}=1035 $\mu A \cdot cm^{-2}$), resulting in a ΔE_p of 167 mV (Figure 68). The efficient electron transfer through the SAM layer was expected due to the extensive conjugation of the aromatic ring to the amine groups at the p-position from the sulfur atom.[288]

---

[285] K.D. Demadis, Maria Paspalaki, and Joanna Theodorou, "Controlled Release of Bis(phosphonate) Pharmaceuticals from Cationic Biodegradable Polymeric Matrices," *Industrial & Engineering Chemistry Research* 50, no. 9 (**2011**): 5873–76.

[286] W. Patungwasa and José H. Hodak, "pH Tunable Morphology of the Gold Nanoparticles Produced by Citrate Reduction," *Materials Chemistry and Physics* 108, no. 1 (**2008**): 45–54.

[287] Li et al., "Controllable Anchoring of Gold Nanoparticles to Polypyrrole Nanofibers by Hydrogen Bonding and Their Application in Nonenzymatic Glucose Sensors," *Biosensors and Bioelectronics* 38, no.1 (**2012**): 402-406.

[288] S.H. Cho, D. Kim and S.M. Park, "Electrochemistry of Conductive Polymers," *Electrochimica Acta* 53, no. 11 (**2008**): 3820–27.

A large increase of ΔE_p up to 464 mV was observed together with a drastic decrease of the anodic peak intensity (I_{pa}) from 1035 to 13 $\mu A \cdot cm^{-2}$ following the modification of the ATP-gold electrode surface with PVA/PEI NFs. This result could be attributed to the electrical insulating properties of PVA/PEI mixture. Further decoration with AuNPs onto the fibers led to a significant improvement of the charge transfer efficiency through the mat. I_{pa} intensities reached 391$\mu A \cdot cm^{-2}$ after the AuNPs loading on the NFs (Figure 68). This result is consistent with the larger electroactive surface exhibited by PVA/PEI/AuNPs modified electrodes. Owing to the conductivity of AuNPs, electrical resistivity decreases with increasing content of the conductive nanoobjects.

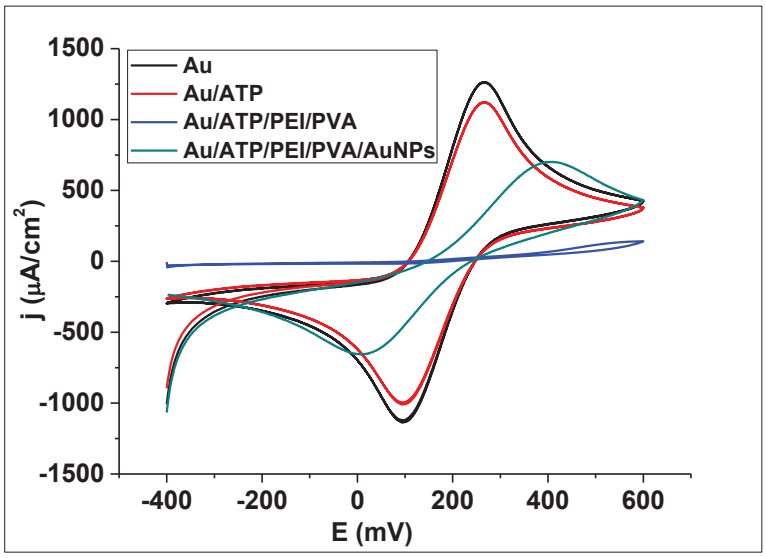

Figure 68. Cyclic voltammograms of gold modified electrodes by ATP SAMs, ATP SAMs/PVA/PEI water-stable electrospun NFs and ATP SAMs/PVA/PEI/AuNPs water-stable electrospun NFs (in $[Fe(CN)_6]^{3-/4-}$ PBS solution, pH 5.0, scan rate 100mV/s.

The electronic transfer properties of the PVA/PEI NFs and PVA/PEI/AuNPs NFs modified gold electrodes were also characterized by EIS by varying frequency in the 100 mHz to 100 kHz range at a constant potential of -300 mV. The Nyquist plot of the gold electrodes modified with ATP and ATP/PVA/PEI/AuNPs NFs are presented in figure 70. They were satisfactorily fitted with a Randles-Ehrshler equivalent electrical circuit (Figure 55). The circuit parameters obtained by fitting the impedance data with the equivalent circuit shown in figure 55 are summarized in Table 8.

Nyquist plot of the ATP/PVA/PEI NFs modified gold electrode (figure 69), shows that the charge transfer resistance is very high (in the range of MΩ) in the absence of AuNPs, in good adequacy with the electrical insulating properties of PVA/PEI polymer. Decoration of the NFs with Au NPs resulted in a significant decrease of R_{ct} (figure 70). This result confirms those obtained with CV: the decrease of charge transfer resistance reflects the enhancement of the charge transfer, due to the increase of the conductivity of the PVA/PEI/AuNPs NFs.

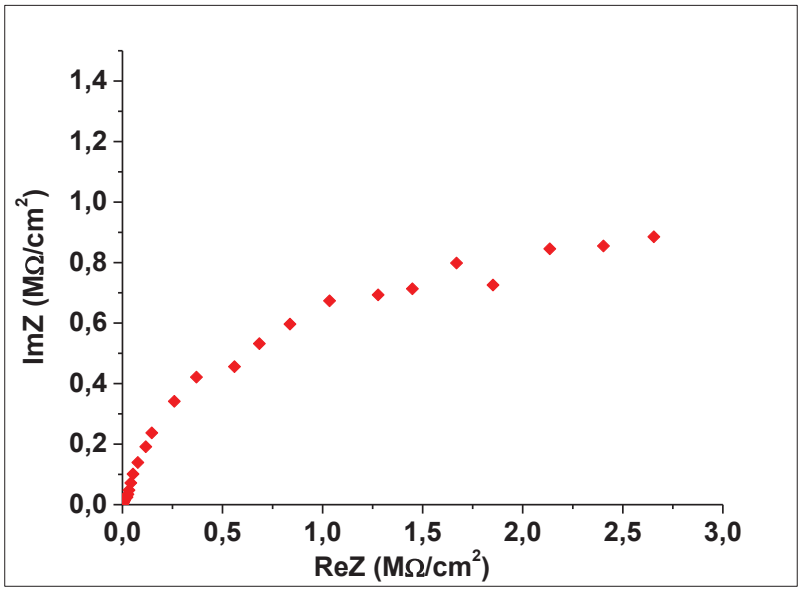

Figure 69. Nyquist plot of impedance spectra obtained for ATP/PVA/PEI water-stable electrospun NFs before immersion in the Au NPs solution. The EIS measurements were performed at -300 mV in the presence of a 10mM $[Fe(CN)_6]^{3-/4-}$ PBS solution by varying frequency in the 100 mHz to 100 kHz range.

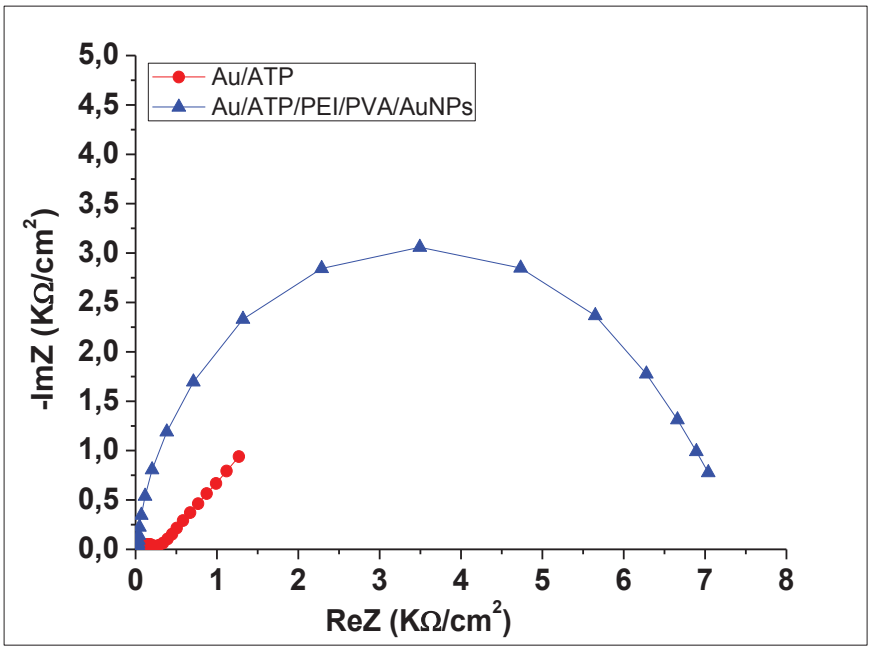

Figure 70. Nyquist plots of impedance spectra obtained for gold electrodes modified with ATP-SAMs and ATP/PVA/PEI/AuNPs water-stable electrospun NFs after immersion in the Au NPs solution pH 5.0. The EIS measurements were performed at -300 mV in the presence of a 10mM $[Fe(CN)_6]^{3-/4-}$ PBS solution by varying frequency in the 100 mHz to 100 kHz range.

Table 8. Fitting parameters obtained from Nyquist plots of impedance spectra by using the equivalent Randles-Ehrshler circuit presented in figure 55.

	R_s ($\Omega \cdot cm^{-2}$)	R_{ct}	CPE ($\mu F \cdot s^{(n-1)}$)	n_{CPE}	x^2
4-ATP	89.7	156 $\Omega \cdot cm^{-2}$	3.41	0.993	0.007
ATP/PVA/PEI/AuNPs	17.2	7.01 $k\Omega \cdot cm^{-2}$	22.72	0.9254	0.0071

III.4.5. Analytical performance of the PVA/PEI/AuNPs/GOx glucose biosensor

The electroanalytic characterization of the PVA/PEI/AuNPs/GOx glucose biosensor was performed by using EIS as the detection technique (Figure 72). Firstly, negative tests were performed by using a PVA/PEI/AuNPs control electrode, and it was demonstrated that the response of the developed sensor was negligible in the absence of enzyme. In a second step, the biosensor response was determined following the injection of various amounts of a glucose concentrated solution to achieve final concentrations in the 1 μM-1 mM range into the measurement cell. Nyquist plots of the resulting impedance spectra (figure 71) were satisfactorily fitted using the Randles-Ehrshler equivalent electrical circuit. The circuit parameters obtained are summarized in Table 9. It was evidenced that the magnitude of impedance increases upon the increasing concentration of glucose (figure 72)[289].

This increase in impedance upon increasing substrate concentration has already been reported in the literature for the glucose-GOx interaction[290] and for the norepinephrine detection using phenylethanolamine N-methyl transerase.[291] This could be explained due to nonspecific binding as well as due to the physical adsorption of the enzymatic reaction products on the modified electrodes surface, acting as a blocker for electron transfer thus increasing the electron transfer resistance.

[289] F. Lisdat and D. Schäfer, "The Use of Electrochemical Impedance Spectroscopy for Biosensing," *Analytical and Bioanalytical Chemistry* 391, no. 5 (**2008**): 1555–67.
[290] T.L. Adamson et al., "The Promise of Electrochemical Impedance Spectroscopy as Novel Technology for the Management of Patients with Diabetes Mellitus," *The Analyst* 137, no. 18 (**2012**): 4179.
[291] B.A. Haselwood and J.T. La Belle, "Development of Electrochemical Methods to Enzymatically Detect Traumatic Brain Injury Biomarkers," *Biosensors and Bioelectronics* 67 (**2015**): 752–56.

Table 9. Fitting parameters obtained from Nyquist plots of impedance spectra by using the equivalent Randles-Ehrshler circuit presented in figure 55 upon the addition of increasing glucose concentration.

Glucose Concentration	R_s (kΩ·cm^{-2})	R_p(kΩ·cm^{-2})	CPE (μF·s$^{(n-1)}$)	n_{CPE}	x^2
0.00 μM	0,01365	7,30757	22.89	0,904	0,005
1.24 μM	0,01214	8,19032	23.32	0,888	0,006
12.31 μM	0,01362	8,72978	25.13	0,873	0,004
24.06 μM	0,00799	9,22854	25.54	0,877	0,005
67.34 μM	0,01806	10,0899	26.89	0,863	0,009
0.1mM	0,01591	11,26132	27.56	0,855	0,005
0.2mM	0,01221	12,21725	28.51	0,876	0,006
1mM	0,01635	13,32444	28.78	0,843	0,007

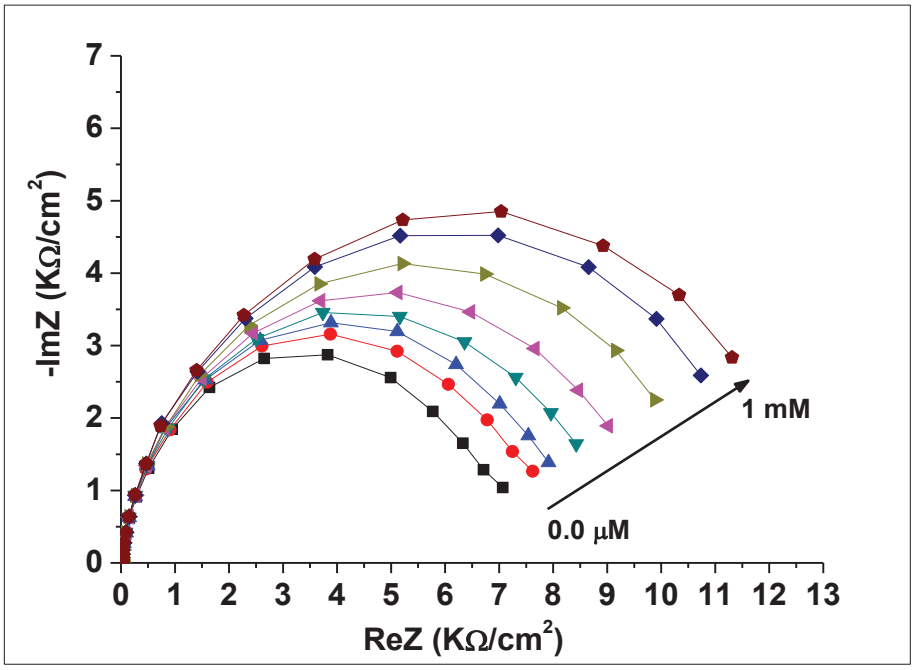

Figure 71. Nyquist plots of impedance spectra obtained for gold electrodes modified with ATP/PVA/PEI/AuNPs/GOx water-stable electrospun NFs upon the increasing concentration of glucose. The EIS measurements were performed at -300 mV in the presence of PBS solution (0.1M, pH 5.0), by varying frequency in the 100 mHz to 100 kHz range.

Figure 72 shows the calibration curve obtained by plotting Rp variations versus log(glucose concentration) for the ATP/PVA/PEI/AuNPs/GOx NFs biosensor. The slope of the logarithmic calibration curve was 2.5KΩ/log[glucose] and the linear range was up to 1mM and the resulting calibtration curve had an R-squared value of 0.986 (Figure 72). The limit of detection (LOD), calculated as the concentration of glucose giving a signal equal to three times the standard deviation on the blank (i.e. in absence of glucose) was 0.15µM. This is ten times lower than the LOD obtained for the PVA/MWCNT-COOHs/GOx NFs described in the previous chapter.

The relative standard deviations calculated from three consecutive measurements on one single biosensor were lower than 4 % in the 1.24µM -1mM range, showing an excellent repeatability of the proposed biosensor. Inter-sensor reproducibility of the method was also rather good as the relative standard deviation, calculated from the analysis of the 1.24 µM glucose solution using five different biosensors, was 14%.

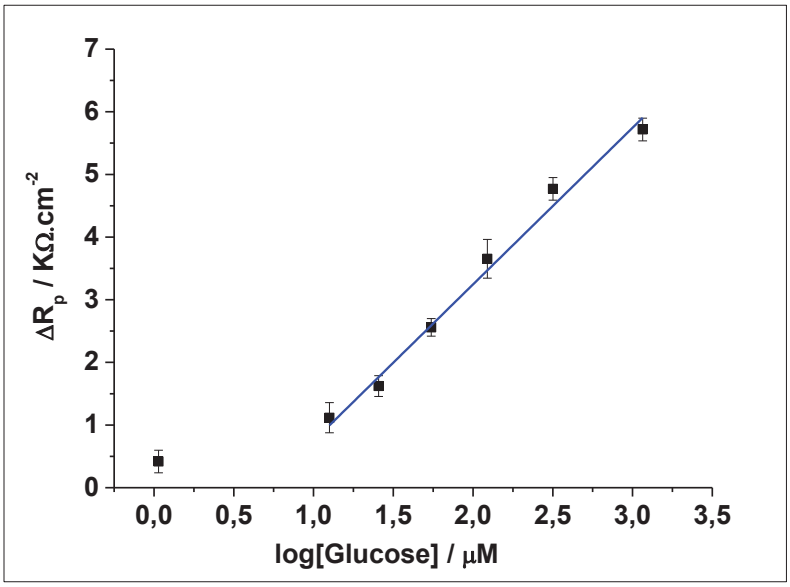

Figure 72. Calibration curve of the ATP/PVA/PEI/AuNPs/GOx NFs biosensor (in PBS 0.1M, pH 5.0). Error bars represent standard deviations obtained from three successive measurements.

Aditionally, operational and storage stabilities of the biosensor were also determined. No significant decrease of the PVA/PEI/AuNPs/GOx biosensor response was observed after 10 measurements of the 0.1 mM glucose solution, performed the same day. In the same way, EIS signal remained stable for 4 days when the biosensor was tested twice per day at the 0.1mM glucose concentration and the biosensor was kept at 4°C between two measurements. The results demonstrate the good operational and storage stabilities of the PVA/PEI/AuNPs/GOx NFs biosensor.

III.5. Conclusion

In the present study, a one-step elaboration of water-stable PVA/PEI/AuNPs/GOx electrospun nanofibrous mats followed by a cross-linking crosslinking step via exposure to GA vapours was proposed and these electroactive surfaces were further evaluated for electrochemical biosensor application. The obtained impedimetric glucose biosensor exhibited linearity in a wide range of glucose concentration (1μM -1mM) and a very low LOD value (0.15 μM) was achieved.

The advantages of this work include the uniform dispersion and pH-tunable assembly of AuNPs on the surface of the electrospun NFs based on hydrogen bonding interactions and physical entrapment of AuNPs into NFs porosity. The AuNPs enhanced the electrical properties of the bioactive electrospun NFs and thus facilitated the electron transfer within the system.

Furthermore, the expression of amino groups on the surface of the electrospun nanofibers, achieved through the incorporation of PEI into the electrospun mixture, served to practical adhesion improvement of the electrospun PVA/PEI/GOx nanofibers onto the gold modified electrode surface. This was achieved by modifying the surface with a conductive self-assembled monolayer, ATP-SAMs, bearing thiol groups for covalent bonding to the gold surface and amine groups which reacted with the amine groups of PEI in a following cross-linking step under GA vapours.

Once again, it was proven that the approach of blending the enzyme inside the water-soluble polymers offers a simple method to produce biologically active water-stable fibers, while enzyme is accessible to the substrate, in one-step synthesis. A ten times improvement of the LOD was achieve using this approach compared to the one described in the previous chapter.

CHAPTER IV: PREPARATION AND CHARACTERIZATION OF CORE-SHELL POLYPYRROLE NANOFIBERS BY COMBINATION OF ELECTOSPINNING AND VAPOUR-PHASE POLYMERIZATION FOR BIOSENSOR APPLICATIONS

IV.1. Introduction

Among the numerous intrinsically conductive polymers (ICPs) prepare to date, polypyrrole (PPy) is by far the most extensively studied and commonly used in biosensing applications, owing to its biocompatibility, high hydrophilic character, and ease of synthesis through electrochemical and chemical routes, high stability at ambient conditions and commercial availability.[292, 293] Hence, PPy presents several advantages including good redox properties and the ability to give high electrical conductivities. Various mechanisms have been proposed for the polymerization of pyrrole monomer, the most probable being radical cation formation, radical coupling and deprotonation. An in-depth study of the mechanism was performed by Sadki et al.[294] Different strategies have been investigated to immobilize biomolecules on PPy, including direct adsorption, entrapment, and chemical grafting on N-[12] or 3-substituted polypyrrole.[293]

Over the past 2 decades, PPy mainly deposited onto an electrode surface as thin films via electropolymerization, has been extensively used for the development of amperometric biosensors for glucose detection.[202, 295] During the deposition process, the enzyme was incorporated into PPy films. This method significantly enhanced the sensor performance, due to the following reasons:

• Tight adherence of PPy to electrode materials, ability to control the properties of the conducting polymer film by changing the conditions during electrochemical polymerization.

• Simple one-step procedure of enzyme entrapment within the film by electrochemical deposition performed under mild conditions thereby preserving enzyme activity.

• PPy layer prevents enzymes from leaching out of the biocatalytic layer.

However, a challenge in thin film based applications is that the active sensing components are embedded in the bulk, which limits the efficiency and sensitivity. In addition, the working area for sensing is limited to its nominal surface area and small surface areas often limiting the sensitivity. Therefore, it is desirable to fabricate conducting polymer nanostructures which offer high porosity and high specific surface area, thus ensuring easy mass transport to and out of the conducting polymer surface.[296]

Production of PPy in a nonwoven fiber mat form has traditionally been accomplished through template synthesis methods by employing mesoporous silica, anodized aluminium oxide membrane, and particle track-etched membranes for various applications including

---

[292] R. Janmanee et al., "Detection of Human IgG on Poly(pyrrole-3-Carboxylic Acid) Thin Film by Electrochemical-Surface Plasmon Resonance Spectroscopy," *Japanese Journal of Applied Physics* 50 (**2011**): 01BK02.

[293] H.Q.A. Lê, H. Sauriat-Dorizon, and H. Korri-Youssoufi, "Investigation of SPR and Electrochemical Detection of Antigen with Polypyrrole Functionalized by Biotinylated Single-Chain Antibody: A Review," *Analytica Chimica Acta* 674, no. 1 (**2010**): 1–8.

[294] S. Sadki, P. Schottland, N. Brodie and G. Sabouraud, "The Mechanisms of Pyrrole Electropolymerization," *Chemical Society Reviews* 29, no. 5 (**2000**): 283–93.

[295] C.M. Hangarter, M. Bangar, A. Mulchandani and N. V. Myung, "Conducting Polymer Nanowires for Chemiresistive and FET-Based Bio/chemical Sensors," *Journal of Materials Chemistry* 20, no. 16 (**2010**): 3131.

sensing and biosensing. After PPy components are grown in these porous templates, the templates are removed via chemical etching to provide PPy nanofibers. However, NFs produced by these methods are typically very short and require further processing to make devices.[296]

On the other hand, the electrospinning process leads to the production of long, continuous fibers directly deposited on electrode surfaces without the need of post-treatment processes. However, it is well known that the ES process is not suitable for direct fabrication of PPy nanofibers. Pristine PPy, without any bulky side groups, is insoluble in all solvents and even though adding bulky side chains to the PPy backbone makes it soluble, the molecular weight is not high enough to form fibers on its own through the ES process.[296] Thus, an alternative ES process can be used instead, in which electrospun fibers of a non-conducting polymer can be used as a template for PPy growth since they provide high surface-to-volume ratios, enhanced mechanical properties and tunable porosity in the nonwoven fiber mat.[219] The coating of the non-conductive backbone NFs can be achieved by using a variety of methods, including the VPP process.[224] When PPy is grown on top of the fiber surface, it should not suffer from the dilution effect by the template polymers, which is inevitable in electrospinning of composite nanofibers.

Finally, in order to secure successful immobilization of the enzyme, pyrrole derivatives containing carboxylic groups[297] are excellent candidates for electrochemical biosensors because they offer suitable interface for covalent grafting of biomolecules, which results to good stability and high immobilization density.[298] They have been studied for the development of immunosensors and aptasensors by a few research groups. [292, 298, 299, 300]

Among them, 3-substituted PPy offers the advantage of maintaining its full intrinsic electrical properties during the construction of immunosensors[301] without interfering with the polymer elongation which typically occurs through coupling at the 2 and 5 positions of the monomer rings.[302] As an example, Yoon et al.[303] reported the successful fabrication of a field-

[296] S. Nair, E.Hsiao and S.H. Kim, "Fabrication of Electrically-Conducting Nonwoven Porous Mats of Polystyrene–polypyrrole Core–shell Nanofibers via Electrospinning and Vapor Phase Polymerization," *Journal of Materials Chemistry* 18, no. 42 (**2008**): 5155-5161.

[297] S. Ko and J. Jang, "Controlled Amine Functionalization on Conducting Polypyrrole Nanotubes as Effective Transducers for Volatile Acetic Acid," *Biomacromolecules* 8, no. 1 (**2007**): 182–87.

[298] R. Janmanee et al., "In Situ Electrochemical-Transmission Surface Plasmon Resonance Spectroscopy for Poly(pyrrole-3-Carboxylic Acid) Thin-Film-Based Biosensor Applications," *ACS Applied Materials & Interfaces* 4, no. 8 (**2012**): 4270–75.

[299] O.S. Kwon, S. J. Park and J. Jang, "A High-Performance VEGF Aptamer Functionalized Polypyrrole Nanotube Biosensor," *Biomaterials* 31, no. 17 (**2010**): 4740–47.

[300] H. Yoon, J. H. Kim, N. Lee, B. G. Kim and J. Jang, "A Novel Sensor Platform Based on Aptamer-Conjugated Polypyrrole Nanotubes for Label-Free Electrochemical Protein Detection," *ChemBioChem* 9, (**2008**): 634-641.

[301] H. Korri-Youssoufi, B. Makrouf, and A. Yassar, "Synthesis of 3-Derivatized Pyrroles Precursors Polymers for Functionalization with Biomolecules toward Biosensor Devices," *Materials Science and Engineering: C* 15, no. 1 (**2001**): 265-268.

[302] E. De Giglio, I. Losito, F. Dagostino, L. Sabbatini, P. G. Zambonin, A. Torrisi and A. Licciardello, "Analytical Characterization of Poly (Pyrrole-3-Carboxylic Acid) Films Electrosynthesised on Pt, Ti and Ti/Al/V Substrates," *Annali Di Chimica* 94, no. 3 (**2004**): 207–18.

effect transistor (FET) thrombin aptasensor using carboxylic-acid-functionalized polypyrrole (CPPy) nanotubes. The carboxylic-acid-functionalized polypyrrole (CPPy) nanotubes were fabricated by copolymerizing pyrrole-3-carboyxylic acid (P3C) with pyrrole by using cylindrical micelle templates in a water-in-oil emulsion system.

However, although many polypyrrole (bio)sensors have been developed by employing the electropolymerization method and some studies have reported the fabrication of enzymatic biosensors based on nanofibrous supports, mainly by employing template methods, to the best of our knowledge there are no studies existing in the literature reporting the fabrication of enzymatic biosensors based on nanofibrous supports fabricated by combination of electrospinning and VPP process.

In this context, the objective of the present work was the fabrication of an original and efficient electroactive platform for electrochemical biosensing, based on conducting core-shell nanofibers produced by the combination of electrospinning and vapour-phase polymerization. To do so, polyacrylonitrile, **PAN,** a well-studied polymer with good stability and mechanical properties, was used to fabricate electrospun PAN NFs.[304] These NFs were used as backbone non-conductive structure (core fibers), whilst facilitating the growth of two different ICPs coatings onto their surface: a) polypyrrole (**PPy**) and b) polypyrrole (**PPy**)/poly(pyrrole-3-carboxylic acid)(**PP3C**), for the elaboration of different glucose biosensors.

The methodology we used was the following:

a) Elaboration of electrospun PAN NFs coated with PPy using vapour-phase polymerization (VPP) process for glucose detection

In a first step, PAN NFs were fabricated by employing the electrospinning technique. Different electrospinning parameters including flow rate, applied voltage, polymer concentration and tip-to-collector distance were tailored to produce PAN nanofibers with minimal beading. Then, PPy was grown onto the surface of the non-conductive PAN NFs via an *in situ* simple two-step VPP method. In this process, the NFs were immersed into a chemical oxidant solution (ferric (III) p-toluenesulfonate, FeTos) of different concentrations (12, 20 and 40wt% respectively) and subsequently, pyrrole monomers were deposited from the gas phase onto the fiber surfaces, which initiated the polymerization reaction producing PPy coatings. The effect of the oxidant concentration on the morphology and conductivity of the NFs was investigated. Finally, glutaraldehyde vapours, were used as cross linking agent during the immobilization process of GOx onto the surface of the PAN/PPy NFs. The electrochemical properties of electrospun PAN/PPy nanofibrous mats were characterized by

[303] Yoon, Ko, and Jang, "Field-Effect-Transistor Sensor Based on Enzyme-Functionalized Polypyrrole Nanotubes for Glucose Detection." *The Journal of Physical Chemistry* 112, (**2008**): 9992-9997.

[304] S.K. Nataraj, K.S. Yang, and T.M. Aminabhavi, "Polyacrylonitrile-Based nanofibers—A State-of-the-Art Review," *Progress in Polymer Science* 37, no. 3 (**2012**): 487–513.

cyclic voltammetry (CV) and electrochemical impedance spectroscopy (EIS). Scanning electron microscopy (SEM) was used to characterize the morphology of the nanofibers.

b) Elaboration of electrospun PAN NFs coated with PPy/PP3C by VPP process for glucose detection

In a second step, the fabrication of a highly sensitive, stable and efficient electrobioactive surface design, by modifying the gold electrode surfaces with electrospun core-shell **PAN- PPy/ PP3C** NFs produced by VVP was optimized for further detection of glucose. To do so, two different approaches were tested. In the first approach, electrospun PAN NFs were used as backbone non-conductive NFs. As previously, different electrospinning parameters were tailored to produce PAN nanofibers with minimal beading. Afterwards, VPP was employed as before to grow a thin PPy/PP3C coating onto the NFs surface. In this process, the NFs were immersed into FeTos solutions of different concentrations (12, 20 and 40 wt% respectively) and subsequently, pyrrole and pyrrole-3-carboxylic acid monomers were deposited from the gas phase onto the fiber surfaces, which initiated the co-polymerization reaction producing PPy/PP3C coatings. The effect of the oxidant concentration on the morphology and conductivity of the NFs was investigated. Alternatively, a the second approach was evaluated in order to produce PPy/PP3C coatings on the backbone fibers in a phenomenally simpler way, the incorporation of the chemical oxidant into the electrospun PAN fibers, by mixing the FeTos solution with PAN solution. To do so, various ratios of FeTos/PAN mixtures were tested in order to electrospin the composite fibers.

The polymerization time of the co-polymer was varied in order to ensure a complete polymerization. The functional monomer P3C was integrated into a copolymer scheme in order to provide sufficient immobilization sites for the enzyme. It was polymerized along with the pyrrole monomer during the VPP process. Finally, the carboxylic acid groups of the PAN/FeTos/PPy/PP3C nanofibers were activated for the covalent immobilization with the amino groups of GOx by using *N*-(3-Dimethylaminopropyl)-*N′*-ethylcarbodiimide hydrochloride (EDC)/ N-hydroxysuccinimide (NHS) chemistry.

The electrochemical properties of electrospun PAN/PPy/PP3C nanofibrous mats were characterized by cyclic voltammetry (CV) and electrochemical impedance spectroscopy (EIS). The obtained biosensor enabled successful detection of glucose by electrochemical impedance spectroscopy. Scanning electron microscopy (SEM) and transmission electron microscopy (TEM) were used to characterize the morphology of the NFs.

The above described approaches employed for the elaboration of impedimetric GOx-based biosensors are summarized in table 10.

Table 10. Different approaches employed for the elaboration of impedimetric glucose biosensors, based on the fabrication of conductive NFs through the combination of ES and VPP process.

Different approaches	NFs Composition	Immersion in FeTos	Mixing with FeTos	Coating layer	Immobilization method of GOx	Section
1	PAN	Yes	No	PPy	GA vapours	IV.4.1.3, IV.4.1.4.
2	PAN/FeTos	No	Yes	PPy/PP3C	–	IV.4.2.1.
3	PAN	Yes	No	PPy/PP3C	Covalent grafting with EDC/NHS	IV.4.2.2.

IV.2. Materials and Methods

Polyacrylonitrile (PAN, average M_w:150,000), Iron(III) p-toluenesulfonate hexahydrate, (FeTos), 1-Butanol (ButOH), Acetonitrile (ACN, 99% anhydrous), *N,N*-Dimethylformamide, (DMF), Glutaraldehyde (GA, 25wt% aqueous solution), N-hydroxysuccinimide (NHS), *N*-(3-Dimethylaminopropyl)-*N*′-ethylcarbodiimide hydrochloride (EDC), Pyrrole-3-carboxylic acid (P3C), Pyrrole (Py), Glucose and Glucose Oxidase (GOx, from *Aspergillus niger* 50KU) was purchased from Sigma-Aldrich (Saint-Quentin-Fallavier, France). Pyrrole was further distilled before usage. Phosphate saline buffer solutions were prepared with mono and dibasic phosphate (pH 7.2, 0.1 M).

Polyacrylonitrile, PAN, is a synthetic, semicrystalline white to yellow organic polymer resin, with the linear formula $(C_3H_3N)_n$. It is a hard, rigid, thermoplastic material that is resistant to most solvents and chemicals, slow to burn anf of low permeability to gases. Almost all PAN resins are copolymers made from mixtures of monomers with acrylonitrile as the main component. It is a versatile polymer used to produce large variety of products. All commercial methods of production of PAN are based on free radical polymerization of Acrylonitrile (AN). In most cases, small amount of other vinyl comonomers are also used (1-10%) along with AN depending on the final application. Anionic polymerization also can be used for synthesizing PAN. For textile applications, PAN with molecular weight in the range of 40,000 to 70,000 is used.

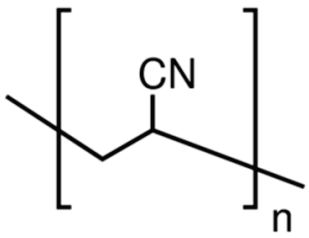

Figure 73. Chemical formula of PAN used in this work.

Iron(III) p-toluenesulfonate hexahydrate, FeTos, is a yellow and solid organic compound with linear formula $(CH_3C_6H_4SO_3)_3Fe{\cdot}6H_2O$ with molecular weight 677.52 g/mol. It is soluble in water, alcohols, and other polar organic solvents. In this work, a ferric tosulate solution was used as the oxidant solution for the vapour-phase polymerization of Py.

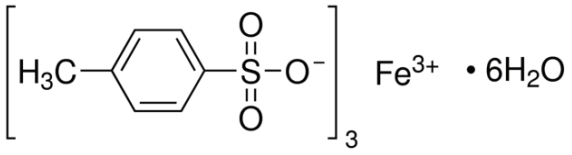

Figure 74. Chemical formula of FeTos used in this work.

***N*-(3-Dimethylaminopropyl)-*N′*-ethylcarbodiimide hydrochloride**, EDC**,** is a carboxyl and amine-reactive zero-length crosslinker with molecular weight 191.7 g/mol. EDC reacts with a carboxyl group first and forms an amine-reactive O-acylisourea intermediate that quickly reacts with an amino group to form an amide bond and release of an isourea by-product (figure 75).

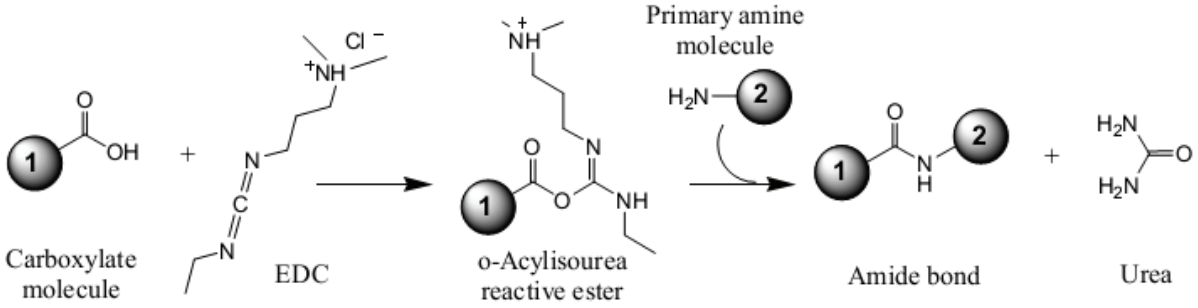

Figure 75. One-step EDC reaction with carboxyl and amine-containing molecules. https://www.lifetechnologies.com/fr/fr/home/life-science/protein-biology/protein-biology-learning-center/protein-biology-resource-library/pierce-protein-methods/carbodiimide-crosslinker-chemistry.html Thermo-Scientific

The intermediate is unstable in aqueous solutions, and therefore, two-step conjugation procedures rely on N-hydroxysuccinimide for stabilization (figure 76). Failure to react with an amine will result in hydrolysis of the intermediate, regeneration of the carboxyl and release of an N-substituted urea. A side reaction is the formation of an N-acylurea, which is usually restricted to carboxyls located in hydrophobic regions of proteins.

N-hydroxysuccinimide, NHS is used to prepare amine-reactive esters of carboxylate groups for chemical labeling, crosslinking and solid-phase immobilization applications. Carboxylate groups may be reacted to NHS in the presence of a carbodiimide such as EDC as mentioned previously, resulting in a semi-stable NHS ester, which may then be reacted with primary amines ($-NH_2$) to form amide crosslinks (Figure 76). Although NHS is not required

for carbodiimide reactions, their use greatly enhances coupling efficiency. Furthermore, using NHS makes it possible to perform a two-step reaction.

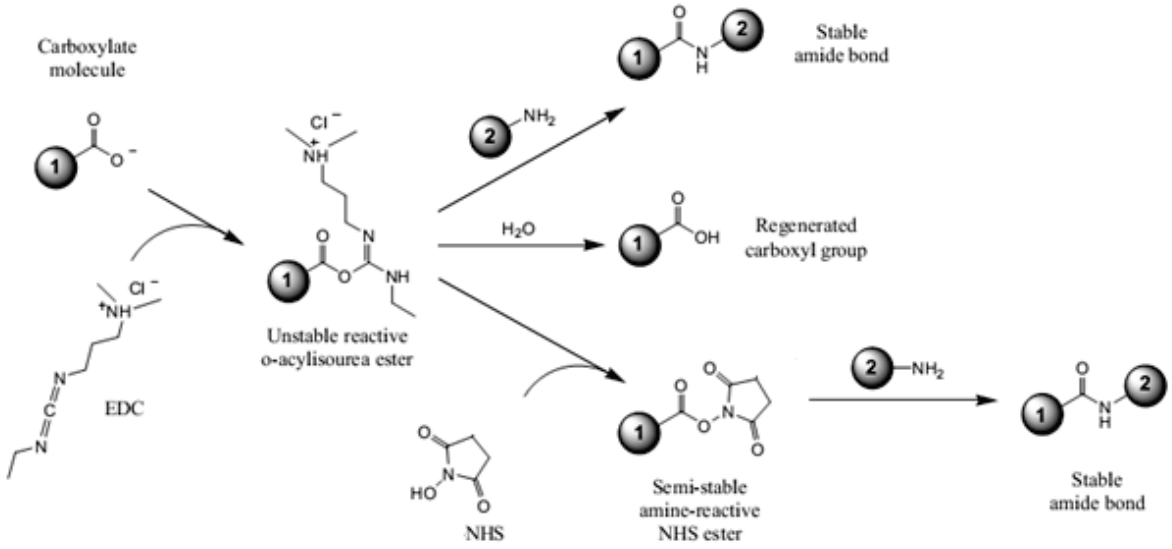

Figure 76. Reactions involving EDC, including activation as an NHS ester. https://www.lifetechnologies.com/fr/fr/home/life-science/protein-biology/protein-biology-learning-center/protein-biology-resource-library/pierce-protein-methods/carbodiimide-crosslinker-chemistry.html Thermo-Scientific

NHS is soluble in aqueous and organic solvents. Activation with NHS, however, decreases water-solubility of the modified carboxylate molecule, while activation with Sulfo-NHS preserves or increases water-solubility of the modified molecule, by virtue of the charged sulfonate group. Although prepared NHS esters are sufficiently stable to process in a two-step reaction scheme, both groups will hydrolyze within hours or minutes, depending on water-content and pH of the reaction solution. (NHS esters have a half-life of 4-5 hours at pH 7, 1 hour at pH 8 and only 10 minutes at pH 8.6). The activation reaction with EDC and NHS is most efficient at pH 4.5-7.2 and reaction of NHS-activated molecules with primary amines is most efficient at pH 7-8, and NHS-ester reactions are usually performed in phosphate-buffered saline (PBS) at pH 7.2-7.5.

Pyrrole, Py, is a 5-membered aromatic heterocyclic organic compound, with chemical formula C_4H_5N. It is a colourless to yellow volatile liquid that darkens readily upon exposure to air and is usually purified by distillation immediately before use.

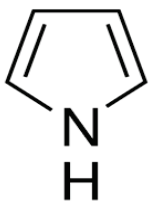

Figure 77. Chemical structure of Pyrrole.

Pyrrole-3-carboxylic acid, P3C, is a pyrrole derivative containing carboxylic groups at 3-position with molecular weight 111.10g/mol.

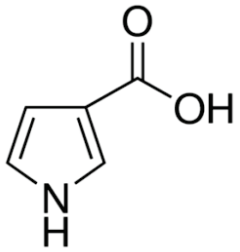

Figure 78. Chemical structure of P3C used in this work.

IV.3. Experimental Section

IV.3.1. Preparation of the working electrodes

Gold electrodes used as working electrodes and their cleaning protocol were the same as described in the second chapter, at section III.3.1.

IV.3.2. Preparation of electrospun solutions

IV.3.2.1. Preparation of PAN suspension

For the fabrication of PAN NFs, a 12 wt% PAN solution was prepared by dissolving PAN powder into DMF at 80 °C for 3 h under magnetic stirring. The solution was cooled down to room temperature before use.

IV.3.2.2. Preparation of PAN/FeTos suspensions

For the fabrication of PAN/FeTos NFs, a 15 wt% PAN solution was prepared by dissolving PAN powder into DMF at 80 °C for 5 h under magnetic stirring. Three different FeTos suspensions (12, 20 and 40wt% in DMF) were also prepared. The FeTos suspensions were added to PAN solutions individually and the resulting PAN/FeTos COOH suspensions were heated at 80 °C under for 3 h under magnetic stirring. Different ratios of PAN and FeTos (1:1, 2:1, 3:1 and 1:2 respectively) were tested for each concentration of the oxidant.

IV.3.3. Electrospinning: Fabrication of electrospun PAN and PAN/FeTos nanofibers

NFs were fabricated using the home-made electrospinning device descrided in section II. 2.2. PAN and PAN/FeTos suspensions were loaded immediately after preparation into a glass syringe fitted with a stainless needle (0.644 mm I.D.), the cleaned working gold electrodes were placed on the collector inside the ES chamber and fibers were spun at room room temperature (23±2 °C). The nanofibers were directly deposited on the surface of the gold electrodes. Electrospinning parameters (e.g. applied voltage, feed rate and collection distance) ranging from 8-22 kV for the applied voltage, 9-23 cm for the tip-to-collector distance and 1-3mL/h for the polymer flow rate, had to be adjusted to limit bead formation.

IV.3.4. Distillation of Pyrrole

Pyrrole darkens very quickly (from colourless to yellow and then brown) upon contact with air. So in order to remove any impurities, distillation by using a vacuum/inert (N_2) gas line [305] was performed before proceeding to VPP method. To do so, the assembly depicted in figure 79 was used. Standard laboratory glassware with ground glass joints was used.

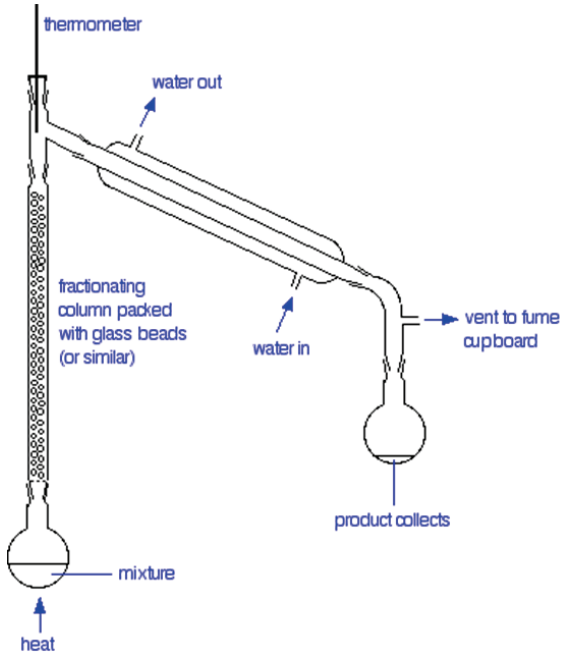

Figure 79. Distillation setup used for pyrrole. Reformed from Ref 305.

Firstly, Py was introduced into a 250mL round-bottom distilling flask and CaH_2 was added and left overnight in it in order to remove all traces of water. Afterwards, the solution was filtered with the help of a funnel in order to remove CaH_2. The assembly (figure 79) was evacuated and 3 cycles of vacuum/inert gas were performed. Then, the pyrrole was introduced in the system, whilst kept under agitation in a nitrogen atmosphere. Within 5 min under vaccum, pyrrole was distilled at 32°C. It was collected in a round-bottom receiving flask which was covered with aluminium foil in order to avoid photopolymerisation and it was kept in the freezer in a sealed dark glass bottle.

IV.3.5. VPP process

An *in situ* VPP process was used to apply the conductive polymer coating onto the surface of NFs, as described in figure 80. In the PPy and PPy/PP3C coating procedures, the PAN NFs were firstly dipped into three oxidant solutions of FeTos (12, 20 and 40 wt% in ButOH) individually. The excess of FeTos solution (defined as the amount of FeTos clogging the porosity of the mat) was removed by using a spincoater (for 20s at 3000 rpm).

[305] W.L.F. Armarego and C.L.L. Chai, *Purification of Laboratory Chemicals*, 5. ed (Amsterdam: Butterworth-Heinemann, 2003).

Subsequently, the FeTos NFs were annealed in air at 70°C on a hot plate for 5min. The NFs were then introduced in a reactor where nitrogen was bubbled through the liquid monomer. The monomer(s) vapours polymerized when they came in contact with the FeTos-coated NFs, producing conductive polymer coating, doped with tosylate anions.

In the PPy coating procedure, a pyrrole solution (0.05M) was prepared by appropriate dilution of the 14M commercial solution in acetonitrile. In the PPy/PP3C coating procedure, pyrrole-3-carboxylic acid was dissolved in acteonitrile (0.1M) and was added to pyrrole suspension (0.05M). The monomers mixture was then placed into the reactor as described above. The polymerization time was varied depending on the monomer used: pyrrole alone polymerized at ambient temperature within a few minutes (7 min), as revealed by the appearance of the characteristic black colour of polypyrrole. The polymerization time for PPy was then set at 15 min to ensure a complete polymerization. On the other hand, Py/P3C polymerized in ambient temperature also but a longer polymerization time was required. The black characteristic colour of the co-polymer started to appear within 20 min, so the polymerization time for PPy/PP3C was set at 30min to ensure a complete polymerization. After the polymerization, the PAN/FeTos/PPy and PAN/FeTos/PPy/PP3C NFs were removed form the reactor and left in ambient atmosphere for 4-5 h to ensure complete evaporation of Py and Py/P3C vapours. They were then ultrasonicated for 1min, rinsed with H_2O/MeOH mixture (1:1) for 10 min and dried under N_2 at room temperature.

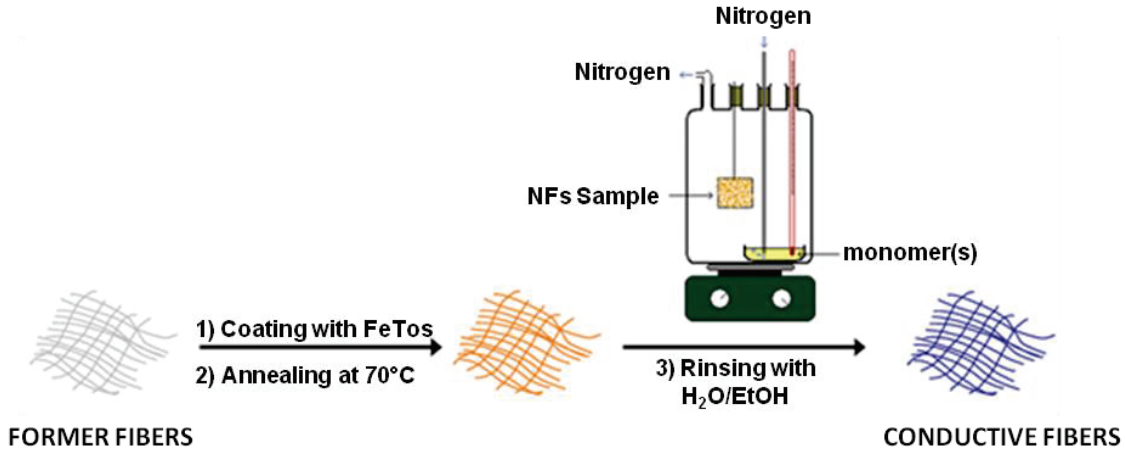

Figure 80. Two-step VPP coating process. Reformed from Ref 309.

IV.3.6. Immobilization of GOx on the surface of PPy coated PAN NFs with GA

A mixture containing 5 mg of GOx, 5 mg of BSA was prepared in 100 μM phosphate buffer (20 mM, pH 7.2). From this mixture, 20 μL were deposited onto the PAN/PPy NFs modified gold electrode surface by spincoating for 15 s at 500 rpm and then for 15 s at 1000 rpm. After the membrane deposition, the electrodes were exposed to GA satured vapours for 30 min. GA allows the cross-linking of the enzyme and BSA through the formation of Schiff bases (-N=CH-). BSA, a lysine-rich protein with no enzymatic activity, was used as crosslinking co-reagent to help forming enzyme immobilization matrices and protect the

enzyme from excessive reaction with GA, which might have compromised its activity.[34] Then, the membranes on top of PAN/PPy NFs were dried at room temperature for 1h and were kept dry overnight at 4°C.

IV.3.7. Covalent immobilization of GOx onto the surface of PPy/P3C coated PAN NFs by using EDC/NHS chemistry

Aqueous solutions of EDC (100 mM) and NHS (100 mM) were prepared by dissolving 1.9 mg EDC in 100 µL and 1.2 mg NHS in 100 µL. Subsequently, the two solutions were mixed together (C_{final} of each=10 mM) and the gold electrodes modified with PAN/PPy/PP3C NFs were immediately immersed into the EDC/NHS mixture for 1 h. Afterwards, the activated surface of the PAN/PPy/PP3C NFs surface was washed 3 times with distilled H_2O to remove the excess of unreacted EDC/NHS moieties. Finally, the modified working electrodes were immersed into the enzyme solution (10 mg GOx in 300 µL of PBS 5 mM, pH 7.2) for 2 h at room temperature, washed with distilled H_2O and immediately used for electrochemical measurements.

IV.3.8. Electrical resistance measurements

A four-point probe (Lucas Lab S-302) which was connected to a digital multimeter with four wires measurement capability (Keithley 2001) were used to measure the electrical resistance of the PAN/FeTos/PPy/P3C NFs. The resistance measurements were carried out using a home-made electrodes design depicted in figure 81. The four electrode design minimizes the influence of the contact impedance which could appear at the electrode/mat interface. The electrodes consisted of a 150-nm thick gold layer deposited by evaporation onto microscope glass slide substrates using an adhesion layer of 20 nm of titanium (Ti).

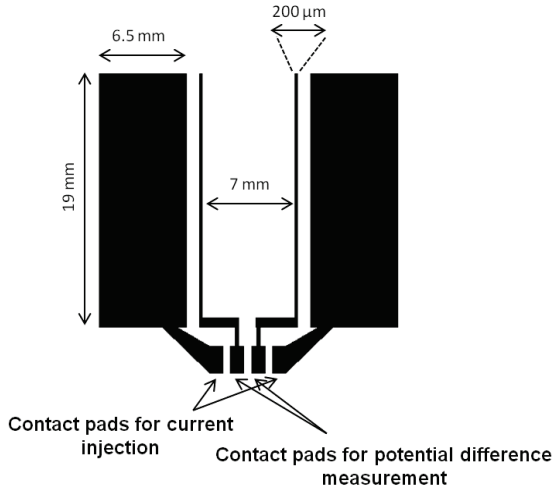

Figure 81. Schematic representation of gold electrodes used for electrical resistance measurements.

IV.3.9. Electrochemical Characterizations

CV and EIS characterizations were all performed at room temperature as described in II.2.1.

IV.3.9.1. PAN NFs, PAN/FeTos/PPy NFs and PAN/FeTos/PPy/PP3C NFs modified electrodes

EIS characterization of PAN NFs and PAN/FeTos/PPy/PP3C NFs modified electrodes were carried out in 0.1 M phosphate buffer saline buffer (PBS) pH 7.2 containing 10 mM $K_3Fe(CN)_6^{3-}$ and $K_4Fe(CN)_6^{4-}$, varying the frequency in the 100 mHz to 100 kHz range and acquiring 5 points per decade. An excitation voltage of 10 mV was superimposed on a dc potential of -300 mV. Impedance data were fitted to equivalent electrical circuits by means of the ZView2 software (Scribner Associates Inc, Southern Pines, USA). The same electrodes were also characterized by CV, the potential being cycled from −400 and +600 mV (versus Ag/AgCl) with a 100 mV/s scan rate. 0.1 M PBS buffer pH 7.2 containing 10 mM $K_3Fe(CN)_6^{3-}$ and $K_4Fe(CN)_6^{4-}$ was chosen as electrolyte. After each measurement, the electrolyte solution was refreshed, and the electrodes were washed with distilled water to remove any residues.

IV.3.9.2. PAN/FeTos/PPy/GOx NFs and PAN/FeTos/PPy/PP3C/GOx NFs modified electrodes

Biosensing experiments were performed by injecting glucose from mother solution into the 4mL electrochemical cell containing either PAN/FeTos/PPy/GOx NFs or PAN/FeTos/PPy/PP3C/GOx NFs modified electrodes and 0.1 M PBS pH 7.2 as electrolyte. EIS measurements were performed by varying the frequency in the 100 mHz to 100 kHz range and acquiring 5 points per decade, on a dc potential of -300 mV. Three replicates were performed for each glucose concentration and related standard deviations were calculated.

IV.3.10. Characterization of NFs morphology

NF mats were characterized by transmission electron microscopy (TEM) using a Philips CM120 instrument operating at an accelerating voltage of 120 kV and by SEM with a TESCAN MIRA3 FEG-SEM microscope after sample metallization (2 nm Pt or Cr).

IV.4. Results and discussion

IV.4.1. Elaboration of electrospun PAN NFs coated with PPy by VVP for glucose detection

IV.4.1.1. Effect of electrospinning parameters on the morphology of PAN electrospun NFs

The influence of PAN concentration on NFs morphology was first investigated. Three concentrations, 7, 12 and 18 wt% of PAN were tested. We observed that it was not possible to produce NFs at the lowest polymer concentration due to the insufficient viscosity of the solution for ES. Increasing PAN concentration from 7 up to 12 wt%, helped solving this issue and pure fibers were generated. However, the 18wt% PAN solutions appeared as hardly electrospinnable due to the very high viscosity that they exhibited. The 12 wt% concentration was therefore selected for further experiments. The influence of applied voltage (ranging from 8-22 kV), the tip-to-collector distance (9-23 cm) and the polymer flow rate (1-3 mL/h) on NFs morphology were further investigated. It was observed that when the applied voltage was fixed at 22 kV, the collection distance at 15 cm and the flow rate was set at 1 mL/h, the electrospinning process was very stable and allowed the continuous production of very uniform PAN NFs, free of beads with average diameter 650±10 nm (figure 82). TEM images of the pure PAN NFs revealed a perfectly smooth fiber surface (figure 82).

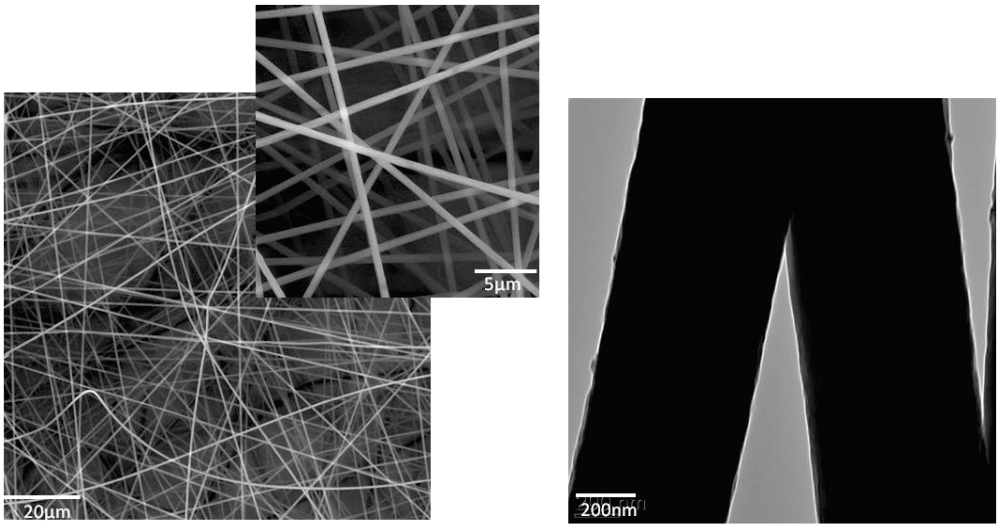

Figure 82. SEM (left) and TEM (right) images of electrospun PAN NFs formed by using an applied voltage of 22 kV, a polymer concentration of 12 wt%, flow rate of 1 mL/h and collection distance of 15 cm.

IV.4.1.2. Morphological Analysis of coated PAN NFs with PPy

Figure 83 shows pictures of PAN NFs, uncoated (a) and coated with a protective mask (b), immersed in FeTos solution (c), annealed at 70°C for 5 min (d), as well as coated with PPy (e, f). The blue protective mask was placed on the NFs in order to ensure a well-established shape (known length and width) necessary for the comparison of the electrical

resistance measurements of the nanofibrous mats. Calculations of resistivity values were not performed, given the fact that a precise and acurate measurement of the coated mat thickness could not be performed.

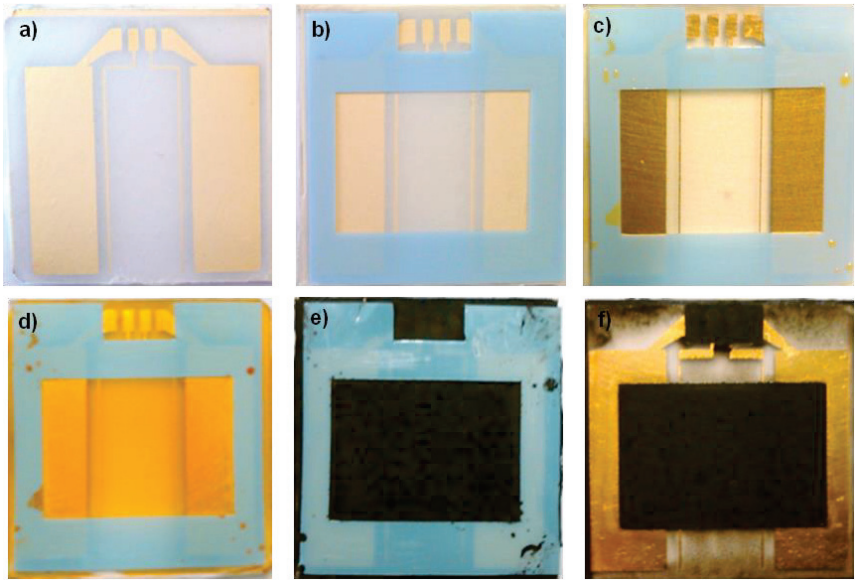

Figure 83. Different steps of PAN NFs PPy coating during the VPP procedure. a) Uncoated PAN fibers, b) placement of blue mask onto the NFs in order to accurately define the shape and size (height and width) of the conductive area to ensure reproducible resistance measurements of the NFs, c) PAN NFs coated with the oxidant after immersion in 20 wt% FeTos solution, d) FeTos coated PAN NFs after annealing at 70°C, d) PPy coated PAN NFs after 15min polymerization time at RT, PPy coated PAN NFs after the removal of protective blue mask.

The NFs mats colour was characteristic of the polymer present at the surface: uncoated PAN NFs exhibited a white colour, whereas PAN NFs immersed in FeTos solution and annealed at 70°C, exhibited the characteristic yellow/orange colour of the oxidant solution. PAN NFs further coated with PPy displayed a black colour, characteristic of the presence of Py. The coatings appeared uniform and homogeneous over the covered NFs.

Core-shell PAN/PPy conductive NFs were obtained by *in situ* VPP polymerization of Py on the surface of PAN fibers. When the electrospun NFs were exposed to Py monomer vapours, redox reaction occurs where Py is oxidized while FeTos is reduced. SEM images revealed that after 15 min of polymerization, the PPy covers completely the surface of PAN NFs. It was observed that cauliflower shaped PPy nanostructures were covering the fiber surface (figure 84), as the PPy was polymerized on top of the PAN/FeTos fibers. The AFD of PAN NFs coated with PPy was roughly estimated, understanding the limitations of the measuring method. A slight increase within the range of 10 to 20nm was observed by calculating the difference in the AFD of uncoated and coated with PPy PAN NFs. The results are in good agreement with what has been reported in the literature.[306]

[306] J. Wang, H. E. Naguib, and A. Bazylak, "Electrospun Porous Conductive Polymer Membranes," *Behavior and Mechanics of Multifunctional Materials and composites* 8342, (**2012**): 83420F-1 -83420F-13.

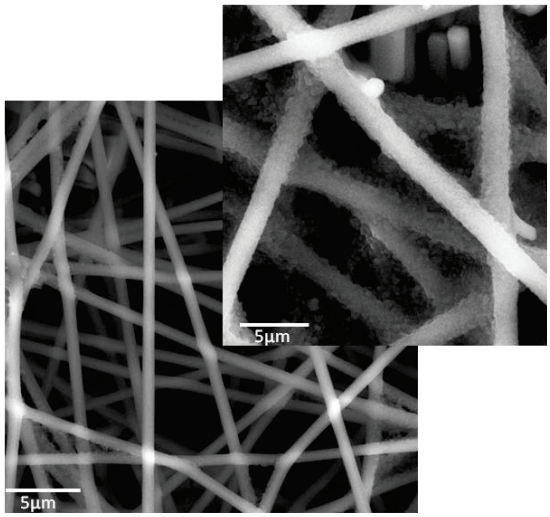

Figure 84. Representative SEM images of conductive PAN NFs coated with PPy, after exposure to Pyrrole vapours for 15min in ambient conditions.

IV.4.1.3. Electrochemical Characterization of PAN/PPy electrospun NFs

CV and EIS were employed to evaluate the electrochemical performance of gold electrodes modified with PAN/PPy NFs upon increasing concentration of the oxidant solution. Polymerization time was set at 15 min. CVs were recorded in 10 mM PBS at pH 7.2 at a scan rate of 100mV/s using $Fe(CN)_6^{3-}/Fe(CN)_6^{4-}$ couple as redox probe. The potential was repetitively cycled until several consecutive curves were superimposed. CVs were recorded before and after the functionalization of the electrode surface with PAN NFs and PAN/PPy NFs when using FeTos solution of 12 wt%, 20 wt% and 40 wt% during the VPP process. It is clearly demonstrated that coating the PAN NFs (initially exhibiting strong insulating properties-figure 85, black curve) with PPy results in the fabrication of conducting NFs (figure 85, red, blue and green curves) with highly capacitive behaviour. The levelled current densities for the PAN/FeTos 40%/PPy/PP3C NFs modified electrode are higher than those of PAN/FeTos 20%/PPy/PP3C NFs electrode and much higher than those of PAN/FeTos 12%/PPy/PP3C NFs electrode. These results are in good agreement with what has been reported in the literature and is consistent with the well-known PPy electrochemical properties.[307, 308]

[307] J.G. Wang et al., "Rational Synthesis of MnO2/conducting Polypyrrole@carbon Nanofiber Triaxial Nano-Cables for High-Performance Supercapacitors," *Journal of Materials Chemistry* 22, no. 33 (**2012**): 16943.
[308] S. Chen and I. Zhitomirsky, "Capacitive Behaviour of Polypyrrole, Prepared by Electrochemical and Chemical Methods," *Materials Letters* 125 (**2014**): 92–95.

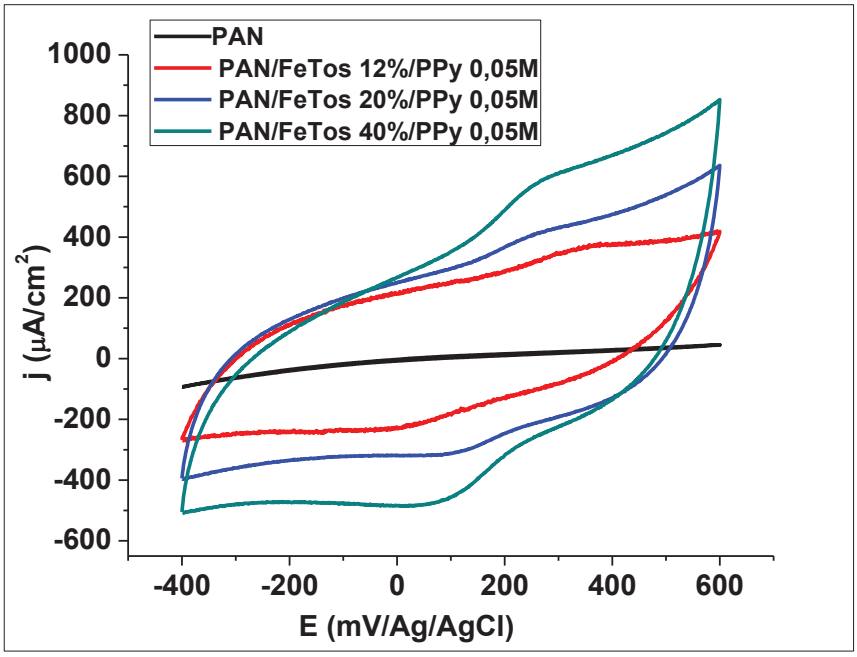

Figure 85. Cyclic voltammograms of gold modified electrodes with PAN NFs and PAN/PPy electrospun NFs by using FeTos solutions of 12, 20 and 40wt% (in $[Fe(CN)_6]^{3-/4-}$ aqueous solution, pH 7.2, scan rate 100mV s^{-1}).

The electronic transfer properties of the PAN/PPy NFs modified gold electrodes were further characterized by EIS by varying frequency in the 100 mHz to 100 kHz range at a constant potential of -300 mV. The Nyquist plots of PAN/PPy NFs electrodes presented in figure 86, were satisfactorily fitted with a Randles-Ehrshler equivalent electrical circuit. Circuit parameters obtained by fitting the impedance data with the equivalent circuit shown in figure 55 are summarized in Table 11.

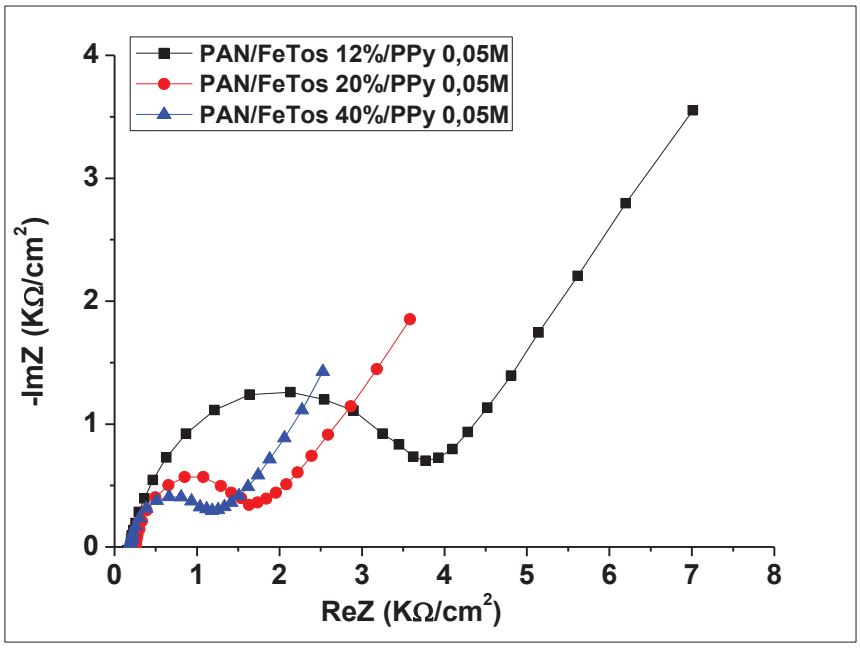

Figure 86. Nquist plots of impedance spectra obtained for gold electrodes modified with **PAN/PPy** electrospun NFs by using FeTos solutions of 12, 20 and 40wt%. The EIS measurements were performed at -300 mV in the presence of a 10mM $[Fe(CN)_6]^{3-/4-}$ PBS solution by varying frequency in the 100 mHz to 100 kHz range.

Table 11. Fitting parameters obtained from Nquist plots of impedance spectra by using the equivalent Randles-Ershler circuit presented in figure 55.

	R_s ($\Omega \cdot cm^{-2}$)	R_{ct} ($k\Omega \cdot cm^{-2}$)	CPE ($\mu F \cdot s^{(n-1)}$)	n_{CPE}	x^2
PAN/FeTos 12wt%/ PPy	0.181	4.107	1.985	0.985	0.004
PAN/FeTos 20wt%/ PPy	0.149	1.544	2.312	0.984	0.004
PAN/FeTos 40wt%/ PPy	0.135	1.151	2.183	0.978	0.003

The transfer charge resistance of PAN/PPy NFs decreased by increasing FeTos concentration, indicating the enhanced electron transfer capability of the PAN/PPy NFs modified gold electrodes.

IV.4.1.4. Electroanalytical characterization of PAN/PPy/GOx electrospun NFs

In subsequent experiments, GOx enzyme was casted and cross-linked on the PAN/PPy NFs modified electrodes prepared at the three FeTos concentrations and EIS measurements were performed by varying the frequency in the 100 mHz to 100 kHz range at a constant potential of -300 mV and injecting different glucose concentrations in order to evaluate the biosensor response. A large number of electrodes were tested, but in all cases Nyquist plots obtained at the different glucose concentrations were superimposed with the curve recorded before glucose injection.

After the removal of the working electrode from the electrochemical cell, the absence of the membrane containing the biomolecule of interest (GOx) was certified, whilst the PAN/PPy NFs were still well attached to the gold substrate. The first protocol tested for the production of PAN/PPy/GOx NFs modified electrodes was therefore not satisfying since it did not enable a firm attachment of the biological sensing membrane onto the fibers. This is why a second strategy of enzyme immobilization was investigated, which consisted in the covalent binding of GOx by incorporating functional carboxylic groups to the PPy coating. This was done by incorporating PP3C containing carboxylic groups in the conductive layer covering the PAN NFs.

IV.4.2. Electrospun PAN NFs coated with PPy/ PP3C by VVP for glucose detection

As already mentioned in the introduction, two different approaches were tested. In the first approach, PAN/FeTos NFs were produced by electrospinning PAN solutions containing FeTos, as described in section IV.3.3. VPP process followed in order to coat the oxidant fibers with a thin layer of PPy/PP3C. In the second approach, pure electrospun PAN NFs (used as backbone (core) fibers) were first immersed into the oxidant solution (FeTos in ButOH) and after the removal of the excess using a spincoater, their exposure to PPy/P3C vapours by using VPP process led to coating their surface with the conductive layer.

IV.4.2.1. First approach: Fabrication of PAN/FeTos composite NFs

The influence of FeTos concentration on the viscosity and the conductivity of the resulting PAN/FeTos electrospun mixtures was first investigated. Three concentrations (12, 20 and 40 wt% of FeTos in DMF) were tested. FeTos solutions exhibited a significant electrical conductivity and varying viscosity depending on the concentration of the solution[309] with those of 40wt% being more conductive and viscous when compared to the others. After the addition of FeTos solutions of different concentrations into 12 wt% PAN solution (1:1 ratio), it was observed that the FeTos presence decreases the viscosity of the resulting mixture.

[309] A. Laforgue and L. Robitaille, "Deposition of Ultrathin Coatings of Polypyrrole and Poly(3,4-Ethylenedioxythiophene) onto Electrospun Nanofibers Using a Vapor-Phase Polymerization Method," *Chemistry of Materials* 22, no. 8 (**2010**): 2474–80.

All mixtures of 12 wt% PAN solutions supplemented with FeTos solution (12, 20 and 40 wt%) exhibited insufficient viscosity for electrospinning, but this issue was overcome by increasing PAN concentration from 12 to 15 wt%. To obtain optimum viscosity and to evaluate the influence of FeTos in the conductivity of the composite NFs, different polymer/oxidant mass ratios were tested. 1:1 and 2:1 (PAN: FeTos) ratios exhibited the required viscosity whereas the viscosity of the solution by using 3:1 ratio became so high that after the addition of the polymer a gel formed at room temperature, leading to the solidification of the mixture. On the contrary, when a ratio of 1:2 (PAN: FeTos) was used, the viscosity of the resulting mixture was insufficient to obtain stable conditions for electrospinning.

By using mixtures of PAN/FeTos (1:1) for all FeTos concentrations, composite oxidant NFs exhibiting the characteristic yellow/orange colour of FeTos, were successfully obtained. However, due to high electrostatic interactions it was hard to achieve deposition of the fibers onto the gold substrate. Instead, we observed the formation of these composite fibers in the air. The phenomenon was more intense upon increasing values of applied voltage and above 15 kV, sparks creation made the process impossible. It was thus concluded that FeTos demonstrates a significant electrical conductivity which greatly affects the conductivity of the electrospun mixture.

Successful fabrication of oxidant FeTos/PS NFs has already been reported in the literature by Laforgue et al.[224] However, in that study the reported FeTos fibers were extremely sensitive to humidity due to the low polymer content used, and they were liquefied within a few min by incorporation of water, if not kept in a very dry environment (relative humidity <15%). So in that study, the electrospinning had to be performed in a controlled chamber kept at 10% of relative humidity to maintain the NF integrity while being produced and the VVP process was carried out under vacuum.

On the contrary in our study, the resulting electrospun oxidant PAN/FeTos NFs were very stable upon their exposure to humidity due to the high polymer content used and the VPP process was simply performed under nitrogen atmosphere. However, the reproducibility of the electrospinning process was limited due to the difficulty in achieving highly stable jets and in controlling all the parameters in order to deposit the NFs onto the gold surface. So in order not to compromise the reproducibility of the glucose sensor, it was decided to produce pure PAN NFs and then immerse them into the oxidant solution (FeTos in ButOH) for the fabrication of the oxidant fibers.

IV.4.2.2. Second approach: Immersion of PAN NFs into FeTos solutions

In this approach, PAN electrospun NFs were produced in the optimal conditions defined in section IV.A.1.1. and immersed in FeTos solutions (12, 20 and 40 wt%) and core-shell PAN/PPy/PP3C conductive NFs were obtained by *in situ* VPP of Py/P3C blends on the surface of PAN NFs.

IV.4.2.2.1. Effect of FeTos concentration on the growth and morphology of conductive PPy/PP3C coating onto core PAN NFs

Two of the most widely used Fe-based oxidants are $FeCl_3$ and ferric tosylate, with the latter being more able to suppress crystallite formation and moderate the solution pH, generally resulting in much smoother and more conducting coatings.[310] In this study, three different FeTos concentrations were tested in order to investigate the way that the final coating thickness and the conductivity of the coated NFs were influenced by the oxidant concentration.

For all FeTos concentrations, after 30 min polymerization time, SEM images revealed that uneven nodular PPy/PP3C thin coating was grown onto the surface of oxidant PAN NFs. Figure 87 shows representative SEM images of coated PAN/PPy/PP3C NFs produced by VPP process after their immersion in 12, 20 and 40 wt% FeTos solution respectively, before the rinsing step with H_2O/MeOH. It was revealed that unreacted oxidant crystallized as FeTos salts, confirming that a significant part of the oxidant has not been consumed by Py/P3C polymerization. An increasing amount of FeTos salts crystals was observed upon increasing the concentration of the oxidant solution.

[310] M.A. Ali et al., "Effects of iron(III) P-Toluenesulfonate Hexahydrate Oxidant on the Growth of Conductive poly(3,4-Ethylenedioxythiophene) (PEDOT) Nanofilms by Vapor Phase Polymerization," *Synthetic Metals* 161, no. 13–14 (**2011**): 1347–52.

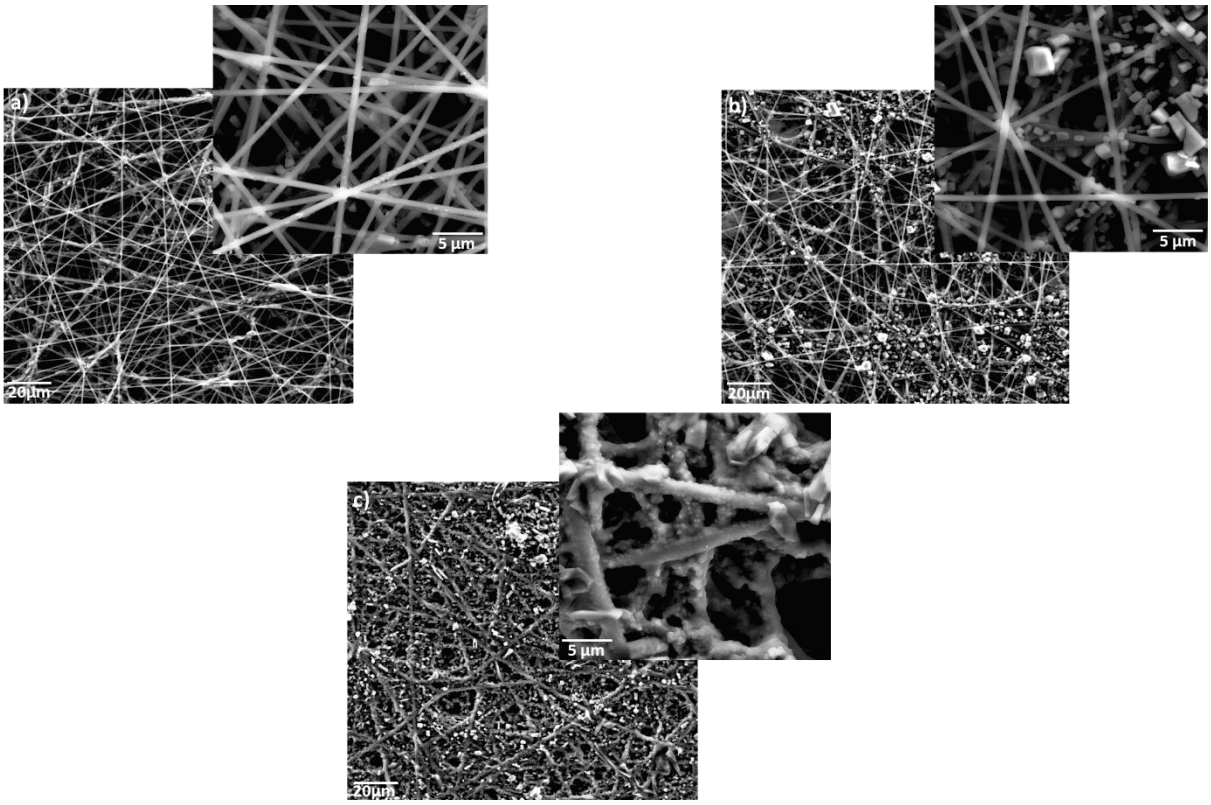

Figure 87. Representative SEM images of PAN NFs covered with PPy/PP3C coatings after VPP process and before the cleaning step. The PAN NFs mats were immersed in a) FeTos 12wt%, b) 20wt% and c) 40wt%, respectively.

As seen in figure 87c, a much thicker film of PPy/PP3C, compared to the one produced at the lowest oxidant concentrations, was obtained for the highest FeTos concentration (40 wt%). This film was formed at almost the whole surface of the mat. This large difference observed could not be attributed only to FeTos concentration in itself, but also to the highest viscosity of the solution that prevented an efficient removal of the excess of oxidant from the mat during the spincoating process. Different speed rates ranging from 0 to 3000 rpm were tested during the spincoating process in order to achieve better removal. It was found that maximum, though partial, removal was achieved at 3000rpm.

By decreasing the concentration of FeTos solution to 20wt% and finally 12wt%, the viscosity of the solution was reduced, allowing more successful but still partial removal of the FeTos excess during the spincoating process thus resulting to coating of individual fibers without filling the entire porosity of the mat (figure 87a and 87b).

Thus, an additional cleanning step was necessary to remove the excess of the unreacted FeTos. To do so, different solvents were tested including distilled H_2O, pure methanol, ethanol and a mixture of H_2O/methanol (1:1) which was found to be the most efficient. Simply rinsing the modified electrodes was not sufficient to remove the totality of FeTos crystals, so the PAN/PPy/PP3C NFs modified gold electrodes were first placed into an ultrasonic bath. The sonication time was varied from 0 to 3 min. For sonication times less than 1 min, the removal of unreacted FeTos was incomplete, independently of oxidant

concentration, and for sonication times higher than 3 min, partial removal of the fibers themselves was observed. Thus, optimum conditions were found at ultrasonication time of 1 min followed by rinsing with H_2O/MeOH. Figure 88 shows SEM images after the rinsing step with H_2O/MeOH.

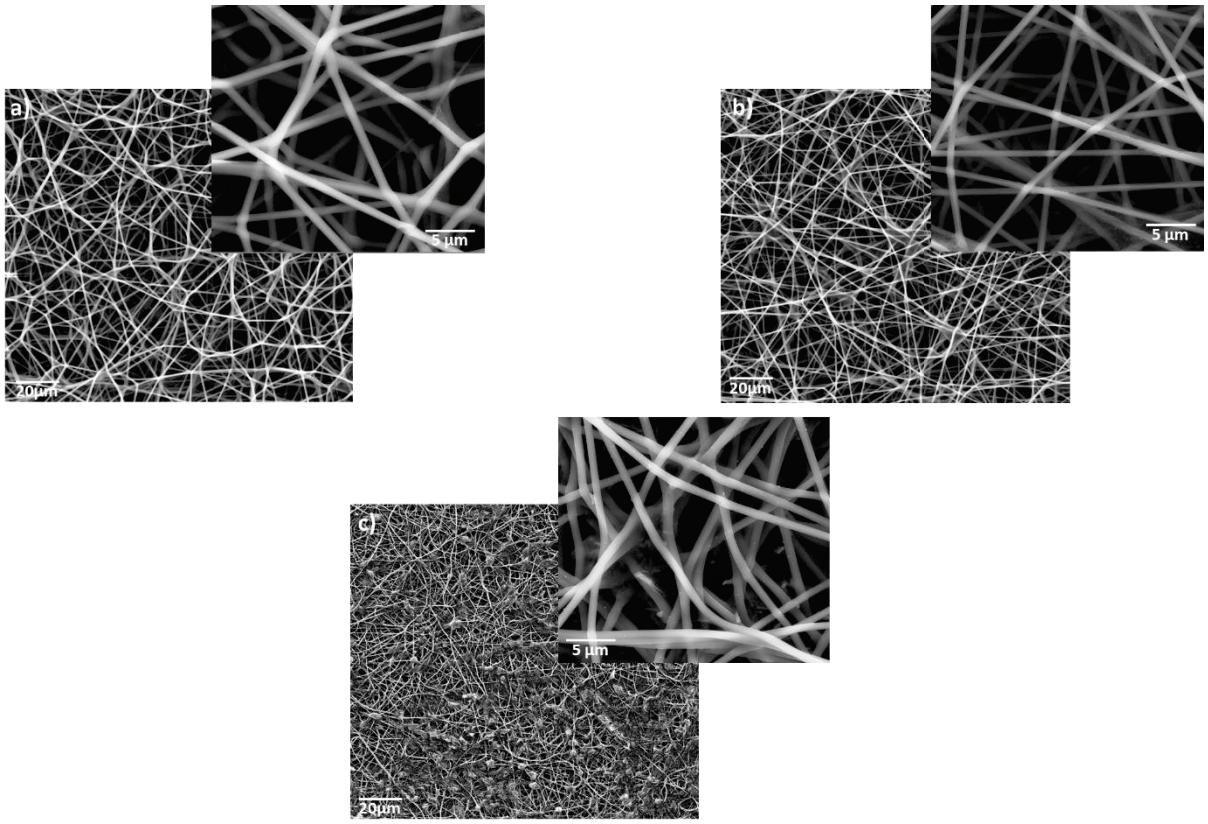

Figure 88. Representative SEM images of PAN NFs covered with PPy/PP3C immersed in a) FeTos 12wt%, b) 20wt% and c) 40wt%, respectively, after ultrasonication for 1min and rinsing with H_2O/MeOH.

SEM images presented in Figure 88a and b confirm the total elimination of crystallized FeTos salts when FeTos solutions of 12wt% and 20wt% are used. The successful removal of FeTos salts after rinsing NFs with methanol has been also reported and confirmed by X-ray diffraction analysis by some authors.[224] At the 40 wt% concentration Figure 88c, only partial removal of FeTos crystals was achieved, also confirming some previous results reported in the literature.[309]

After the cleaning step, all the coated NFs maintained the fibrous morphology and the surfaces were cauliflower shaped, and some NFs were bonded at the fiber-fiber intersections. A possible reason for the formation of the bonding structure is the capillary effect occurring during the coating of the NFs with FeTos solution, in a way that extra FeTos was adsorbed at these intersections and therefore more PPy/PP3C was formed in these areas.[311] As a result, the

[311] H. Wang et al., "Polypyrrole-Coated Electrospun Nanofibre Membranes for Recovery of Au(III) from Aqueous Solution," *Journal of Membrane Science* 303, no. 1–2 (**2007**): 119–25.

PPy/PP3C coating makes the individual fibers less distinguishable when compared to uncoated PAN NFs. (figure 89)

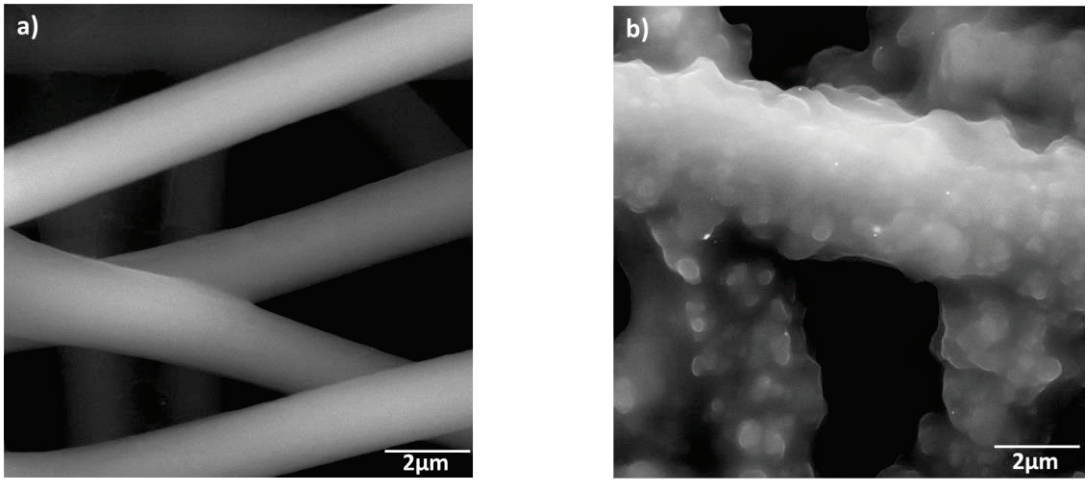

Figure 89. Representative SEM images of a) uncoated PAN fibers and b) PPy/PP3C coated PAN NFs after rinsing with H_2O/MeOH (polymerization time: 30min, FeTos concentration: 20wt%, PPy/PP3C ratio: 1:2.

Moreover, it was noted that the AFD of the PAN/PPy/PP3C NFs was not affected during the rinsing step, which was expected given the fact that PAN does not swell in H_2O and alcohols. The AFD of PAN/PPy/PP3C NFs was 660±10 nm, 670±5 nm and 710±10 nm for 12, 20 and 40 wt% FeTos concentration respectively, when the polymerization time was set at 30 min. The PPy/PP3C coating thickness, roughly estimated by calculating the difference in the AFD of uncoated and PPy/PP3C coated PAN NFs, was in the 10 to 20 nm range, when using 12 wt% and 20 wt% oxidant concentrations. The coatings were found to be thicker at higher oxidant concentration, most likely because of the increase of the oxidant solution viscosity that produced thicker overlayers on the nanofibers.

IV.4.2.2.2. Effect of Polymerization time on the conductive polymer coating

Different polymerization times, ranging from 30 min to 3 h, were tested in order to ensure complete co-polymerization. Preliminary tests were firstly performed, in order to roughly estimate the polymerization kinetics of the two monomers. By keeping the concentration of the two different monomers the same (0.05M), VPP was performed with a) PPy and b) PP3C. From our previous work, we have observed that during the coating of electrospun PAN NFs with PPy by VPP process, pyrrole alone polymerized at ambient temperature within a few minutes (7 min), as revealed by the appearance of the characteristic black colour of polypyrrole onto the NFs. The observed results are in good agreement with what has been reported in the literature during the coating of NFs with PPy by using VPP process.[311]

Additional experiments were performed for the fabrication of conductive PAN/PP3C core-shell NFs, by *in situ* VPP of PP3C on the surface of PAN fibers. P3C polymerized also in ambient temperature but a longer polymerization time was required, probably due to slower evaporation rate of the P3C momoner. When PAN NFs were exposed for 15 min to Py/P3C vapours generated from a Py/P3C (1:2 w/w) solution, the nanofibrous mat turned grey/black, indicating the presence of PPy/PP3C on the NFs.

Polymerization times of 30 min and 3 h were subsequently tested in order to determine the evolution of the NFs diameter with the PPy/PP3C synthesis time. In both cases, the whole membrane looked very uniform, without any colour variations and physical defects. Average fiber diameters of PAN/PPy/P3C NFs after exposure times of 30 min and 3 h, estimated by SEM analysis, are summarized in Table 12. It was observed that AFD slightly increased upon the increasing exposure time to Py/P3C vapours.

Table 12. Influence of FeTos solution concentration and polymerization time on AFD of NFs prepared by VPP of Py/P3C (1:2 w/w).

FeTos Concentration (wt%)	Reaction time: 30min	Reaction time: 3h
12	660±10nm	680±10nm
20	670±5nm	690±10nm
40	710±10nm	735±30nm

IV.4.2.2.3. Electroconducting properties

To characterize the electroconducting properties of the PAN/PPy/PP3C NFs (PPy/PP3C: 1:2 w/w; polymerization time: 30 min), surface resistance was measured by using a four-point probe technique, as described in section IV.3.8.. Increasing FeTos concentration resulted in a significant decrease of the resistance of PAN/PPy/PP3C mats, values being 37.6 kΩ, 9.2 kΩ and 3.3 kΩ for the 12, 20 and 40 wt% concentration, respectively.

Such low resistance values may be assigned to the soldering phenomenon revealed by SEM images at fiber intersections after polymerization, this phenomenon being more intense upon the increasing concentration of FeTos solution. This suggests that the fibers are interconnected at multiple junctions, which ensures a good contact between the fibers and therefore a low ohmic barrier to the charge transport from one fiber to another. Especially at the highest oxidant concentration, the fibers are almost compacted (as revealed by SEM pictures) thus forming a continuous conductive path and significantly reducing the contact resistance between fibers. The observed results are consistent with what it is generally reported in the literature.[309, 312]

The low resistance values exhibited by the conductive nanofibrous mats produced in our study may also be attributed due to a possible semi-crystalline nature of the PPy/PP3C

[312] J.Y. Lee et al., "Polypyrrole-Coated Electrospun PLGA Nanofibers for Neural Tissue Applications," *Biomaterials* 30, no. 26 (**2009**): 4325–35.

coatings. Laforgue and Robitaille showed by X-ray diffraction analysis (XRD)[309] that PPy coatings produced by VPP method are crystalline. The crystallinity of the coatings was attributed to the fact that the VPP method is a solvent-free polymerization process where the tosylate anions produce a templating effect during the growth of the polymers, resulting in the production of particularly ordered polymers by π-π interactions.[313, 314] Additional characterization by X-ray diffraction analysis (XRD) should be performed to confirm our assumption.

IV.4.2.2.4. Electrochemical Characterization of PAN/PPy/PP3C core-shell electrospun NFs

CV and EIS were employed to evaluate the influence of increasing FeTos concentration on the electrochemical characteristics of the gold electrodes modified with PAN/PPy/PP3C NFs. Polymerization time was set at 30 min. CVs were recorded in 10 mM PBS at pH 7.2 at a scan rate of 100mV/s using $Fe(CN)_6^{3-}/Fe(CN)_6^{4-}$ couple as redox probe. The potential was repetitively cycled until several consecutive curves were superimposed. CVs were recorded before and after the functionalization of the electrode surface with PAN NFs and PAN/PPy/PP3C NFs when using FeTos solution of 12 wt%, 20 wt% and 40 wt% during the VPP process. Figure 92 evidences that PAN NFs is highly insulating (black curve) and becomes conductive, with a strong capacitive behaviour, when coated with PPy/PP3C thin films (figure 92, red, blue and green curves). The capacitive current observed for the PAN/FeTos 40%/PPy/PP3C NFs modified electrode is higher than that of PAN/FeTos 20%/PPy/PP3C NFs electrode and much higher than that of PAN/FeTos 12%/PPy/PP3C NFs electrode. These results are in good agreement with what has been reported in the literature.[310]

[313] B. Winther-Jensen et al., "High Current Density and Drift Velocity in Templated Conducting Polymers," *Organic Electronics* 8, no. 6 (**2007**): 796-800.

[314] B. Winther-Jensen et al., "Order–disorder Transitions in poly(3,4-Ethylenedioxythiophene)," *Polymer* 49, no. 2 (**2008**): 481-487.

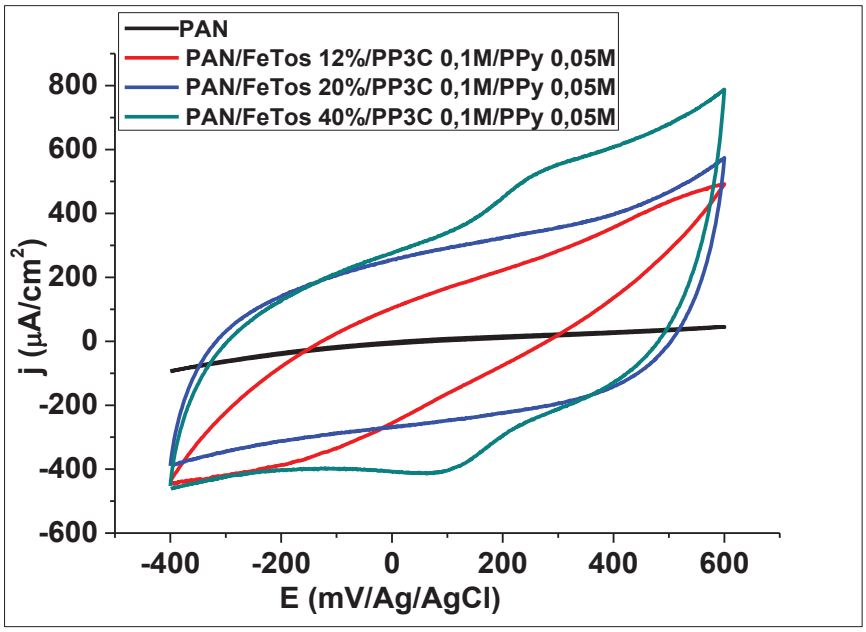

Figure 90. Cyclic voltammograms of gold modified electrodes with PAN NFs and PAN/FeTos/PPy/PP3C electrospun NFs by using FeTos concentrations of 12, 20 and 40 wt%. The CVs were performed in a 10mM $[Fe(CN)_6]^{3-/4-}$ PBS solution, pH 7.2, at a scan rate of 100mV/s.

The electronic transfer properties of the PAN NFs and PAN/PPy/PP3C NFs modified gold electrodes were further characterized by EIS by varying frequency in the 100 mHz to 100 kHz range at a constant potential of -300 mV. The Nyquist plot of bare modified with PAN NFs and PAN/PPy/PP3C NFs electrodes presented in figures 91 and 92 respectively, were satisfactorily fitted with a Randles-Ershler equivalent electrical circuit (Figure 55). The circuit parameters obtained are summarized in Table 13.

The R_{ct}-values of PAN/PPy/PP3C NFs modified electrodes revealed a slight increase in the magnitude of impedance when compared to those of PAN/PPy NFs modified electrodes (Table 11), fabricated under the same conditions. This slight increase in impedance was attributed to the incorporation of the functional monomer pyrrole-3-carboxylic acid (P3C) into the co-polymer scheme, even though it is well-known[301, 302] that 3-substituted pyrroles demonstrate the ability to maintain their intrinsic electrical properties without interfering with the polymer elongation.

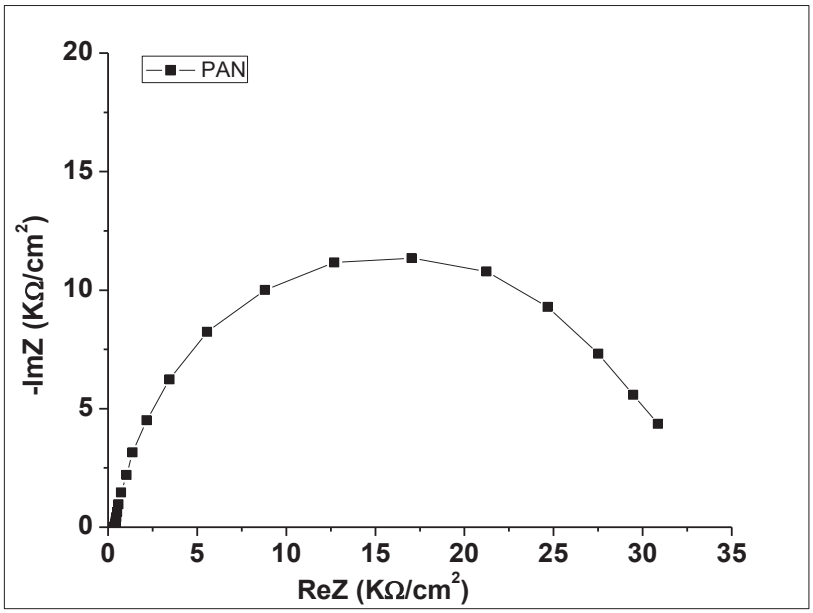

Figure 91. Nyquist plots of impedance spectra obtained for gold electrodes modified with PAN NFs. The EIS measurements were performed at -300 mV in the presence of a 10mM $[Fe(CN)_6]^{3-/4-}$ PBS solution by varying frequency in the 100 mHz to 100 kHz range.

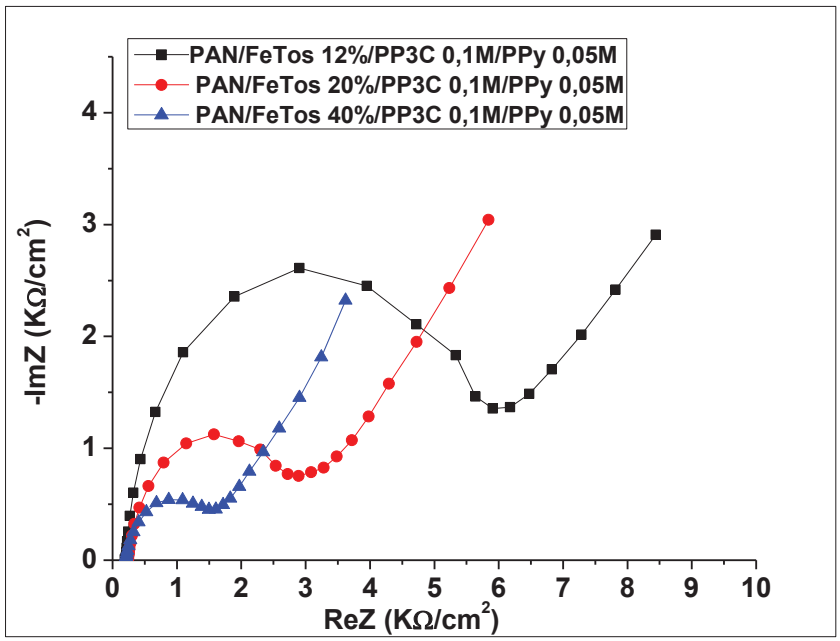

Figure 92. Nyquist plots of impedance spectra obtained for gold electrodes modified with PAN/FeTos/PPy/PP3C NFs by using FeTos concentrations of 12, 20 and 40 wt%. The EIS measurements were performed at -300 mV in the presence of a 10mM $[Fe(CN)_6]^{3-/4-}$ PBS solution by varying frequency in the 100 mHz to 100 kHz range.

Table 13. Results of fitting the Nyquist plots of impedance spectra recorded for gold electrodes modified by PAN NFs and PAN/PPy/PP3C with the equivalent Randles-Ehrshler circuit (figure 55).

	R_s ($\Omega \cdot cm^{-2}$)	R_{ct} ($k\Omega \cdot cm^{-2}$)	CPE ($\mu F \cdot s^{(n-1)}$)	n_{CPE}	x^2
PAN NFs	0.270	32.17	4.945	0.995	0.003
PAN/FeTos 12wt%/ PPy/PP3C	0.177	6.130	1.640	0.988	0.005
PAN/FeTos 20wt%/ PPy/PP3C	0.168	2.998	1.656	0.981	0.004
PAN/FeTos 40wt%/ PPy/PP3C	0.191	1.705	2.332	0.977	0.003

The decrease of R_{ct}-values observed by coating the PAN NFs with PPy/PP3C indicate that the electron transfer capability of the PAN/PPy/PP3C NFs modified gold electrodes is significantly enhanced in comparison to the one of PAN NFs modified electrode, this phenomenon being accentuated by increasing FeTos concentration. These results confirm CV measurements, the diminution of the charge transfer resistance reflecting the increase of the conductivity of the PAN/PPy/PP3C NFs with oxidant concentration.

IV.4.2.2.5. Electroanalytical characterization of PAN/PPy/PP3C/GOx electrospun NFs

For the development of the glucose biosensor, 20 wt% FeTos solution was selected as the oxidant solution in which the PAN NFs were immersed prior to the VPP process, since the mats exhibited high conductivity and uniform coating with PP3C/PPy, and were free of FeTos crystals, as the results of the electrochemical characterization and SEM analysis after the cleaning step had revealed. Although the PAN/40 wt% FeTos/PPy/PP3C NFs exhibited a lower charge transfer resistance than the other fibers, the excess of FeTos crystals could not be totally removed form the mats and would jeopardize the reproducibility of the sensor.

In order to study the influence of the proportion of non carboxylated Py and carboxylated Py in the monomers solution on the final glucose biosensors response, different electrodes were prepared using pure P3C, and 1:1 or 1:2 (w:w) Py/P3C mixtures. PP3C carboxyl groups were then activated for further GOx binding. Each electrode was measured by EIS in PBS solution in presence of different glucose concentrations. Glucose could not be detected, neither with the PAN/P3C/GOx NFs nor with the PAN/Py/P3C(1:1)/GOx NFs modified electrode.

The first result may be attributed to the too high density of carboxyl groups present on the surface, which may hamper activation reaction and/or subsequent binding of a sufficient amount of enzyme. The same issue and/or a slower evaporation rate of the P3C momoner compared to PPy may explain the absence of signal observed for the PAN/Py/P3C(1:1)/GOx NFs modified electrode. PPy alone polymerizes at ambient temperature within a few minutes (7 min), whereas for P3C a longer polymerization time is required (15min). By setting the ratio of Py/P3C monomers at 1:2, EIS measurements enabled successful detection of glucose, thus validating the successful incorporation of carboxylic groups onto the NFs surface (Figure

93). Impedance decreased upon the increasing concentration of glucose, probably due to the fact that the electron transfer is facilitated by the presence of the enzymatic reaction products. No signal was detected from the PAN/PPy/PP3C control electrode.

The Nyquist plots recorded at the different glucose concentrations for PAN/PPy/PP3C/GOx NFs modified electrodes were satisfactorily fitted with a Randles-Ehrshler equivalent electrical circuit (figure 55). The circuit parameters obtained by fitting the impedance data to the equivalent circuit are summarized in Table 14. Values of Rp were used to built the calibration curve of the proposed PAN/PPy/PP3C/GOx NFs biosensor and determine its analytical performances.

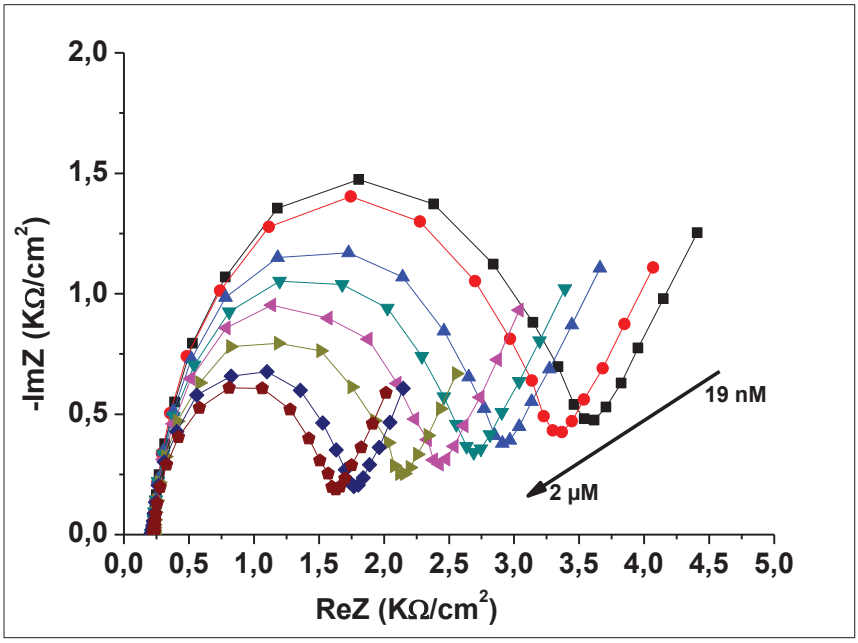

Figure 93. Nyquist plots of impedance spectra obtained for gold electrodes modified with PAN/FeTos 20wt%/PPy0.05M/PP3C0.1M/GOx electrospun NFs upon the increasing concentration of glucose. The EIS measurements were performed at -300 mV in the presence of PBS solution (0.1M, pH 7.2), by varying frequency in the 100 mHz to 100 kHz range.

Table 14. Fitting parameters (Randles-Ehrshler model) obtained from Nyquist plots of impedance spectra recorded at increasing glucose concentration for the PAN/PPy/PP3C/GOx NFs biosensor.

Glucose Concentration	R_s (kΩ·cm^{-2})	R_p (kΩ·cm^{-2})	CPE (μF·s$^{(n-1)}$)	n_{CPE}	x^2
0.00 nM	0,0213	3.381	1.879	0,995	0,003
19 nM	0,0216	3.350	2.027	0,993	0,005
46 nM	0,0214	2.719	2.341	0,996	0,003
103 nM	0,0214	2.493	2.553	0,989	0,007
206 nM	0,0217	2.218	1.793	0,991	0,004
412 nM	0,0226	1.931	2.142	0,990	0,006
1 μM	0,0224	1.565	2.431	0,993	0,004
2 μM	0,0228	1.402	2.836	0,997	0,005

IV.4.2.2.6. Analytical performances of the glucose biosensor

Figure 94 shows the calibration curve obtained by plotting ΔR_p versus log(glucose concentration) for the PAN/FeTos 20wt%/PPy/PP3C/GOx NFs biosensor. The signal was linear in the 19nM-2μM range ($R^2 = 0.977$) with a slope of 0.98 KΩ/log[glucose] (Figure 95).

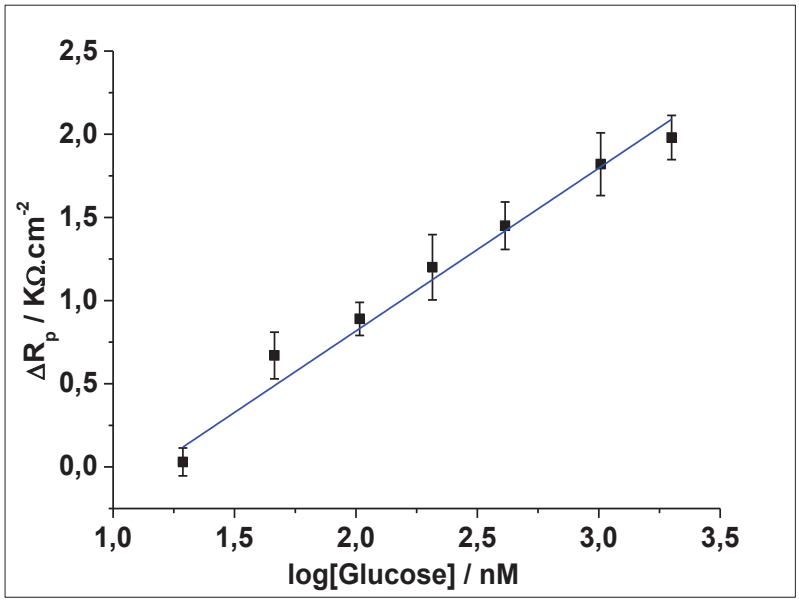

Figure 94. Calibration curve of the PAN/FeTos 20wt%/PPy/PP3C/GOx NFs biosensor (in PBS 0.1M, pH 7.2). Error bars represent standard deviations obtained from three successive measurements.

The limit of detection (LOD), defined as the concentration of glucose giving a signal equal to three times the standard deviation on the blank (i.e. in absence of glucose) was calculated for several electrodes coming from the same and from different batches of the VPP process in order to evaluate the reproducibility of the VPP method. The LOD values are illustrated in Table 15. It is important to point out that even though the LOD slightly varies when the sensor used is coming from different batches (while keeping the same conditions during VPP), all sensors tested exhibited linearity within the same range (19 nM-2 μM), implying that even though the thickness of the conducting PPy/PP3C coating during the VPP was not accurately controlled, the impact of this fact on the reproducibility demonstrated by the developed glucose biosensors was negligible.

Table 15. Limit of detection calculated for six electrodes coming from two different batches of VPP process.

	Batch 1			**Batch 2**		
LOD (nM)	Sensor 1: 1.49	Sensor 2: 1.28	Sensor 3: 2.67	Sensor 4: 2.46	Sensor 5: 5.14	Sensor 6: 2.38
Mean LOD (nM)	1.8			3.3		
Slope (KΩ/log[glucose])	0.98	0.96	0.97	0.57	0.33	0.86

The relative standard deviations calculated from three consecutive measurements on one single biosensor were lower than 2% in the 19nM-2μM range, showing an excellent repeatability of the proposed biosensor. Inter-sensor reproducibility of the method was also rather good as the relative standard deviation, calculated from the analysis of the 46nM glucose solution using six different biosensors, was 15%.

Additionally, operational and storage stabilities of the biosensor were determined. According to the operational stability measurement results, no significant decrease of the PAN/PPy/PP3C/GOx biosensor response was observed after 10 measurements of the 1μM glucose solution, performed the same day. In the same way, EIS signal remained stable for 10 days when the biosensor was tested twice per day at the 1μM glucose concentration and the biosensor was kept at 4°C between two measurements. The results demonstrate the good operational and storage stabilities of the PAN/PPy/PP3C/GOx NFs biosensor.

IV.5. Conclusion

In the present study, different approaches of fabricating core-shell conductive NFs, by combination of electrospinning process and vapour-phase polymerization process, were tested for biosensor elaboration.

In the first approach, electrospun PAN NFs were used as backbone non-conductive NFs which were then coated with conductive PPy coating, through the VPP process. GA vapours were used as cross-linking agent for the immobilization of GOx onto the PAN/PPy NFs surface. By using the VPP method, uniform coating of PAN NFs with PPy was achieved as SEM images revealed, and the resulting fibers exhibited high conductivity as electrochemical characterization results revealed. However, this first approach was not satisfying since it did not enable a firm attachment of the biological sensing membrane onto the fibers and the biosensing layer detached rapidly.

To overcome this issue, covalent immobilization of the enzyme onto the surface of the NFs was decided, and the incorporation of carboxylated functions into the conductive coating through the evaporation of Py/PP3C mixtures instead of Py alone, was investigated. Owing to the poor electrospinnability of PAN/FeTos solutions, immersion of PAN NFs into FeTos oxidant solution was found to be the best way to produce the PAN/FeTos oxidant NFs used as support for subsequent Py and Py/PP3C polymerization. Based on this approach, the successful and rapid elaboration of an original electrochemical glucose biosensor based on electrospun PAN NFs covered with conducting PPy/PP3C coatings via VPP, followed by covalent grafting of GOx onto the surface of the NFs, was illustrated.

The resulting glucose biosensor exhibited enhanced performance, by achieving linearity in a wide range of glucose concentration (19nM-2µM), good stability (shelf life time of 10 days) and very low LOD values (2-5 nM) when compared to LODs obtained via the two approaches described in chapter II and III, and to conventional film-based polypyrrole electrochemical glucose biosensors. Although the thickness of the conducting coating was not accurately controlled, as in an electropolymerisation process, biosensors coming from different batches exhibited linearity in the same ranges thus implying good reproducibility of the VPP method. Moreover by employing the electrospinning technique for the fabrication PAN/PPy/PP3C NFs instead of template synthesis methods, are commonly used for the elaboration of nanostructured polyppyrole based biosensors, we eliminated the need of post-synthetic treatment of the electrospun nanofibers while significantly increasing the specific surface of the biosensor.

GENERAL CONCLUSION AND PERSPECTIVES

GENERAL CONCLUSION AND PERSPECTIVES

In the present dissertation, we reported the simple, rapid and successful fabrication of three pioneering, highly sensitive and electroactive platforms based on conductive electrospun nanofibrous composite materials for further application to electrochemical biosensors elaboration. Glucose oxidase was used as a model enzyme to validate the performance of the developed biosensors. The enzyme was either incorporated into the NFs or covalently immobilized onto their surface. These original biosensors, characterized by various microscopic and electrochemical techniques, enabled successful detection of glucose by employing cyclic voltammetry and electrochemical impedance spectroscopy, whilst demonstrating enhanced performances over conventional biosensors in terms of sensitivity, reproducibility and stability.

Optimizing the processing parameters during the electrospinning process, including flow rate, applied voltage, distance between tip and collector, and polymer solution parameters such as polymer concentration, is of high importance to fabricate nanofibrous mats with minimal beading. This is important in order to decrease the variability of the mats morphology and subsequently increase the reproducibility of the resulting biosensors.

The modification of gold electrodes with electrospun PVA-SbQ/MWCNTs-COOH/GOx NFs, followed by a rapid and facile photochemical cross-linking step which rendered the NFs water-stable, resulted in the production of a highly sensitive voltammetric glucose biosensor exhibiting a wide linear range (5 μM-4 mM) and a very low LOD value (2 μM). Judging from the exhibited high I_{max}, it was concluded that introducing MWCNTs-COOH as conducting filler into the polymeric NFs, improved their conducting properties thus enhancing the electron transfer ability of the generated nanofibrous mats. Moreover, this approach of blending enzyme, MWCNTs-COOH, and water-soluble polymers offers a simple method to electrospin biologically active fibers and thus fabricate a novel electroactive platform for enzyme immobilization in a one-step synthesis approach. Most importantly, it was proven that the enzyme remained active and accessible to the substrate.

In the second approach, water-stable PVA/PEI electrospun NFs incorporating GOx were produced and uniformly decorated with pH-tunable densities of citrate AuNPs. The AuNPs enhanced the electrical properties of the bioactive electrospun NFs and thus facilitated the electron transfer within the system. The obtained impedimetric glucose biosensor exhibited linearity in a wide range (1μM -1mM) of glucose concentration and very low LOD value (0.15μM). Furthermore, the expression of amino groups on the surface of the electrospun nanofibers, achieved through the incorporation of PEI into the electrospun mixture, served to practical adhesion improvement of the electrospun PVA/PEI/GOx nanofibers onto the gold modified electrode surface. This was achieved by modifying the surface with a conductive self-assembled monolayer, ATP-SAMs, bearing thiol groups for covalent bonding to the gold surface and amine groups which reacted with the amine groups of PEI in a following cross-linking step under GA vapours.

Finally, the successful elaboration of a pioneering electrochemical glucose biosensor based on core-shell PAN/PPy/PP3C nanofibrous mats fabricated by combination of electrospinning process and vapour-phase polymerization process, was illustrated. The originality of this work derives from the fact that the combination of ES and VPP technique was employed for the first time for the elaboration of an electrochemical biosensor instead of the use of template synthesis methods, which have traditionally been employed for the elaboration of nanostructured polypyrrole based biosensors.

The advantages of this work include the uniform coating of the surface of the electrospun NFs with PPy/PP3C in a rapid and simple way by carefully setting parameters such as polymerization temperature and time, during the VPP process. The uniform covering of electrospun PAN NFs with conducting PPy/PP3C coatings, contributed to improved electrochemical activity of the nanofibers, thus facilitating the electron transfer within the system. Furthermore, the successful expression of –COOH groups onto the NFs surface, enabled the covalent immobilization of the enzyme, thus decreasing common problems such as diffusion, instability etc. encountered at non-covalent immobilization techniques. Tunable conductivity of the NFs was achieved by immersing the NFs into oxidant solutions of different concentrations before the VPP process.

The resulting glucose biosensor exhibited enhanced performance, by achieving linearity in a wide range of glucose concentration (19 nM-2 μM) and very low LOD values (2-5 nM) when compared to conventional film-based polypyrrole electrochemical glucose biosensors. Although the thickness of the conducting coating was not accurately controlled, whereas in an electropolymerization process it is, biosensors coming from different batches of VPP (while keeping the same conditions during VPP) exhibited linearity in the same ranges thus implying good reproducibility of the VPP method.

The above mentioned analytical performances of the three developed biosensors are summarized in table 16.

Table 16. Analytical performances of the developed biosensors.

	Detection method: CV	**Detection method: EIS**	
	Sensor 1	**Sensor 2**	**Sensor 3**
Linearity range	5 μM-4 mM	1 μM-1 mM	19 nM-2 μM
Limit of detection	2 μM	0.15 μM	2-5 nM
Storage ability	5 days	4 days	10 days
Intra-sensor Reproducibility	lower than 5%	lower than 4%	lower than 2%
Inter-sensor Reproducibility	12%	14%	15%

The elaboration of an impedimetric biosensor based on PVA-SbQ/MWCNTs/GOx would have been interesting in order to be able to perform a more complete comparison between this sensor and the two impedimetric biosensors developed in this work and to evaluate their performance. Only the second and third biosensors can be really compared as they are based on the same transduction mode.

The higher sensitivity achieved using the third approach, compared to the second one, may be due to the fact that when the NFs are covered with a conducting coating instead of being decorated with a certain amount of AuNPs, enhanced electrical properties are achieved, resulting in enhanced electron transfer within the system. The improved electrical properties of PAN/PPy/PP3C nanofibers over PVA/PEI/AuNPs nanofibers were attributed to the fact that during the coating step with PPy/PP3C, a continuous conductive path was created which significantly reduced the contact resistance between the fibers and facilitated the charge transfer whereas in the case of PVA/PEI/AuNPs NFs the electrons are transferred through the insulating polymer NFs by a tunneling mechanism through conduction, which leads to a lower charge transfer efficiency through the mat. An attempt to improve the electrical properties of PVA/PEI/AuNPs NFs was performed, by trying to increase the coverage of their surface with a higher amount of AuNPs. However, the results presented in this work were the optimal ones, since AuNPs aggregated for pH values lower than 4.

The higher sensitivity of PAN/PPy/PP3C/GOx biosensor may be also due to the fact that the enzyme is covalently grafted onto the surface of the nanofibers instead of being encapsulated within the fibers. It is therefore more accessible to the substrate.

Finally, the improved storage ability of PAN/PPy/PP3C/GOx biosensor over PVA/PEI/AuNPs/GOx biosensor, was attributed to the fact that even though the cross-linking of PVA/PEI NFs under GA vapours was successful, after a certain time (4 days) they finally lost their water-insolubility, whereas PAN NFs remained stable since PAN is a water-insoluble polymer. Except that, given the fact that the decoration of PVA/PEI NFs with AuNPs is based on hydrogen bonding and physical entrapment by the cavities of the nanofibrous mats, it was assumed that due to the relatively weak interaction between the NFs and the AuNPs, the latter are being progressively removed from the NFs surface after a given time.

As a conclusion, elaboration of core-shell nanofibrous mats by combination of electrospinning process and vapour-phase polymerization process is a novel and very exciting area of research that opens new perspectives, not only for engineering biosensing systems with improved sensitivity and superior performances compared to existing biosensors, but also for a wide range of applications, e.g. biofuels. Nevertheless, in spite of the promising results we have already obtained, additional characterizations of the systems we developed as well as some technological improvements in their elaboration are still to be done in order to achieve optimal performances. For example, additional experiments able to monitor and quantitatively determine the incorporation of the P3C monomer into the co-polymer scheme would be helpful to optimize Py/PP3C ratio to achieve higher sensitivity of the developed

sensors. For instance, the amount of –COOH coming from the incorporation of the P3C monomer might be determined through the grafting of amino-terminated fluorophores to the PAN/PPy/PP3C NFs surface.

Moreover, in order to evaluate the nature of the produced PPy/PP3C and to see if they have a semi-crystalline nature, which possibly contributes to the low resistance values that PAN/PPy/PP3C nanofibrous mats exhibited or not, X-ray diffraction analysis (XRD) measurements are necessary in order to prove the speculations made within this dissertation.

Finally, it would be interesting to better control of the deposition of the NFs on the electrodes to master the alignment and thickness of the fibers to improve the reproducibility of the final devices produced, by using more advanced electrospinning setups.

Grafting other types of biomolecules (DNA, antibodies, aptamers,…) on these novel hybrid nanofiber based platforms may be also envisaged, enabling to expand their application to the development of other classes of biosensors such as immunobiosensors, nucleic acid biosensor, etc.

Résumé (détaillé)
Introduction générale

Les biocapteurs sont des dispositifs analytiques rapides, sélectifs et à bas coûts présentant une large gamme d'applications dans différents domaines tels que la santé, l'environnement et l'alimentaire. Ils combinent un élément biologique actif, reconnaissant sélectivement une espèce chimique ou bien une famille d'espèces chimiques, et un transducteur physico-chimique pour fournir des mesures complexes de biologie analytique avec un système simple et facile à utiliser. Les biocapteurs électrochimiques présentent un intérêt particulier car ils proposent des méthodes analytiques rapides, précises et à bas coût et offrent de nombreux avantages tels que la possibilité d'être facilement intégrés dans l'électronique tout en satisfaisant les demandes de puissances requises pour des tests décentralisés, ce qui montrent leur fort potentiel notamment pour les applications biomédicales.

D'importants efforts ont été portés sur la miniaturisation de transducteur électrochimique, résultant en une diminution significative de la quantité suffisante de l'entité biologique nécessaire pour la réalisation d'un biocapteur, et également une intégration simplifiée dans des *lab-on-chip*. Malgré les avantages associés à cette diminution de taille des électrodes, la sensibilité des biocapteurs diminuera car la surface spécifique des électrodes, et donc les sites d'immobilisation disponibles pour l'élément de reconnaissance biologique, seront moins nombreux. Cependant, cette difficulté peut être surmontée avec succès en nanostructurant la surface des électrodes et notamment au traver de l'utilisation de nanostructures flexibles.

La conception de nouveaux capteurs intégrant des matériaux nanométriques est un sujet interdisciplinaire en plein essor notamment grâce à leur surface spécifique élevée et leurs propriétés optiques, mécaniques et catalytiques particulières. Une large gamme de matériaux nanométriques tels que les nanoparticules et les nanotubes, avec des formes et des compositions différentes, ont prouvé leur efficacité pour améliorer les performances des biocapteurs.

En particulier, les fibres électrofilées remplissent de nombreuses conditions nécessaires à l'amélioration des performances d'un biocapteur du fait qu'ils présentent de très faibles diamètres (d'une centaine de nanomètre à quelques micromètres), des longueurs élevées, des surfaces spécifiques par unité de masse élevées, et donc un rapport surface/volume élevé et des tailles de pores modulables. Les nanofibres électrofilées ont été utilisées avec succès dans différents domaines d'application tels que l'ingénierie tissulaire, le stockage de l'énergie, la catalyse etc, mais leur utilisation en tant que matrice d'immobilisation pour un biocapteur n'est pas très répandue. Cependant, l'intérêt d'utiliser l'électrofilage pour la fabrication de nanofibres fonctionnalisées, pour la biodétection, croît rapidement en raison de nombreux avantages de cette technique tels que son utilisation simple ne nécessitant pas d'équipements coûteux, la possibilité de contrôler la géométrie des

nanofibres électrofilées, sa haute *ré-utilisabilité* et sa polyvalence. Des biocapteurs basés sur des nanofibres électrofilées fabriqués par quelques groupes de chercheurs ont été rapportés dans la littérature et ont montré des sensibilités supérieures à celles de biocapteurs conventionnels.

Dans les travaux présentés, nous étudions et comparons différentes approches pour la nanostructuration de surface d'électrodes en or avec des nanofibres électrofilées conductrices pour le développement de biocapteurs enzymatiques électrochimiques.

Ce manuscrit est organisé en quatre chapitres. Le premier chapitre est dédié à une revue bibliographique des biocapteurs et en particulier les biocapteurs électrochimiques, les nanomatériaux et leurs utilisations pour l'élaboration de biocapteurs, la technique de l'électrofilage, les polymères conducteurs et leur intégration dans des systèmes de biodétection.

Les travaux présentés dans les chapitres II, III et IV décrivent chacun le développement d'une nouvelle plateforme innovante basée sur des nanofibres électrofilées en matériaux hybrides pour leur application dans l'élaboration de biocapteurs électrochimiques. La glucose oxydase a été utilisée comme enzyme modèle pour valider les performances des biocapteurs développés et des électrodes d'or ont été utilisées comme transducteur. La première plateforme électroactive à être décrite implique la fabrication en une étape simple et rapide de nanofibres électrofilées d'alcool polyvinylique résistantes à l'eau avec des groupes styryle pyridine pendants (PVA-SbQ) contenants des nanotubes de carbones multifeuillets (MWCNTs-COOH) et de la glucose oxydase (GOx) pour la détection du glucose. La seconde surface électroactive décrite implique la modification de la surface d'une électrode d'or avec la réalisation en une étape de nanofibres de copolymère d'alcool polyvinylique/polyéthylèneimine (PVA/PEI) dans lesquelles est incorporée la glucose oxydase comme dans le précédent cas, et la surface de ces nanofibres a été recouverte uniformément par des nanoparticules d'or dont la densité est fonction du pH. La troisième plateforme électroactive développée pour la biodétection à être décrite est basée sur l'utilisation de nanofibres conductrices cœur-enveloppe de polyacrylonitrile (PAN) – polypyrrole(PPy)/acide poly(pyrrole-3-carboxylique) (PP3C) produites par la combinaison du procédé d'élctrofilage avec la technique de polymérisation en phase vapeur. Les fonctions carboxyliques présentes en surface des nanofibres PAN/PPy/PP3C ont été utilisées pour le greffage de façon covalente de la glucose oxydase en réagissant avec les fonctions amine de cette dernière.

Une synthèse des résultats les plus significatifs sera présentée en conclusion, elle mettra en avant les avantages et les inconvénients de chacune des différentes approches employées pour le développement de biocapteurs, et également pour illustrer leur contribution pour le développement de système de biodétection de nouvelle génération menant à des performances supérieures. Ce manuscrit se conclura par une brève discussion sur les perspectives des travaux présentés.

Conclusion générale

Dans ce manuscrit, la fabrication simple, rapide et efficace de trois plateformes électroactives basées sur des nanofibres électrofilées de matériaux composites présentant des sensibilités très élevées ont été présentées pour leur application dans l'élaboration de biocapteurs. La glucose oxydase a été utilisée comme enzyme modèle pour valider les performances des biocapteurs développés. L'enzyme a été soit incorporée directement dans les nanofibres, soit greffée de façon covalente en leur surface. Ces biocapteurs originaux, caractérisés par de nombreuses techniques microscopiques et électrochimiques, ont permis de détecter avec succès du glucose en employant la voltammétrie cyclique et la spectroscopie d'impédance électrochimique, tout en montrant des performances supérieures en termes de sensibilité, reproductibilité et stabilité par rapport aux biocapteurs conventionnels.

L'optimisation des conditions opératoires du procédé d'électrofilage, notamment le débit, la différence de potentiel appliquée, la distance entre la pointe et le collecteur, et les paramètres de la solution de polymère avec notamment sa concentration, sont déterminants dans la fabrication de tapis de nanofibres avec le minimum de perlage. Il est important de maîtriser ce phénomène dans le but de diminuer les variations de morphologie des tapis et donc ainsi augmenter la reproductibilité des biocapteurs développés.

La modification des électrodes d'or avec les nanofibres électrofilées PVA-SbQ/MWCNTs-COOH/GOx, suivie par une étape rapide et simple de réticulation photochimique rendant les nanofibres résistantes à l'eau, a permis la production de biocapteur de glucose à haute sensibilité en voltammétrie montrant une large domaine linéaire (5 µM-4 mM) et une faible LOD (2µM). Les hautes valeurs de I_{max} retrouvées sur ces biocapteurs ont été attribuées à l'introduction de MWCNTs-COOH comme renfort conducteur dans les nanofibres polymères, améliorant ainsi leur propriétés conductrices et en particulier en améliorant la capacité de transfert des électrons des tapis de nanofibres. De plus, cette approche consistant à mélanger l'enzyme, les MWCNTs-COOH et un polymère hydrosoluble offre une méthode de synthèse simple et en une étape pour l'électrofilage de fibres biologiquement actives, et donc la fabrication de nouvelles plateformes électroactives pour l'immobilisation. En particulier, il a été prouvé que l'enzyme reste active et accessible pour la solution. Cette étude ouvre la voie vers de nouveaux systèmes de biodétection avec une sensibilité et des performances supérieures à celles des biocapteurs conventionnels.

Dans une deuxième approche, des nanofibres résistantes à l'eau de PVA/PEI contenant la GOx ont été produites et uniformément recouvertes avec des nanoparticules d'or (AuNPs) dont la densité est fonction du pH. Les AuNPs améliorent les propriétés électriques des nanofibres électrofilées bioactives et donc facilite le transfert d'électrons dans le système. Les biocapteurs du glucose par impédance obtenus ont montré une linéarité sur un large domaine de concentration de glucose (1µM – 1 mM) et une très faible valeur de LOD. De plus, la présence des groupes amines en surface des nanofibres électrofilées, due à la présence de PEI dans le mélange électrofilé, permet d'améliorer l'adhérence des nanofibres PVA/PEI/GOx

électrofilées sur l'électrode en or fonctionnalisée. Les électrodes étant au préalable fonctionnalisées avec une monocouche conductrice comportant une fonction thiol pour le greffage covalent à la surface d'or et une fonction amine réagissant avec les fonctions amines du PEI lors de l'étape de réticulation sous les vapeurs de glutaraldéhyde (GA).

Enfin, l'élaboration avec succès d'un biocapteur électrochimique innovant pour la détection du glucose basé sur un tapis de nanofibres cœur-enveloppe PAN/PPy/PP3C fabriqué par la combinaison du procédé d'électrofilage et celui de la polymérisation par phase vapeur a été présenté. L'originalité de ce travail provient du fait que c'est la première fois que le procédé d'électrofilage est combiné à celui de la polymérisation par phase vapeur pour l'élaboration d'un biocapteur électrochimique, passant outre l'utilisation des techniques conventionnels de nanostructuration utilisées pour l'élaboration de biocapteurs basés sur des nanostructures en PPy.

Les travaux présentés permettent le dépôt homogène sur des nanofibres électrofilées de PPy/PP3C de façon rapide et simple en ajustant correctement les paramètres expérimentaux tels que la température de polymérisation et la durée du procédé de polymérisation par phase vapeur. Le recouvrement uniforme de nanofibres électrofilées PAN avec un dépôt conducteur de PPy/PP3C contribue à l'amélioration de l'activité électrochimique des nanofibres, et donc facilite le transfert d'électron dans le système. De plus, la présence de fonctions carboxyliques en surface permet le greffage covalent de l'enzyme, évitant ainsi les problèmes communément retrouvés tels que la diffusion, l'instabilité (etc…) lors de greffages non covalents des enzymes. La variation de la conductivité des nanofibres a été maîtrisée par l'immersion des nanofibres dans des solutions oxydantes de différentes concentrations avant le procédé de polymérisation par phase vapeur.

Les biocapteurs de glucose ainsi réalisés ont montré des performances supérieures, en possédant une linéarité sur une large gamme de concentration de glucose (19 nM – 2 μM) et de très faibles valeurs de LOD (2-5 nM) par rapport aux biocapteurs électrochimiques de glucose conventionnels basés sur un film de PPy. Bien que l'épaisseur de PPy déposée par VPP n'est pas précisément contrôlée, contrairement à celles déposés par électroplolymérisation, les biocapteurs réalisés séparément mais sous les même conditions expérimentales ont montré une linéarité similaire sur le même domaine, montrant ainsi une bonne reproductibilité du procédé VPP.

Les performances analytiques des trois biocapteurs innovants présentés ci-dessus sont résumées dans la table 1.

Table 17: Synthèse des performances analytiques des biocapteurs développés.

	Méthode detection : VC	**Méthode de detection : SIE**	
	Capteur 1	**Capteur 2**	**Capteur 3**
Domaine de linéarité	5 µM-4 mM	1 µM-1 mM	19 nM-2 µM
Limite de détection	2 µM	0.15 µM	2-5 nM
Capacité de stockage	5 days	4 days	10 days
Reproductibilité des mesures sur un capteur	lower than 5%	lower than 4%	Lower than 2%
Reproductibilité des mesures sur différents capteurs	12%	14%	15%

Etant donné que les performances électroanalytiques du premier biocapteur développé ont été réalisées par voltammétrie cyclique tandis que celles des deux autres biocapteurs ont été étudiées par spectroscopie d'impédance électrochimique, une comparaison de ces performances ne sera faite que pour ces derniers. Tel que démontré précédemment, lorsque les nanofibres de PAN recouvertes d'un film conducteur de PPy/PP3C ont été utilisées, de meilleurs résultats ont été obtenus en terme de sensibilité et de capacité de stockage par rapport aux biocapteurs basés sur des nanofibres de PVA/PEI recouvertes de nanoparticules d'or.

Une explication possible à ce phénomène vient du fait que lorsque les nanofibres sont couvertes avec un dépôt conducteur, plutôt qu'avec des nanoparticules métalliques, elles possèdent de meilleures propriétés électriques de surface et donc un meilleur transfert d'électron. L'amélioration des propriétés électriques des nanofibres PAN/PPy/PP3C par rapport aux PVA/PEI/AuNPs a été attribuée au fait que durant l'étape de dépôt de PPy/PP3C, un film continu conducteur est ainsi créé entre certaines nanofibres diminuant fortement la résistance de contact entre les fibres et facilitant le transfert de charges, tandis que dans le cas des nanofibres PVA/PEI/AuNPs les électrons ne peuvent être transférés aux nanofibres isolantes que par des mécanismes d'effet tunnel, ce qui mène à une efficacité de transfert de charges plus faible dans le tapis. Pour améliorer les propriétés électriques des nanofibres PVA/PEI/AuNPs, des essais ont été réalisés pour augmenter le taux de recouvrement des nanofibres par les AuNPs. Cependant, les résultats présentés dans ces travaux sont déjà les plus optimaux, étant donné que pour des valeurs de pH inférieures à 4 les AuNPs se sont aggrégées.

De plus, concernant la plus grande sensibilité des biocapteurs PAN/PPy/PP3C/GOx, il peut aussi être envisagé que comme l'enzyme ait été greffée de façon covalente à la surface des nanofibres au lieu d'être encapsulée dans les fibres, elle demeure plus accessible par la solution.

Enfin, la capacité de stockage supérieure des biocapteurs PAN/PPy/PP3C/GOx, par rapport aux biocapteurs PVA/PEI/AuNPs, a été attribuée au fait que même si la réticulation des nanofibres de copolymère PVA/PEI sous des vapeurs de glutaraldéhyde (GA) a fonctionné, après un certain temps (4 jours) les nanofibres perdent leur résistance à l'eau tandis que les nanofibres de PAN reste stables étant donné que le PAN est insoluble dans l'eau. Par ailleur, étant donné que le recouvrement des nanofibres PVA/PEI avec les AuNPs est basé sur des laisons hydrogènes et par l'ancrage mécanique dans les rugosités des nanofibres, il a été présumé qu'en raison de l'unique présence d'interactions faibles entre les AuNPs et les nanofibres, après un certain temps, les AuNPs sont progressivement retirées de la surface des nanofibres.

Concernant les perspectives de travaux présentés, il peut être mentionné que la réalisation d'expériences supplémentaires pourrait être menée dans le but de contrôler et de déterminer les proportions de monomère P3C dans le copolymère. L'incorporation de la proportion optimale de P3C est un paramètre clé pour la sensibilité des biocapteurs développés étant donné que ce sont ces fragments qui permettent l'immobilisation de l'enzyme. Par exemple, des fluorophores aminés peuvent être utilisés pour être greffés sur les nanofibres PAN/PPy/PP3C permettant ainsi de quantifié la quantité de sites COOH disponibles pour l'enzyme par spectroscopie infra-Rouge à transformée de fourrier, déterminant ainsi de façon indirecte la proportion de P3C dans le copolymère.

De plus, pour déterminer la nature des nanofibres PPy/PP3C, plus particulièrement leur nature semi-cristalline ou non qui pourrait expliquer les faibles valeurs de résistance des tapis de nanofibres PAN/PPy-PP3C, des analyses par diffraction des rayons X seraient nécessaires pour appuyer les hypothèses formulés dans ce manuscrit.

D'un autre côté, la réalisation d'un biocapteur d'impédance basé sur un tapis de nanofibres de PVA-SbQ/MWCNTs/GOx aurait été intéressante dans le but d'être capable de réaliser une comparaison plus complète, du point de vue des performances analytiques, entre ce biocapteur et les deux autres développés dans ces travaux.

Pour conclure, il est important de noter que l'application de ces plates-formes innovantes basées sur des nanofibres en matériaux hybrides n'est pas seulement limitée aux biocapteurs enzymatiques mais peut également être utilisée pour le développement d'autres types de biocapteurs tels que les biocapteurs immunologiques ou des biocapteurs d'acides nucléiques. De plus, au lieu d'utiliser des équipements conventionnels d'électrofilage pour la fabrication de tapis de nanofibres aléatoirement réparties, des équipements plus sophistiqués peuvent être utilisés pour fabriquer des tapis de nanofibres alignées ce qui contribuera à une meilleure reproductibilité des biocapteurs fabriqués.